THE APPLICATION OF COMPUTATIONAL AND EXPERIMENTAL TECHNIQUES TO METAL DEFORMATION IN COLD ROLL FORMING

Rohana Sarath Kumar Senanayake

Doctor of Philosophy

University of Aston, Aston Triangle, Birmingham

1998

Thesis Summary

The Application of Computational and Experimental Techniques to Metal Deformation in Cold Roll Forming

University of Aston, Birmingham
Rohana Sarath Kumar Senanayake
Doctor of Philosophy
1998

The quality of roll formed products depends to a large extent on the strains to which the material is subjected during the cold roll forming process. The main objective of this research has been to achieve a better understanding of the behaviour of the material during the process of cold roll forming. To achieve this objective, strains developed in the material during forming have been studied. The effect of the parameters such as interpass distance and the material on these strains has been investigated. A reliable method of predicting these strains using a commercially- available finite element package has also been achieved. During the design of roll tooling, a reasonably accurate assessment of the material behaviour can be provided by finite element analysis. Measurement of grid markings on specimens to calculate plastic strains using optical microscopes is time-consuming and prone to errors. Hence a technique was developed using computer vision methods to calculate plastic strains automatically.

Keywords

Cold Roll Forming
Finite Element Analysis
Elastic Strains induced during Cold Roll Forming
Plastic Strains in Cold Roll Forming
Cold Roll Forming Mills

Acknowledgements

Thanks to:

Dr I.M.Cole, my supervisor for the guidance and support given to me throughout the period of this research project.

A/Prof S. Thiruvarudchelvan, my supervisor in Singapore for his support and advice.

My wife for her constant encouragement, support and patience while I worked during evenings and weekends.

Dr Sisira Amarasinghe, Dr Yeo Song Huat , Dr Gerald Seet for all their help.

Mr Tia Nan Heng and Mr Ting Poh Ming for helping with the experimental work.

Mr Chan Weng Fatt and Mr Chua Yoke Kee for helping with the fabrication of the Cold Roll Forming mill.

BHP Lysaught Pte Ltd, Singapore for loaning a Cold Roll Forming mill.

Nanyang Technological University, Singapore for providing me with an Applied Research Grant to fund the experimental work and the building of a Cold Roll Forming Mill.

Abstract

The quality of roll formed products depends to a large extent on the strains to which the material is subjected during the cold roll forming process. The main objective of this research has been to achieve a better understanding of the behaviour of the material during the process of cold roll forming. To achieve this objective, strains developed in the material during forming have been studied. The effect of the parameters such as interpass distance and the material on these strains has been investigated. A reliable method of predicting these strains using a commercially- available finite element package has also been achieved. During the design of roll tooling, a reasonably accurate assessment of the material behaviour can be provided by finite element analysis. Measurement of grid markings on specimens to calculate plastic strains using optical microscopes is time-consuming and prone to errors. Hence a technique was developed using computer vision methods to calculate plastic strains automatically.

List Of Contents

		Page
Abstract		4
List of Contents		5
List of Figures		12
List of Tables		23
CHAPTER 1	**INTRODUCTION**	24
1.1	**Background**	24
1.2	**Objective**	25
CHAPTER 2	**COLD ROLL FORMING**	26
2.1	**Basic Approach to a simple shape**	26
2.2	**Tolerance and speeds of rolls**	29
2.3	**Roller Material**	30
2.4	**Cold Roll Forming: Problems and Solutions**	30
2.5	**Roll Forming High Tensile Steels**	31
2.6	**Number of Passes**	32
2.7	**Roll Form Design - Locating the Vertical Guideline**	34
2.8	**Roll Form Design - Driving Diameters**	34
2.9	**Strip Width Calculations and the Section Flower**	35
2.10	**Rules for Designing Cold Roll Formed Sections**	35
2.11	**Cold Roll Forming Profiles from Material of Non-Uniform Thickness**	36

CHAPTER 3 PREVIOUS RESEARCH INTO COLD ROLL FORMING 37

3.1 Experimental Research 37

3.2 Computer simulation of Cold Roll Forming 45

3.3 Theoretical Investigations 51

CHAPTER 4 DESIGN AND FABRICATION OF A COLD ROLL FORMING MILL 58

4.1 Cold Roll Forming Mill No: 1 59

4.2 Design and fabrication of the CRF Mill No: 2 60

4.2.1 Frame 61

4.2.2 Roll Stations 67

4.2.3 Drive System 67

4.3 Design of Roll Tooling for the CRF Mills 70

4.3.1 Tooling for the CRF Mill No: 1 71

4.3.2 Tooling for the CRF Mill No: 2 74

4.4 Quality testing of the Roll Formed Sections 75

4.4.1 Factors that affect the quality of roll formed products 75

4.4.2 Measurement of the Longitudinal bow of the roll-formed section 77

4.4.3 Measurement of the Springback effect on the roll-formed channel 79

CHAPTER 5 EQUIPMENT, MATERIALS AND EXPERIMENTAL PROCEDURES 81

5.1 Equipment 81

5.1.1 CRF mills 81

5.1.2 Specimens 82

	5.1.3	Strain measurement	84
	5.2	**Experimental Procedures**	92
	5.2.1	Static forming tests	92
	5.2.2	Dynamic forming tests	95
	5.2.3	Comparison between Static and Dynamic tests	96
	5.2.4	Plastic strain measurement	97
	5.3	**Experimental Results**	98
CHAPTER 6		**AN APPROXIMATE METHOD TO PREDICT STRAIN DEVELOPMENT IN COLD ROLL FORMING USING FINITE ELEMENT ANALYSIS**	105
	6.1	**Previous Research Work in the Simulation of Cold Roll Forming Process using Finite Element Analysis and other Analytical Methods.**	105
	6.2	**MARC Finite Element Analysis Program**	107
	6.3	**Modelling the Cold Roll Forming Process**	120
	6.4	**Program Output / Results**	125
CHAPTER 7		**INTRODUCTION TO COMPUTER VISION TECHNIQUES**	132
	7.1	**Basics of Digital Image Processing**	132
	7.2	**Imaging Software Package MATROX ITOOLS® and Matrox Imaging Library Software**	136
	7.2.1	Image processing capabilities	136
	7.2.2	Graphics capabilities	137
	7.2.3	Blob analysis capabilities	137
	7.2.4	Pattern recognition capabilities	137
	7.2.5	MIL objects	137
	7.2.6	Image Pixel Depth	138
	7.2.7	The library	138
	7.2.8	Matrox imaging library interpreter (MILINTER)	138

7.3 **Image Processing** 138

7.3.1 Improving the image quality 139

7.3.2 Techniques to improve images 140

7.3.3 Thresholding images 141

7.3.4 Binarizing 141

7.3.5 Clipping 142

7.3.6 Advanced Image Manipulation 142

7.4 Blob Analysis 143

7.4.1 MIL and blob analysis 144

7.4.2 Typical steps to perform blob analysis 145

7.4.3 Setting up for blob analysis 145

7.4.4 Adjusting blob analysis processing controls 146

7.4.5 Controlling the image lattice 146

7.4.6 The pixel aspect ratio 147

7.4.7 Analysing the blobs 148

7.4.8 The area and perimeter 148

7.5 Pattern Recognition 150

7.5.1 Defining the model 150

7.5.2 Image alignment 150

7.5.3 Searches, models and model search parameters 151

7.5.4 Positional accuracy 151

7.5.5 Sub-pixel accuracy 152

7.6 Specifying and Managing Data Buffers 152

7.6.1 Allocation of data buffers 152

7.6.2 Managing data buffers 153

7.7 MIL Program Structure 153

CHAPTER 8 STRAIN MEASUREMENT USING COMPUTER VISION 155

8.1 Description of the Image Grabbing Procedure 156

8.2 Procedure involved in Measuring the co-ordinates of the Grid Points 156

8.3	**Description of the Procedure**	162
8.4	**Measurement of Strains**	166
8.4.1	Special considerations	167
8.4.2	Retrieving the co-ordinates of the grid points	167
8.4.3	Organisation of grid point co-ordinates	168
8.5	**Algorithm for the Organisation of Grid Points**	173
8.5.1	The choice of the origin of the local co-ordinate system of the grid points	173
8.5.2	Columns of grid points	173
8.5.3	Classification of columns of grid points	173
8.5.4	Calculation procedure	173
8.5.5	Calculation of strains	175
8.5.6	Printing of the results	176
8.5.7	Comparative tests	176
8.5.8	Conclusion	177
CHAPTER 9	**DISCUSSION AND CONCLUSION**	178
9.1	**Elastic-Plastic Strain Analysis**	178
9.1.1	Longitudinal strains in the web	178
9.1.2	Longitudinal strains in the flange	180
9.1.3	Lateral strains in the flange	185
9.1.4	Principal strain analysis	188
9.1.5	Influence of material	191
9.1.6	Effect of number of roll stations and interpass distance	197
9.2	**Comparison of Experimental and Theoretical Strain Distributions**	204
9.3	**Finite Element Analysis**	205
9.3.1	Strains Predicted by the Finite Element Model	206
9.3.2	Incremental-Iterative Solutions	207
9.4	**Plastic Strain Analysis**	207
9.5	**Conclusions**	209
9.6	**Recommendations for future work**	211

LIST OF REFERENCES 213

APPENDICES

Appendix A **Theoretical Strain distributions** 219

(see under list of figures for details)

Appendix B **Experimental Strain distributions** 224

(see under list of figures for details)

Appendix C **Flowcharts for MIL Programs** 256

Flowchart for the programs Cogimag1.cl, Cogimag2.cl,

Cogmark1.cl and Cogmark2.cl 237

Appendix D **Flowcharts for C Programs** 260

Flowchart for Main Program 261

Flowchart for Function *FileOpen* 262

Flowchart for Change of Function 263

Flowchart for Translation vector 264

Flowchart for Rotation Angle 265

Flowchart for Rotation of points and translation of points 266

Flowchart for Determination of the base 267

Flowchart for Obtaining the column of base 268

Flowchart for function *classification* 269

Flowchart for function *arrange* 270

Flowchart for function *calculus* 271

Flowchart for the program LINK.cl 272

Flowchart for the programs MFOCUS1.cl, MFOCUS2.cl,

MFOCUS3.cl, MFOCUS4.cl, 273

Appendix E	**MIL Programs for image processing**	274
	Program COGIMAG1.CL	275
	Program COGIMAG2.CL	279
	Program COGMARK1.CL	283
	Program COGMARK2.CL	287
	Program LINK.CL	291
	Program MFOCUS1.CL	293
	Program MFOCUS2.CL	294
	Program MFOCUS3.CL	296
	Program MFOCUS4.CL	298
Appendix F	**C Programs for calculating plastic strains**	300
	Program STRAINS.C	301
Related Publications		317

List of Figures

		Page
Figure 2.1	Typical Roll Formed Shapes	26
Figure 2.2	Illustration of Forming Angle α of a channel section	28
Figure 2.3	Flower Pattern	29
Figure 2.4	Bend Radii in Conventional Forming	31
Figure 2.5	Helical Path of the Edge of a Section	32
Figure 2.6	Metal Movement	33
Figure 2.7	Path of the Least Length of the Strip Edge	33
Figure 3.1	Typical Strain Distribution at a Roll Station	38
Figure 3.2	Inlet Angle α	39
Figure 3.3	Inlet Angle of Centre Line of Web Part in the Forming Process from Bend Angle θ_i to θ_{i+1}	39
Figure 3.4	Channel Sections	40
Figure 3.5	Membrane Strain Traces using Multiple Roll Stations	42
Figure 3.6	Membrane Strain Traces using two Roll Stations	42
Figure 3.7	Curved Surface of the Sheet Metal	47
Figure 3.8	Roll Forming a Channel Section	52
Figure 3.9	Bend Angle Diagram	52
Figure 3.10	Geometric Restriction Resulting from the Roll Cross-section	53
Figure 3.11	Bend Angle Diagram showing Bottom Roll at the End of Pass	54
Figure 3.12	Bottom Roll for Forming a Channel Section	55
Figure 3.13	Theoretical Strain Distribution	56

Figure 4.1	Roll Forming Mill No:1	59
Figure 4.2	Horizontal and Vertical Shaft Distance	60
Figure 4.3	View of the Cold Roll Forming Mill No:2	61
Figure 4.4	General Assembly of the Cold Roll Forming Mill	62
Figure 4.5	Bottom Frame assembly	63
Figure 4.6	Exploded View of Bottom Frame Assembly	64
Figure 4.7	Top Frame Assembly	65
Figure 4.8	Exploded View of the Top Frame Assembly	66
Figure 4.9	General Assembly of a Roll Station	68
Figure 4.10	Exploded View of a Roll Station	69
Figure 4.11	Chain Drive System of the CRF Mill No:2	67
Figure 4.12	Top and Bottom Rolls for producing a Trapezoidal Section	70
Figure 4.13	Trapezoidal Section (CRF Mill No:1)	71
Figure 4.14		
	(a) Top Roll Assembly	72
	(b) Top Roller after Modification	72
Figure 4.15	Profile of bottom roll	73
Figure 4.16	Flower pattern of the Trapezoidal Section	74
Figure 4.17	Trapezoidal Section (CRF Mill No:2)	74
Figure 4.18	Factors Affecting Straightness	75
Figure 4.19	Springback	76
Figure 4.20	Longitudinal Bow of an Aluminium Roll Formed Section	78
Figure 4.21	Longitudinal Bow of a Mild Steel Roll Formed Section	78
Figure 4.22	Graph of Springback Factor Vs Forming Angle	80

Figure 5.1	Cold Roll Forming Mill No:1	81
Figure 5.2	Cold Roll Forming Mill No:2	82
Figure 5.3	Dimensions of Tensile Test Specimen	83
Figure 5.4	Tensile Test Specimen	83
Figure 5.5	Instron Tensile Testing Machine	83
Figure 5.6	Stress-Strain Diagrams for Steel and Aluminium Specimens	84
Figure 5.7	Location of Strain Gauges - Specimen No:1	85
Figure 5.8	Location of Strain Gauges - Specimen No:2	86
Figure 5.9	SYS4000 Datalogger and Peripherals	87
Figure 5.10	SYS4000 Main Menu	87
Figure 5.11	System Block Diagram	88
Figure 5.12	Dynamic Data Acquisition System	89
Figure 5.13	OMIS II - Optical Measurement Inspection System	91
Figure 5.14	Measurement Screen	91
Figure 5.15	Main Menu Screen	92
Figure 5.16	Test with 6 Roll Stations 127 mm apart (CRF Mill No:1)	94
Figure 5.17	Test with 3 Roll Stations 2 x 127 mm apart (CRF Mill No:1)	94
Figure 5.18	View of strain gauges during strain measurement	95
Figure 5.19	Comparisons of static and dynamic principal strain distributions	96
Figure 5.20	Partially Formed Specimen	97
Figure 5.21	Longitudinal strains (static) in the flange	98
Figure 5.22	Lateral strains (static) in the flange	98
Figure 5.23	Longitudinal strains (static) in the web	99
Figure 5.24	Longitudinal strains (dynamic) in the flange	99

Figure 5.25	Lateral strains (dynamic) in the flange	100
Figure 5.26	Maximum and Minimum Principal Strains in the Steel Specimen	100
Figure 5.26	Maximum and Minimum Principal Strains in an Aluminium Specimen	101
Figure 6.1	MARC Finite Element Program Structure	108
Figure 6.2	Basic Uniaxial Tension Behaviour of the combined Hardening Model.	116
Figure 6.3	Work Hardening Slopes	118
Figure 6.4	MARC Program Flow Diagram	119
Figure 6.5	Roll Form Layout	120
Figure 6.6	Schematic Layout of the Section Height at each Pass, the Forming Angles and Total Forming Length	121
Figure 6.7	Partially formed workpiece with grid marks	122
Figure 6.8	Trapezoidal Section (CRF Mill No:1)	123
Figure 6.9	Plot of the MARC output of longitudinal strain near the edge of the specimen	125
Figure 6.10	Plot of the 3rd component of nodal displacement against horizontal distance using MARC® Finite Element Simulation output	126
Figure 6.11	Band Contour Plot of Longitudinal Strain Variation	126
Figure 6.12	Band Contour Plot of Lateral Strain Variation	127
Figure 6.13	Plot of 3rd Component of Nodal Displacement	128
Figure 6.14	Plot of Equivalent Plastic Strain	129
Figure 6.15	Plot of Equivalent von Mises Stress	129
Figure 6.16	Plot of Deformed Specimen (Sheet 1)	130
Figure 6.17	Plot of Deformed Specimen (Sheet 2)	131

Figure 7.1	Conversion of an Analogue Video Signal	133
Figure 7.1a	Signal conversion for display on standard TV monitor	133
Figure 7.1b	Signal conversion for image processor use	133
Figure 7.2a	Voltage pulse train from (5 x 5 array) solid state camera and resultant pixel values in image array	134
Figure 7.2b	An image with brightness gradient	134
Figure 7.3	Pixel Arrangement	135
Figure 7.4	Lattices with neighbour connections	146
Figure 7.5	Circle with aspect ratio	147
Figure 7.6	Area and perimeter of a pixel	148
Figure 7.7	Convex perimeter of a blob	148
Figure 7.8	Pixel aspect ratio	149
Figure 7.9	Feret diameter	149
Figure 7.10	MIL Program Structure	154
Figure 8.1	Image of a sheet of metal before deformation without sufficient illumination.	158
Figure 8.2	Binarization of the image (thresholding value:130)	159
Figure 8.3	Binarization of the image (thresholding value:120)	159
Figure 8.4	Binarization of the image (thresholding value:100)	160
Figure 8.5	Image of a blob and the noise around it.	162
Figure 8.6	The centres of gravity are marked with a cross hair.	164
Figure 8.7	Image of a blob, and its centre of gravity (marked by a cross hair)	165
Figure 8.8	Position of the specimen before deformation.	167
Figure 8.9	Position of the specimen after deformation.	168

Figure 8.10 Example of a co-ordinate system 169

Figure 8.11 Translation Vector 169

Figure 8.12 Determination of the rotation angle. 170

Figure 8.13 Transformation of the co-ordinates system. 171

Figure 8.14 Rotation in the co-ordinates system after deformation 172

Figure 8.15 Classification of grid points 174

Figure 8.16 Deformation of a plane element. 175

Figure 8.17 Test Specimens for strain measurement using computer vision techniques 176

Figure 9.1 Longitudinal strain distribution in the web (CRF Mill No: 2) 179

Figure 9.2 Longitudinal strain distribution in the web (CRF Mill No: 1) 179

Figure 9.3 Longitudinal strain in the outer edge of the flange (CRF Mill No: 2) 180

Figure 9.4 Longitudinal strain near the bend line (CRF Mill No: 2) 181

Figure 9.5 Longitudinal strain distributions in the flange (CRF Mill No: 1) 182

Figure 9.6 Bend angle curve 182

Figure 9.7 Comparison of Longitudinal Strain distributions at different locations of the flange for Steel and Aluminium Specimens (CRF Mill No:2) 183

Figure 9.8 Localised deformation during cold roll-forming 184

Figure 9.9 Edge of strip elongated during forming 185

Figure 9.10 Lateral strain in the outer edge of the flange (CRF Mill No: 2) 185

Figure 9.11 Lateral strain in the bend corner of the flange 186

Figure 9.12 Comparison of Lateral Strain distributions at different locations of the flange for Steel and Aluminium Specimens (CRF Mill No:2) 187

Figure 9.13 Lateral strain distributions in the flange (CRF Mill No:1) 188

Figure 9.14 Maximum principal strain distribution (CRF Mill No:2) 189

Figure 9.15 Comparison of maximum and minimum principal strain distributions for Steel and Aluminium Specimens (CRF Mill No:2) 190

Figure 9.16 Comparison of maximum and minimum principal strain distributions (CRF Mill No:1) 191

Figure 9.17 Influence of material on longitudinal strain (CRF Mill No:2) 192

Figure 9.18 Influence of material on lateral strain (CRF Mill No: 2) 192

Figure 9.19 Influence of material on longitudinal strain (CRF Mill No: 1) 193

Figure 9.20 Influence of material on lateral strain (CRF Mill No: 1) 193

Figure 9.21 Comparison of strain distributions for Steel and Aluminium Specimens (CRF Mill No:2) 194

Figure 9.22 Comparison of 6 roll stations and 3 roll stations (CRF Mill No: 1) 198

Figure 9.23 Comparison of longitudinal strains for 2x127 mm spacing and 127 mm spacing (CRF Mill No: 1) 199

Figure 9.24 Comparison of longitudinal and lateral strain distributions for different interpass distances. (CRF Mill No:2, Aluminium and Steel Specimens) 200

Figure 9.25 Graph of maximum and minimum principal strains at varying interpass distances (CRF Mill No:2, Steel and Aluminium Specimens) 203

Figure 9.26 Comparison of experimental and theoretical strain distributions (CRF Mill No:1) 205

Figure 9.27 Longitudinal strain distribution in the flange of a steel specimen using MARC finite element simulation (CRF Mill No:1) 206

Figure 9.28 Longitudinal strain distribution in the flange of a steel specimen determined experimentally using the CRF Mill No:1 206

Figure 9.29 Comparison of experimental longitudinal strain distribution with strains predicted by finite element analysis. 207

Figure 9.30 Plastic strain distributions (a) Longitudinal Strains 209

Figure 9.30 Plastic strain distributions (b) Lateral Strains 210

List of Figures (Appendices A and B)

Figure A1. Theoretical bend angle curve and strain distribution in folding from 0 to 19.69° 220

Figure A2. Theoretical bend angle curve and strain distribution in folding from 19.69° to 35.59° 220

Figure A3. Theoretical bend angle curve and strain distribution in folding from 35.59° to 47.04° 221

Figure A4. Theoretical bend angle curve and strain distribution in folding from 47.04° to 55.04° 221

Figure A5. Theoretical bend angle curve and strain distribution in folding from 55.05° to 60.79° 222

Figure A6. Theoretical bend angle curve and strain distribution in folding from 60.79° to 65.03° 222

Figure A7. Theoretical bend angle curve and strain distribution in folding from 19.69° to 47.04° 223

Figure A8. Theoretical bend angle curve and strain distribution in folding from 47.04° to 65.03° 223

Figure B1. Graph of Strain Vs Distance travelled 225
CRF Mill No:1, Mild Steel Specimen, 6 rollers with 127mm spacing

Figure B2. Graph of Strain Vs Distance travelled 226
CRF Mill No:1, Mild Steel Specimen, 6 rollers with 127mm spacing

Figure B3. Graph of Strain Vs Distance travelled 227
CRF Mill No:1, Aluminium Specimen, 6 rollers with 127mm spacing

Figure B4. Graph of Strain Vs Distance travelled 228
CRF Mill No:1, Aluminium Specimen, 6 rollers with 127mm spacing

Figure B5. Graph of Strain Vs Distance travelled 229
CRF Mill No:1, Mild steel Specimen, 3 rollers with 2x127mm spacing

Figure B6. Graph of Strain Vs Distance travelled 230
CRF Mill No:1, Mild steel Specimen, 3 rollers with 2x127mm spacing

Figure B7. Graph of Strain Vs Distance travelled 231
CRF Mill No:1, Aluminium Specimen, 3 rollers with 2x127mm spacing

Figure B8. Graph of Strain Vs Distance travelled 232
CRF Mill No:1, Aluminium Specimen, 3 rollers with 2x127mm spacing

Figure B9. Graph of Strain Vs Distance travelled 233
CRF Mill No:1, Mild steel Specimen, 3 rollers with 127mm spacing

Figure B10. Graph of Strain Vs Distance travelled 234
CRF Mill No:1, Mild steel Specimen, 3 rollers with 127mm spacing

Figure B11. Graph of Strain Vs Distance travelled 235
CRF Mill No:1, Aluminium Specimen, 3 rollers with 127mm spacing

Figure B12. Graph of Strain Vs Distance travelled 236
CRF Mill No:1, Aluminium Specimen, 3 rollers with 127mm spacing

Figure B13. Graph of Strain (Dynamic) Vs Distance travelled 237
CRF Mill No:1, Mild Steel Specimen, 6 rollers with 127mm spacing

Figure B14. Graph of Strain (Dynamic) Vs Distance travelled 238
CRF Mill No:1, Mild Steel Specimen, 6 rollers with 127mm spacing

Figure B15. Graph of Strain (Dynamic) Vs Distance travelled 239
CRF Mill No:1, Mild Steel Specimen, 3 rollers with 127mm spacing

Figure B16. Graph of Strain (Dynamic) Vs Distance travelled 240
CRF Mill No:1, Mild steel, 3 rollers with 127mm spacing

Figure B17. Graph of Strain (Dynamic) Vs Distance Travelled 241
CRF Mill No:1, Mild steel, 3 rollers with 2x127mm spacing

Figure B18. Graph of Strain (Dynamic) Vs Distance Travelled 242
CRF Mill No:1, Mild steel Specimen 3 rollers with 2x127mm spacing

Figure B19. Graph of Principal Strain Vs Distance Travelled 243
CRF Mill No:1, Steel and Aluminium Specimens, 6 and 3 Roll Stations

Figure B20. Graph of Principal Strain Vs Distance Travelled 244
CRF Mill No:1, Steel and Aluminium Specimens, 6 and 3 Roll Stations

Figure B21. Graph of strain Vs Distance travelled for different interpass distances 246
CRF Mill No:2, Mild Steel Specimen

Figure B22. Graph of strain Vs Distance travelled for different interpass distances 247
CRF Mill No:2, Mild Steel Specimen

Figure B23. Graph of strain Vs Distance travelled for different interpass distances 248
CRF Mill No:2, Mild Steel Specimen

Figure B24. Graph of strain Vs Distance travelled for different interpass distances 249
CRF Mill No:2, Mild Steel Specimen

Figure B25. Graph of Principal Strain Vs Distance Travelled 250
for varying interpass distances
CRF Mill No:2, Mild Steel Specimen

Figure B26. Graph of Strain Vs Distance travelled for varying interpass distances 251
CRF Mill No:2, Aluminium Specimen

Figure B27. Graph of Strain Vs Distance travelled for varying interpass distances 252
CRF Mill No:2, Aluminium Specimen

Figure B28. Graph of Strain Vs Distance travelled for varying interpass distances 253
CRF Mill No:2, Aluminium Specimen

Figure B29. Graph of Strain Vs Distance travelled for varying interpass distances 254
CRF Mill No:2, Aluminium Specimen

Figure B30. Graph of Principal strain Vs Distance travelled for varying 255
interpass distances
CRF Mill No:2, Aluminium Specimen

List of Tables

		Page
Table 4.1	Bend angle for the six bottom rolls	74
Table 4.2	Bend angle and Springback factor of roll-formed trapezoidal section	79
Table 5.1	Dimensions of specimens used for tests with CRF Mills 1 & 2	82
Table 5.2	Properties of Mild steel and Aluminium	84
Table 5.3	Schedule of tests carried out on CRF Mill No:1	93
Table 5.4	Schedule of tests carried out on CRF Mill No:2	95
Table 5.5	Schedule of tests carried out on CRF Mill No:1 in Dynamic Mode	96
Table 5.6	Schedule of tests carried out for plastic strain measurement	97
Table 5.7	Schedule of experimental results listed in Appendix B (CRF Mill No:1)	102
Table 5.8	Schedule of experimental results listed in Appendix B (CRF Mill No:2)	104
Table 9.1	Forming angles with different roll stations	197

CHAPTER 1

INTRODUCTION

1.1 Background

The process of cold roll forming first gained acceptance in the early part of this century and has since evolved and been mastered by experienced toolmakers, machinists, technicians and engineers. These craftsmen learned more from experience, occasional failures and word of mouth than from textbooks, formulae and scientifically proven equations. In spite of the huge quantities of metals processed by roll forming world-wide, the process is still considered more of a "black art" than a science.

Cold roll forming is usually described as a continuous process of bending metals in a straight line without changing the material's thickness, using successive pairs of rotating tools. In practice, the formed lines could be curved and the material thickness may change. The high productivity of roll formers and the continuing demand to reduce product costs have led to the evolution of including more and more operations in the roll forming line. Aiming to produce finished products from coils without intermittent storage and material handling, roll forming lines now include operations such as punching, piercing, curving, welding, embossing and packaging plus many more.

During the last ten years or so CAD/CAM techniques have been increasingly applied to the design and manufacture of roll forming tooling. Traditionally, the design of forming rolls relies mainly on the experience of the designer. Little or no consideration is given to the behaviour of the material during the design process. The material undergoes a complex sequence of forming and stretching as the work passes through the roll stands

during the roll forming operation. Experienced designers are capable of designing tooling to roll form virtually any section .

The forming angle method is used to determine the interpass distance and the roll angles. These limit the plastic strains at the edges of the workpiece. Other parts of the workpiece may also be stretched beyond its elastic limit. It has been established practically that it is essential to keep the elongation of the metal below a predetermined maximum stretch in order to achieve good roll design. Metal movement is measured on a scale layout of the forming progression called a "section flower".

1.2 Objective

The main objective of this research is to achieve a better understanding of the material behaviour during the cold roll forming process. Using finite element analysis it is possible to determine the strains at any point on the workpiece with reasonable accuracy. This enables the elimination of most of the guesswork in form roll design. Modelling of roll forming presents difficulties due to the awkward geometry of the problem. The problem has been studied as a three-dimensional problem in order to understand the actual deformation process. The finite element analysis has proved to be considerably promising.

Initially experimental investigation of the stresses was carried out using an outboard type cold roll forming mill with fixed interpass distances. A second, much larger mill, with adjustable roll centres was designed and built to investigate the effect of interpass distance and the size of the specimen on the forming process. A grid method was used to measure plastic strains in the workpiece. A technique was also developed to calculate strains using computer vision methods.

CHAPTER 2

COLD ROLL FORMING

2.1 Basic Approach to a Simple Shape

Since Cold Roll Forming (CRF) is a well established commercial production process, this chapter describes the traditional approach to the design of cold roll formed sections in industry. Cold Roll Forming is a means of converting a flat sheet of steel or alloy to a desired shape by passing the stock material through a series of rollers with progressively designed profiles until the desired shape is achieved. During the process, corners are rolled rather than stretched.

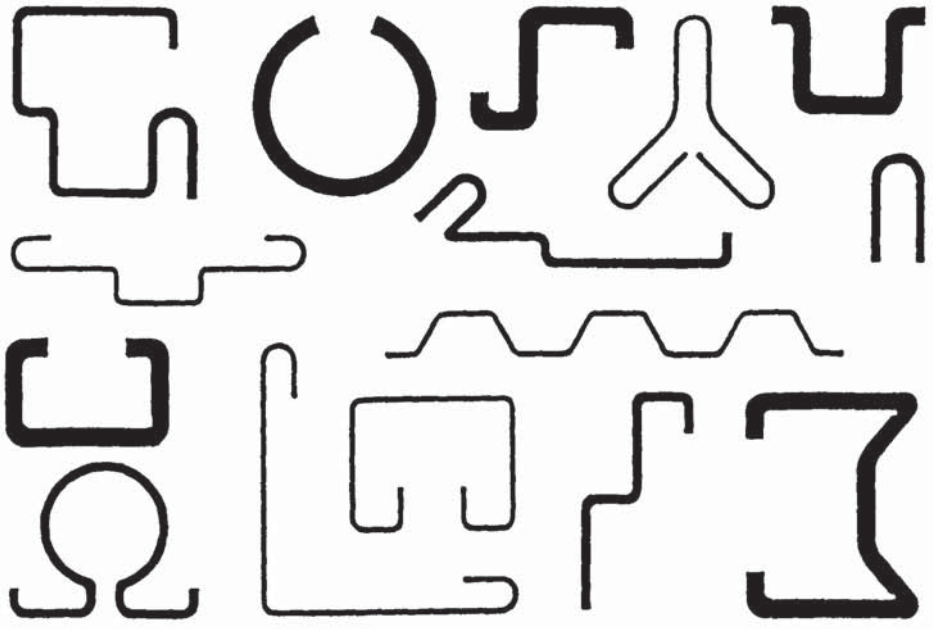

Figure 2.1. Typical shapes produced by Roll Forming [Rhodes5].

CRF is a continuous, high production process for forming metal from sheet, strip or coils into shapes of essentially uniform cross-section. Because of the diversity in materials, product shape [Figure 2.1] and markets, the cold roll forming process has enjoyed steady growth. It is a quiet and clean process. In automotive, aircraft, building and transportation industries roll formed products from trim to structural members are being produced. This diversity is partly the result of the variety of materials that can be roll formed as well as the range of material thicknesses. Components can be roll formed from metals as thin as 0.1mm to plate steel as thick as 20 mm. As far as length of component parts are concerned the limitations are only due to the feed stock and material handling. Widths from a few mm to panels approaching 2 m can be roll formed. Basically any ductile material that can withstand bending to a desired radius can be roll formed. Stainless steel available in a wide variety of compositions and properties can be somewhat more difficult to form than carbon steel but are routinely formed in thicknesses ranging from 0.15 to 7.6 mm. Another important aspect of cold roll forming is the ability to combine two or more different materials into a single product.

Deformation proceeds by successive local operations at each station rather than by a gradual process over the machine length. There is no thinning of the material during cold roll forming. Thin gauge material (0.25 mm to 1.52 mm) can be successfully roll formed with from 150 to 450 mm centres whereas thicker material gives better results with centres of 450 mm upwards. The thinner the material and the shallower the section, the smaller the permissible centre distance between stations.

Dividing the required bending of the strip into a number of increments requires some method. The forming angle method is a rule-of-thumb used by some roll designers to

determine the approximate number of roll passes and the distribution of forming at each pass. Figure 2.2 illustrates the forming angle of a simple channel section.

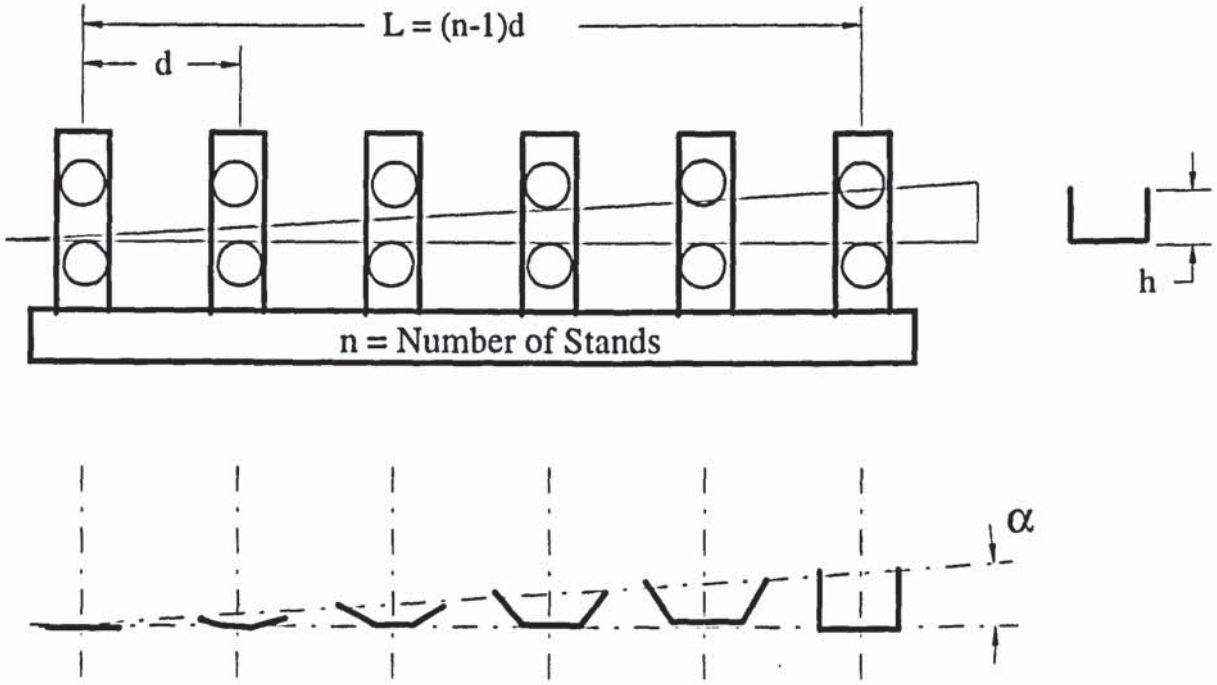

Figure 2.2. Illustration of Forming Angle ∝ of a channel section[Beecher].

- Cotangent of Forming Angle: $\alpha = \frac{L}{h} = \frac{(n-1)d}{h}$
- Conservative Forming Cot $\alpha = 40.5$ $\alpha = 1\frac{1}{2}°$
- An estimate of number of stands: $n = \frac{40.5h}{d} + 1$

Forming angle should never exceed 2° and more generally 1° for good results, which is a conservative figure.

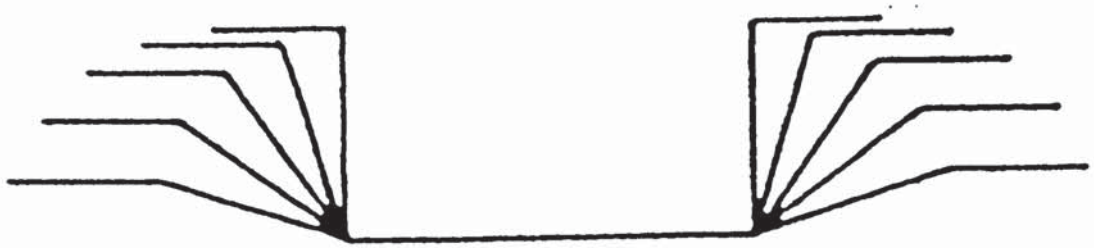

Figure 2.3 Flower Pattern [Halmos4]

Before designing the rolls, the developed width of the coil stock must be calculated accurately. During the process, the material is formed, but not permanently stretched. The amount of material flow should be accurate. (A selection of ½ the thickness of the material as a developed minimum bend radius can be used). A flower pattern [Figure 2.3] must now be finalised. When a relatively thin material is being rolled, it is important to allow for the temporary linear stretch due to elastic strains. Otherwise buckling of the workpiece could occur between roll stations. This can be done by adding 0.25 mm to each base roll diameter from station 2 onwards. This increases the surface speed of the roll and thereby taking up the stretch between stations.

2.2 Tolerance and Speeds of Rolls

Tolerances must be kept within 25 μm on both overall width and diameters. Tighter tolerances will result in a finer product. Rolls must be in true relationship to each other from station to station. The dimensions are critical on most machines from the inboard side of the machine only. The inboard side of the machine is the datum for all dimensions. The spacers on the inboard side must be strictly toleranced. Strict

tolerancing of the rolls alone is of no use. The machine must line up from station to station.

A speed ratio between top and bottom surfaces is desirable. For shallow sections a 1:1 ratio is practical. When rolling deep sections, a speed ratio has to be applied between the top and bottom shafts, otherwise the rolls will become excessively large in size resulting in high costs in material and handling. A way of overcoming this problem is to let the top rolls freewheel. This allows the top rolls to be of random diameters. Freewheeling of top rolls affects the driving power and is often undesirable. The surface speeds at the top and bottom roll peripheries should be identical, otherwise scuffing will occur and the surface finish will be affected. Distortion could be another result.

2.3 Roller Material

Roll material is related to the type of material being rolled and the expected length of the production run. Hot rolled steel strip is extremely hard on the forming rolls. A suitable roll material for such a situation is heat treated and hardened to 68-70 degrees Rockwell C. For short production runs (2 to 3 years) a relatively cheap steel can be selected. Case hardened steel rolls with 58-60 Rockwell C at a depth of 0.5/0.6 mm has been used very successfully.

.

2.4 Cold Roll Forming: Problems and Solutions

Cold roll forming is an efficient, reliable production method. Tight roll gaps can cause problems. If the gap between top and bottom rolls which should be a sliding fit is not set properly, excessive pressure will cause undue stresses in the material. This causes the material to twist and distort. Defective strip can also result in problems. Camber can prove troublesome. Use of a straightener can help to overcome this problem.

2.5 Roll Forming High Tensile Steels

Conventional Bend Radii						
Thickness t mm	Yield Strength N/mm^2					
	310	345	380	415	450	480
up to 4.75	1t	1.5t	1.5t	2t	3t	3.5t
4.75 to 6.35	1t	2t	2.5t	3t	3.5t	4t
6.35 to 12.5	2t	2.5t	3t	3.5t	4t	4.5t
12.5 and over	Usually Formed Hot					

Figure 2.4. Bend radii in conventional forming [Halmos4].

The Figure 2.4 shows the bend radii used in conventional forming, such as press braking. They range from t to more than 4t where t is the thickness. In general material thicknesses of more than 12 mm are formed hot. Sharper bend radii can be obtained with roll forming compared to other metal forming methods. Whenever possible roll formed products of high strength should be designed with conservative bend radii. In roll forming strip material, corner radii are always formed parallel to the direction of mill grain and this presents a hazard as the material could split or crack. In order to avoid this, in the case of short pieces formed in a press brake, the blanks are usually sheared and bent perpendicular to grain direction. When roll forming continuous strip this choice does not exist. Proper tool design is important at each roll stand. A forming angle of 1½ degrees can be kept in mind as a rule-of-thumb.

2.6 Number of Passes

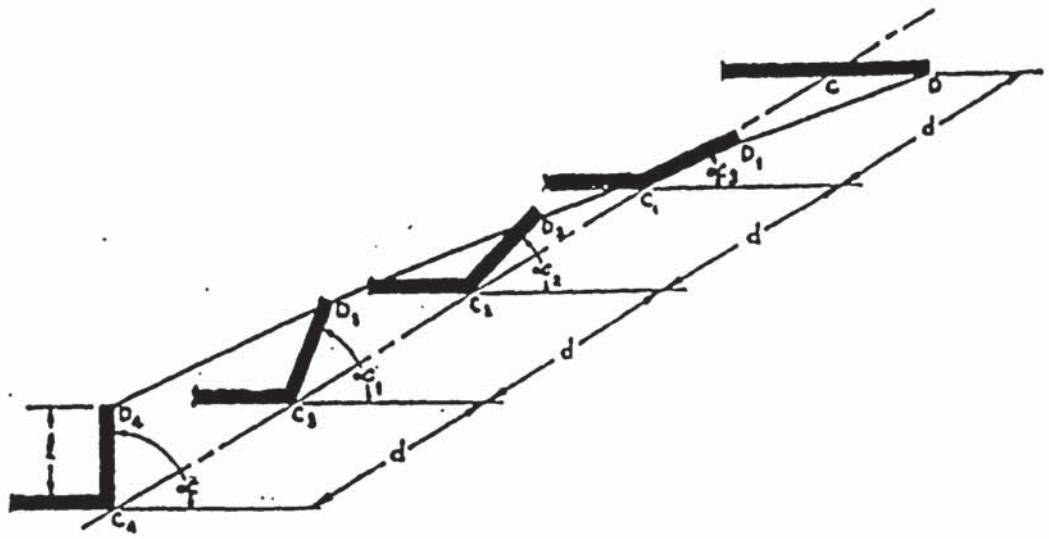

Figure 2.5. Helical Path of the edge of a section [Halmos4].

To determine the number of passes four factors have to be considered

- Material Properties
- The forming rate or metal movement
- Specification of available machines
- Order of forming, mainly of short legs

Figure 2.5 shows half of a "U" section, as it is formed at the planes of roll shafts. DD_4 is a curve longer than cc_4. Curve DD_4 is the edge of the metal strip being formed. Plastic elongation may occur at the strip edges if there is too much elongation. Other portions of the section may also be stretched beyond the elastic limit of the material.

Twists, ripples, bows and other quality problems may result due to plastic deformation. The secret in good roll design is to keep the elongation of the metal below a predetermined maximum stretch.

Material	Yield Strength (S_y) N/mm^2	Allowable elastic strain (Sy/E)	Metal Movement
Cold rolled Steel	170	0.0008	$\sqrt{0.0016} = 0.040$
Aluminium	75	0.0011	$\sqrt{0.0022} = 0.046$
Stainless Steel	275	0.0013	$\sqrt{0.0026} = 0.050$

Figure 2.6. Metal Movement [Halmos4].

The portion of the strip that is being stretched will tend to compress the remainder of the strip and thus reduce the calculated stretch. The metal movements shown in figure 2.6 have been used on standard forming machines. Figure 2.7 shows the path of the least length of the strip edge during forming, which is a helix. The length of this helical curve is equal to $(1+\varepsilon)$.

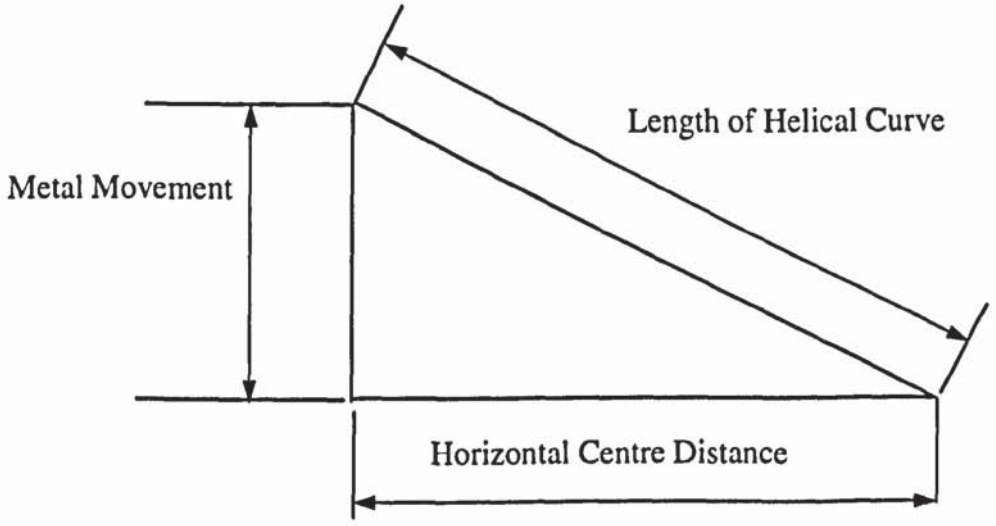

Figure 2.7 Path of the least length of the strip edge

Metal movement can be determined from the triangle shown and is calculated on the basis of per unit length of horizontal centre distance.
Metal movement will be equal to $\sqrt{(1+\varepsilon)^2 - 1^2} = \sqrt{2\varepsilon + \varepsilon^2} \approx \sqrt{2\varepsilon}$

Metal movement is measured on a scale layout of the forming progression called the "section-flower". The section-flower is the first step in roll design. Machine selection depends on the strip section, amount of forming and material. The depth of section determines the roll diameter necessary. The horizontal centre distance and the allowable metal movement of the section material per unit length of horizontal centre distance determines the metal movement per pass.

2.7 Roll Form Design - Locating the Vertical Guideline

Location of the vertical guide line in the section and its position relative to the centre of the roll forming machine should never change.

2.8 Roll Form Design - Driving Diameters

Use of small diameter rolls reduces tool costs by reducing material and machining costs but causes problems in production. Typical problems which result from poor driving diameter design and small rolls are

- Buckling of the section between passes
- High rubbing velocities necessitating low rolling speeds because of poor finish and galling problems
- Increased metal movement as a consequence of abrupt changes in section profile or pass-to-pass direction

2.9 Strip Width Calculations and the Section Flower

The approximate strip width of a roll formed section can be calculated with sufficient accuracy for section flower development and roll design. In calculating strip width , the section drawing is divided into elements. The length of each element is determined individually and the total length will be equal to the strip width. Machine specifications must always be considered in developing section flowers. The amount of metal movement that can be accomplished in a pair of rolls is related to the horizontal centre distance of the machine.

2.10 Rules for Designing Cold Roll Formed Sections

Many non-symmetrical sections are roll formed without difficulty, but the section that is symmetrical about its vertical sections allows for an equal amount of forming to be done on each edge of the metal, as it passes through the form rolls. When this condition occurs, the stress and strain imparted by the forming process are equalised. Extreme depth of cross-section should be avoided. The strains in roll forming are much more complex than in other types of bending.

In deep sections, the metal movement around the arc of the bend is much greater and thus so is the resulting edge strain. Whenever possible, bend radii should be equal to or greater than the metal thickness. In forming a radius smaller than the material thickness, grooving or cutting of the metal must be done. This practice can cause thinning and even fracturing of the metal at the bends. To form tight radii without grooving takes an excessive amount of pressure and leaves the metal work hardened in bend areas. Minimum practical leg length including the bend should be three times the metal thickness. A short leg does not allow the rolls to form and results in waves along the edge of the finished part. In cold roll forming, varying metal thickness causes problems.

If metal strip with less than accepted commercial tolerance is used, many of the control and dimensional problems will be resolved. Otherwise section tolerances are increased and generally the section uniformity suffers.

Ona and Jimma [Ona2]studied the design of successive shapes of the rolls and the determination of the number of roll passes necessary to form a given section. The following equation was derived for the formulation of empirical designs.

$$\cos\,\theta_i = 1 + (1-\cos\theta_0)\left\{i^2\,\frac{(2i-3N)}{N^3}\right\}$$

where θ_i is the bend angle of the i^{th} stand, θ_0 is the last bend angle and N the total number of stands. This method has been successfully applied to design sash and track frames for windows.

2.11 Cold Roll Forming Profiles From Material of Non-Uniform Thickness

Cold roll forming of strip material from material varying in thickness in a ratio of 5.6 to 1 has been accomplished on a production basis. Advanced roll forming systems that will accommodate materials of wide thickness variations, without changing machine set-up, opens new possibilities in forming of strip into desired profiles[Beecher].

CHAPTER 3

PREVIOUS RESEARCH INTO COLD ROLL FORMING

Research carried out in the field of cold roll forming can be classified broadly under the categories of experimental work, computer aided simulation of the forming process and theoretical work to predict the behaviour of metal during forming.

3.1 Experimental Research

Noble and Sarantidis carried out research in the field of cold roll forming [Noble]. Their research interests were mainly confined to simple symmetrical channel sections produced by air bending, using a mill with nine stations. All top rolls were of the same design. Actual forming was done by the first four rolls. Subsequent bottom rolls having the same included angle as the fourth were used for straightening purposes. All rolls were positively driven at the same speed. All roll stations were 101.6 mm apart.

Inspection of a mild steel strip removed from the mill after partial forming revealed that the deformation had taken place locally and had increased successively at each roll station and put into question the notion of "Forming angle" concept. Localised deformation was examined in more detail. Steel strips were grid marked (2.5 mm pitch), the co-ordinates of intersection points were measured before and after forming and the longitudinal strain distribution was determined.

Figure 3.1 shows the typical strain distribution at a roll station. At the edges of the flange, longitudinal strain changed from tensile to compressive. In the middle, strain changed from compressive to tensile. The range reducing after the first station until the 6th and subsequent stations exhibiting a uniform small residual extension.

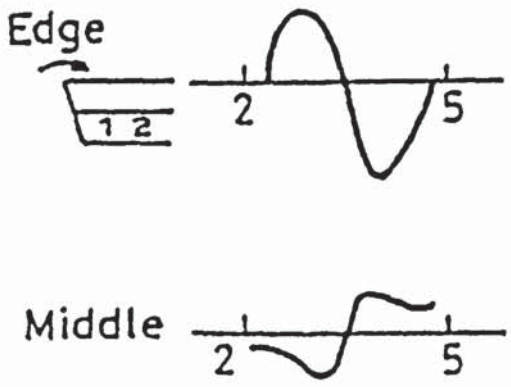

Figure 3.1. Typical strain distribution at a roll station [Noble].

In order to investigate the effect of roll station spacing, stations 2, 4, 6 & 8 were removed and the experiment repeated. The result was more severe deformations and the final residual tensile stresses are slightly higher. Of particular note was the fact that prior to the last station the distributions are of inverted form compared with the results from the previous test; edge compression precedes tension and centre tension precedes compression in each station. Similar results were obtained again when the station pitch was reduced to 101.6 mm, concluding that roll station pitch is of little consequence and need only be such as to give reasonable physical clearance. The most important criterion appears to be the severity of change in shape while the work passes through a particular roll station.

Jimma and Ona [Jimma3] tried forty two combinations of seven pairs of forming rolls for the forming of symmetrical channels from carbon steel, stainless steel and aluminium strip. A slight buckle was noticed on the web part of a strip during progressive forming, just in front of each roll stand and a method was proposed for using the slight buckle as a direct measure of the severity of the cold roll forming

process. Figure 3.2 shows the slight buckle, which grows just in front of the rolls and disappears soon after passing through the rolls. According to the findings, the magnitude of this slight buckle was strongly related to the severity of forming at the roll stand. These inlet angles α along the centre line of the waved web were measured as shown in Figure 3.2

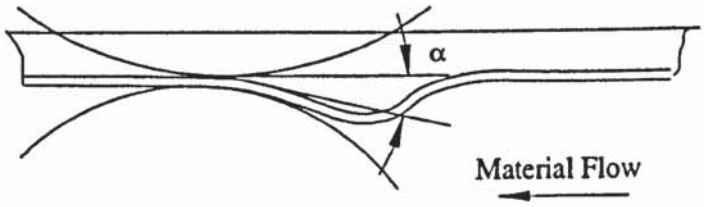

Figure 3.2. Inlet angle α [Jimma3].

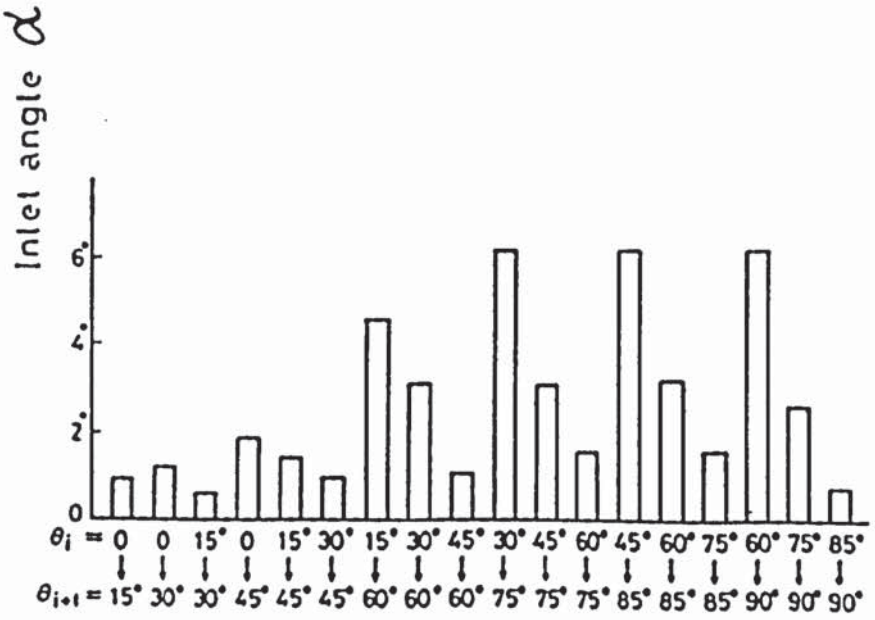

Figue 3.3. Inlet angle of centre line of web part in the forming process from bend angle θ_i to θ_{i+1} [Jimma3].

Figure 3.3 shows the inlet angle α in the forming process as the bend angles increase from θ_i to θ_{i+1}. Forming becomes difficult with increasing α. Seven pairs of rolls with bend angles 15°, 30°, 45°, 60°, 75°, 85°, 90° were used to form symmetrical channels I and II (Fig 3.4). The rolls were designed so that the pitch diameter of each successive roll pair is increased by 0.5 mm.

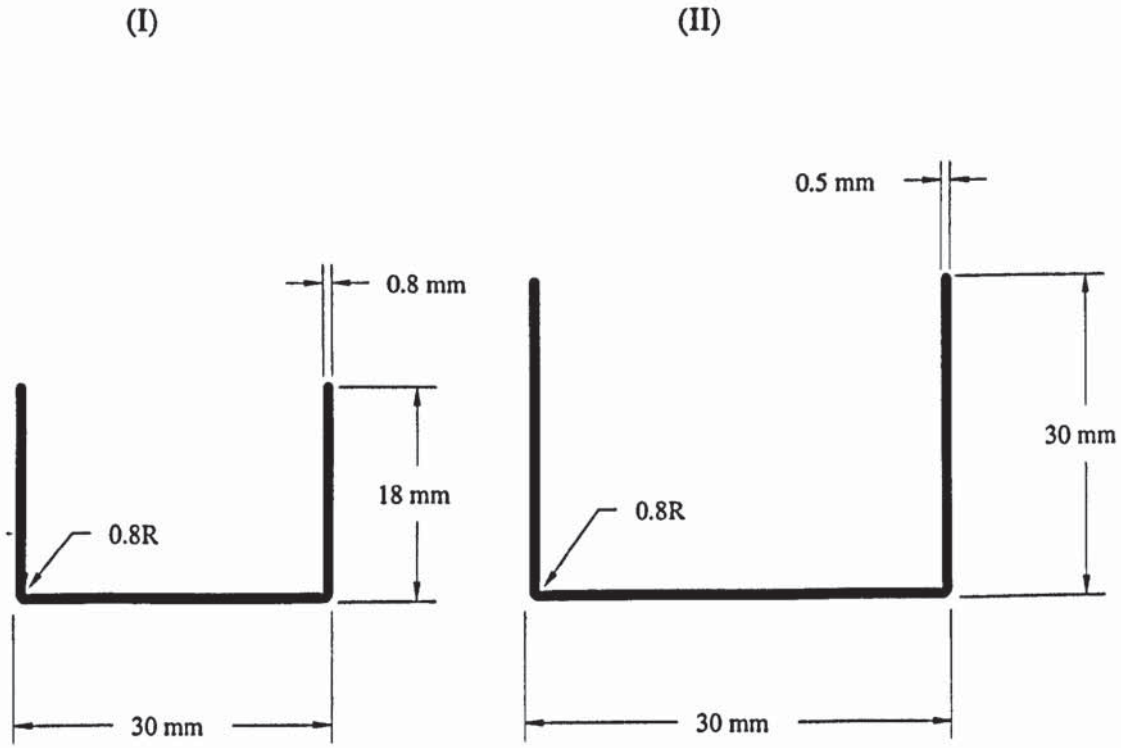

Figure 3.4. Channel Sections [Jimma3].

Bhattacharyya and Smith [Bhattacharyya1] investigated the development of strains during cold roll forming of symmetrical sections from mild steel. The roll forming mill was of the cantilevered type. All the rolls had the same base diameter of 106 mm and the base surface of all driven rolls lay in a straight horizontal plane. The lower

driven rolls were shaped to give the fold angle while all the upper rolls were flat faced. Strips were formed into symmetrical channel sections of trapezoidal form. The instantaneous strain histories of flanges and webs have been obtained (Figure 3.5 and Figure 3.6) using strain gauges bonded to the upper and lower surfaces of a the strip 1.5 mm away from the flange edge and on the centre line of the web, which gave continuous recordings of strain for various stages of channel forming.

From the average of the two readings, the longitudinal membrane strains $\bar{e}_F$ and $\bar{e}_W$ were obtained. The level of strains imposed directly affect the formation of wrinkles in the flanges and straightness of the product. The former is directly related to the peak longitudinal strains imposed by the folding process. Straightness is a function of the level of final residual longitudinal strain differences between the extreme surfaces of the web and the flanges of the product. The peak longitudinal strain $\bar{e}_{FP}$ = peak value of $0.5(e_1 + e_2)$ and the residual strain difference $\Delta\bar{e}_R = \bar{e}_{FR} - \bar{e}_{WR}$, remaining in a free-formed product were studied by passing the strip through a single roll station with the roll angle varying between 20° and 50°. Slightly ahead of the roll centre, a discrete deformation zone was observed where significant tensile strains induced in the flanges peaked. On passing beyond the roll station, a rapid strain recovery occurred. Strains in the web were much lower, typically less than $0.1\bar{e}_{FP}$

It was concluded that the magnitude of the peak flange strain at any roll station bears a direct relationship to the incremental fold angle applied at the roll station and has no direct relationship to the roll angle used at that station. It is also not significantly affected by the incremental fold angle applied at the subsequent roll stations. The maximum peak strain that can be permitted is determined by the tendency to wrinkle.

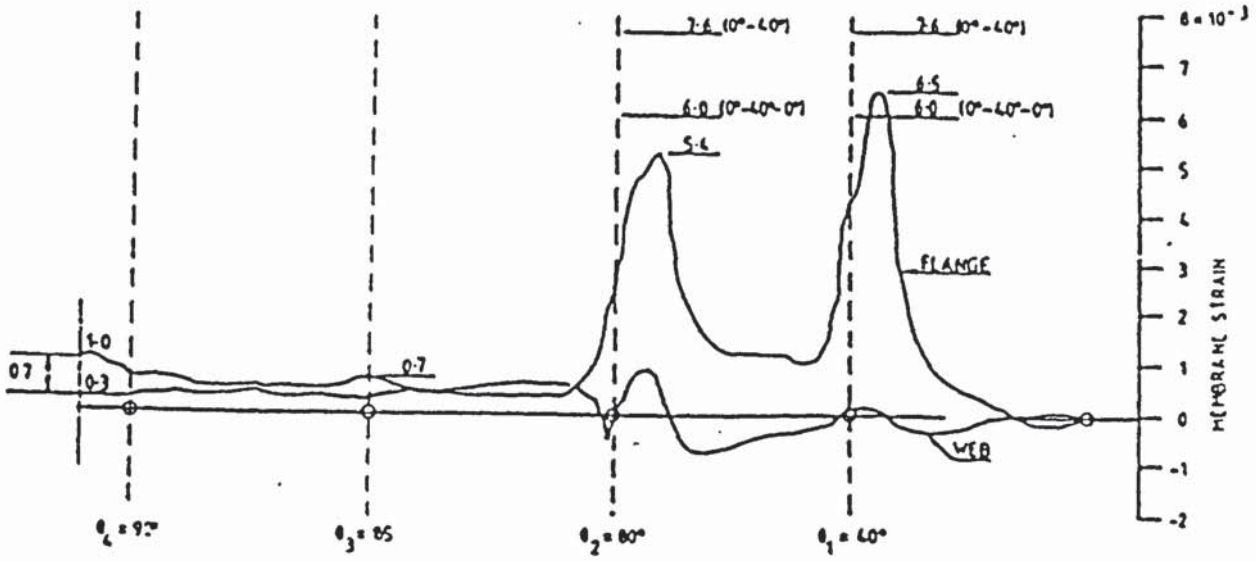

Figure 3.5. Membrane strain traces using multiple roll stations [Bhattacharyya1].

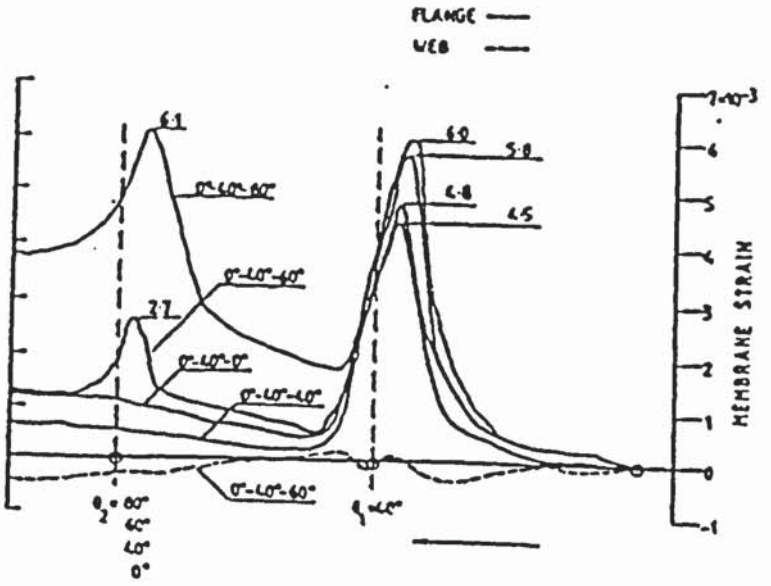

Figure 3.6. Membrane strain traces using two roll stations [Bhattacharyya1].

Jimma and Morimoto [Jimma1] applied grid strain analysis to the cold roll forming of channel-type cross-sections from stainless steel strip. Small strains of the order of microstrain produced in the forming process were measured. Near the edge of the flange, the longitudinal membrane strain showed a maximum at a distance nearly equal to the width of web from the centre line of the roll. On the flange near the bending

corner and on the web, the membrane strains were almost zero or negative. In both the flange and web, near the centre line of the roll, the strains showed a compressive maximum and the absolute values decreased after passing the roll stand.

Jimma and Morimoto [Jimma1] investigated the CRF process by grid stress analysis using stainless steel channels. The displacement readings were corrected for spring-back. According to their findings, (i) in the flange, the plate on the convex roll side is elastic throughout the whole forming process except near the surface and near the centre of the plate (ii) in the web, most of the plate is elastic except near the surface and (iii) the residual bending moment which is tensile on the concave roll side of cross-section in the flange and web is greater near flange edge and in the web.

Bhattacharyya et al [Bhattcharyya2] have concluded that the traditional "forming angle" method used for the determination of the number of stations is only reasonably dependable and agrees more with the findings of Noble and Sarantidis[Noble] that the deformation during the cold roll forming process is intermittent under each roll station and extends only up to a limited distance preceding the forming roll. This deformation length (not to be confused with the 'forming length') not only plays its role in the calculation of strains but also influences the positioning of the two subsequent rolls. They have predicted the deformation length by minimising the energy required for bending and stretching in a roll station. It has been claimed that their theoretical predictions agree well with experimental results and that the length of deformation is very much dependent on flange length, prescribed fold angle and material thickness but the mechanical properties of the material have little effect. The material was treated as rigid-perfectly plastic.

The expression for deformed length is

$$L = a\sqrt{8a\theta_p / 3t}$$

where a is the flange length

t is the thickness of the material and

θ_p is the prescribed fold angle in one particular stage.

From the experimental and theoretical research performed by Masuda [Masuda] on the cold-roll forming of metal strips to form cross-sections of circular arcs, it has been found that the membrane strain in the strip was negligibly small compared to bending strain.

Experimental investigations have been carried out by many researchers in Japan since 1963 [Onoda] on basic problems of cold roll-forming such as deformation of strip, shape defects (edge wave, web buckling and longitudinal curvature), roll pressure distribution and roll force. Much research effort has also been directed towards the study of forming pipes.

Experimental research into the forming of light gauge steel members has been done by Ona and Jimma on symmetrical and asymmetrical channel sections and wide profiles. Roll pass schedules for channel forming has been investigated to,

- arrive at a finished product with minimum surface damage to the finished surfaces
- eliminate buckling of the flange
- reduce longitudinal curvature and elastic distortion of sections in the neighbourhood of cut-off edges
- remove distortion such as vertical and horizontal bends and twists

The mechanism causing defects such as web-buckling, cracks and distortion in the forming of wide profiles has also been experimentally investigated by Ona and Jimma.

Kato, Saito and Shinto experimentally investigated [Kato2] the relationship between the shape of the product and properties of strip metals in single stand roll forming of circular section. In the roll forming process, the strip material is subjected to stretching and shrinking. Consequently the roll formed products often bend longitudinally. This phenomenon is also called edge stretch. According to their findings, the edge stretch and

longitudinal bending decreased but the springback of the cross-section increased as the alloying elements in the carbon steel increased.

Ona and Jimma [Ona1] experimentally investigated the oil-canning and edge buckling of wide profiles during cold roll forming. All the wide profiles produced compressive strains in the longitudinal direction. The degree of oil-canning and edge buckling increased with the longitudinal compressive strains. The application of tension to wide profiles in the forming process was effective in eliminating oil-canning. The wave heights of oil-canning and edge buckling were measured with non-contacting displacement sensors. The degree of oil-canning or edge buckling was defined by the sum of the heights of the waves which appeared on the web centre or the flange edges per unit length of the wide profile. The longitudinal normal strains of the wide profiles were measured by comparing the length of a roll formed section with its length before rolling. No oil-canning appeared provided that the average longitudinal compressive strain was restricted to within $200x10^{-6}$. According to Ona and Jimma, oil-canning was due to elastic buckling. The mechanism of oil-canning was explained by assuming that the bend corners of the wide profile are plastically extended in the width direction while being compressed in the longitudinal direction. Edge buckling increased with the average longitudinal compressive strain and it was found that edge buckling could be suppressed provided that the average strain is restricted to within $300x10^{-6}$. Edge buckling could be either elastic or plastic.

3.2 Computer Simulation of Cold Roll Forming

Kiuchi, Koudabashi & Sato [Kiuchi1][Kiuchi3] have developed a computer aided simulation and design system capable of attaining optimum roll profiles. When the dimensions of the required product such as the diameter and wall thickness of a circular pipe are given, this system is capable of giving a series of roll profiles which can satisfy various requirements such as (i) edge stretch of the sheet metal occurring during the forming process (ii) the driving power of each roll.

The authors have developed a mathematical theory which makes it possible to simulate deformation behaviour of sheet metal in the roll forming process. Through this study, a computerised simulation technique which can analyse characteristics of deformation of sheet metal in the process has been developed to automate the design of roll profiles. This CAD system has the necessary functions to design roll profiles for a required product, and the procedure to optimise them. The shape of the deformed sheet metal, which is a three-dimensional curved surface, is mathematically expressed using an approximated function.

Once the deformed shape of the sheet metal is approximately expressed by this function, deformation behaviour of each element of the sheet metal which is considered to move from one roll to the next along this curved surface, is analysed by using the incremental theory of plasticity. According to the energy method, the values of the adjustable parameters included in the specific function are selected so as to make the total power of deformation of the sheet metal a minimum. When this minimisation is accomplished, the optimised mathematical expression of the deformed shape of the sheet metal is obtained. Stress and strain distributions occurring in the sheet metal were calculated from this optimised mathematical expression of the deformed shape.

From the results it was found that large tensile strains ε_{xm} occur at the edge of sheet metal during the forming process between two roll stands. The peak value of ε_{xm} occurred at the edge, which is known as the edge stretch, causes edge wave and other defects of the roll formed product. It was found that ε_{xm} was an important parameter that had to be controlled in the determination of the optimum roll pass schedule.

The main drawback of this method was the requirement that an approximate mathematical expression had to be assumed in order to represent the deformed shape of the sheet metal in three dimensions.

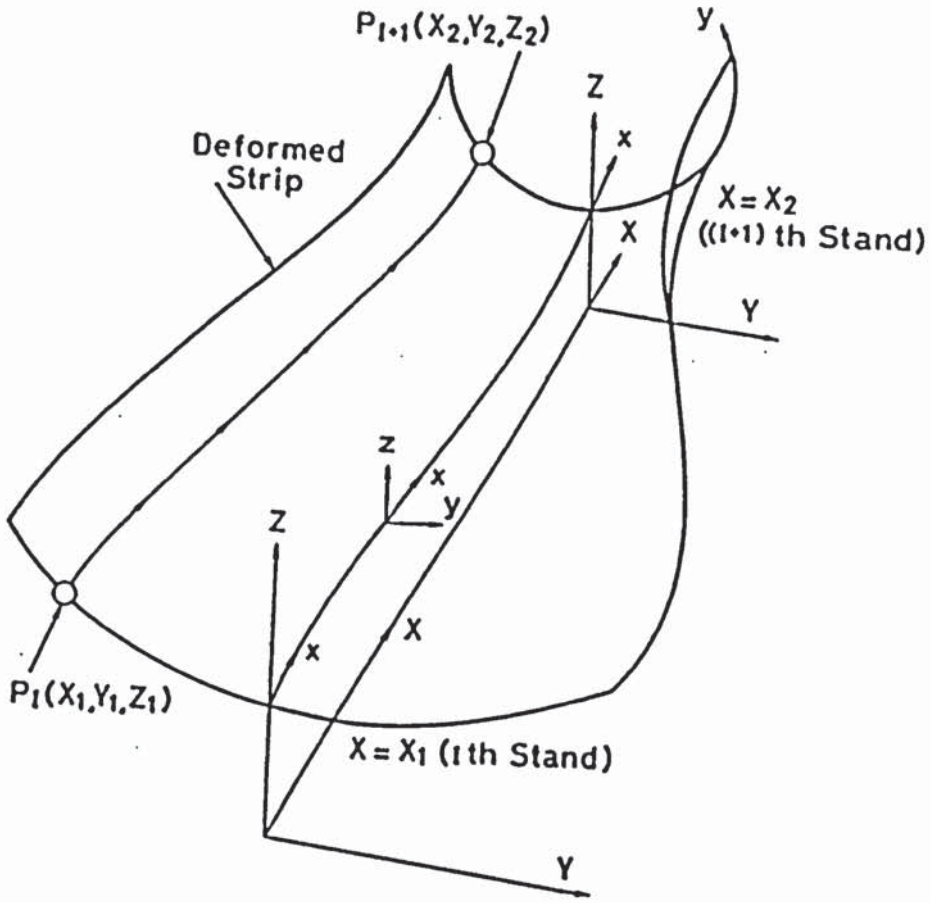

Figure 3.7. Curved surface of the sheet metal [Kiuchi2].

Figure 3.7 shows the curved surface of the sheet metal between two roll-stands[Kiuchi2]. In this figure, $x = x_1$ and $x = x_2$ represent the positions of i^{th} roll stand and $(i + 1)^{th}$ roll stand respectively. The equation for the three dimensional curved surface is expressed by using the shape function

$$S(X) = \sin\left(\frac{\pi}{2}\left(\frac{X}{L}\right)^n\right)$$

where $L = (x_2 - x_1)$ is the distance between two neighbouring rolls.

Computer simulation of the cold roll forming process has also been carried out by Kiuchi since 1982 in order to estimate the stress and strain distributions produced in the strip during passage through the rolls. In this approximate analytical method for the simulation of the forming process, geometrical shapes of deformed strips between successive stands was expressed by the same shape function as above, where the parameter n is determined by the minimisation of deformation energy. Applications of this method have been done in the forming of circular arcs, C channel and top hat sections. In these studies, the variation of strain in the strip has not always been estimated precisely.

Simulation has shown that

$$\dot{W} \propto t^{2.18}$$

where $\dot{W}$ is the total power of deformation and t is the thickness of the sheet metal.

This is in good agreement with the empirical formula that the power of deformation is proportional to t^2 in various sheet forming processes in which bending deformation is dominant compared to other types of deformations.

The Machine Tool Industry Research Association (MTIRA) has developed methods [Eyres] to aid the roll designer in selecting a suitable forming sequence and then processing this information to manufacture a set of rolls. The design programs at MTIRA make simplifying assumptions about the geometry of the material as it deforms. A constant material thickness is assumed throughout the forming process and any transverse strain induced in the material is taken into account by defining a 'neutral axis'. This neutral axis is similar to the one used in presswork when estimating bend allowances. It is the distance from the surface at the inner radius of the material to the plane, which is assumed to remain unstrained throughout bending, expressed as a proportion of the initial thickness of the material. A neutral axis of 0.5 therefore

assumes both a constant volume to be associated into a bend and equal tensile and compressive strains about the neutral axis.

When strip material is cold roll-formed into radii very much greater than its thickness and the rate of forming is such that plastic yielding in the direction of motion of the strip can be kept low, then plane strain conditions can be assumed to apply. Assuming a material with an elastic/perfectly plastic stress-strain characteristic it is possible to calculate the elastic 'springback' that will occur after forming and hence, using the reciprocal relationship, calculate what 'overbend' to apply in order to achieve a given final radius or angle. A further point of interest is that, using the same relationships, it is possible to calculate the radius to which material can be bent, but still springback to a flat condition.

Springback Calculations

$$N = \frac{\sigma_y . r\,(1-\nu^2)}{E.t}$$

$$\frac{r_f}{r} = \frac{1}{(1-3N+4N^3)}$$

$$\alpha_f . r_f = \alpha . r$$

For springback to flat $3N - 4N^3 = 1$

where

N = Intermediate calculation variable

σ_y = yield stress

r = bend radius to neutral axis

α = bend angle

E = Young's Modulus

ν = Poisson's ratio

t = material thickness

r_f = final radius (after springback)

α_f = final angle (after springback)

The calculations of the geometrical properties of the constant cross-section are based upon the use of the finite-element method. In adopting such a technique, it was recognised that the use of the finite elements would have great potential for the long-term development of predicting cold roll-forming effects.

The Machine Tool Industry Research Association (MTIRA) [Rhodes4] has developed computer aided design programs to design form rolls. The program Flower III, can produce six different types of output. Two of these are centre-line flower patterns, three are roll designs of different type and one is a template drawing. The flower pattern can also be drawn with the origin at a defined pass height or radius at each stage. The pass radii at the different stages are input as data and can either be fixed throughout the machine or varied. The reason for varying the pass radius of the origin from stage to stage is in order to attempt to equalise stretching of the section. Although it is not straightforward to relate stress to strain in the operation since it is the plastic flow of the material with which the process is concerned, it is desirable to attempt to equalise the stretch of the section about its centroid in order to reduce the distortion caused by twisting and bowing.

The relationship between a shape factor Φ_3 and the number of roll passes necessary to form light gauge wide profile steel sections has been investigated by Ona, Jimma, Konzono, Nakako[Ona4]. It is claimed that relationships for symmetrical, asymmetrical wide profile sections and pipes have been validated.

$$\text{Shape factor} \quad \Phi_3 = \frac{nW_1 h}{W_2},$$

where W_1 is the the half width of sheet steel plate

W_2 is the half width of final section

h is the height of cross-section and

n is the number of bend corners respectively.

The allocation of roll bend angle at any stage was carried out by assuming that the locus

of the edge of the section on the horizontal plane is a modified cubic curve. This technique has been incorporated in to a CAD system for the design of Cold Rolled sections.

Roll forming a new section requires a new set of rolls and it is with this aspect that CAD/CAM has come to be very useful in industry [Rhodes2][Rhodes3]. Complex sections require rolls of complex form and it is to minimise the work in both design and manufacture of the rolls that much effort has been devoted. Most of the design work is in trigonometrical calculation of one type or another and in this field a computer is a very powerful tool, being able to complete in seconds, calculations which would take days to complete manually. Most of the work in this area has been concerned with the development of suitable programs to carry out much of the design / drawing previously done by the designer and the automatic generation of CNC input data for manufacturing the rolls. Traditionally the rolls are made on manually operated centre-lathes which rely greatly upon the skill of the operator.

3.3 Theoretical Investigations

Panton, Zhu and Duncan [Panton4] introduced a new method of indicating forming severity and the bend angle curve which shows the bend angle distribution and geometric restrictions imposed by the shape of the rolls. The concept of geometric constraint is illustrated by considering one pass in roll forming a channel section as shown in Figure 3.8.

The strip exits at stage 1 with a bend angle θ_1 and deforms to a bend angle θ_2 at stage 2. The assumptions are as follows:

- The strip bends along a discrete line.
- The base of the strip is straight and horizontal along the Z axis as shown in the figure.
- The sides are straight with a current angle θ which is a function only of z.
- A normal section transverse to the strip remains plane and normal.
- Springback can be neglected.

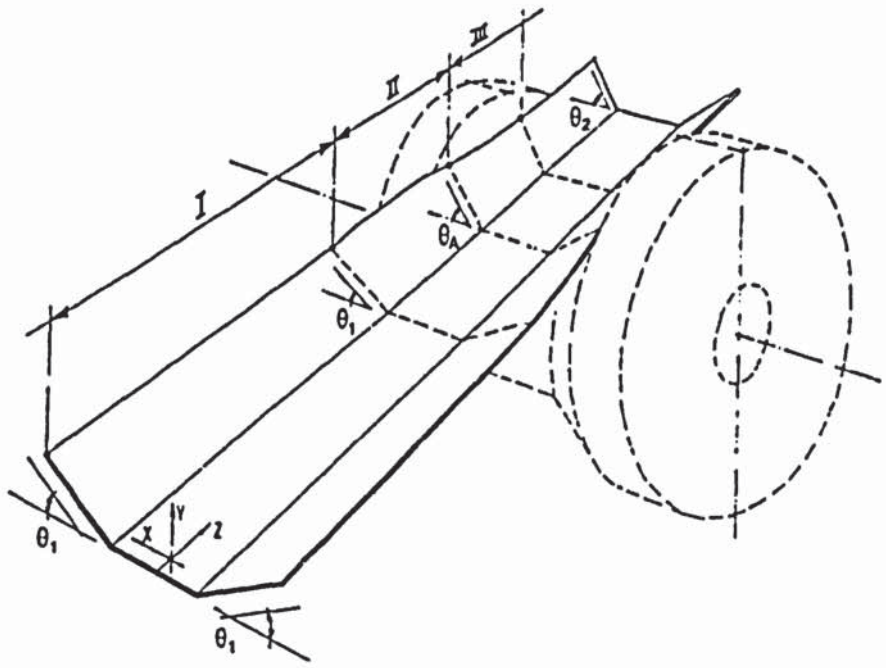

Figure 3.8. Roll-forming a channel section [Panton3].

Since springback is neglected, a graph of the bend angle θ against distance along the path z can be plotted as shown in Figure 3.9. It comprises of two regions: region A where the bend angle does not change and region B where the bend angle changes from θ_1 to θ_2. In fact, the later part of region B is further complicated by the geometrical restriction of the roll when the strip comes in contact with the roll. This is illustrated in Figure 3.10.

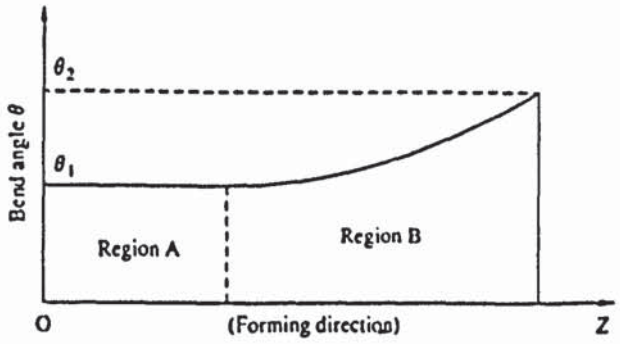

Figure 3.9. Bend angle diagram [Panton3].

At section CC' the value of θ must be equal to θ_2. Now at section AA', since it has been assumed that bending takes place only about the fold line and the 'leg' of the channel remains straight, it can be said that the bend angle at section AA' must be greater than or equal to θ_2. (It has been assumed that the roll is sufficiently wide that the tip of the strip would contact the roll before any other point on the cross-section). This argument could be repeated to obtain a minimum value for θ at any cross-section of the roll. Hence the geometrical restriction imposed by the roll can be mapped on to the bend angle diagram as the shaded region in Figure 3.10.

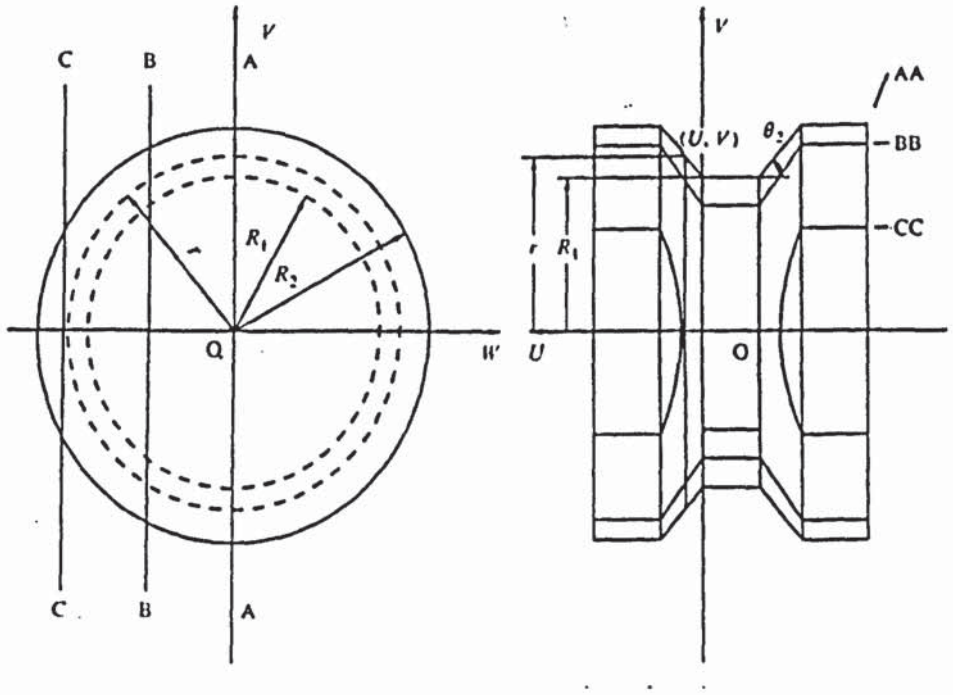

Figure 3.10. Geometric restriction resulting from the roll cross-section [Panton3].

The bend angle diagram can now be considered to consist of three regions (Figure 3.11): region I where the bend angle does not change, region II where the bend angle changes but the strip does not contact the roll and region III where the bend angle changes as a function of the roll geometry.

The geometric restriction imposed by the bottom roll can be found by considering Figure 3.12. With some trigonometrical manipulation, the following relationship between θ and z are obtained :

$$z = L - \sqrt{\frac{a^2 \cos^2\theta}{\cos^2\theta_2} + 2aR_1 \frac{\sin(\theta_2 - \theta)}{\cos\theta_2} - a^2}$$

where L - Distance between 2 roll stations;

a - Flange length;

θ - Bend angle;

θ_2 - Bend angle at end of pass; and

R_1 - Base roll radius

z - Distance in the forming direction

This is the boundary of the shaded region in Figure 3.10 and defines the bend angle curve in region III.

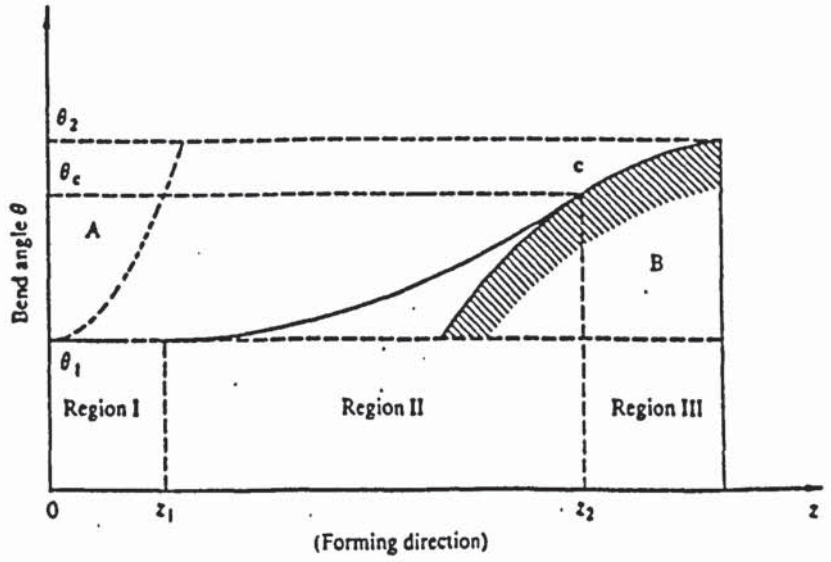

Figure 3.11. Bend angle diagram showing bottom roll at the end of pass [Panton3].

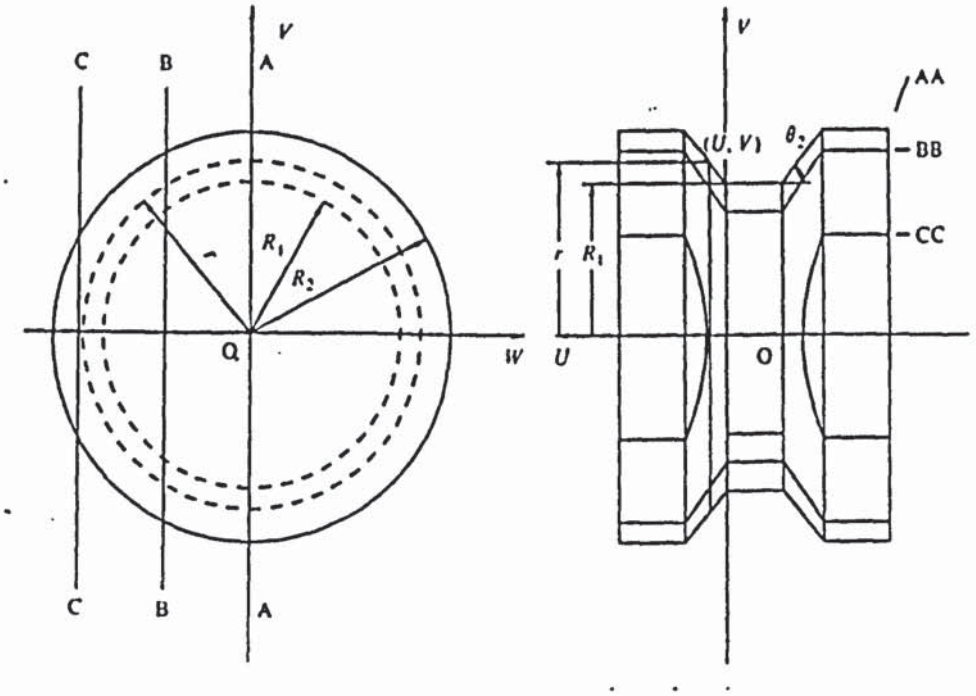

Figure 3.12. Bottom roll for forming a channel section [Panton3].

To describe the bend angle distribution completely, it is necessary to determine the bend angle distribution in region II. Bhattacharyya has shown that if the following assumptions are made [Bhattacharyya2]:

- Transverse sections of the strip remain plane, orthogonal and a constant distance apart during deformation;
- Bending takes place only along the fold line and out of plane bending in the flange and any deformation in the web are neglected; and
- The forming material is rigid plastic.

then the bend angle distribution which minimises the plastic work is given by the expression :

$$\theta(z) = \theta_1 + \frac{3t}{8a^3}(z - z_1)^2$$

where z_1 is the start of the deformation region for a strip previously bent to an angle θ_1 and 'a' and 't' are the flange length and strip thickness respectively. This relationship is illustrated in Figure 3.11.

Bhattacharyya also shows that :

$$\varepsilon = \frac{s^2}{2}\left(\frac{d\theta}{dz}\right)^2$$

where ε is the longitudinal strain and s is the distance from the fold line. $d\theta/dz$ can be found directly from the bend angle diagram and hence the bend angle diagram can be used to indicate the severity of the process. The peak ε occurs at the boundary of region II and region III. Figure 3.13 shows the theoretical strain distributions on the flange at different distances from the fold line compared with experimental strain distribution.

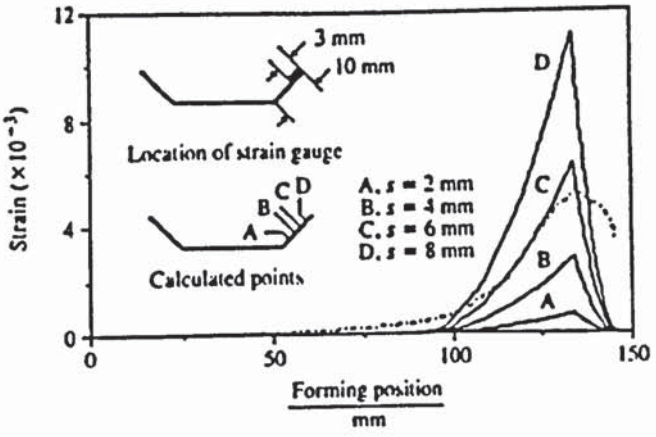

Figure 3.13. Theoretical strain distribution compared with experimental strain distribution [Panton3].

Panton, Zhu and Duncan [Panton4] identified four fundamental deformation types in roll forming. These are the longitudinal stretching, longitudinal bending, transverse bending and shear. Expressions were developed for the strain and work associated with each deformation type in the roll forming of a section with a single action bend. The shear strain was shown to be potentially far greater in magnitude than the longitudinal strain and hence must be considered a significant factor in roll-forming.

Zhu, Panton, and Duncan [Zhu] investigated the effects of geometric variables such as flange length, thickness, bend angle, bend angle increment and roll diameter on the longitudinal strain developed in roll forming channel sections. The peak longitudinal strain was found to increase with flange length and then drop when the flange length reaches a critical value. The peak longitudinal strain was found to increase with thickness. In general, increasing the bend angle increment was found to increase the peak longitudinal strain despite the fact that the deformation length also increases. Increasing the roll diameter was found to decrease the peak longitudinal strain.

CHAPTER 4

DESIGN AND FABRICATION OF A COLD ROLL FORMING MILL

One of the main objectives of this research is the experimental investigation of the cold roll forming process. The CRF mill used in the earlier part of the research has fixed interpass distances, i.e. fixed roll stations. This mill will be referred to as the 'CRF Mill No:1'. It was felt that this feature was a serious drawback for experimental investigation and it was decided to design and fabricate a much larger CRF mill with variable interpass distances. This second mill will be referred to as 'CRF Mill No: 2'.

Tooling was designed for both the mills using the forming angle method. During the design of the second mill, Autocad's Advanced Modelling Extension, which defines 3-dimensional objects as solid forms, has been used for modelling. Solid modelling aids visualisation, checks interference of mating parts and offers better presentation. The design was kept simple and identical parts were used as far as possible. This is to reduce the number of unique parts to allow maximum interchangeability. Both the forming mills used for the experimental work are of the outboard type with 6 roll stations. The outboard type mill has certain distinct advantages over the more conventional inboard type mill for experimental work.

These are

- accessibility to the workpiece
- accessibility to the strain gauges and their connecting leads
- better control over the workpiece movement during roll forming
- the ease of dismantling the rolls to remove a partially formed workpiece from the mill for the measurement of plastic strains.
- roll tooling can be changed without dismantling the drive system

CRF Mill No: 1 is a high quality commercial roll forming mill supplied by BHP Lysaught Ltd. Quality checks were carried out for the specimens formed with the CRF Mill No: 2 which was designed by the author.

4.1 Cold Roll Forming Mill No: 1

The roll forming mill shown in Figure 4.1, consists of six roll stations which are interconnected by a chain and sprockets to a DC motor/ gearbox. This motor/gearbox has a rated output of 0.37 kW running at a constant speed of 24 rpm. The horizontal and vertical roll shaft distances are 127 mm and 96 mm respectively. At each station a bolt and nut is used in conjunction with a sliding support block to control the roll-gap to cater for different strip thicknesses as shown in Figure 4.2. All the top rolls are identical. Shape is imparted to the formed section by the bottom rolls which are of trapezoidal form.

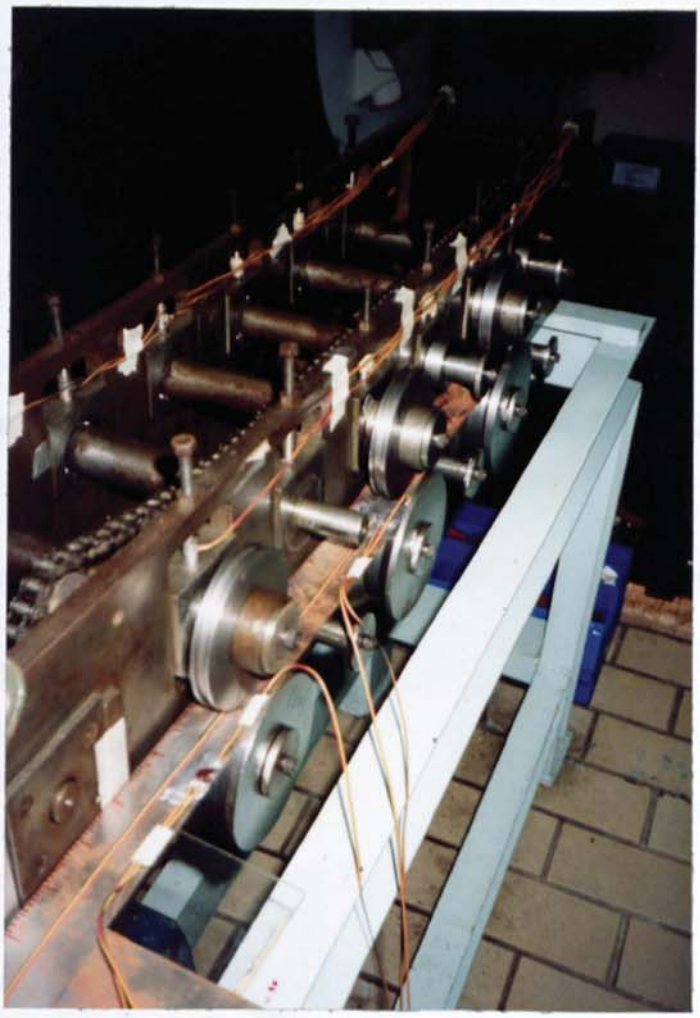

Fig 4.1 Roll Forming Mill No:1

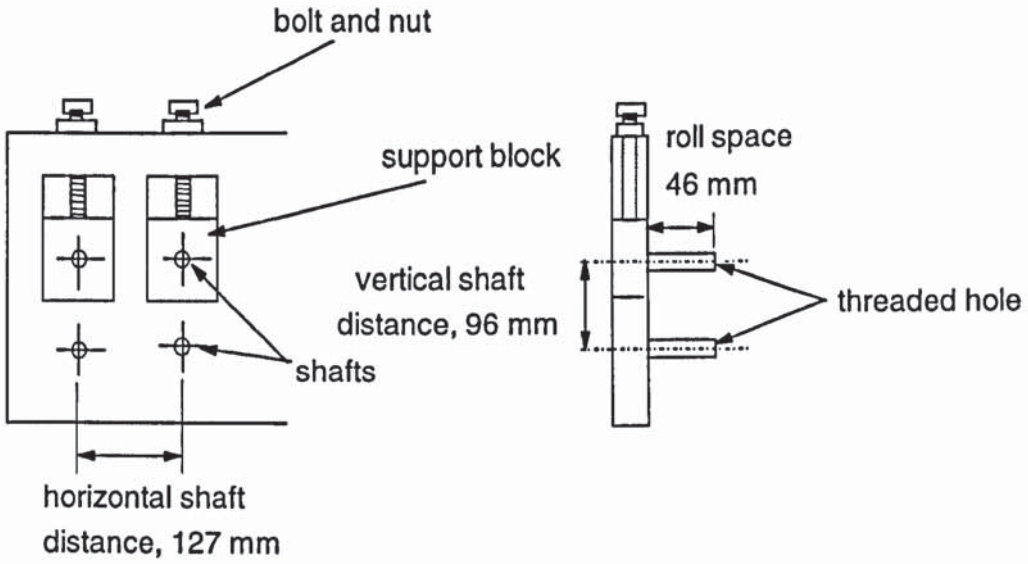

(a) Front view (b) Side elevation

Figure 4.2 Horizontal and vertical shaft distance

4.2 Design and Fabrication of the Cold Roll Forming Mill No: 2

The following design guidelines were decided at the commencement of the project:

- The overall length of the mill shall not exceed 2 metres
- The distance between roll stations should be adjustable
- The maximum thickness of the strip to be rolled is 1 mm
- Parts should be designed for maximum interchangeability
- Structure could be easily dismantled for easy relocation
- Electrical drives to have variable speed
- Easy accessibility to the workpiece for strain measurement.
- Easy removal of partially formed workpiece from the machine.

The main features of cold roll forming mill are:

- machine structure
- roll stations
- drive system
- roll tooling

Figure 4.4 shows the general assembly of the CRF Mill No:2.

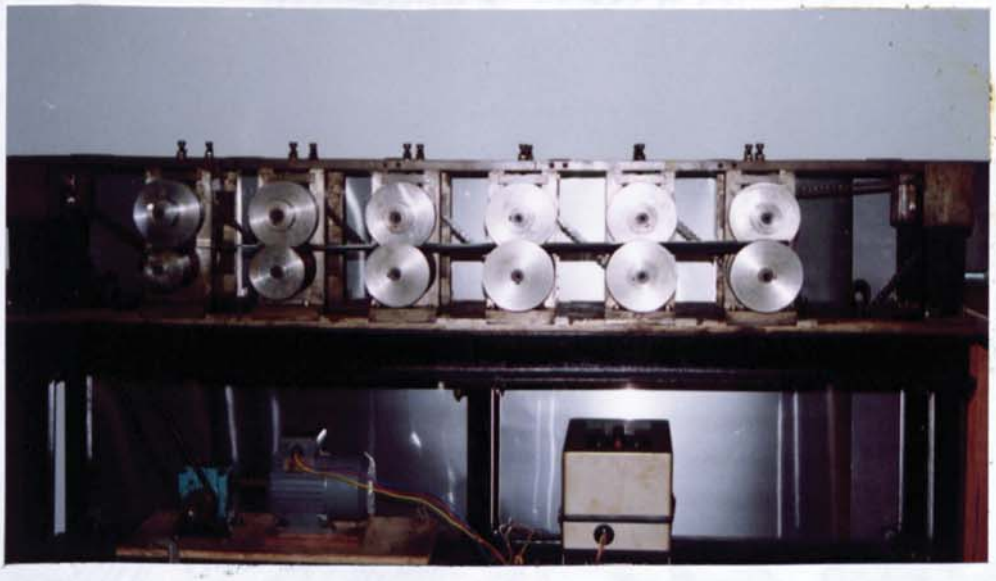

Fig 4.3 View of Cold Roll Forming Mill No:2

4.2.1 Frame

The machine frame is made of two main sub-assemblies, the top frame assembly and the bottom frame assembly. The bottom frame is made up of a base plate, two I-beams and several hollow square sections welded together as shown in Fig.4.5. The frame is of bolted construction. This is to facilitate easy dismantling and relocation of the mill in the laboratory. Figure 4.6 shows the exploded view of the bottom frame assembly. The base plate has two T-slots running parallel along its length to guide the movement of the station assemblies. To reduce the weight of this plate, a rectangular hole is cut out in the centre. The two holes near the end of the plate are for the chain to pass through. The two I-beams support the base plate and the station assemblies. All the other members of the frame are rectangular hollow sections.

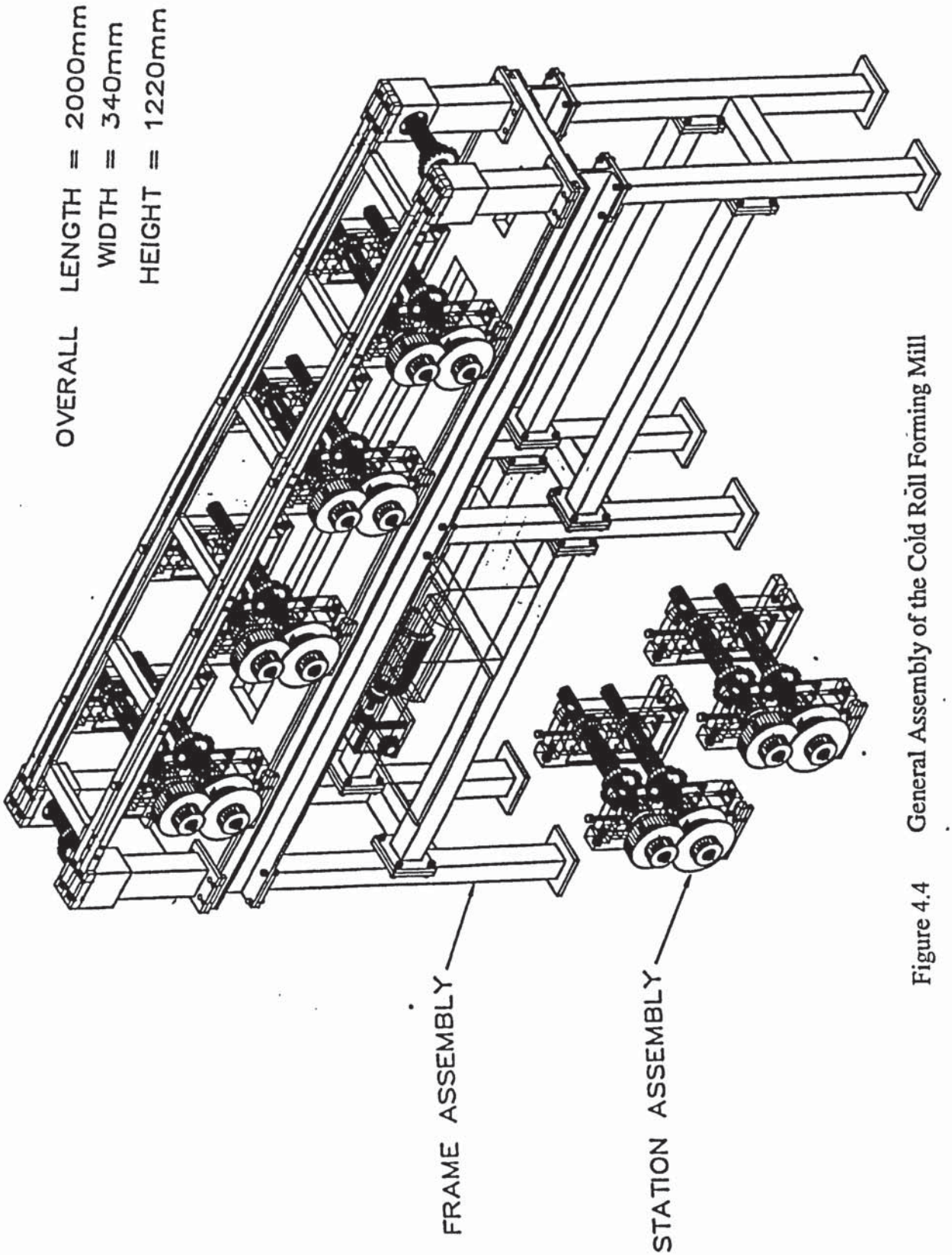

Figure 4.4 General Assembly of the Cold Roll Forming Mill

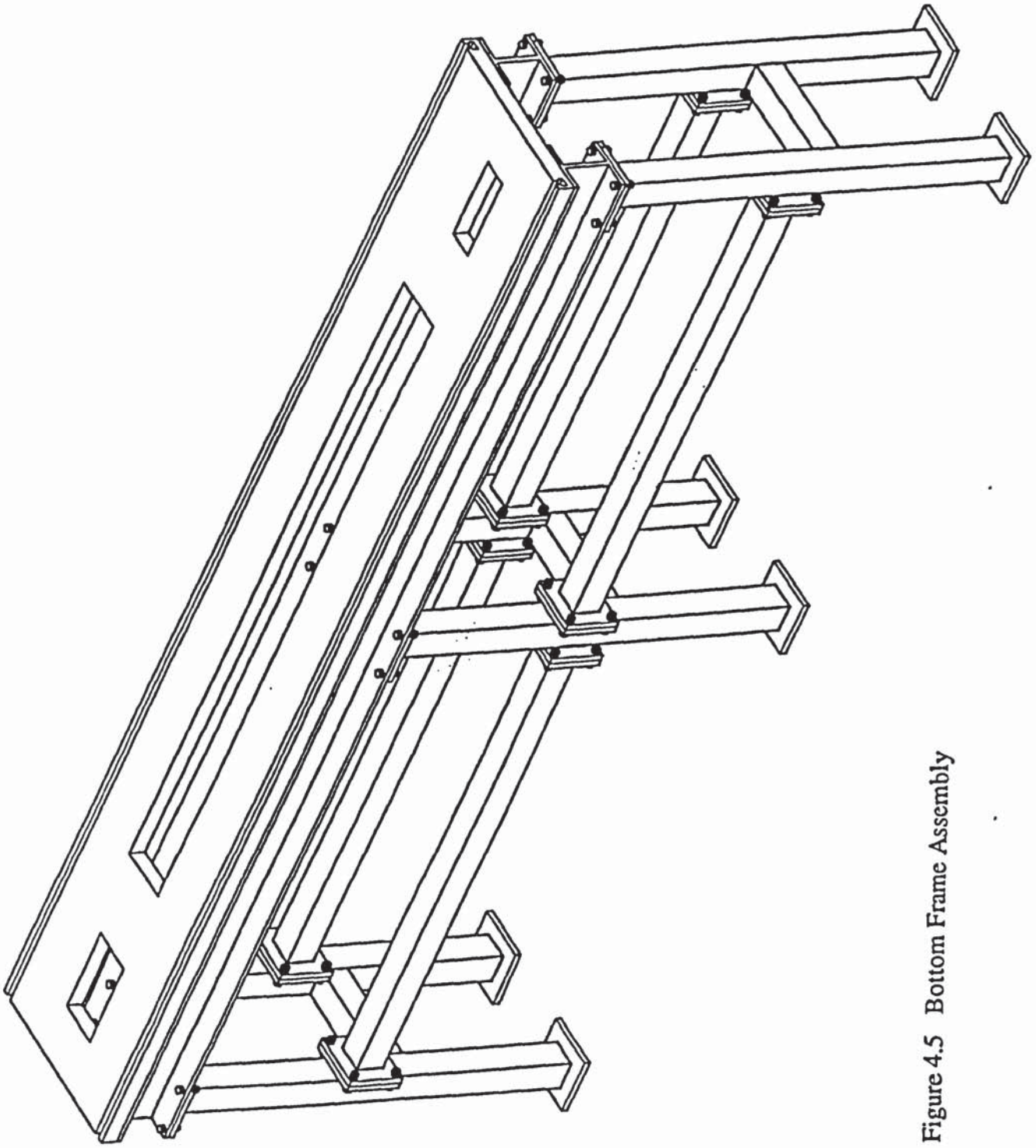

Figure 4.5 Bottom Frame Assembly

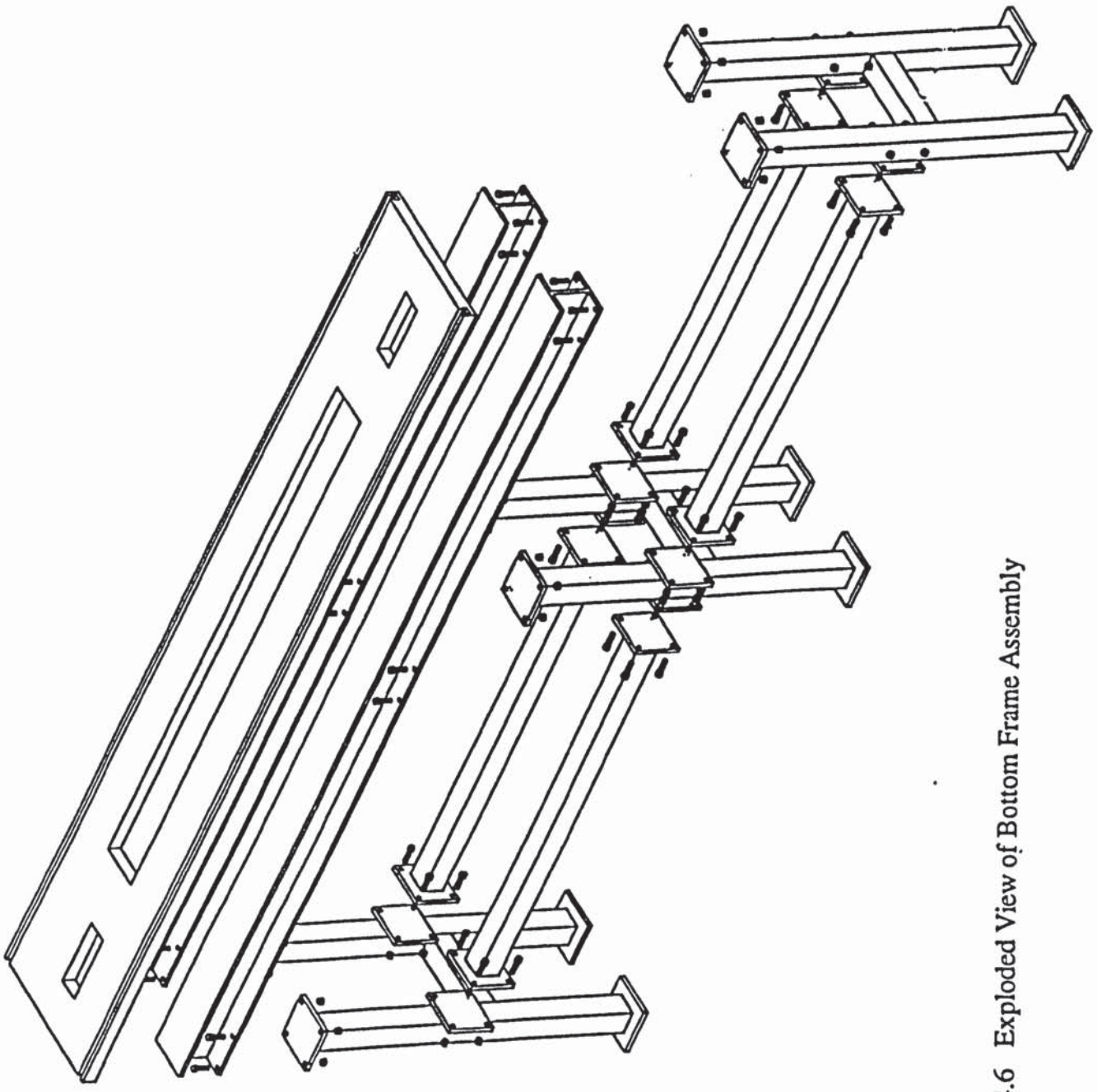

Figure 4.6 Exploded View of Bottom Frame Assembly

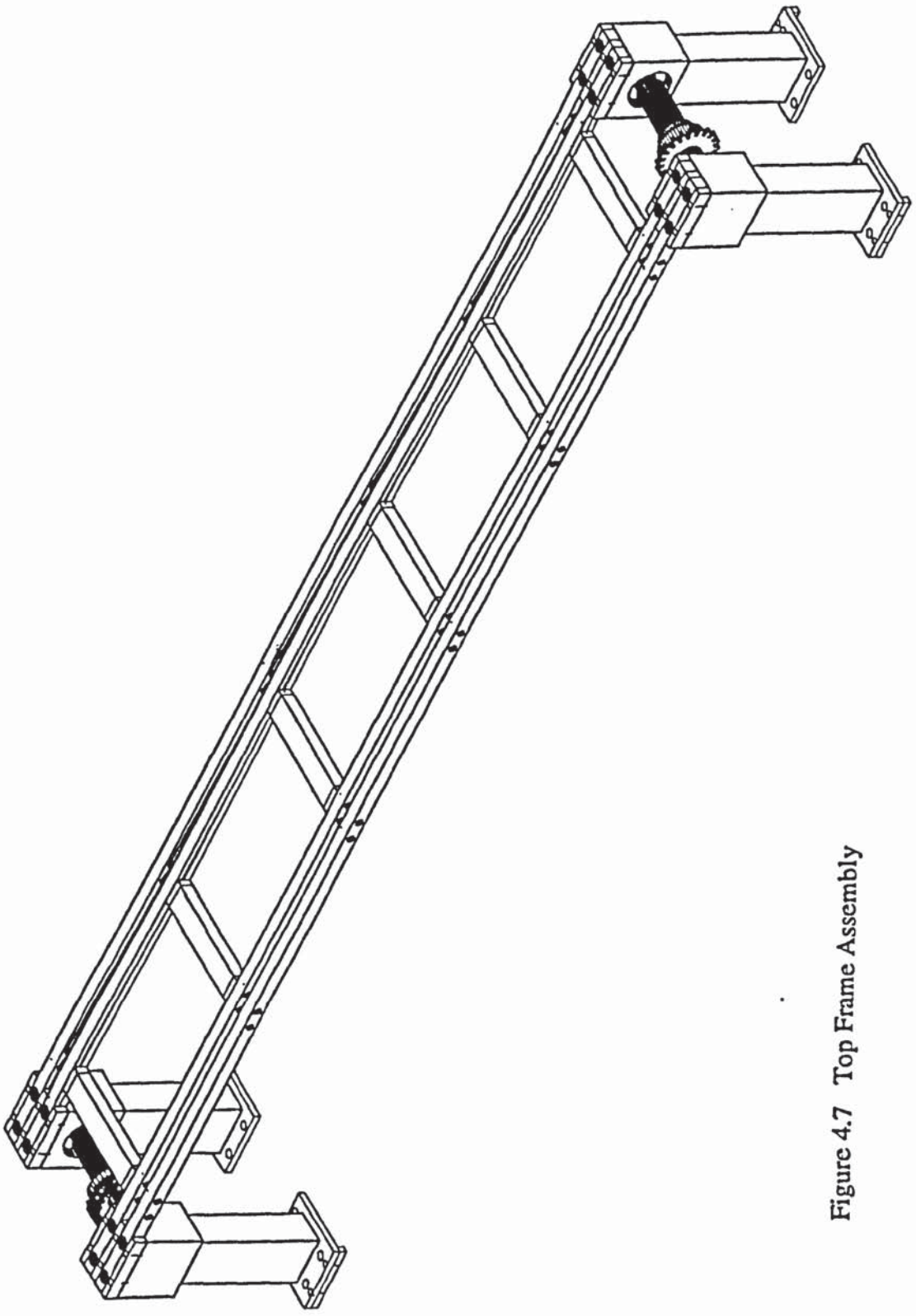

Figure 4.7 Top Frame Assembly

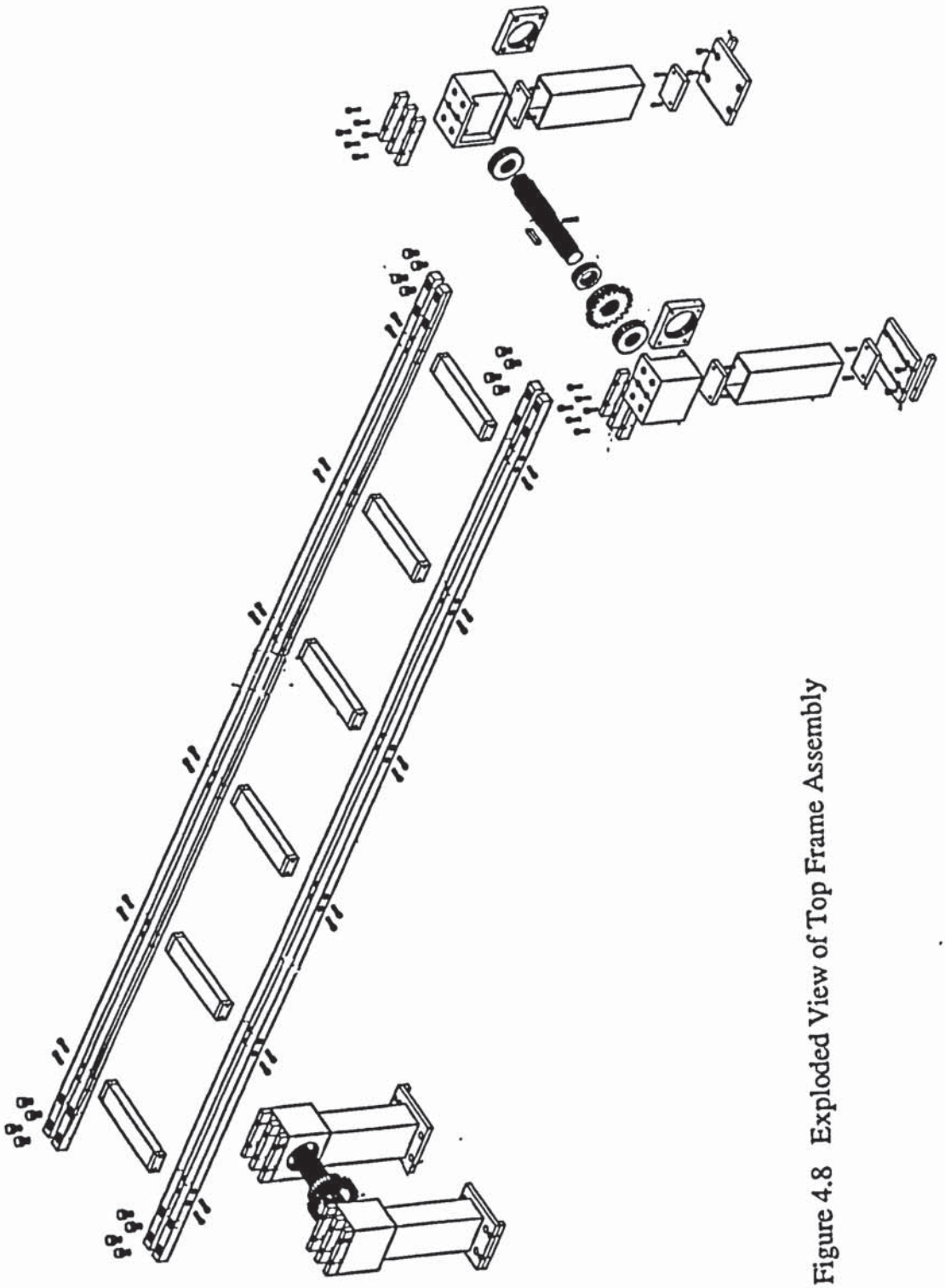

Figure 4.8 Exploded View of Top Frame Assembly

The top frame assembly consists of two longitudinal rails to anchor the roll stations. The main function of the top frame is to support the two gear wheels for the chain drive system. Figures 4.7 and 4.8 shows the construction of the top frame assembly.

4.2.2 Roll Stations

The roll stations are responsible for forming the workpiece into the desired form. Roll stations are designed as independent modules. Any one of the six stations can be moved without affecting the other stations. This is a useful feature for experimental investigations and repair and maintenance of the mill. Figure 4.9 illustrates one of the stations. An exploded version of the station is shown in Fig. 4.10.

4.2.3 Drive System

A chain drive system is used to drive the top rolls and bottom rolls. All the rolls rotate at the same speed. This is achieved by using identical sprockets on all the roll shafts. Figure 4.11 shows the chain drive system. A chain drive system was adopted in the design for simplicity. A gear drive system demands tighter tolerances and more accurate machining and fabrication.

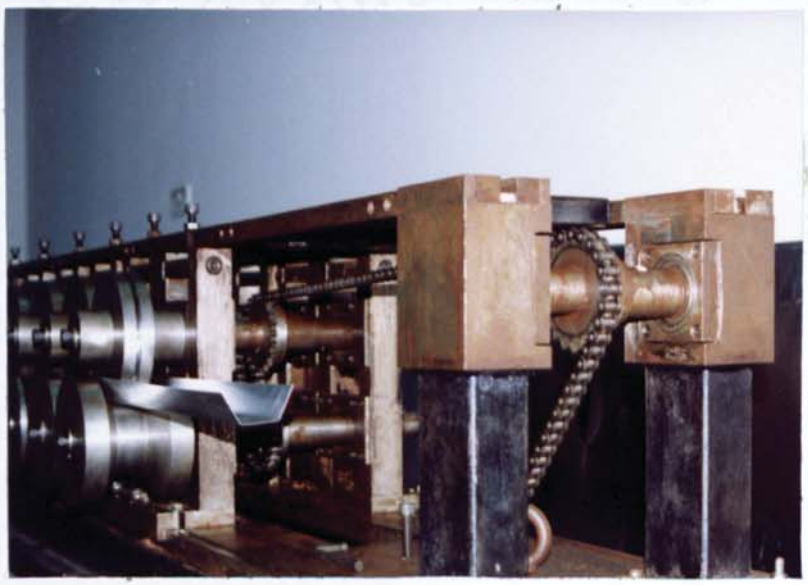

Fig 4.11 Chain Drive system of the CRF Mill No:2

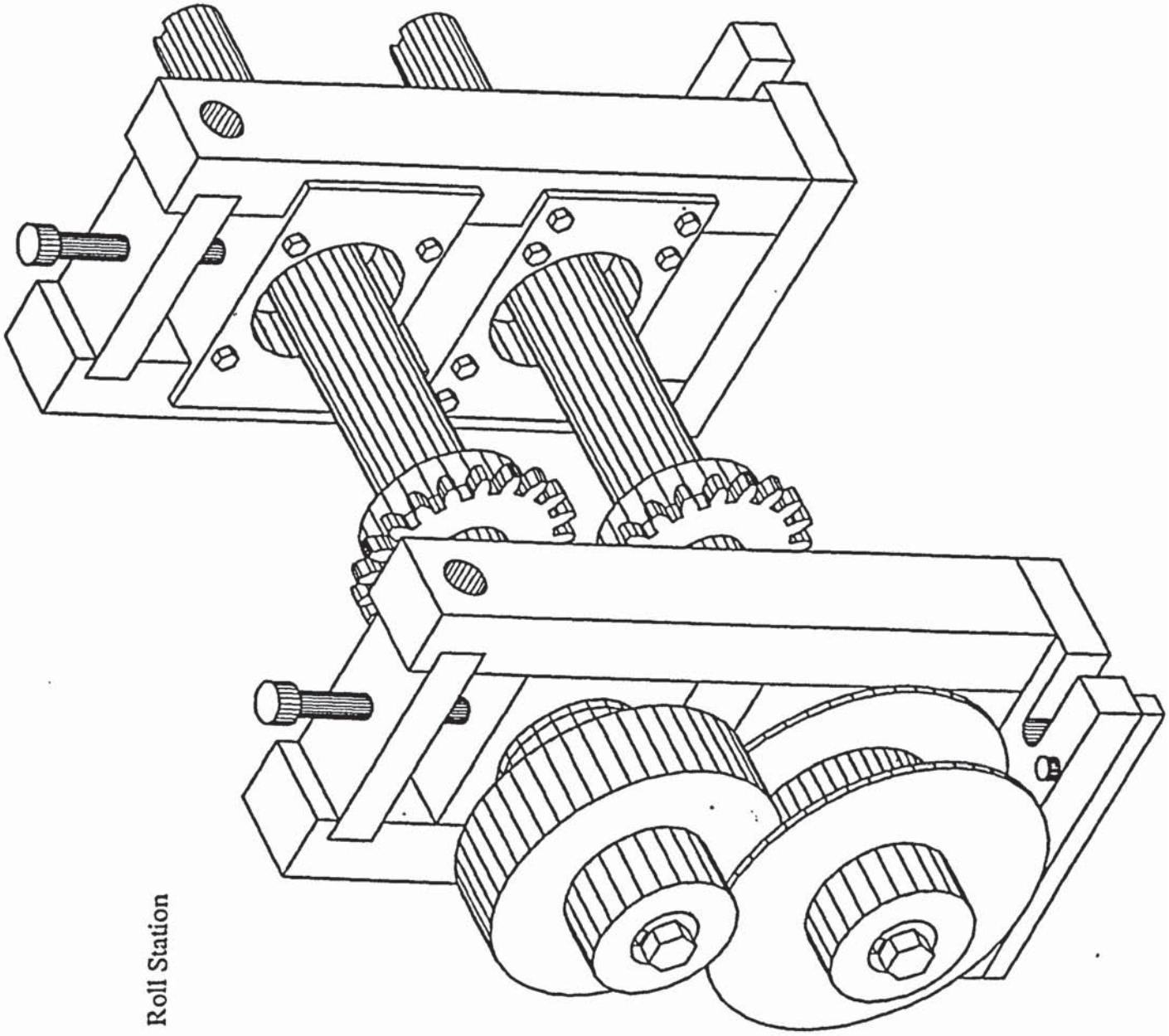

Figure 4.9 General Assembly of a Roll Station

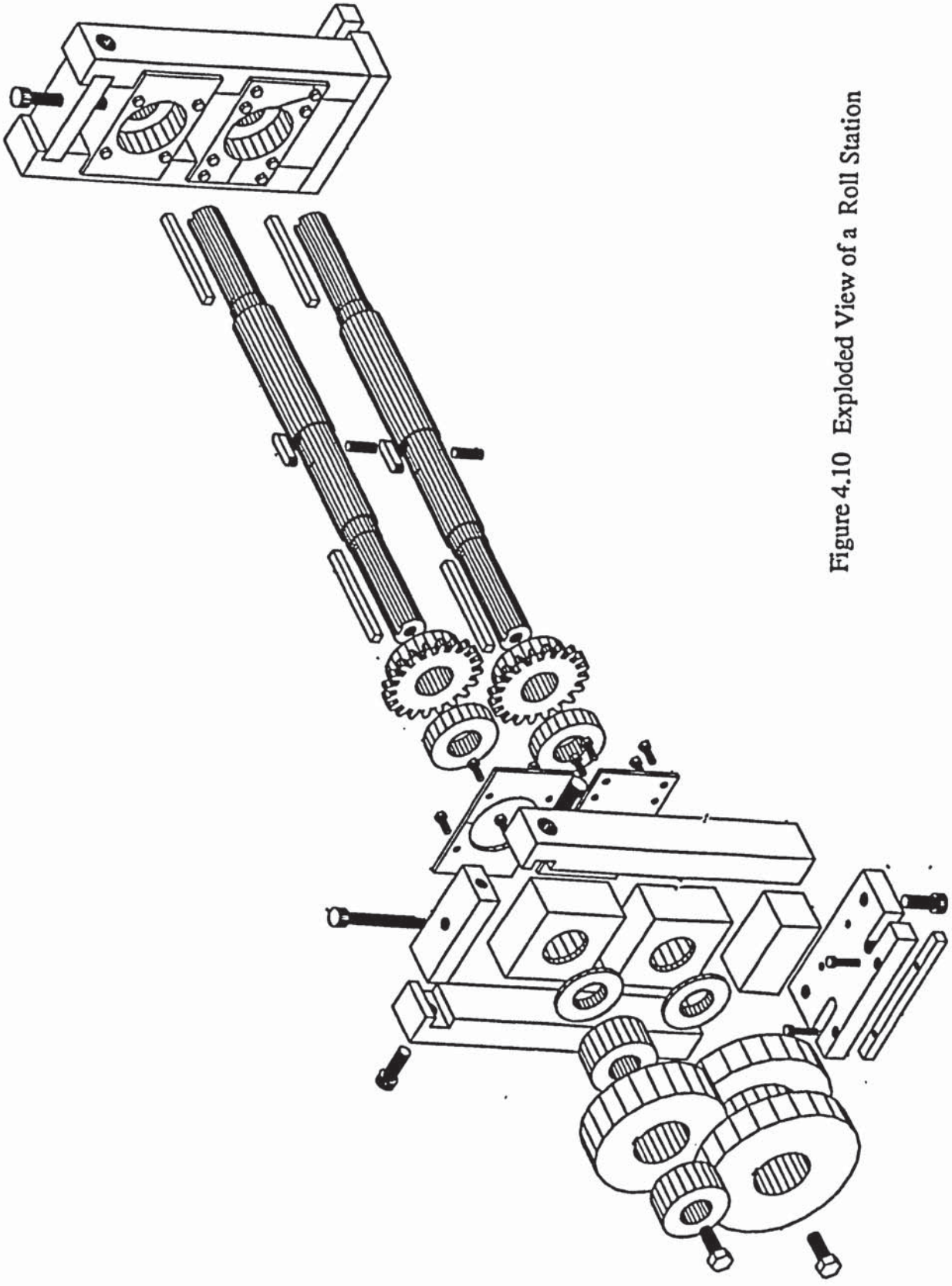

Figure 4.10 Exploded View of a Roll Station

4.3 Design of Roll Tooling for the CRF Mills

Special consideration was given to tooling design during the experimental work to facilitate strain measurement. Commercial tooling normally comes in matching pairs of contoured rolls. This design cannot accommodate strain gauges without some modifications. The usual method is to machine grooves on top rolls to allow the strain gauge to pass through. Roll design is based on air-bending where the top roll is of cylindrical shape. This set-up allows the use of strain gauges on the inside face of the flanges. The bottom roll is of special design which is made of two halves. This has the following advantages:

- The common face can be ground or shimmed to make dimensional adjustments to correct defects in the formed product. There is very little leeway for modifying a one-piece bottom roll.

- Partially formed workpieces can be removed from the mill for the measurement of plastic strains by removing one half of the bottom roll.

Figure 4.12 shows the typical arrangement of a roll station. If a conventional inboard type roll forming mill with conventional tooling is used for experimental work, the mill will have to be virtually dismantled to remove a partially formed work piece.

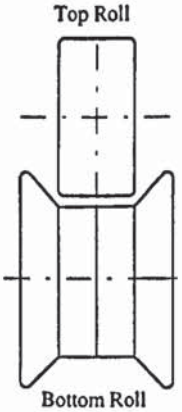

Fig 4.12 Top and Bottom Rolls for producing a trapezoidal section

4.3.1 Tooling for the CRF Mill No: 1

(a) Roll diameter

Roll diameters are determined by the depth of the trapezoidal shape and the capacity of the machine. Larger diameter of rolls are preferred as it permits higher production speeds, lower rubbing velocity and permits more roll regrinds. Larger rolls also provide a larger transition distance which reduces the amount of curvature in the edge of the section and the actual metal movement.

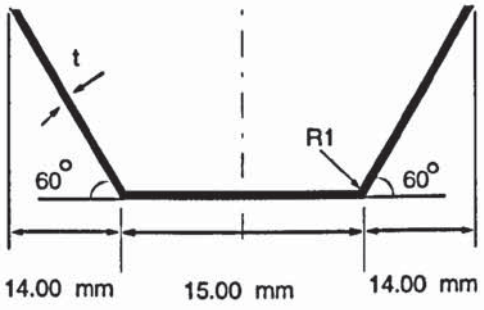

Fig 4.13. Trapezoidal Section (CRF Mill No:1).

To ensure that the top roll is always in contact with the bottom roll, the diameter of rolls must be greater than 96 mm, which is the vertical shaft distance. However, this should not exceed 127 mm to prevent cutting into the path of successive roll.

$$96.0 \text{ mm} < \text{Diameter of Roll} < 127 \text{ mm}$$

For the above reasons, a roll diameter of 101.6 mm was chosen for all the rolls.

(b) Top roll design

Figure 4.14 shows the different parts of a top roll assembly. The 6 mm slot at the middle of the top roll is to provide clearance for the strain gauge mounted on the to-be-formed metal strip. As shown in Figure 4.13, the base length of the trapezoidal section is 15 mm. The width of the upper roll is:

$$\text{width of upper roll} = \text{Base} - 2 \times \text{Strip metal thickness} - \text{Allowance}$$
$$= 15 - (2 \times 0.5) - 0.2 = 13.8 \text{ mm}$$

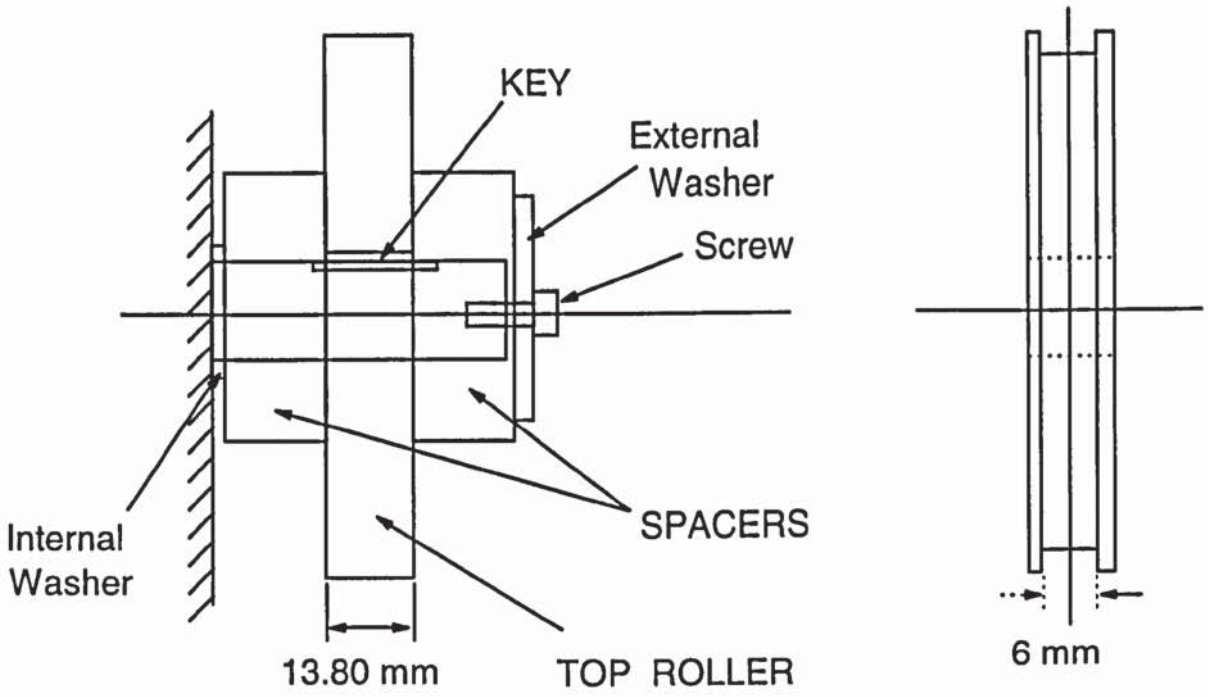

Figure 4.14 (a) Top roll assembly (b) Top roller after modification

(c) Bottom roll design

The design of bottom rolls is crucial in the process of rolling as they shape the metal strip. Figure 4.15 shows the profile of the bottom roll. The roll or bend angle θ varies from roll station 1 to 6. The constant forming angle method was employed to determine the bend angles. In the design, a forming angle of 2.34° was adopted . As a rule-of-thumb, the forming angle varies from 1.25° (for steel) to 3.0° for ductile materials. The bend angles for the six bottom rolls are shown in Table 4.1.

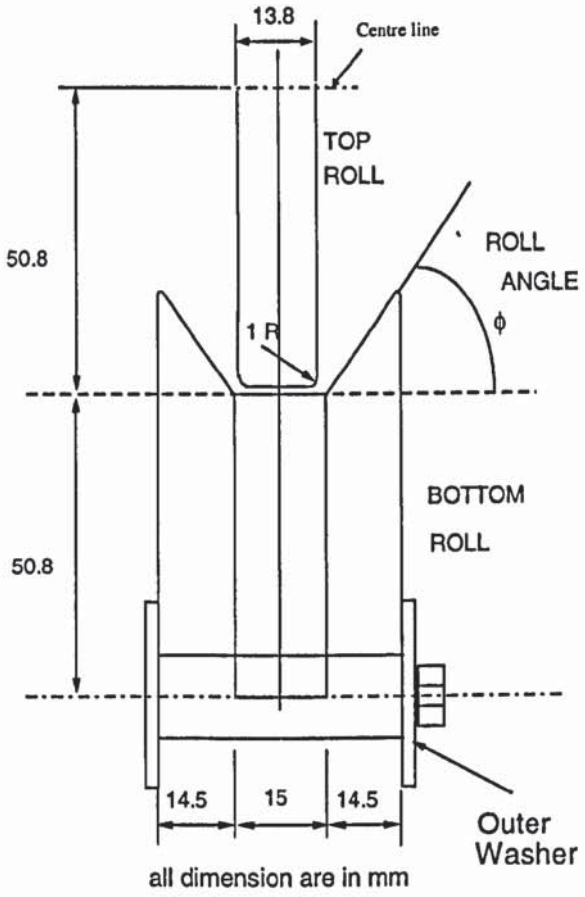

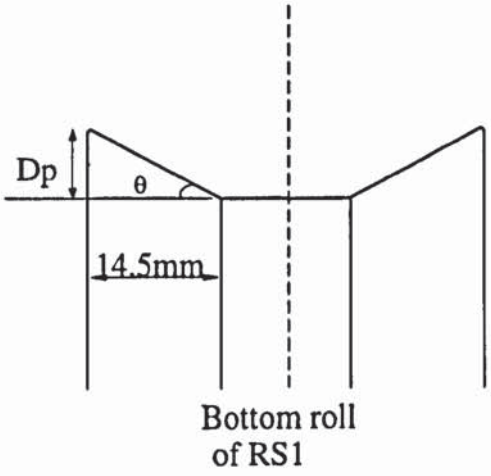

Figure 4.15 Profile of bottom roll

$$\theta_1 = \tan^{-1}\frac{5.19}{14.5} = 19.69^{\circ}$$

Roll Station	Depth of section, Dp	Bend angle of bottom roll, θ
1	5.19 mm	19.69°
2	10.37 mm	35.59°
3	15.57 mm	47.04°
4	20.75 mm	55.05°
5	25.94 mm	60.79°
6	31.14 mm	65.03°

Table 4.1 Bend angle for the six bottom rolls

A 'flower' pattern as shown below is used to illustrate this design.

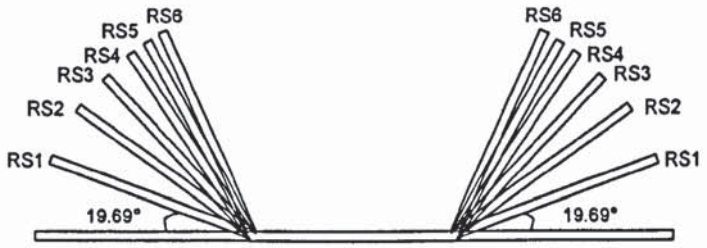

Figure 4.16 Flower pattern of the trapezoidal section

4.3.2 Tooling for the CRF Mill No:2

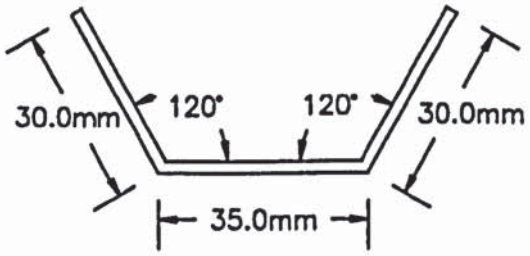

Fig 4.17 Trapezoidal Section (CRF Mill No:2)

A set of roll tooling was also designed and fabricated for the CRF Mill No:2 to form the trapezoidal section shown in Fig 4.17. The two sets of rolls are identical in principle.

4.4 Quality Testing of the Roll Formed Sections

Since the author had no previous experience in the design of either roll forming mills or forming tools, both these were designed according to the information found in published literature. The quality of the roll formed sections appeared to be satisfactory when inspected visually. Straightness and springback of the roll formed sections were measured to ensure that they were suitable for experimental purposes.

4.4.1 Factors that affect the quality of roll formed products

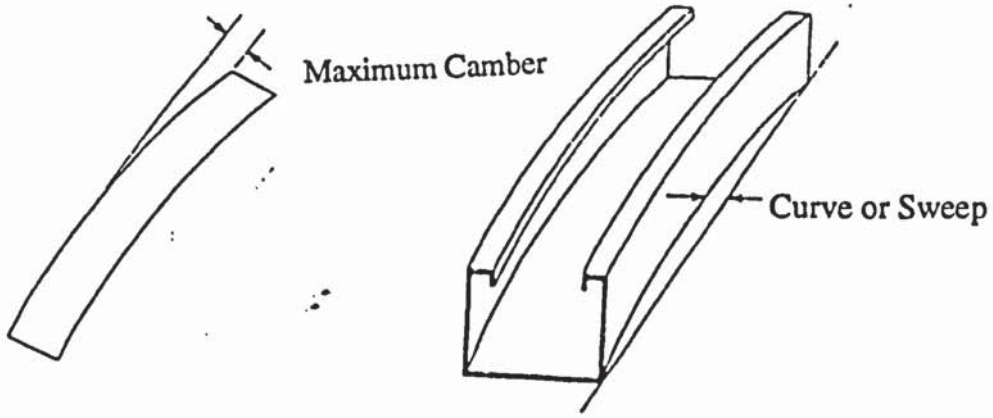

(a) Camber (b) Curve

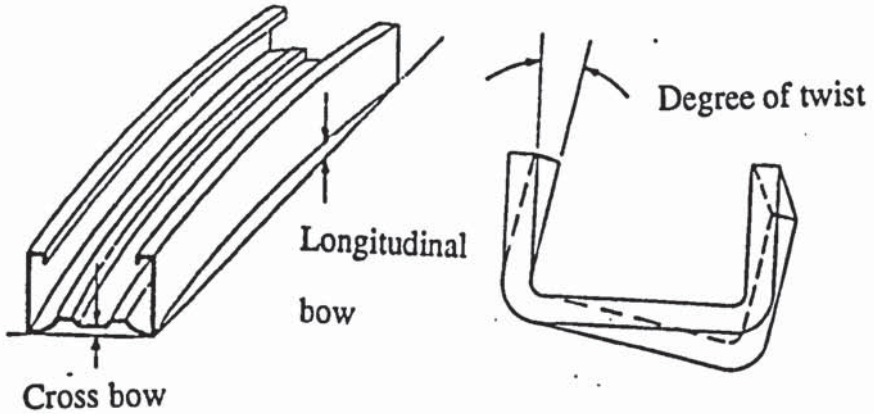

(c) Bow (d) Twist

Figure 4.18 Factors Affecting Straightness

Factors that affect the quality of roll formed products are

- Straightness
- Springback
- End Flare
- Material of the formed section

(a) Straightness

Parameters that determine straightness are camber, curve, bow and twist. Figure 4.18 gives a pictorial explanation of these parameters.

(b) Springback

Springback is a phenomenon that occurs when the material being formed has not been stressed beyond its elastic limit as shown in Fig 4.19. When the metal is released from the rolls, the elastic band tries to return to the original conditions but due to restriction by the plastic deformation zone, only some partial return occurs. The amount of springback varies with metal properties such as yield stress and elastic modulus.

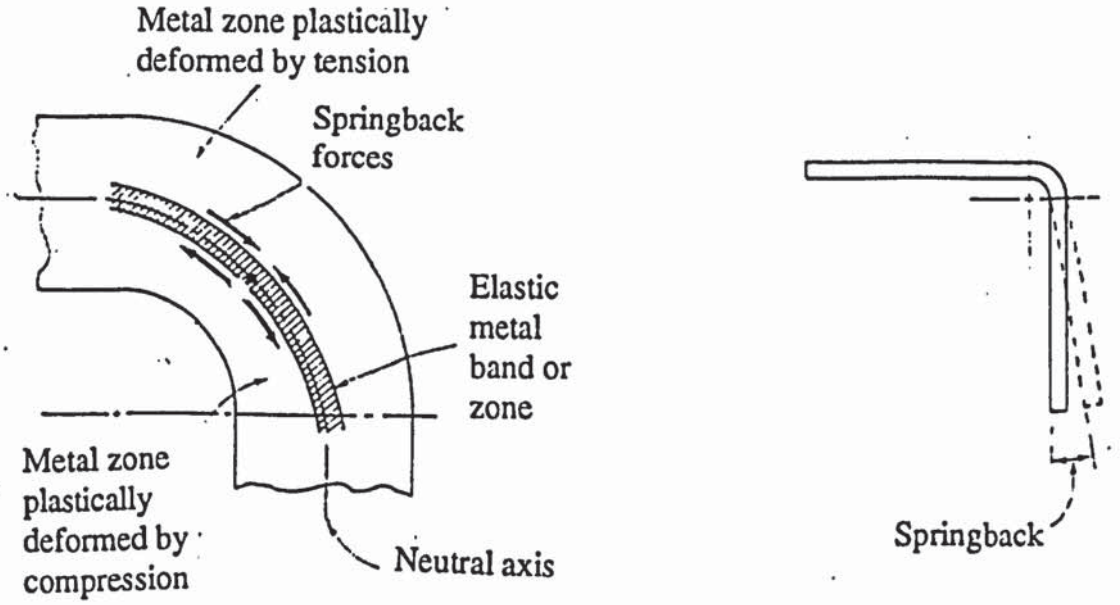

Figure 4.19 Springback

(c) End flare

End flare is the distortion that appears at the end of a roll-formed part. This can be minimised by having extra roll passes, avoidance of prepunched edges at the cut-off zone and the use of more ductile material.

(d) Material of the formed section

Any ductile material that can withstand bending to a desired radius can be roll-formed. The material can be non-ferrous or ferrous, cold rolled, hot rolled, polished, painted or plated. Multiple sections from several different strips of material can be combined to produce one section through roll forming. Some materials that have poor forming characteristics can be heated and then formed on specially designed roll machines[Halmos4].

4.4.2 Measurement of the Longitudinal bow of the roll-formed section

A Zeiss co-ordinate measuring machine (CMM) was used to measure the longitudinal bow of the cold roll formed section. CMM's are essentially universal measuring machines and need not be dedicated to a particular task. They can measure almost any dimensional characteristic of a part. No special fixtures or gauges are required. Because probe contact is light, most parts can be inspected without being clamped to the table. CMM is used to measure the longitudinal bow of the formed product in this experimental work.

The general behaviour of the longitudinal bow of an aluminium and a mild steel roll-formed section can be seen in Figures 4.20 and 4.21 respectively. The bowing is very much dependent upon the material. A Mild steel specimen exhibits larger longitudinal curvature over a span of 500 mm when compared with an identical aluminium specimen. The measured longitudinal bow for the specimens are within the limits of longitudinal bow of specimens rolled by commercial roll forming machines.

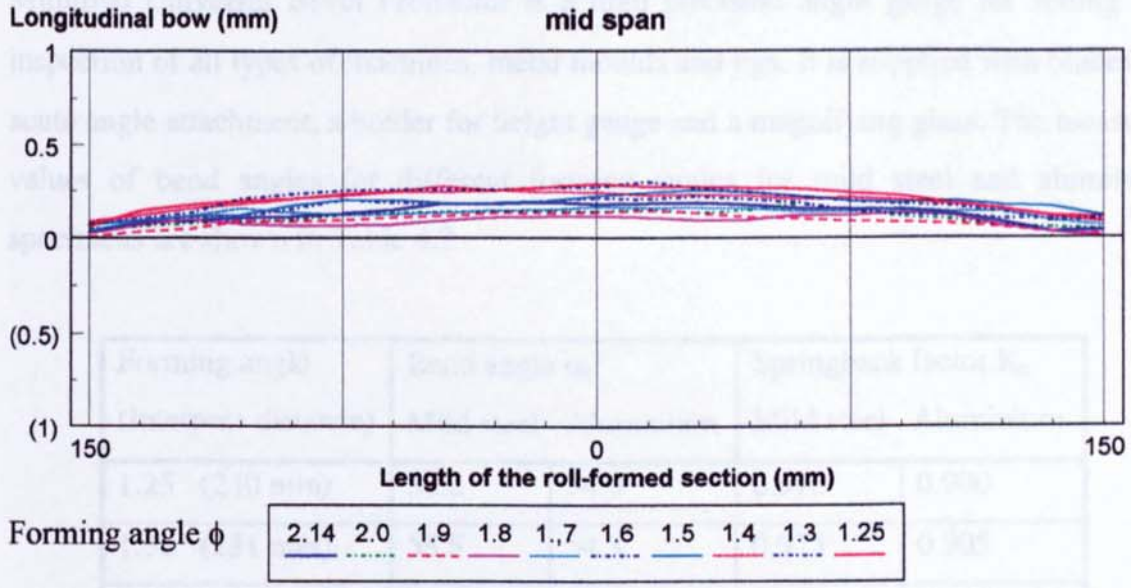

Figure 4.20 Longitudinal bow of an Aluminium roll-formed section

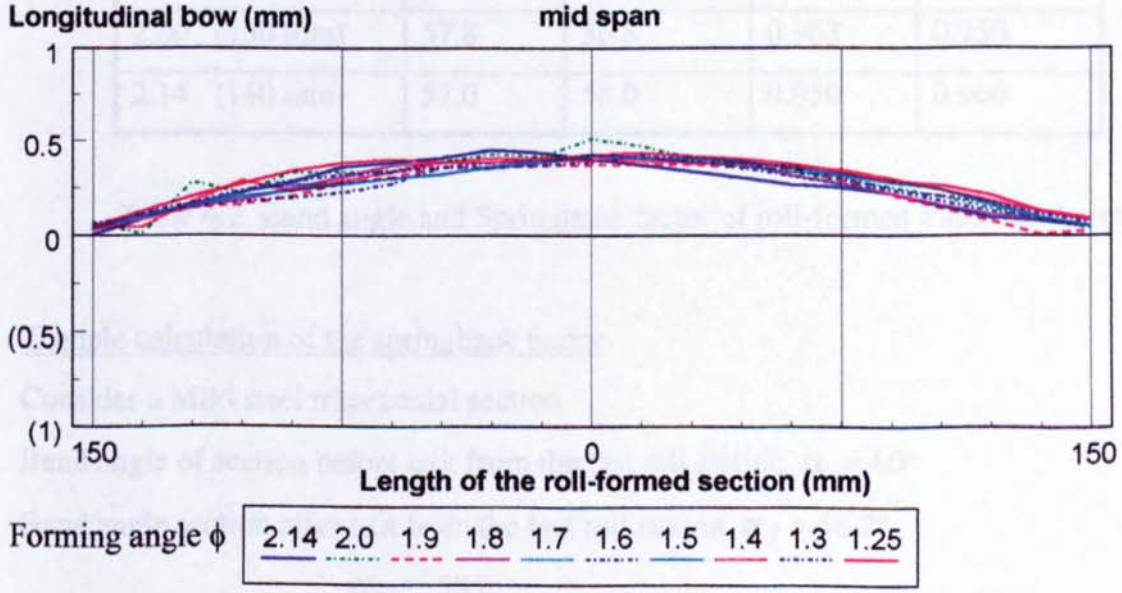

Figure 4.21 Longitudinal bow of the mild steel roll-formed section

4.4.3 Measurement of the Springback effect on the roll-formed channel

A Mitutoyo bevel protractor was used to measure the bend angle of formed sections. Mitutoyo Universal Bevel Protractor is a high precision angle gauge for setting and inspection of all types of machines, metal moulds and jigs. It is supplied with blades, an acute angle attachment, a holder for height gauge and a magnifying glass. The measured values of bend angles for different forming angles for mild steel and aluminium specimens are shown in Table 4.2

Forming angle (Interpass distance)	Bend angle $\alpha_f°$		Springback factor K_s	
	Mild steel	Aluminium	Mild steel	Aluminium
1.25 (240 mm)	58.2	54.0	0.970	0.900
1.30 (231 mm)	58.5	54.3	0.975	0.905
1.40 (214 mm)	59.5	54.8	0.990	0.913
1.50 (200 mm)	60.0	55.0	1.000	0.916
1.60 (187 mm)	60.0	55.2	1.000	0.920
1.70 (176 mm)	59.9	55.3	0.998	0.922
1.80 (167 mm)	59.8	55.4	0.996	0.923
1.90 (158 mm)	58.5	56.0	0.975	0.933
2.00 (150 mm)	57.8	56.8	0.963	0.950
2.14 (140 mm)	57.0	58.0	0.950	0.966

Table 4.2 Bend angle and Springback factor of roll-formed trapezoidal section

Sample calculation of the springback factor

Consider a Mild steel trapezoidal section

Bend angle of section before exit from the last roll station $\alpha_i = 60°$

Bend angle section after exit from the last roll station $\alpha_f = 58.2°$

Springback factor $K_s = \frac{\alpha_f}{\alpha_i} = \frac{58.2}{60.0} = 0.970$

Springback Analysis

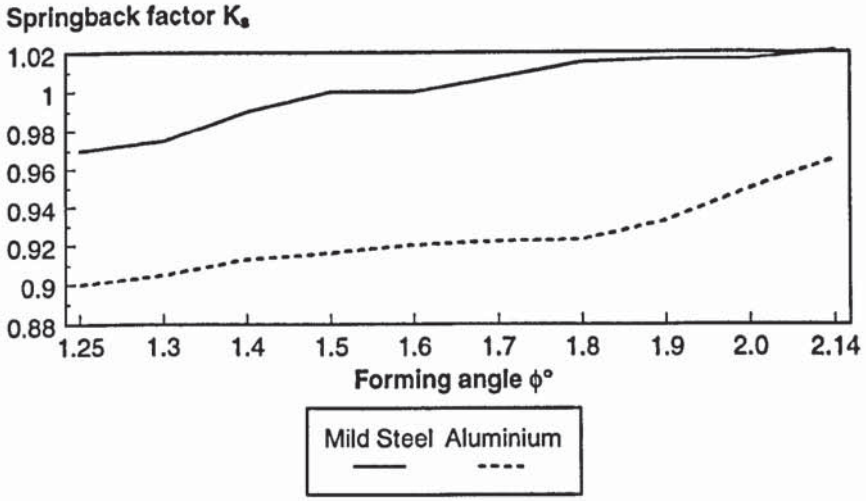

Figure 4.22 Graph of Springback factor Vs Forming angle

The general behaviour of the springback effect of the materials is shown in Figure 4.22. A springback factor of K_s =1 indicates no springback and K_s = 0 indicates complete elastic recovery. A springback factor of $K_s > 1$ indicates springforward. As can be seen in Figure 4.22, the springback factor is very dependent upon the forming material and the forming angle. Mild steel exhibits minimum springback when the forming angle is within the range of 1.5°-1.6°. The springback effect for mild steel decreases as the forming angle increases. This also implies that the elastic recovery of the material decreases (due to more deformation) as the interpass distance between station decreases. In fact a spring-forward tends to occurs.

Figure 4.22 compares the effect of the forming angle ϕ on the springback factor K_s for the steel and aluminium specimens. The quality of the roll formed specimens is considered to be satisfactory.

CHAPTER 5

EQUIPMENT, MATERIALS AND EXPERIMENTAL PROCEDURES

The main factors that affect the process of cold roll forming are strains induced in the workpiece during forming, workpiece material, and interpass distance between the rolls. In experimental work it is generally assumed that the rate of forming has no effect on the induced strains. To justify this assumption, the dynamic strains induced during forming are also measured and compared with static strains. In this Chapter, experiments conducted to investigate the influence of these factors during cold roll forming are described.

5.1 Equipment

5.1.1 CRF mills

The two cold roll forming mills used for the experimental work are shown below.

Figure 5.1 Cold Roll Forming Mill No:1

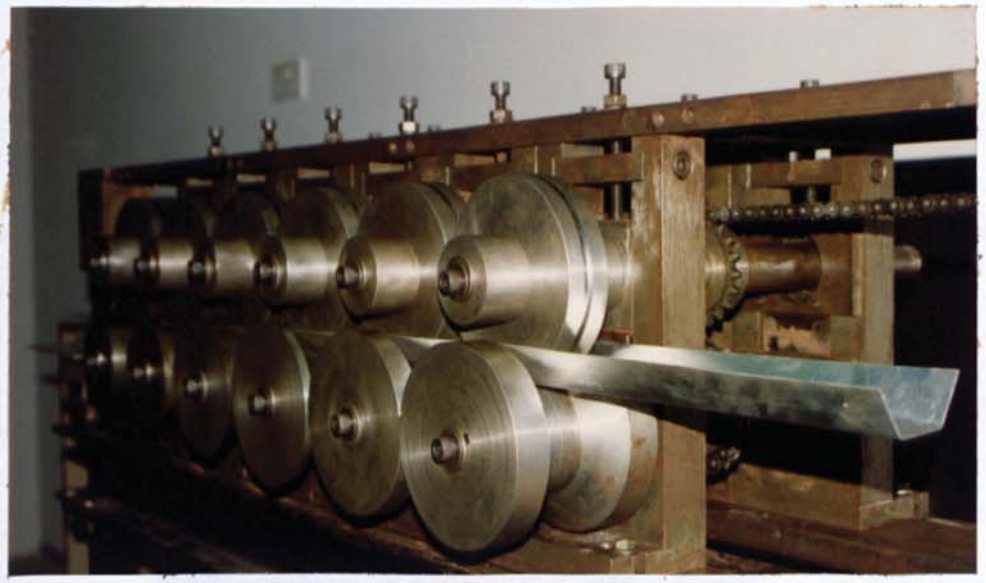

Figure 5.2 Cold Roll Forming Mill No:2

5.1.2 Specimens

Mild steel and Aluminium strips are used to investigate the effect of material properties on the strains developed during cold roll forming. The specimens are formed into trapezoidal sections as described in Chapter 4. The specimen dimensions before forming are listed in Table 5.1.

Table 5.1. Dimensions of specimens used for tests with CRF Mills 1 &2.

Strips	Length (mm)	Width (mm)	Thickness (mm)
Type A	1000	43	0.5
Type B	1220	95	0.5

Specimen types A and type B strips were used on the CRF mills 1 and 2 respectively. An Instron 4204 tensile testing machine is used to determine the mechanical properties of both materials. This test is carried out in accordance with the "*ASTM Standard Test Methods for Tension Testing of Metallic Materials (Metric)*".

A test specimen (Figure 5.3 and Figure 5.4) with a gauge length of 80 mm is subjected to a tensile load until failure at a constant rate of 0.5 mm/min. A tensile testing machine (Figure 5.5) is used to measure the strain during the test. Mechanical properties such as Young's Modulus, Yield strength at 0.2% offset and Ultimate tensile strength are obtained and tabulated in Table 5.2.

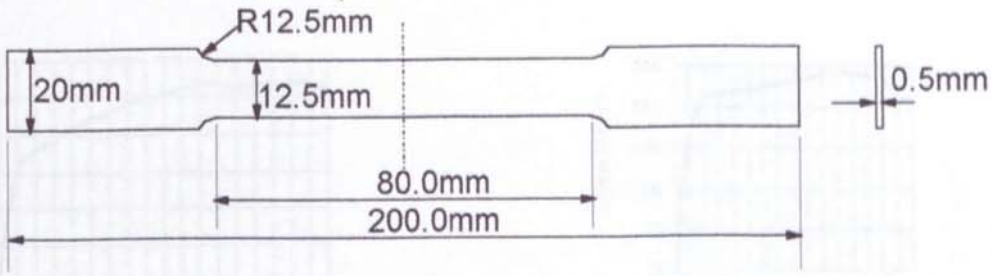

Figure 5.3. Dimensions of Tensile test specimen.

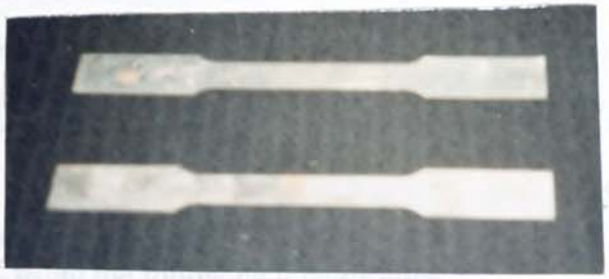

Figure 5.4. Tensile Test Specimens.

Figure 5.5. Instron Tensile Testing Machine.

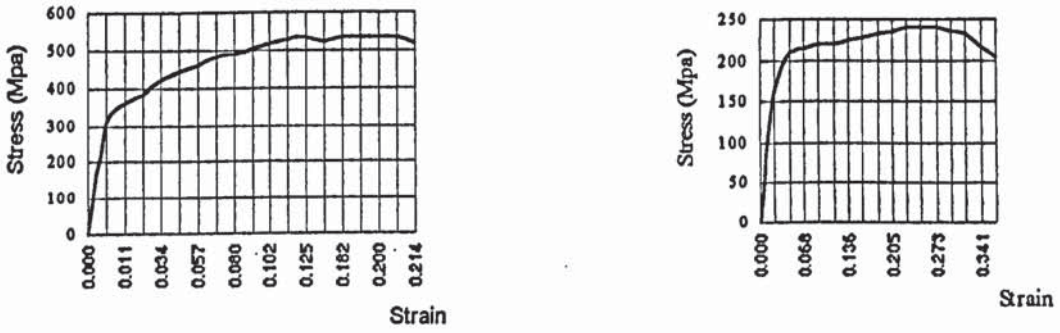

(a) Steel (b)Aluminium

Figure 5.6. Engineering Stress vs Linear Strain Diagrams for Steel and Aluminium Specimens

Figure 5.6 shows the engineering stress-strain diagrams for Steel and Aluminium specimens. The true stress- true strain curves can be derived from the engineering stress-strain values, using the following relationships:

$\varepsilon_{true} = \ln(1 + \varepsilon_{eng})$ and $\sigma_{true} = \sigma_{eng}(1 + \varepsilon_{eng})$.

Table 5.2 Properties of Mild steel and Aluminium Specimens

Material	Aluminium Alloy	Mild steel AISI 1030
Young's Modulus (GPa)	80	210
Yield Strength (MPa)	206	318
Ultimate Tensile Strength (MPa)	237	525

5.1.3 Strain measurement

Strain gauges are mounted on the specimens to measure longitudinal and lateral strains at various locations along the strips. The TML foil strain gauges are used. The lead wires of the strain gauge are connected to a datalogger via a quarter bridge operation. Figures 5.7 and 5.8 shows the locations of strain gauges on specimens for CRF mills 1 and 2 respectively.

(a) Static strain measurement

The cold roll forming mills are hand cranked to prescribed positions to measure the strains induced in the workpiece during forming. It is assumed that the forming speed has no effect on the induced strains. The strains developed are recorded using the SYS4000 datalogger as shown in Figure 5.9. The main menu is shown in Figure 5.10.

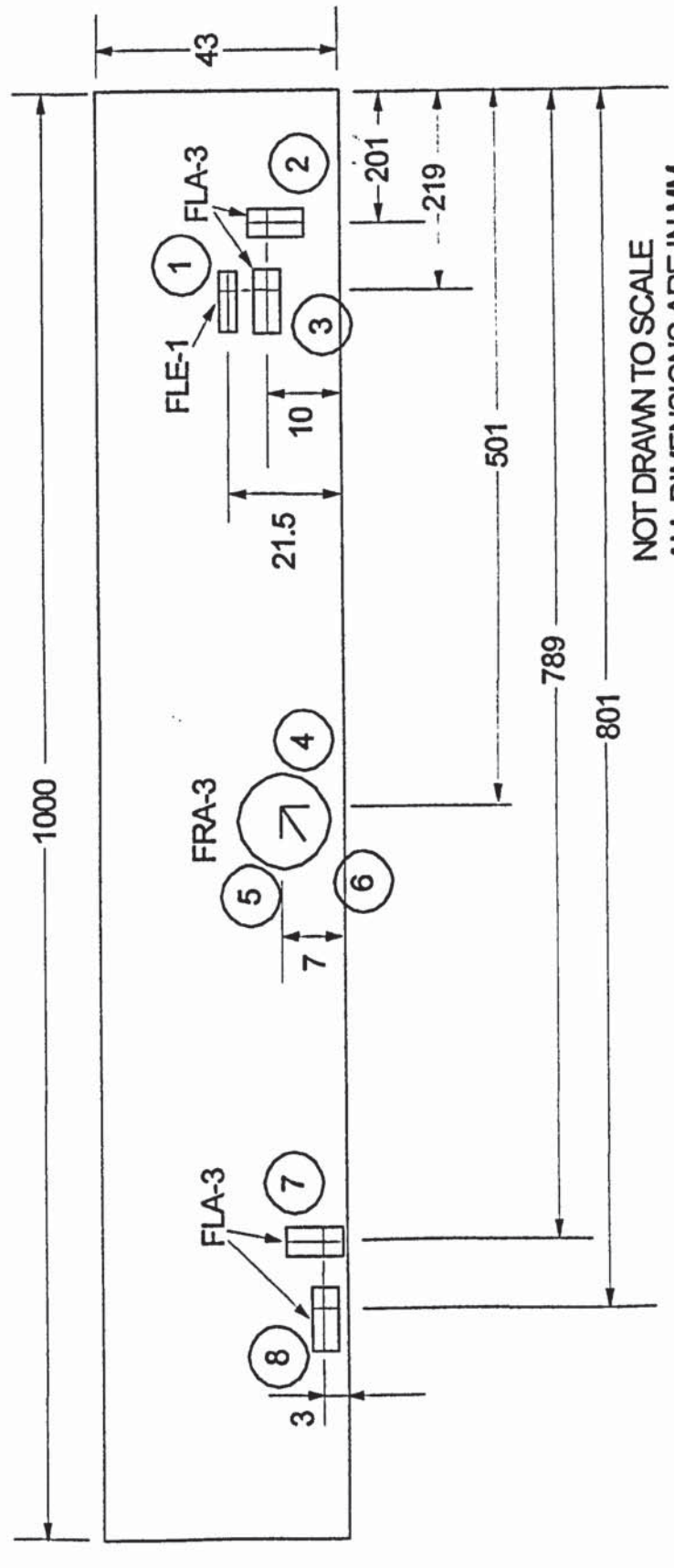

Figure 5.7. Location of Strain Gauges - Specimen No:1.

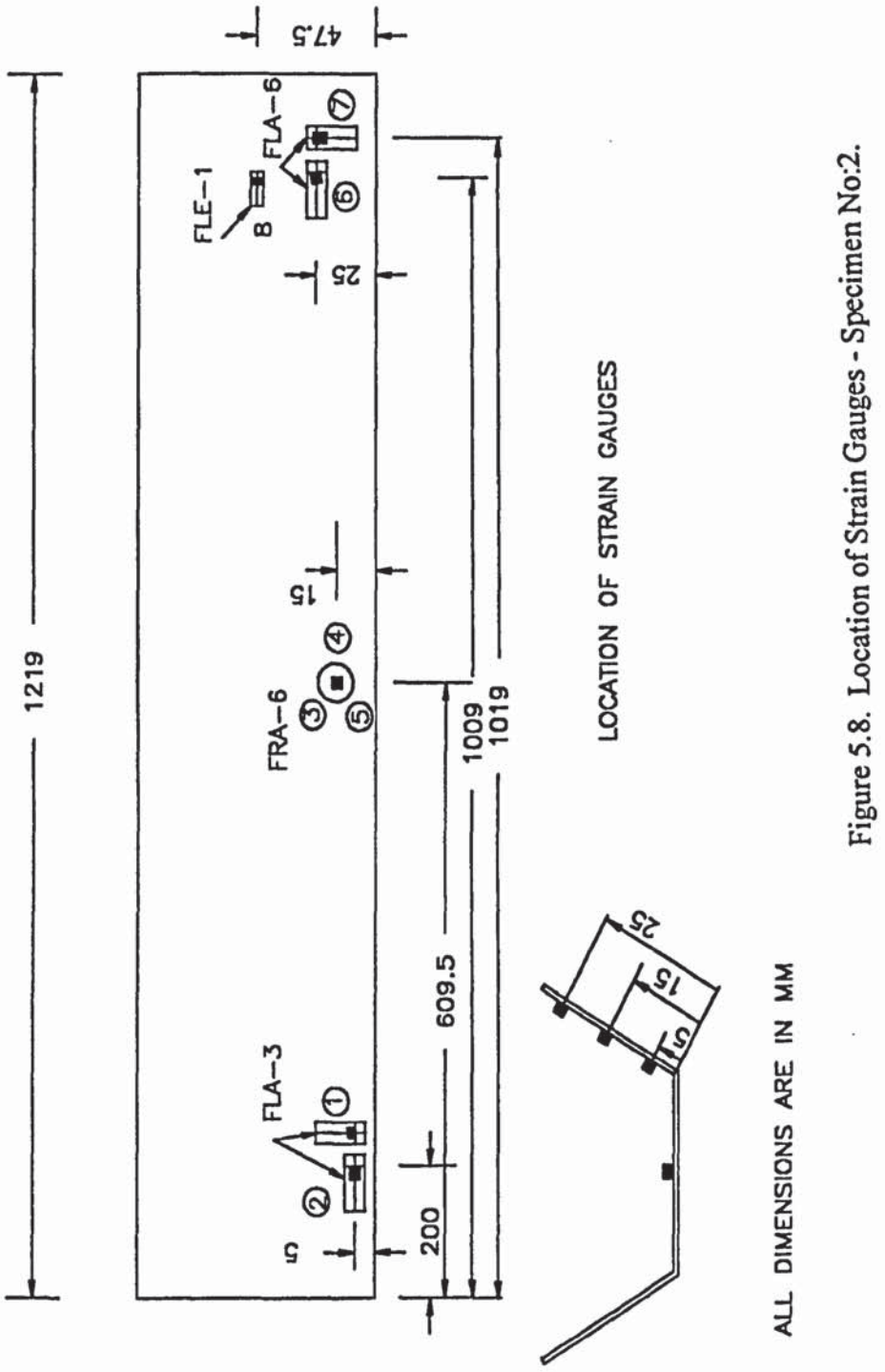

Figure 5.8. Location of Strain Gauges - Specimen No:2.

The datalogger system comprises a 486DX33 computer, standard system software, and strain gauge scanners. It accepts and stores test parameters, controls the scanning operations, records input signals, and corrects and reduces the data to provide direct engineering information. The system block diagram is shown in Figure 5.11.

The strain gauge scanner accepts input from up to 20 quarter, half, or full strain gauge bridges, or strain gauge based transducers. Every channel incorporates 14 terminals, each identified according to standard wiring codes.

Figure 5.9 SYS4000 Datalogger and peripherals

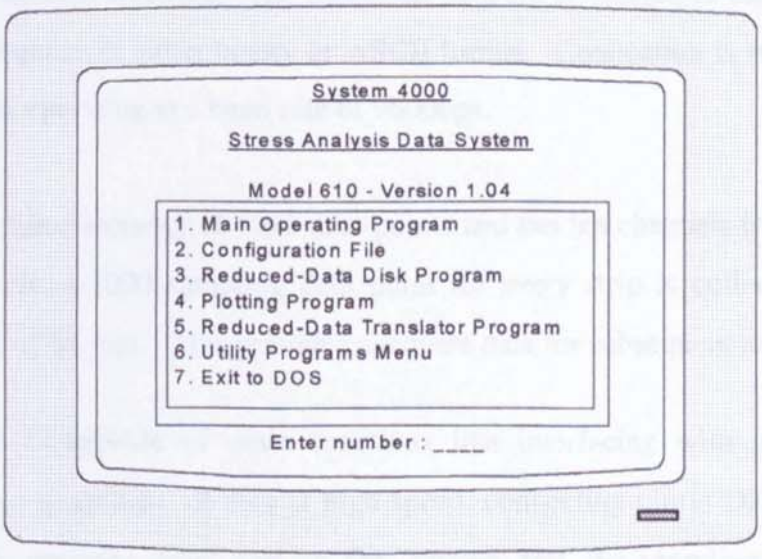

Figure 5.10. SYS4000 Main Menu.

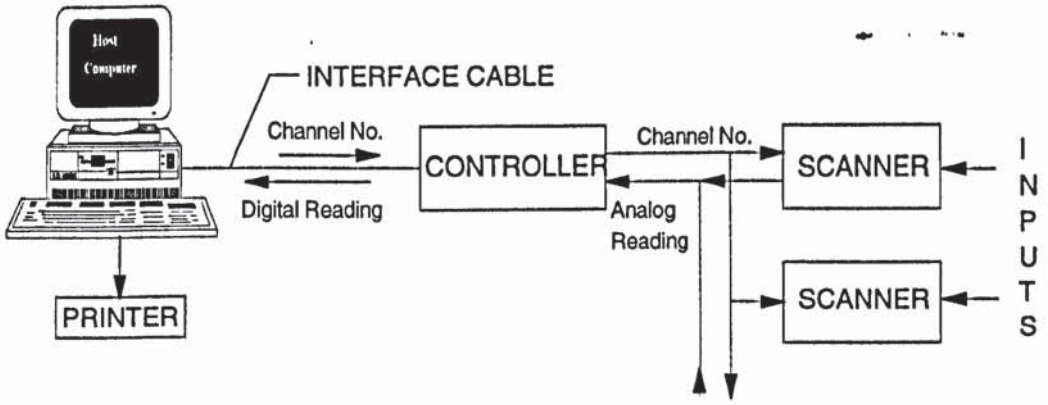

Figure 5.11 System Block Diagram

(b) Dynamic strain measurement

The dynamic strains induced in the workpiece during forming are measured by operating the cold roll forming mills at a fixed speed. A dynamic datalogger, the DRA10A Dynamic Digital Strain meter, is used to measure the strains induced during the process of cold roll forming.

The dynamic datalogger is interfaced to an external computer (Figure 5.11). The computer issues commands to and receives data from the DRA10A through a special Windows application software. The measured data are converted to digital signals and sent to the computer in either binary or ASCII format. Connection is made via an RS-232C interface, operating at a baud rate of 9600bps.

The DRA10A has a memory of 4096 data-points and has ten channels for data input. In the dynamic test, a 1000 sampling data point for every strip is collected with a roll forming speed of 24 rpm. This provides adequate data for subsequent analysis.

The DRA10A is capable of other functions like interfacing with an oscilloscope, transfer of large quantities of data at high speed, connecting plural DRA10A on same line etc. In the program developed for the dynamic test, the sampling data point was selected to be 1000 (see sample calculation). The time required for the complete data transfer from the DRA10A to the computer memory in the ASCII output mode is about 30mins.

(a) Computer and DRA10A

(b) 8 BNC Connectors

Figure 5.12 Dynamic Data Acquisition System

Sample calculation

Radius of roll = 51mm
Roll speed = 24 rpm

Assume that the specimen does not slip on rolling,

$$\text{Transverse speed of specimen} = 51*(24*\frac{2\pi}{60})$$
$$= 128 \text{ mm/s}$$

Every 3mm movement required 1 scan from DRA10A
The **data sampling rate** $= 1000 \div (\frac{128}{3}) = 23.4$ ms

Total travel = Length of specimen + Distance between first and last shaft
= 1000 + (5*127)
= 1635 mm
≡ 545 scans
≡ 12.77 sec

An allowance of 5 sec is given for the initialisation of DRA10A

No. of data points required = (12.77 + 5) / 0.0234
= 759

(c) Plastic strain measurement

An optical measurement inspection system, the OMIS II, is used to measure the plastic strains induced during forming. The system comprises of an optical comparator, a microscope and a coordinate measuring table as shown in Figure 5.13.

The OMIS II is incorporated with a software-based dimension measurement tool. The software supports three operation modes : Measurement, Analysis, and Programming. The Measurement and Analysis modes are used to perform dimensional measurements manually and at the same time to record the inspection sequence. Figure 5.14 shows the measurement screen. The details of the main menu are shown in Figure 5.15. Under the Programming mode, an inspection sequence can be stored, loaded or run either automatically or step by step.

Figure 5.13 OMIS II-Optical Measurement Inspection System

Figure 5.14 Measurement Screen

Figure 5.15. Main Menu Screen.

5.2 Experimental Procedures

5.2.1 Static forming tests

The static forming tests are carried out with the DC motor disconnected to permit manual forward motion of strips by turning the shaft. The metal strip bonded with strain gauges is connected to the SYS4000 datalogger via a Quarter bridge. The datalogger is set with the gauge factors of the strain gauges used.

During the test, the metal strip is first inserted into the first roll. The strip is then advanced through the mill forward manually and is stopped at every 3 mm interval of material rolling distance to activate the datalogger. The strains developed during the roll forming process is recorded. When the mild steel strip passes through the last roll station, the operation is terminated. The collected data after processing will enable a strain-distance graph to be plotted, showing the changes of strains in the strip during the forming process.

Tests on CRF mill No:1

Six tests are conducted using the CRF mill No:1 (Table 5.3), with different strip materials, interpass distances, and number of roll stations. Figure 5.16 shows the 6 station mill, with a 127 mm spacing between each roll station. In order to investigate the effect of fewer forming rolls on the strains developed in the strip, tests are conducted with 3 roll stations as shown in Figure 5.17, with an interpass distance of 2x127 mm. Both mild steel and aluminium strips are used.

Table 5.3 Schedule of tests carried out on CRF Mill No:1

CRF mill No:**1** Test mode : **Static**			
Test No.	Material	Interpass Distance	No. of Roll stations
1	Mild Steel	127 mm	6
2	Aluminium	127 mm	6
3	Mild Steel	127 mm	3
4	Aluminium	127 mm	3
5	Mild Steel	2 x 127 mm	3
6	Aluminium	2 x 127 mm	3

(b) Tests on CRF mill No:2

Four tests are conducted using the CRF mill No:2 (Table 5.4), with different strip materials, interpass distances, and 6 roll stations. The objective is to investigate how the forming strains are affected by the interpass distance calculated using the forming angle method. Both mild steel and aluminium strips are used.

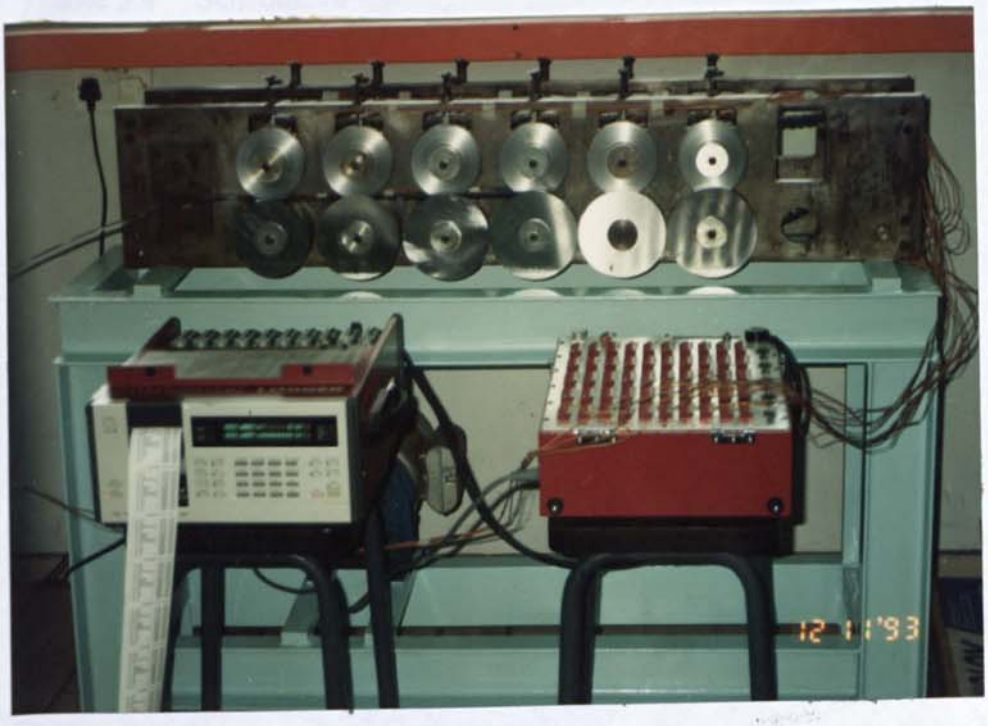

Figure 5.16 Test with 6 roll stations placed 127 mm apart (CRF Mill No:1)

Figure 5.17 Test with 3 roll stations placed 2x127 mm apart (CRF Mill No:1)

Table 5.4 Schedule of tests carried out on CRF Mill No:2

CRF mill No: **2** Test mode : **Static**			
Test No.	Material	Interpass Distance	No. of Roll stations
1	Mild Steel	140 mm	6
2	Mild Steel	240 mm	6
3	Aluminium	240 mm	6
4	Aluminium	140 mm	6

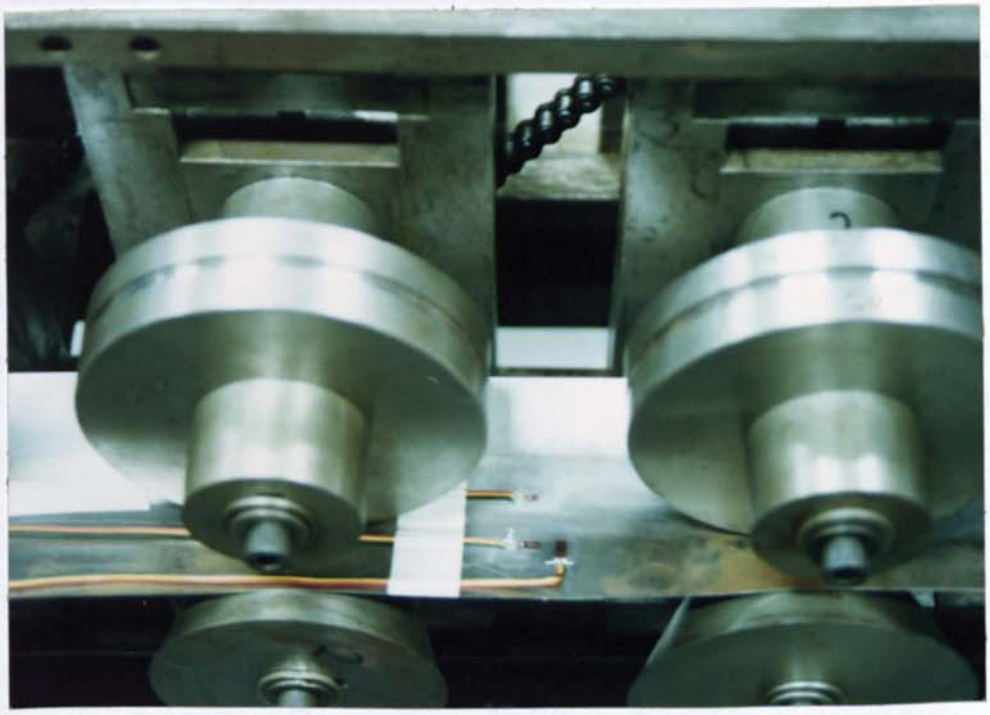

Figure 5.18 View of strain gauges during strain measurement

5.2.2 Dynamic forming tests

The dynamic forming tests are similar to the static ones but instead of manual turning, a DC motor is used to drive the rolls at 24 rpm. A dynamic datalogger, the DRA10A Dynamic Digital Strain meter, is used to measure the forming strains in-process.

At the start of experiment, a test procedure developed using the dynamic datalogger is retrieved and executed to initialise the system before feeding the mild steel strip. The output signals from the strain gauges through successive roll stations are recorded. The data can then be processed to obtain plots of strain as a function of distance travelled.

Three tests are conducted using the CRF Mill No:1 (Table 5.5), with different strip materials, interpass distances, and numbers of roll stations.

Table 5.5 Schedule of tests carried out on CRF Mill No:1 in Dynamic Mode

CRF mill number : **1** Test mode : **Dynamic**			
Test No.	Material	Interpass Distance	No. of Roll stations
1	Mild Steel	127 mm	6
2	Mild Steel	127 mm	3
3	Mild Steel	2 x 127 mm	3

5.2.3 Comparison between Static and Dynamic Tests

Comparison of experimental strain distributions obtained for static and dynamic tests using mild steel specimens are shown in Figure 5.19. The strains developed for the two cases are similar in terms of magnitude and distribution. This implies that strain measurement can be based on static tests which are much easier to perform.

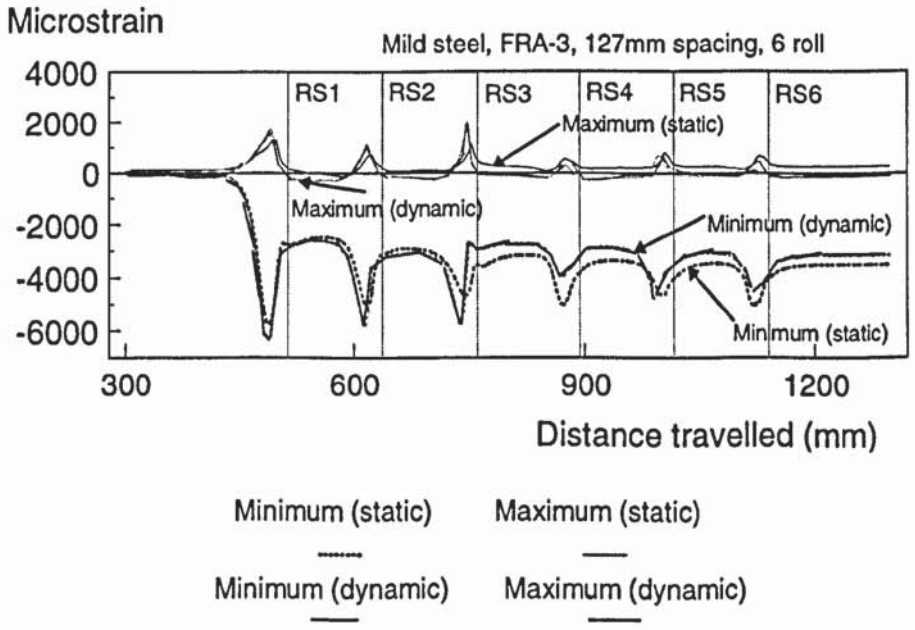

Figure 5.19. Comparison of static and dynamic principal strain distributions.

5.2.4 Plastic strain measurement

In order to measure the plastic strain, a dotted grid (2.0 mm x 2.0 mm) is marked on the surface of the mild steel strip using a milling machine and a pointed tool. The horizontal and vertical grid distances are measured using the OMIS II (Optical Measurement Inspection System) before deformation. During the forming, the partially roll-formed strip is removed from the mill, enabling grid measurements to be made (Figure 5.20).

Figure 5.20 Partially Formed Specimen.

Two tests are conducted using the CRF mill No:2 (Table 5.6), with mild steel strips and 3 and 6 roll stations. Two different interpass distances, 200 mm and 140 mm, are selected to investigate its influence on plastic strain during forming.

Table 5.6 Schedule of tests carried out for plastic strain measurement

CRF mill No: 1 Test mode : Plastic strain measurement			
Test No.	Material	Interpass Distance	No. of Roll stations
1	Mild Steel	200 mm	3
2	Mild Steel	140 mm	6

5.3 Experimental Results

Figures 5.21 to 5.25 show samples of different types of strain distributions measured as the workpiece is formed. A detailed discussion of the behaviour pattern of the strains will be given in Chapter 9 (Discussion and Conclusion).

(a) Longitudinal strains (static) in the flange near the edge

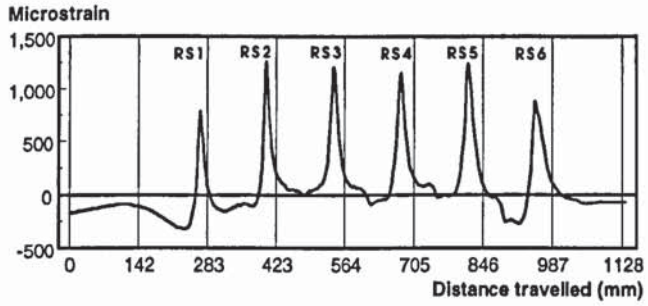

Figure 5.21. Longitudinal strains (static) in the the flange

The longitudinal strains near the free edge of the flange typically follows the pattern shown in Figure 5.21. The longitudinal strains are positive slightly ahead of each roll station. As the material passes through the roll centre line there is a sharp drop in the magnitude of the strain and becomes compressive.

(b) Lateral strains (static) in the flange near the edge

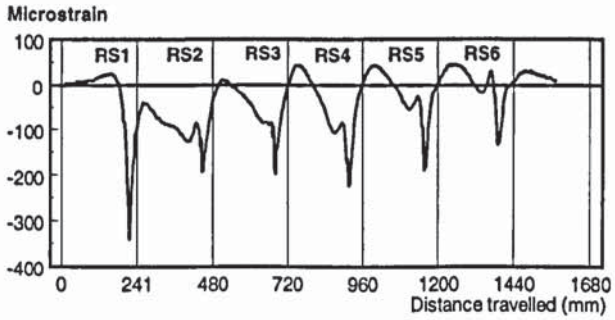

Figure 5.22 Lateral strains in the flange (static)

The lateral strains near the edge are compressive as the material approaches the roll station. As the material passes through the roll centre line, the strains become positive.

(c) Longitudinal strains in the web (static)

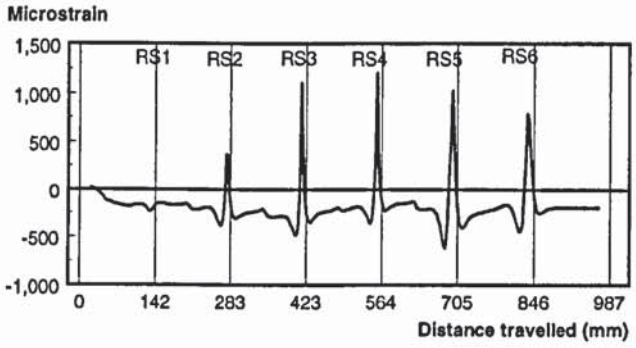

Figure 5.23 Longitudinal strains in the web (static)

The longitudinal strains at the centre line of the web have been measured and they reach tensile peaks slightly ahead of the roll centres. These strains become compressive as the material exits the roll stations.

(d) Longitudinal strains (dynamic) in the flange near the edge

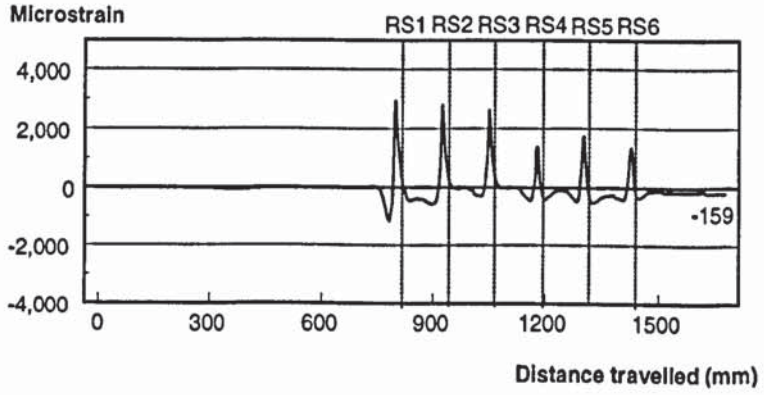

Figure 5.24. Longitudinal strains (dynamic) in the flange.

The dynamic longitudinal strains follow the same pattern as the static strains.

(e) Lateral strains (dynamic) in the flange near the edge

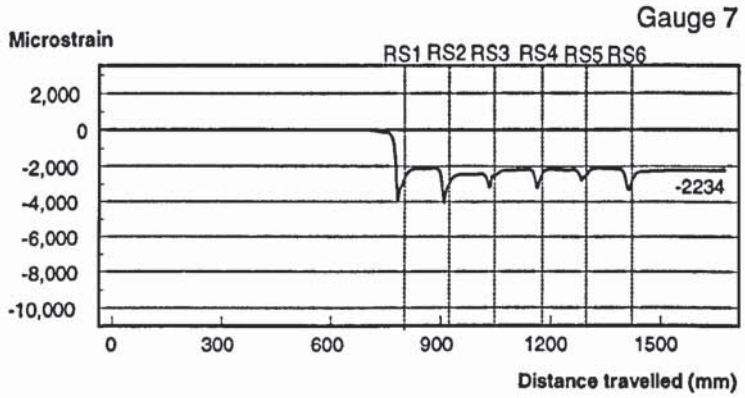

Figure 5.25. Lateral strains (dynamic) in the flange.

The dynamic lateral strains follow the same pattern as the static strains.

(f) Principal Strains

The maximum and minimum principle strains in the steel and aluminium specimens are shown in Figures 5.20 and 5.27 respectively.

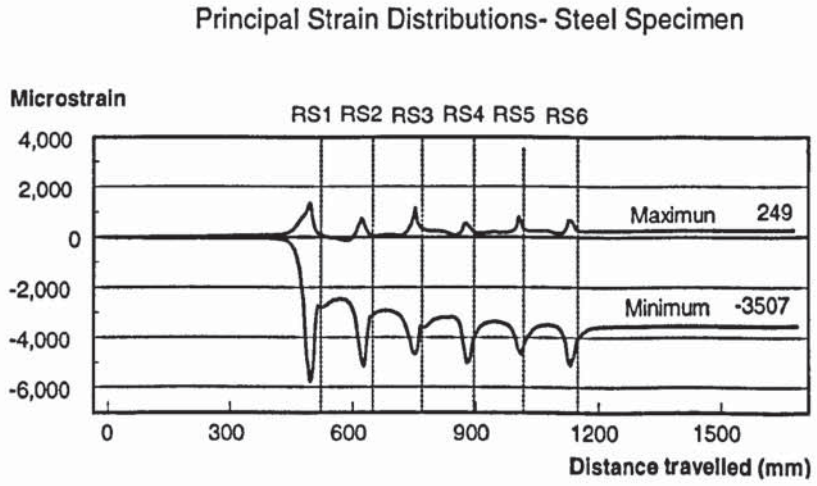

Figure 5.26. Maximum and Minimum Principal Strains in the Steel Specimen

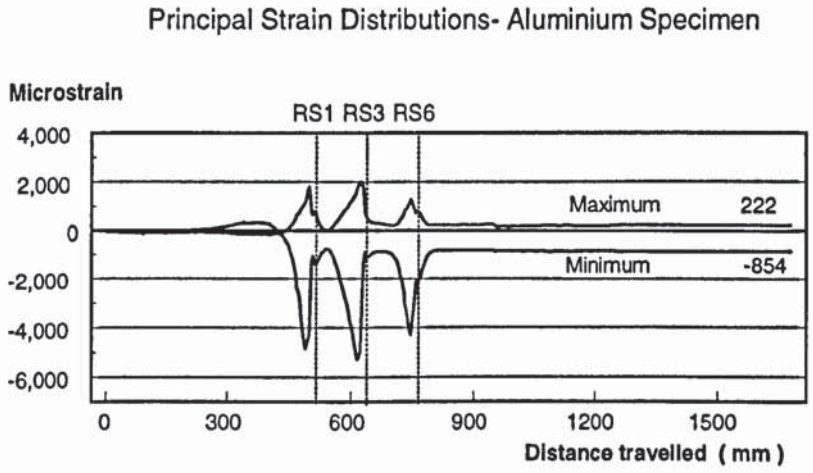

Figure 5.27 Maximum and Minimum Principal Strains in an Aluminium Specimen

Tables 5.7 and 5.8 show a comprehensive listing of results for the experiments carried out to measure static and dynamic strains for steel and aluminium specimens using CRF mills 1 and 2.

Table 5.7. Schedule of experimental results listed in Appendix B (CRF Mill No:1).

Figure (Appendix B)	Gauge	Material	No: of rollers	Interpass distance (mm)	Mode	Quantity
B1	1	Mild Steel	6	127	Static	$\varepsilon_{longitudinal}$ - Web
B2	2	Mild Steel	6	127	Static	$\varepsilon_{lateral}$ - Flange
B1	3	Mild Steel	6	127	Static	$\varepsilon_{longitudinal}$ - Flange
B2	4	Mild Steel	6	127	Static	$\varepsilon_{lateral}$ - Flange
B1	5	Mild Steel	6	127	Static	$\varepsilon_{longitudinal}$ - Flange
B2	6	Mild Steel	6	127	Static	$\varepsilon_{45°}$ - Flange
B2	7	Mild Steel	6	127	Static	$\varepsilon_{lateral}$ - Flange
B1	8	Mild Steel	6	127	Static	$\varepsilon_{longitudinal}$ - Flange
B3	1	Aluminium	6	127	Static	$\varepsilon_{longitudinal}$ - Web
B4	2	Aluminium	6	127	Static	$\varepsilon_{lateral}$ - Flange
B3	3	Aluminium	6	127	Static	$\varepsilon_{longitudinal}$ - Flange
B4	4	Aluminium	6	127	Static	$\varepsilon_{lateral}$ - Flange
B3	5	Aluminium	6	127	Static	$\varepsilon_{longitudinal}$ - Flange
B4	6	Aluminium	6	127	Static	$\varepsilon_{45°}$ - Flange
B4	7	Aluminium	6	127	Static	$\varepsilon_{lateral}$ - Flange
B3	8	Aluminium	6	127	Static	$\varepsilon_{longitudinal}$ - Flange
B5	1	Mild Steel	3	2 x 127	Static	$\varepsilon_{longitudinal}$ - Web
B6	2	Mild Steel	3	2 x 127	Static	$\varepsilon_{lateral}$ - Flange
B5	3	Mild Steel	3	2 x 127	Static	$\varepsilon_{longitudinal}$ - Flange
B6	4	Mild Steel	3	2 x 127	Static	$\varepsilon_{lateral}$ - Flange
B5	5	Mild Steel	3	2 x 127	Static	$\varepsilon_{longitudinal}$ - Flange
B6	6	Mild Steel	3	2 x 127	Static	$\varepsilon_{45°}$ - Flange
B6	7	Mild Steel	3	2 x 127	Static	$\varepsilon_{lateral}$ - Flange
B5	8	Mild Steel	3	2 x 127	Static	$\varepsilon_{longitudinal}$ - Flange
B7	1	Aluminium	3	2 x 127	Static	$\varepsilon_{longitudinal}$ - Web
B8	2	Aluminium	3	2 x 127	Static	$\varepsilon_{lateral}$ - Flange
B7	3	Aluminium	3	2 x 127	Static	$\varepsilon_{longitudinal}$ - Flange
B8	4	Aluminium	3	2 x 127	Static	$\varepsilon_{lateral}$ - Flange
B7	5	Aluminium	3	2 x 127	Static	$\varepsilon_{longitudinal}$ - Flange
B8	6	Aluminium	3	2 x 127	Static	$\varepsilon_{45°}$ - Flange
B8	7	Aluminium	3	2 x 127	Static	$\varepsilon_{lateral}$ - Flange
B3	8	Aluminium	3	2 x 127	Static	$\varepsilon_{longitudinal}$ - Flange
B9	1	Mild Steel	3	127	Static	$\varepsilon_{longitudinal}$ - Web
B10	2	Mild Steel	3	127	Static	$\varepsilon_{lateral}$ - Flange
B9	3	Mild Steel	3	127	Static	$\varepsilon_{longitudinal}$ - Flange
B10	4	Mild Steel	3	127	Static	$\varepsilon_{lateral}$ - Flange
B9	5	Mild Steel	3	127	Static	$\varepsilon_{longitudinal}$ - Flange
B10	6	Mild Steel	3	127	Static	$\varepsilon_{45°}$ - Flange
B10	7	Mild Steel	3	127	Static	$\varepsilon_{lateral}$ - Flange
B9	8	Mild Steel	3	127	Static	$\varepsilon_{longitudinal}$ - Flange

Table 5.7 (Continued)

Figure (Appendix B)	Gauge	Material	No: of rollers	Interpass distance (mm)	Mode	Quantity
B11	1	Aluminium	3	127	Static	$\varepsilon_{longitudinal}$ - Web
B12	2	Aluminium	3	127	Static	$\varepsilon_{lateral}$ - Flange
B11	3	Aluminium	3	127	Static	$\varepsilon_{longitudinal}$ - Flange
B12	4	Aluminium	3	127	Static	$\varepsilon_{lateral}$ - Flange
B11	5	Aluminium	3	127	Static	$\varepsilon_{longitudinal}$ - Flange
B12	6	Aluminium	3	127	Static	$\varepsilon_{45°}$ - Flange
B12	7	Aluminium	3	127	Static	$\varepsilon_{lateral}$ - Flange
B11	8	Aluminium	3	127	Static	$\varepsilon_{longitudinal}$ - Flange
B13	1	Mild Steel	6	127	Dynamic	$\varepsilon_{longitudinal}$ - Web
B14	2	Mild Steel	6	127	Dynamic	$\varepsilon_{lateral}$ - Flange
B13	3	Mild Steel	6	127	Dynamic	$\varepsilon_{longitudinal}$ - Flange
B14	4	Mild Steel	6	127	Dynamic	$\varepsilon_{lateral}$ - Flange
B13	5	Mild Steel	6	127	Dynamic	$\varepsilon_{longitudinal}$ - Flange
B14	6	Mild Steel	6	127	Dynamic	$\varepsilon_{45°}$ - Flange
B14	7	Mild Steel	6	127	Dynamic	$\varepsilon_{lateral}$ - Flange
B13	8	Mild Steel	6	127	Dynamic	$\varepsilon_{longitudinal}$ - Flange
B15	1	Mild Steel	3	127	Dynamic	$\varepsilon_{longitudinal}$ - Web
B16	2	Mild Steel	3	127	Dynamic	$\varepsilon_{lateral}$ - Flange
B15	3	Mild Steel	3	127	Dynamic	$\varepsilon_{longitudinal}$ - Flange
B16	4	Mild Steel	3	127	Dynamic	$\varepsilon_{lateral}$ - Flange
B15	5	Mild Steel	3	127	Dynamic	$\varepsilon_{longitudinal}$ - Flange
B16	6	Mild Steel	3	127	Dynamic	$\varepsilon_{45°}$ - Flange
B16	7	Mild Steel	3	127	Dynamic	$\varepsilon_{lateral}$ - Flange
B15	8	Mild Steel	3	127	Dynamic	$\varepsilon_{longitudinal}$ - Flange
B17	1	Mild Steel	3	2 x 127	Dynamic	$\varepsilon_{longitudinal}$ - Web
B18	2	Mild Steel	3	2 x 127	Dynamic	$\varepsilon_{lateral}$ - Flange
B17	3	Mild Steel	3	2 x 127	Dynamic	$\varepsilon_{longitudinal}$ - Flange
B18	4	Mild Steel	3	2 x 127	Dynamic	$\varepsilon_{lateral}$ - Flange
B17	5	Mild Steel	3	2 x 127	Dynamic	$\varepsilon_{longitudinal}$ - Flange
B18	6	Mild Steel	3	2 x 127	Dynamic	$\varepsilon_{45°}$ - Flange
B18	7	Mild Steel	3	2 x 127	Dynamic	$\varepsilon_{lateral}$ - Flange
B17	8	Mild Steel	3	2 x 127	Dynamic	$\varepsilon_{longitudinal}$ - Flange
B19	Rosette	Aluminium	6	127	Static	Principal Strain
B19	Rosette	Mild Steel	6	127	Static	Principal Strain
B19	Rosette	Aluminium	3	127	Static	Principal Strain
B19	Rosette	Mild Steel	3	127	Static	Principal Strain
B20	Rosette	Aluminium	3	2 x 127	Static	Principal Strain
B20	Rosette	Mild Steel	3	2 x 127	Static	Principal Strain
B20	Rosette	Mild Steel	6	127	Dynamic	Principal Strain
B20	Rosette	Mild Steel	3	127	Dynamic	Principal Strain

Table 5.8. Schedule of experimental results listed in Appendix B (CRF Mill No:2).

Figure (Appendix B)	Gauge	Specimen Material	No: of rollers	Interpass distance (mm)	Mode	Quantity
B21	1	Mild Steel	6	140	Static	$\varepsilon_{lateral}$ - Flange
B21	1	Mild Steel	6	240	Static	$\varepsilon_{lateral}$ - Flange
B21	2	Mild Steel	6	140	Static	$\varepsilon_{longitudinal}$ - Flange
B21	2	Mild Steel	6	240	Static	$\varepsilon_{longitudinal}$ - Flange
B22	3	Mild Steel	6	140	Static	$\varepsilon_{lateral}$ - Flange
B22	3	Mild Steel	6	240	Static	$\varepsilon_{lateral}$ - Flange
B22	4	Mild Steel	6	140	Static	$\varepsilon_{longitudinal}$ - Flange
B22	4	Mild Steel	6	240	Static	$\varepsilon_{longitudinal}$ - Flange
B23	5	Mild Steel	6	140	Static	ε_{45° - Flange
B23	5	Mild Steel	6	240	Static	ε_{45° - Flange
B23	6	Mild Steel	6	140	Static	$\varepsilon_{longitudinal}$ - Flange
B23	6	Mild Steel	6	240	Static	$\varepsilon_{longitudinal}$ - Flange
B24	7	Mild Steel	6	140	Static	$\varepsilon_{lateral}$ - Flange
B24	7	Mild Steel	6	240	Static	$\varepsilon_{lateral}$ - Flange
B24	8	Mild Steel	6	140	Static	$\varepsilon_{longitudinal}$ - Web
B24	8	Mild Steel	6	240	Static	$\varepsilon_{longitudinal}$ - Web
B25	Rosette	Mild Steel	6	140	Static	Principal Strain
B25	Rosette	Mild Steel	6	240	Static	Principal Strain
B25	Rosette	Mild Steel	6	140	Static	Principal Strain
B25	Rosette	Mild Steel	6	240	Static	Principal Strain
B26	1	Aluminium	6	140	Static	$\varepsilon_{lateral}$ - Flange
B26	1	Aluminium	6	240	Static	$\varepsilon_{lateral}$ - Flange
B26	2	Aluminium	6	140	Static	$\varepsilon_{longitudinal}$ - Flange
B26	2	Aluminium	6	240	Static	$\varepsilon_{longitudinal}$ - Flange
B27	3	Aluminium	6	140	Static	$\varepsilon_{lateral}$ - Flange
B27	3	Aluminium	6	240	Static	$\varepsilon_{lateral}$ - Flange
B27	4	Aluminium	6	140	Static	$\varepsilon_{longitudinal}$ - Flange
B27	4	Aluminium	6	240	Static	$\varepsilon_{longitudinal}$ - Flange
B28	5	Aluminium	6	140	Static	ε_{45° - Flange
B28	5	Aluminium	6	240	Static	ε_{45° - Flange
B28	6	Aluminium	6	140	Static	$\varepsilon_{longitudinal}$ - Flange
B28	6	Aluminium	6	240	Static	$\varepsilon_{longitudinal}$ - Flange
B29	7	Aluminium	6	140	Static	$\varepsilon_{lateral}$ - Flange
B29	7	Aluminium	6	240	Static	$\varepsilon_{lateral}$ - Flange
B29	8	Aluminium	6	140	Static	$\varepsilon_{longitudinal}$ - Web
B29	8	Aluminium	6	240	Static	$\varepsilon_{longitudinal}$ - Web
B30	Rosette	Mild Steel	6	140	Static	Principal Strain
B30	Rosette	Mild Steel	6	240	Static	Principal Strain
B30	Rosette	Mild Steel	6	140	Static	Principal Strain
B30	Rosette	Mild Steel	6	240	Static	Principal Strain

CHAPTER 6

AN APPROXIMATE METHOD TO PREDICT STRAIN DEVELOPMENT IN COLD ROLL FORMING USING FINITE ELEMENT ANALYSIS

In order to design roll tooling to produce a roll formed section successfully, a means of predicting the maximum strains induced in the workpiece during the forming process is essential. Finite Element Analysis of the cold roll forming process is used in this research for this purpose. The trapezoidal section formed by the CRF Mill No:1 was analysed. The commercially available MARC® Finite Element Analysis package has been used in the analysis. As a large number of relatively cheap finite element packages are commercially available today, the use of such a package is useful in the practical design of CRF tooling.

6.1 Previous Research Work in the Simulation of Cold Roll Forming Process using Finite Element Analysis and other Analytical Methods.

Due to the complexities involved in the deformation of the sheet metal, the design of roll formed products, roll pass sequences and forming tools remains more of an art than a science. There are several CAD programs available on the market for the design of forming tools and roll pass sequences. However, these programs are based on rather simplified formulae or empirical rules and to a large extent, perform the same experience based functions as is done by the experienced designer, only faster and more accurately. Duggal et al has developed a computer aided simulation program, Roll Forming Profile Analysis and Simulation Software (RFPASS), based on deformation mechanics[Duggal]. Simulation results have been compared with

experimental measurements found in the literature. The program, RFPASS, has been used to analyse simple cross sectional profiles such as U, V and the C channels.

Finite element modelling of cold roll forming was validated by McClure and Li. ABAQUS® finite element modelling software was used to simulate experiments involving roll forming of symmetrical channel sections from mild steel. A comparison was made between measured and computed longitudinal membrane strains at two positions on the workpiece. Results were obtained at four bend angles. The simulation was able to reproduce the essential features of the experimentally determined membrane strain traces[McClure].

Kiuchi and his fellow researchers have developed a computerised numerical simulation system for cold roll-forming. It was applied to various roll-forming processes of electric resistance welded pipes and light gauge steel sections. Through simulations, the effects of roll pass-schedules, roll geometry, dimensions of the product, stresses and strains occurring in the product, roll separating forces and roll driving torque were clarified. The system is now being used for design of profiles of forming rolls, roll positions and other operation factors. It is also being successfully used to design roll pass-schedules for new products[Kiuchi4].

Nefussi and Gilormini has proposed a kinematical approach for predicting the optimal shape and the deformed length of a metal sheet during cold-roll forming, before the first roll stand. The middle surface of the sheet is described as a Coons patch depending on one geometrical parameter. A velocity field is then defined on this surface so that the plastic work rate depends only on this single geometrical parameter. Its minimisation gives the optimal shape for a strain-hardening rigid-plastic material. This approach has been implemented on a workstation, and it allows a very fast simulation of the process. Moreover, this method can be extended to different shapes, and the whole process including several roll stands can also be calculated [Nefussi].

The traditional design of roll-former tooling calls not only for laborious drafting techniques and hand calculations to ensure geometric accuracy, but also is extremely error-prone due to the tedious procedures involved and lack of a scientific basis for the examination of possible design options. Hence, lengthy trials are often required, with subsequent costly alterations, before full production can commence. Haritos, Ghosh and Milner have investigated the feasibility of linking a finite-element package such as PAFEC® to a CAD/CAM system for cold roll-forming [Haritos].

6.2 MARC® Finite Element Analysis Program

The MARC system consists of the following series of integrated programs. **MARC,** MESH3D, MARC-PLOT, MARC-PIPE, **MENTAT.** Fig 6.1 shows how various modules corresponding to pre-processing, analysis and post-processing are inter-connected to form the MARC system. MARC is capable of performing linear or non-linear stress analysis in the static and dynamic regimes. The non-linearities may be due to material behaviour, large deformation or boundary conditions.

MESH3D automatically generates three-dimensional mesh data using either 8-node or 20-node brick elements (MESH3D will not be used for this project).

MARC-PLOT is a post-processor plotting program. (MARC-PLOT will not be used for this project).

MARC-PIPE is a program for generating mesh for analysing a piping system consisting of straight and curved sections (MARC-PIPE will not be used for this project).

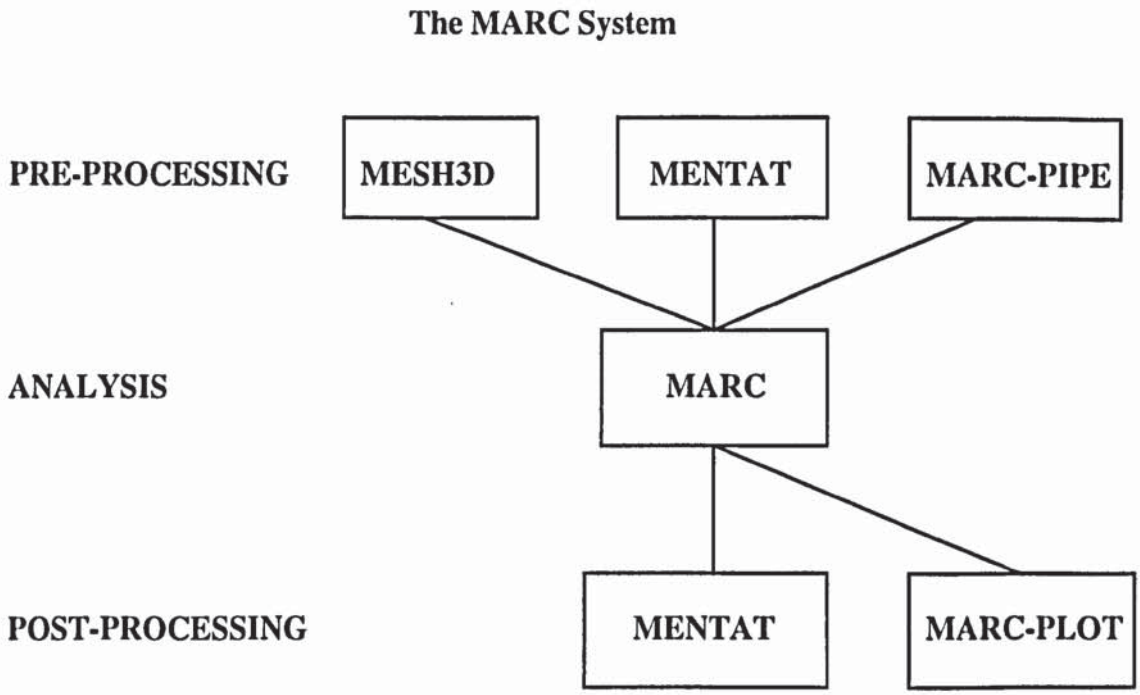

Fig 6.1. MARC Finite Element Analysis Program Structure [MARC].

MENTAT is an interactive program for pre- and post processing. *MENTAT* can process both two- and three- dimensional meshes to carry out the following:

- Generate and display a mesh
- Generate and display boundary conditions and loadings
- Perform post-processing to generate the contour, deformed shape and time history plots

The data that is processed includes:

- Nodal co-ordinates
- Element Connectivity
- Nodal boundary conditions
- Nodal co-ordinate systems
- Element material properties

- Element geometric properties
- Element and nodal sets
- Element loads
- Nodal loads/ non zero boundary conditions

The MARC program has four libraries. These contain structural procedures, materials, elements and program functions.

Non-linear Analysis

MARC finite element program can be used for non-linear , as well as linear problems. Non-linear finite element techniques are essential in analysing metal forming problems. A problem is non-linear if the force-displacement relationship depends on the current state (i.e., current displacement, force and stress-strain relationship).

Let **u** be a generalised displacement vector, **P**, a generalised force vector, and **K** the stiffness matrix. The expression of the force-displacement relations for a non-linear problem is

$$\mathbf{P} = \mathbf{K}(\mathbf{P}, \mathbf{u})\,\mathbf{u} \qquad (1)$$

Linear problems form a subset of non-linear problems. For example , the above equation becomes

$$\mathbf{P} = \mathbf{K}\,\mathbf{u} \qquad (2)$$

where, the stiffness matrix **K** is independent of both **u** and **P.**

There are three sources of non-linearity: material, geometric, and non-linear boundary conditions.

- Material non-linearity results from the non-linear relationship between stresses and strains. Models for these relationships cannot be derived along purely mathematical lines, but rather are rather based on experimental data.

- Geometric non-linearity results from large strain effects and large deflections with small strains. As displacements grow in size, the displaced co-ordinates of a finite

element can change the structural stiffness in a variety ways. Typically, the problem is non-linear and it is necessary to iterate to obtain a valid solution.

Large Displacements with Large Strains

The overall stiffness of a structure depends on the orientation and individual stiffness of its component parts. As the nodes of an element undergo displacement, the contribution from the element to the overall structural stiffness can change in two ways. First, as the shape of the element changes, its individual element stiffness will change. Second, if the orientation of the element changes, the transformation of its local stiffness into global stiffness will also change.
Small deflection and small strain analyses assume that displacements are small enough that the resulting stiffness changes are insignificant. This assumption of unchanging stiffness implies that one iteration, using the structural stiffness based on original geometry is sufficient to calculate displacements in a small-deformation analysis.

In contrast, large strain analyses account for the stiffness changes that result from changes in the shape and orientation of the element. Because the stiffness is affected by the displacements, and vice-versa, an iterative solution is required to obtain the correct displacements in a large strain analysis. For large displacement, large strain problems, the constitutive relation must be defined in the correct frame of reference and transformed from this frame of reference to the one in which the equilibrium equations are written.

Large Deflections with small strains

Some elements support large rotation effects, but do not support large shape changes. A limited form of the large strain feature called large deflection is available for such elements. In a large deflection analysis, element rotations can be large, but the strains are assumed to be small. For large displacement and small strain problems, changes in the stress-strain law may be neglected, but the

contributions from non-linear terms in the strain displacement relations must not be neglected.

- Contact and friction problems may also cause non-linearity. Contact and friction problems lead to non-linear boundary conditions. This type of non-linearity plays an important role in metal forming problems.

Non-linear analysis is more complex and expensive than linear analysis. The frontal solver of the program operates on a set of linear equations to predict the response of an engineering system. However, a non-linear behaviour of a structure cannot be represented directly with such a set of linear equations . A series of successive linear approximations with corrections are needed to solve non-linear problems.

In general, the solutions of non-linear problems always require incremental solution schemes and sometimes require iterations (or recycles) within each load/time increment to ensure that equilibrium is satisfied at the end of each step. Superposition cannot be applied in non-linear problems.

Non-linear analyses require good judgement and use considerable computing time. Since they often require several runs, the first run should extract the maximum amount of information with the minimum amount of computing time. Some considerations for a *preliminary run* are as follows:

1. Minimise degrees of freedom whenever possible
2. Use a small number of load increments to reduce computing time
3. Use a coarse tolerance on convergence to reduce the number of iterations. A course tolerance on convergence determines the area of most rapid change where additional load increments may be required.

MARC solves large displacement non-linear static problems according to the tangent modulus method. This method requires at least the following three controls:

1. A tolerance on convergence
2. A maximum to the maximum allowable number of recycles
3. Specification of a minimum number of recycles

Several load incrementation options are available in the program to input mechanical load increments.

LOAD	OPTIONS
Mechanical (Force / Displacement)	Proportional Increment Point Load Distributed Load Auto Load Boundary Change Displacement Change Auto Time

The model definition option RESTART creates a restart tape for the current analysis which may be used in a subsequent analysis. It may also be used to read in a previously generated tape to continue the analysis. The RESTART option is important for any multi-increment analysis as it allows the user to continue the analysis at a later time.

MARC uses the incremental method in plasticity analysis. Load incrementation can be prescribed automatically or manually through a variety of options. The program control is based upon iteration. The two extreme approaches to solving non-linear equations are to solve a large number of small steps with few iterations or to solve one large step with many iterative cycles. Generally it is best to employ a combination of both. Whenever multiple substeps are used, it is necessary to achieve a balance between accuracy and economy. Using more substeps (i.e., small time step sizes) usually result in better accuracy, but at a cost of increased run times.

The residual load is applied as a correcting force to ensure that equilibrium is maintained and hence an accurate solution is obtained for non-linear problems. The residual load correction enforces global equilibrium at the start of each new increment. This prevents the accumulation of out-of-equilibrium forces from increment to increment and makes the solution less sensitive to step size. The residual load correction is the difference between the internal forces and the externally applied loads.

There are two fundamentally different approaches for the description of large deformation problems: the Eulerian method and the Lagrangian method. In the Eulerian method, the finite element mesh is fixed in space and the material flows through the mesh. This approach is particularly suitable for analysis of steady-state processes such as extrusion.

The approach is not advantageous when the constitutive equations depend on the current strains or deformation histories. These problems are more easily handled by the Lagrangian method. In this method, the finite element mesh is attached to the material and moves through space along with the material. There are two varieties of Lagrangian method: the total Lagrangian method, where the mesh co-ordinates are not updated to new positions and the updated Lagrangian method where the co-ordinates of the mesh are updated after each increment.

The total Lagrangian approach is useful for problems in plasticity and creep, where moderately large rotations but small strains occur. In the total Lagrangian approach, the large displacement formulation is based on the initial element geometry. To input tolerances for large displacement analysis, the model definition option CONTROL is used.

In the updated Lagrangian approach, the element stiffness matrix is assembled in the current configuration of the element, and the stress and strain output are given with respect to the co-ordinate system in the updated configuration of the element. The

updated Lagrangian approach is useful in (a) analysis of shell and beam structures in which rotations are large so that the non-linear terms in the curvature expressions may no longer be neglected and (b) large strain plasticity analysis, for calculations in which the plastic deformations cannot be assumed to be infinitesimal. The combination of LARGE DISP, UPDATE and FINITE results in a complete large strain plasticity formulation. The program internally uses true (Cauchy) stress and true deformation rate. For large displacements and strains, the solution is obtained as a series of piece-wise linear increments, so that suitable small load steps must be taken. When extremely large deformations occur, the element mesh should be designed so that it can follow these deformations without complete degeneration of elements. The shape of the structure after the application of the loads must be borne in mind and the mesh adapted in order to obtain a reasonable solution. It is possible to use re-zoning when using the lower order incompressible elements.

In the analysis of metal forming problems by the finite element method, an Eulerian flow-type approach and a total Lagrangian approach can be used for steady-state and transient problems. The updated Lagrangian procedure is most suitable for analysis of large strain plasticity problems. The main reasons for this are,

- its ability to trace free boundaries and
- the flexibility of taking history effects into account.

The large strain capability of MARC allows the analysis of problems of large-strain, elastic-plastic material behaviour. The analysis involves both material and geometric non-linearities. In performing finite deformation elastic-plastic analysis, there are some special considerations. These are:

- Correct choice of finite element types
- In addition to the usual criteria for selection, the element selected needs to be insensitive to strong distortion and for three-dimensional problems, the element mesh must be able to represent non-dilational (incompressible) deformation modes.

- Nearly incompressible behaviour
- MARC recommends the use of lower order elements, invoking the constant dilation option.
- Treatment of boundary conditions
- In many large strain problems, especially in metal forming problems , the metal slides over curved surfaces with or without friction. The MARC gap friction element and contact option can model these boundary conditions.
- Severe mesh distortion
- Because the mesh is attached to the material, severe distortion of the mesh occurs during deformation
- Instabilities in the material description

For the large strain plasticity option, the work hardening slope for plasticity is the true stress/true plastic strain rate. The work hardening curve must therefore be entered as the true stress/logarithmic plastic strain in a uniaxial tension test.

Yield stress and work hardening are two experimentally related phenomena that characterise plastic material behaviour. A flow rule is essential in establishing the incremental stress-strain relations for plastic material. The flow rule describes the differential changes in the plastic strain components $d\varepsilon^P$ as a function of the current state of stress.

The Prandtl-Reuss representation of the flow rule is available in MARC.

$$d\varepsilon^P = d\bar{\varepsilon}^P \frac{\partial \bar{\sigma}}{\partial \sigma}$$

where $d\bar{\varepsilon}^P$ and $\bar{\sigma}$ are equivalent plastic strain increment and equivalent stress, respectively. The above equation expresses the condition that the direction of inelastic straining is normal to the yield surface. This condition is called either the normality condition or the associated flow rule. If the von Mises yield surface is used, then the normal is equal to the deviatoric stress.

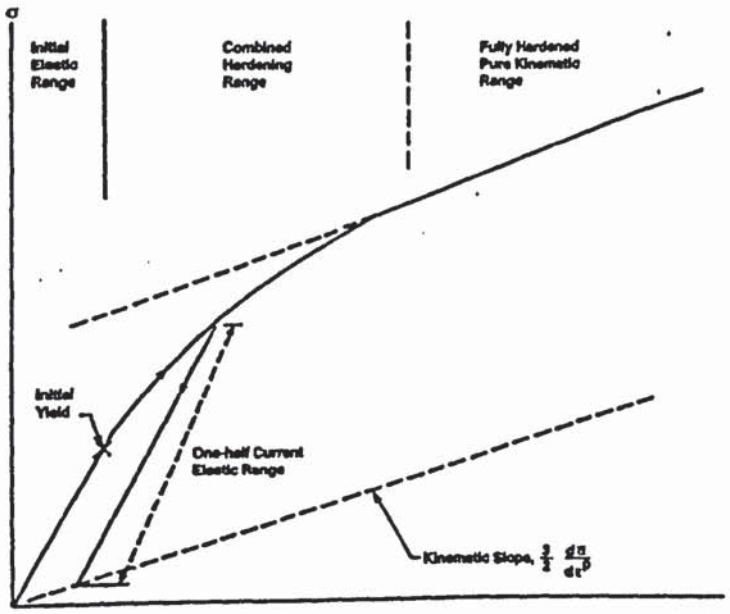

Figure 6.2. Basic Uniaxial Tension Behaviour of the combined Hardening Model [MARC].

The significance of this representation is illustrated in Figure 6.2. This figure illustrates the "stress-space" for the two-dimensional case. The solid curve gives the yield surface (locus of all stress states causing yield) as defined by the von Mises criterion.

The full Newton-Raphson method is the default in the MARC program for the solution of non-linear equations. This method has quadratic convergence properties. This means that, in subsequent iteration, the relative error decreases quadratically. If material non-linearities are present, some approximations slow down convergence. The full Newton-Raphson method provides good results for most non-linear problems, but is expensive for large, three-dimensional problems, when the direct solver is used.

A number of history definition options are available for input of multiple load increments. For example, the AUTO LOAD option generates a specified number of

increments, all having the same load increment, and is useful for non-linear analysis with proportional loads

MARC can minimise the nodal bandwidth of a structure in a number of ways. The amount of storage is directly related to the size of the bandwidth and the computation time increases in proportion to the square of the average bandwidth. The OPTIMIZE option allows the choice of several bandwidth optimization algorithms. The Cuthill-McKee algorithm is used in this analysis. The combination of LARGE DISP, UPDATE and FINITE results in a complete plasticity formulation. The program internally uses true (Cauchy) stress and the true deformation rate.

Work hardening Rules

In a uniaxial test, the work hardening slope is defined as the slope of the stress-plastic strain curve. The work hardening slope relates the incremental plastic strain in the inelastic region and dictates the conditions of subsequent yielding. A number of work hardening rules (isotropic, kinematic and combined) are available in MARC. A uniaxial stress-plastic strain curve may be represented by a piecewise linear function through the WORK HARD option. As an alternative, work hardening can be specified through the user subroutine WKSLP.

There are two methods to enter this information, using the WORK HARD option. In the first method, work hardening slopes for uniaxial stress data as a change in stress per unit of plastic strain (Figure 6.3) and the plastic strain at which these slopes become effective (breakpoints) .

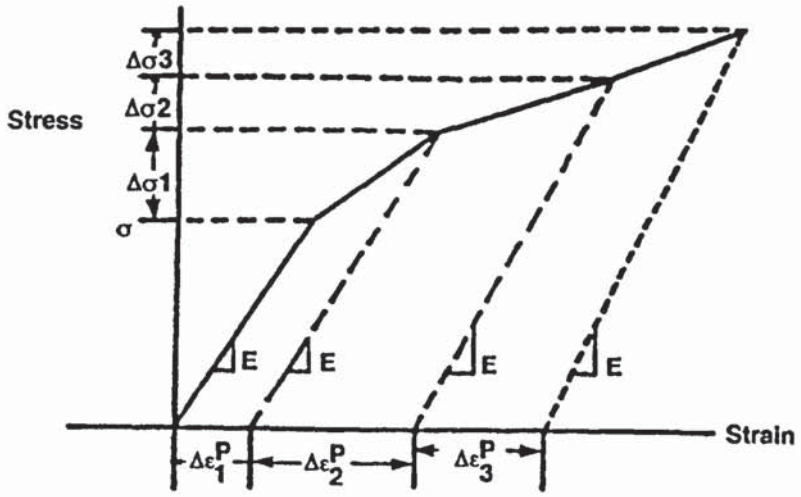

Figure 6.3. Work hardening slopes[MARC].

Singularity Ratio

The singularity ratio is a measure of the conditioning of the matrix. The ratio is printed each time there is a solution of the matrix equation. The influence of the non linearities in the structure can be measured by examining the change in singularity ratios between increments.

Convergence

During the execution of the program, several messages are printed that concern the convergence of the solution. These messages indicate the displacement, velocity or residual error and are very important because they provide information concerning the accuracy of the solution procedure. These messages also indicate the ratio of the error and its relative quantity. This ratio must be less than that given in CONTROL option for convergence to occur.

Solution of Linear Equations

The finite element formulation leads to a set of linear equations. The solution is obtained through numerically inverting the system. Figure 6.4 shows the MARC program flow diagram.

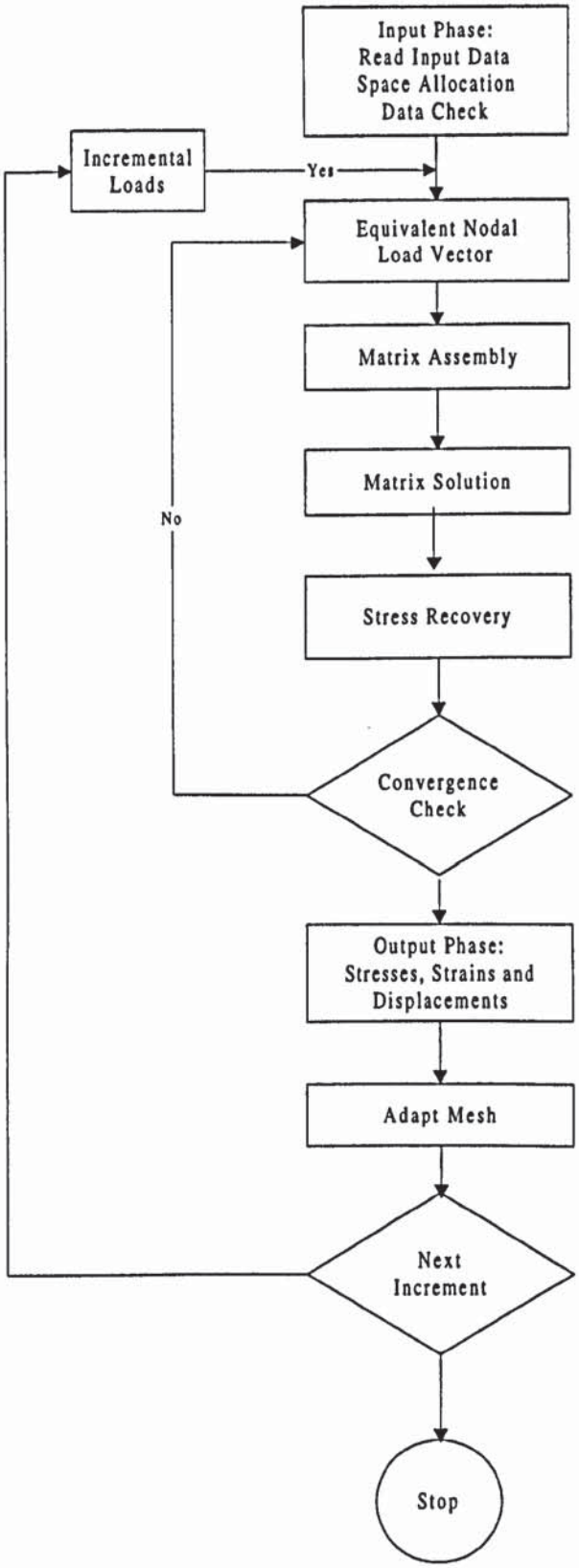

Figure 6.4. MARC Program Flow Diagram [MARC].

6.3 Modelling the Cold Roll Forming Process

In this simulation the sheet metal is modelled with a 4-node shell element (type 75) with global displacements and rotations as degrees of freedom[MARC]. Bi-linear interpolation is used for the co-ordinates, displacements and rotations. The above 4-node shell element is a very efficient and simple element and it exhibits correct behaviour in the limiting case of thin shells. It can be used in curved shell analysis as well as in the analysis of complicated plate structures. Due to its simple formulation when compared with the standard higher order shell elements, it is less expensive and, therefore, very attractive in non-linear analysis. Seven layers are used through the thickness of the shell.

The ISOTROPIC work-hardening (with a work slope of zero) is the default option in MARC. To explicitly specify the isotropic hardening option in MARC, the model definition options ISOTROPIC or ORTHOTROPIC option is used together with work hardening data.

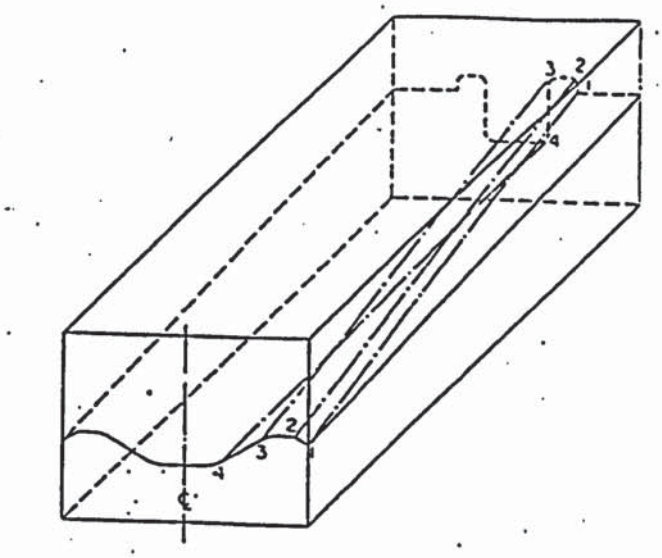

Figure 6.5 Roll form layout [Angel2].

Theoretically, a roll form layout may be compared with a solid block of die material which is machined to the shape to be formed from flat to finished section (Figure 6.5). If this block were divided into an infinite number of slices, each slice would be converted into a roll with identical profile and become a roll form pass. The greater the number of passes or greater the length from flat to finished shape, the easier would be the progressive forming operation.

In the finite element analysis, boundary conditions have to be applied to the metal workpiece. During the cold roll forming process, the longitudinal free edge of a strip of metal (Figure 6.6) of length AF (in the original undeformed state) is stretched so that its length is A′F′. After the forming process, the length of the workpiece would be AF. The length of the free edge is increased from AF to A′F′ temporarily.
It is assumed that

- Point A moves to A′and point F moves to F′, the intermediate points B,C,D,E moving to B′, C′, D′, E′ respectively
- These points A,B,C,D,E and F also lie in planes passing through the roll centres

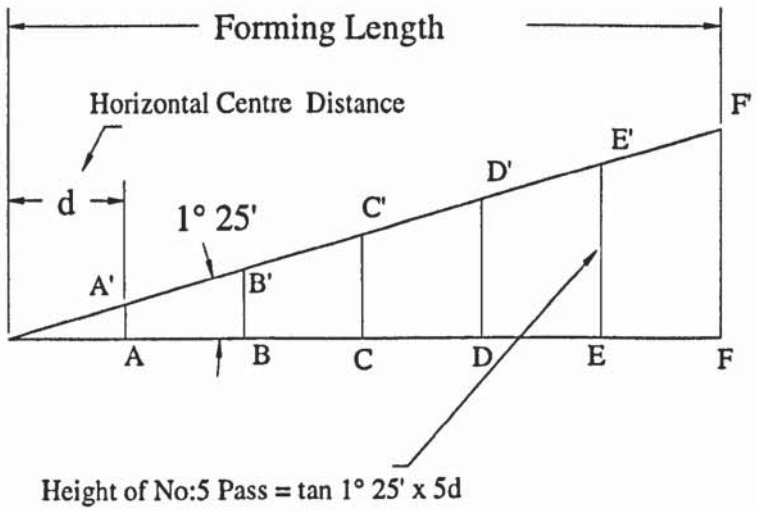

Figure 6.6. Schematic layout of the section height at each pass, the forming angles and total forming length.

An experiment was carried out to determine the validity of the above assumption. A fine grid representing the mesh used in the finite element model was engraved on a strip of metal (identical to the specimen used for strain measurement) using a milling machine. The specimen was then partially formed on the CRF mill No:1 by stopping the forming process when the leading edge of the specimen reached the centre line of the last roll station. The partially formed specimen was then removed from the mill. The specimen (Figure 6.7) was placed on a flat granite table and the grid lines were observed. It was observed that the deformation was such that the lateral grid lines engraved on the undeformed specimen were now vertical, similar to the model in Figure 6.6. This confirmed that the forming angle model is correct.

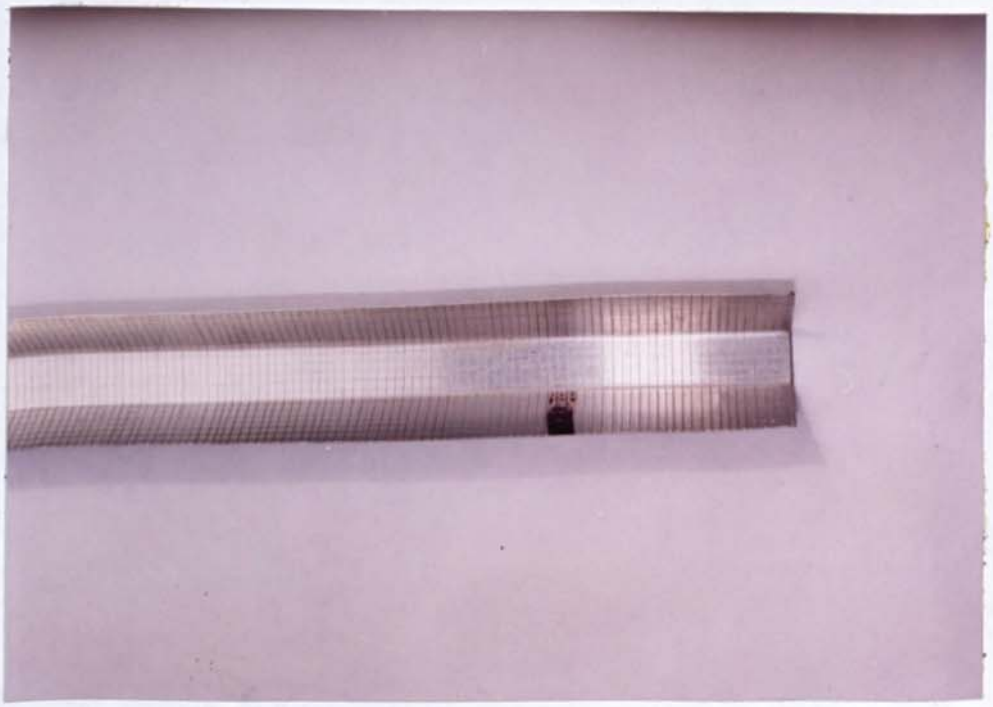

Figure 6.7. Partially formed specimen with grid markings.

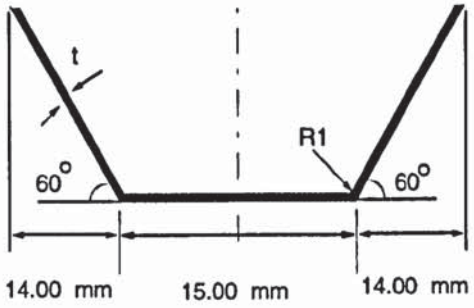

Fig 6.8. Trapezoidal Section (CRF Mill No:1).

When applying boundary conditions in the finite element analysis, points A,B,C,D,E,F (Figure 6.6) are constrained to move in the vertical planes through the roll centrelines until they reach their final positions A′,B′, C′, D′, E′ and F′.

From results obtained through years of experience in the field, a longitudinal forming angle of 1°25′ has been found applicable as a guide by designers in determining the number of roll passes required for simple shapes. In the finite element analyses that follow, the same basic idea is used.

The procedure used to predict the strains is only an approximate method. The boundary condition applied are derived from observation and experimentation. The main factor missing in this analysis is the roll radius at the forming edge. The strain distributions before and after each roll station starting from the first roll station through to the last roll station describes the strain history of a particular point on the workpiece during the cold roll forming process.

A 'more accurate simulation' could be performed as a 'CONTACT' problem, where the rolls are modelled as rigid bodies using their exact dimensions. Here the roll radii will be taken into account. In a simulation of this nature, the roll loads and friction between the rolls and the material being roll formed has to be used in modelling for the program to work out its own 'boundary conditions'. Here subjectivity enters the simulation resulting in inaccuracies.

In any kind of finite element analysis/simulation, the roll geometries have to be assumed or determined by some other method and input as data or boundary conditions. Hence the usefulness of the finite element method is limited to estimating or predicting the strains in the workpiece. It is not possible to design the roll tooling using this method. This is the possible reason for the commercial roll forming companies to concentrate on a CAD/CAM approach to design and manufacture the roll tooling. In commercial roll form design programs such as COPRA® [dataM] and PROFIL® [Ubeco] the longitudinal stresses in the flanges are estimated and their values kept below critical values.

The trapezoidal profile formed on CRF Mill No:1 (Figure 6.8) was modelled as described in the preceding sections and analysed using the MARC® finite element program. The roll angles through A, B, C, D, E and F are 19.69°, 35.59°, 47.04°, 55.05°, 60.79° and 65.03° respectively.

In the finite element model, the nodes lying on planes through A,B,C,D,E and F are prescribed incremental displacements. These incremental displacements should be small enough to prevent any buckling of the sheet at any node. 300 equal increments are applied until the sections through F confirm to the prescribed trapezoidal shape. In history definition, a 300-increment analysis is performed with a maximum of twenty recycles (iterations) per load step and the sheet metal is formed into the final shape.

The overall length and thickness of the finite element model is identical to the length and thickness of the specimen used on the CRF mill No:1. Since the workpiece is symmetrical about a longitudinal axis through the centre line of the CRF mill, only half the workpiece is modelled for analysis. This finite element model comprised of 129 rectangular elements and 176 nodes.

6.4 Program Output/Results

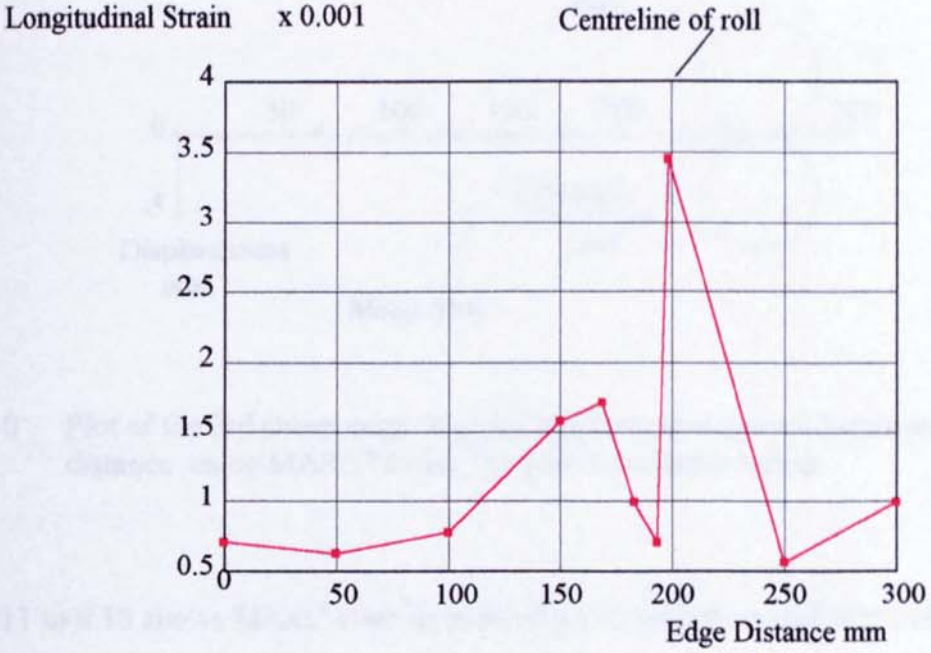

Fig 6.9 Plot of the MARC output of longitudinal strain near the edge of the specimen.

Figure 6.9 shows the typical MARC output of longitudinal edge strains plotted against the distance. These strains display a peak slightly ahead of the roll centres which is in agreement with the experimental results. If a finer mesh is used in the modelling, a smoother curve , resembling an experimental strain trace would result, but at the cost of longer computing time.

An interesting observation made by Jimma & Ona [Jimma3] during their research into cold roll forming was the buckling of the sheet metal immediately before entering each roll station. The angle of entry at each roll stand was used as an indicator to measure the degree of severity of forming. This is confirmed by the finite element analysis and Figure 6.10 shows a typical plot of the profile immediately before entering a roll station.

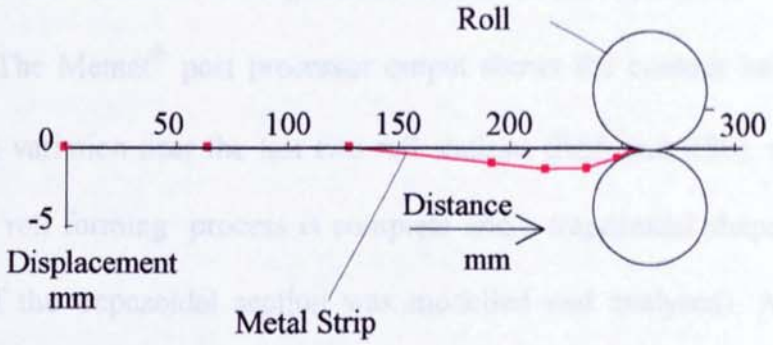

Figure 6.10 Plot of the 3rd component of nodal displacement against horizontal distance using MARC® Finite Element Simulation output.

Figures 6.11 to 6.15 shows MARC contour plots of stress and strain distributions in the workpiece during roll forming. Figures 6.16 and 6.17 shows the deformed specimen. As the workpiece is symmetrical about the longitudinal centreline of the web, only half the workpiece has been modelled.

MARC® Contour Plots

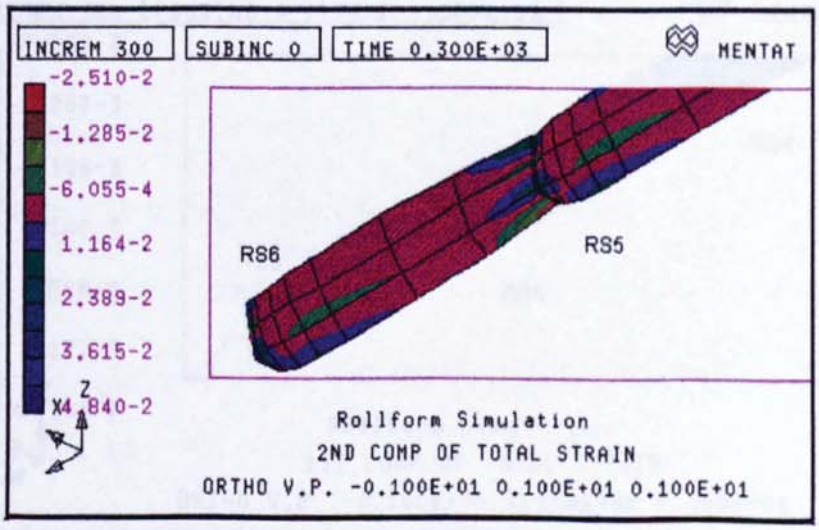

Figure 6.11 Band Contour plot of Longitudinal Strain Variation.

Figure 6.11 shows the variation of longitudinal strains in the workpiece during the forming process. The Mentat® post processor output shows the contour bands of the longitudinal strain variation near the last two roll stations (RS5 and RS6). At the last station (RS6), the roll forming process is complete and a trapezoidal shape has been formed (only half the trapezoidal section was modelled and analysed). As the roll station is approached, the strain in the flange is nearly zero or positive. The strain then becomes compressive for a short distance before it reaches a tensile maximum just before passing through the roll centre line. As the specimen passes through the roll stand the strain drops sharply and turns compressive briefly before reaching a near zero value.

The longitudinal strain variations near the fold line and along the longitudinal centre line of the web also can be seen in Figure 6.11.

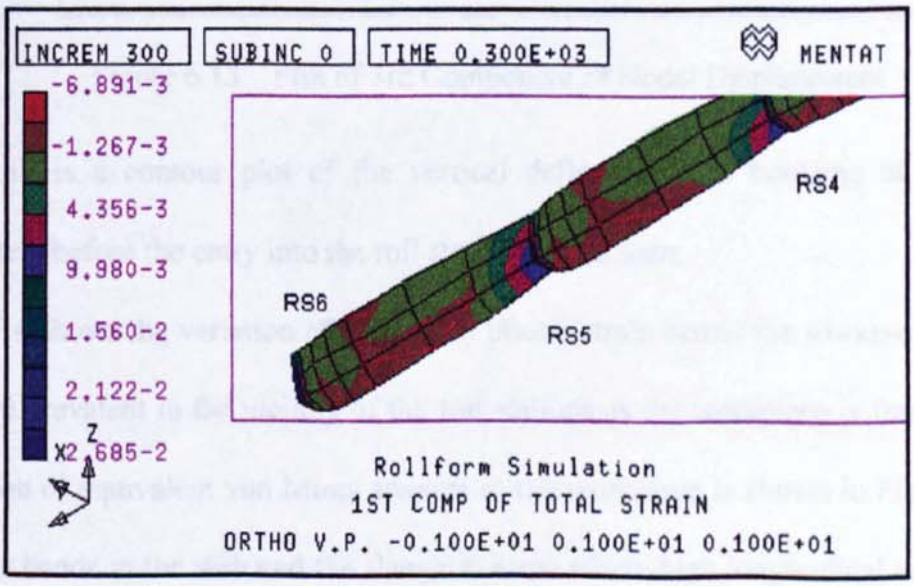

Fig 6.12. Band Contour Plot of Lateral Strain Variation

The lateral strain variation in the flange and web in the workpiece as it approaches, passes through and exits a roll station can be seen in Figure 6.12. The lateral strain in the flange which is negative decreases further as the roll station is approached. Immediately before entering the roll station, the absolute value of the lateral strain decreases and continues to decrease while passing through the roll stand and beyond. The lateral strain variation in the web can also be seen in this contour plot.

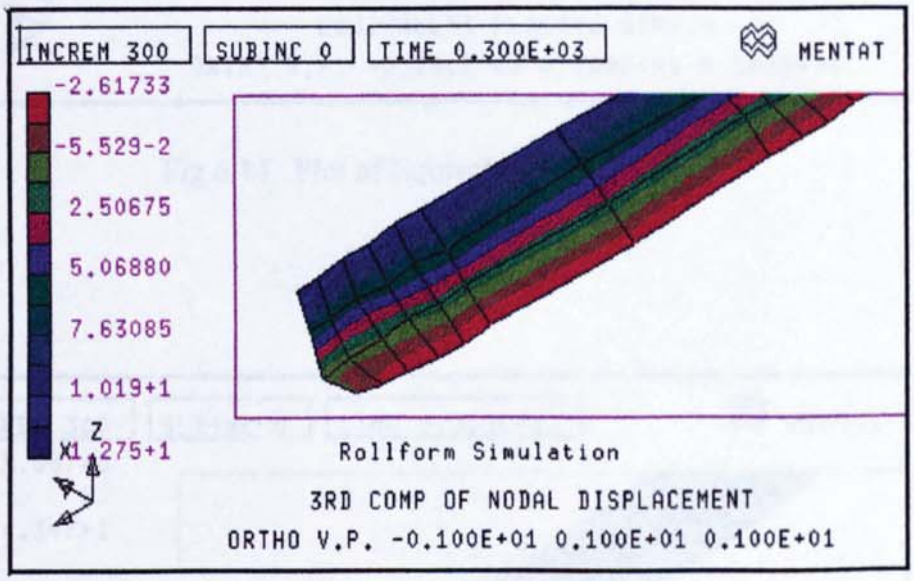

Figure 6.13 Plot of 3rd Component of Nodal Displacement

Figure 6.13 is a contour plot of the vertical deflection. The buckling of the web immediately before the entry into the roll station can be seen.

Figure 6.14 shows the variation of equivalent plastic strain across the workpiece. These strains are prevalent in the vicinity of the roll stations as the workpiece is formed. The distribution of equivalent von Mises stresses in the workpiece is shown in Figure 6.15. The stress bands in the web and the flange in areas where high longitudinal and lateral strains are present can be clearly seen.

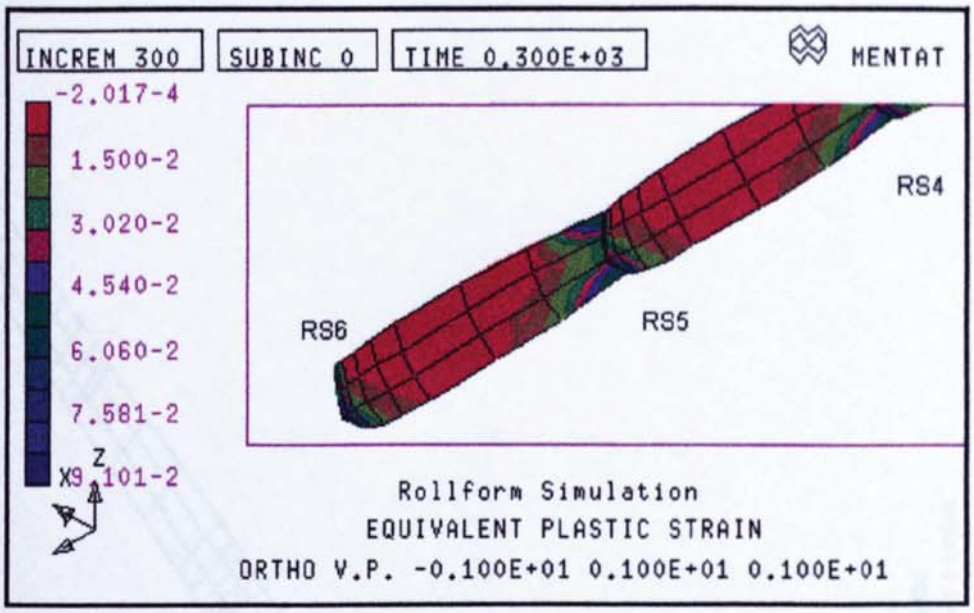

Fig 6.14 Plot of Equivalent Plastic Strain

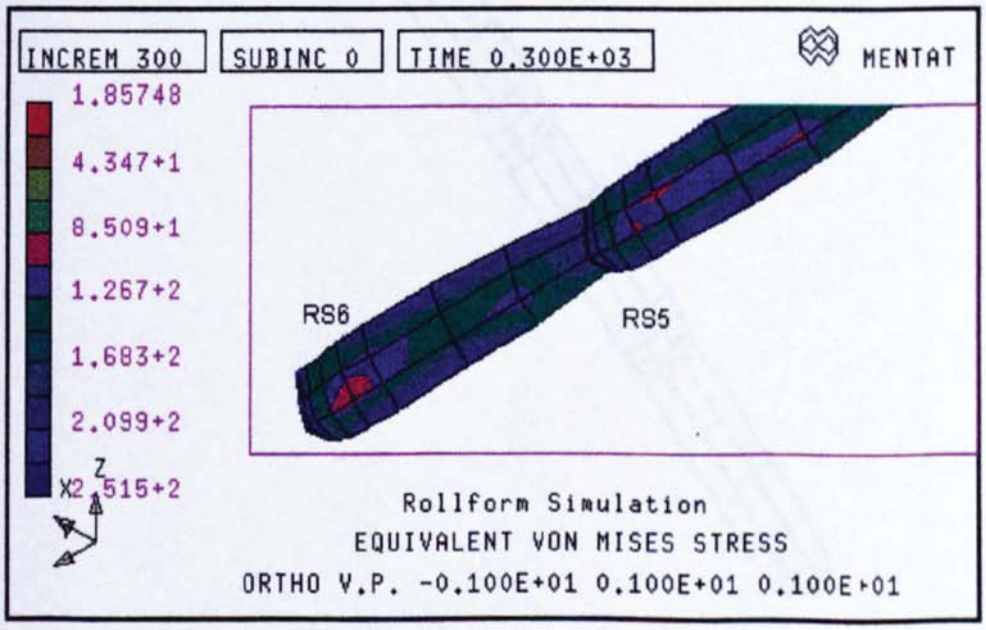

Fig 6.15 Plot of Equivalent von Mises Stress

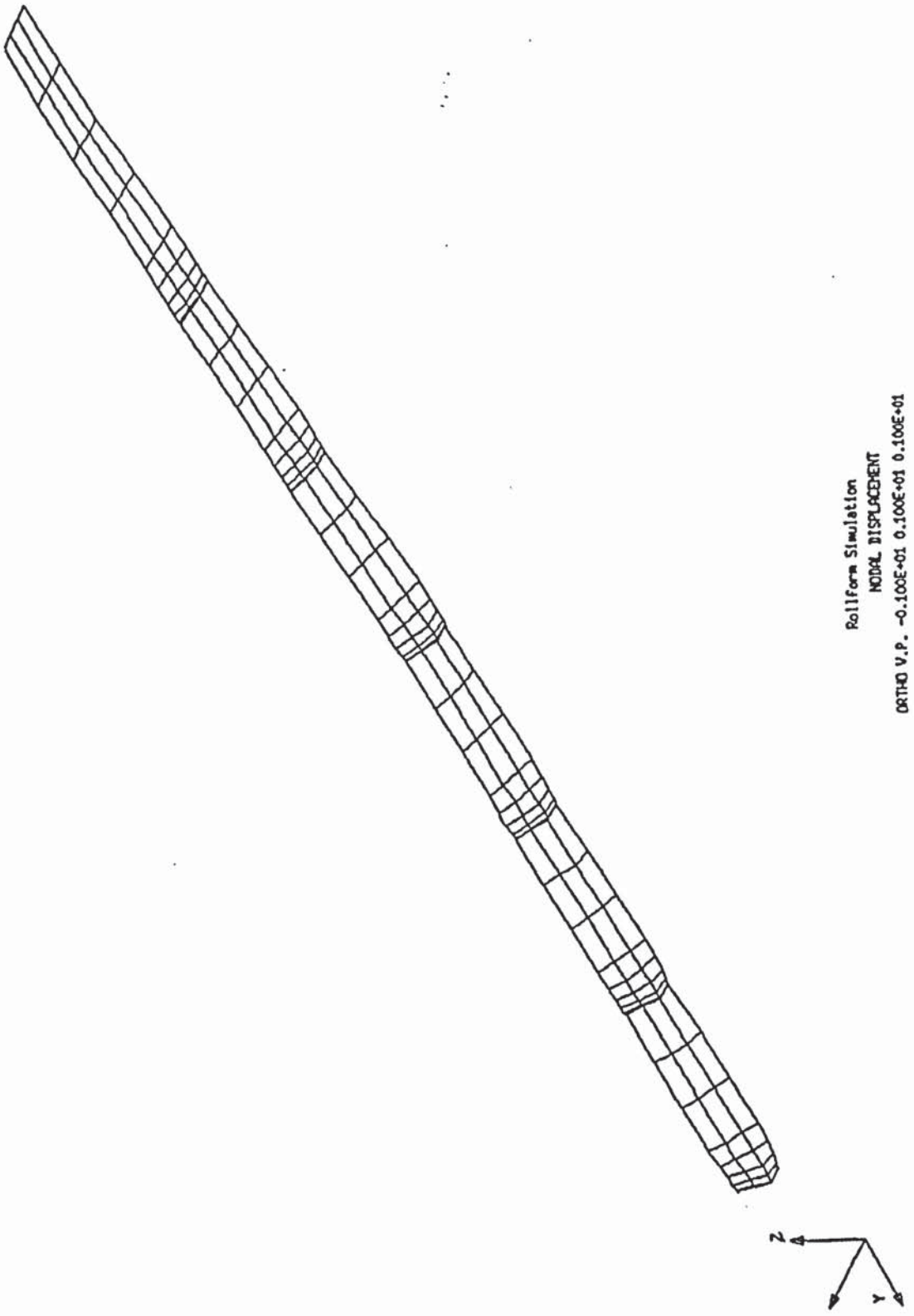

Figure 6.16 Plot of Deformed Specimen (Sheet 1)

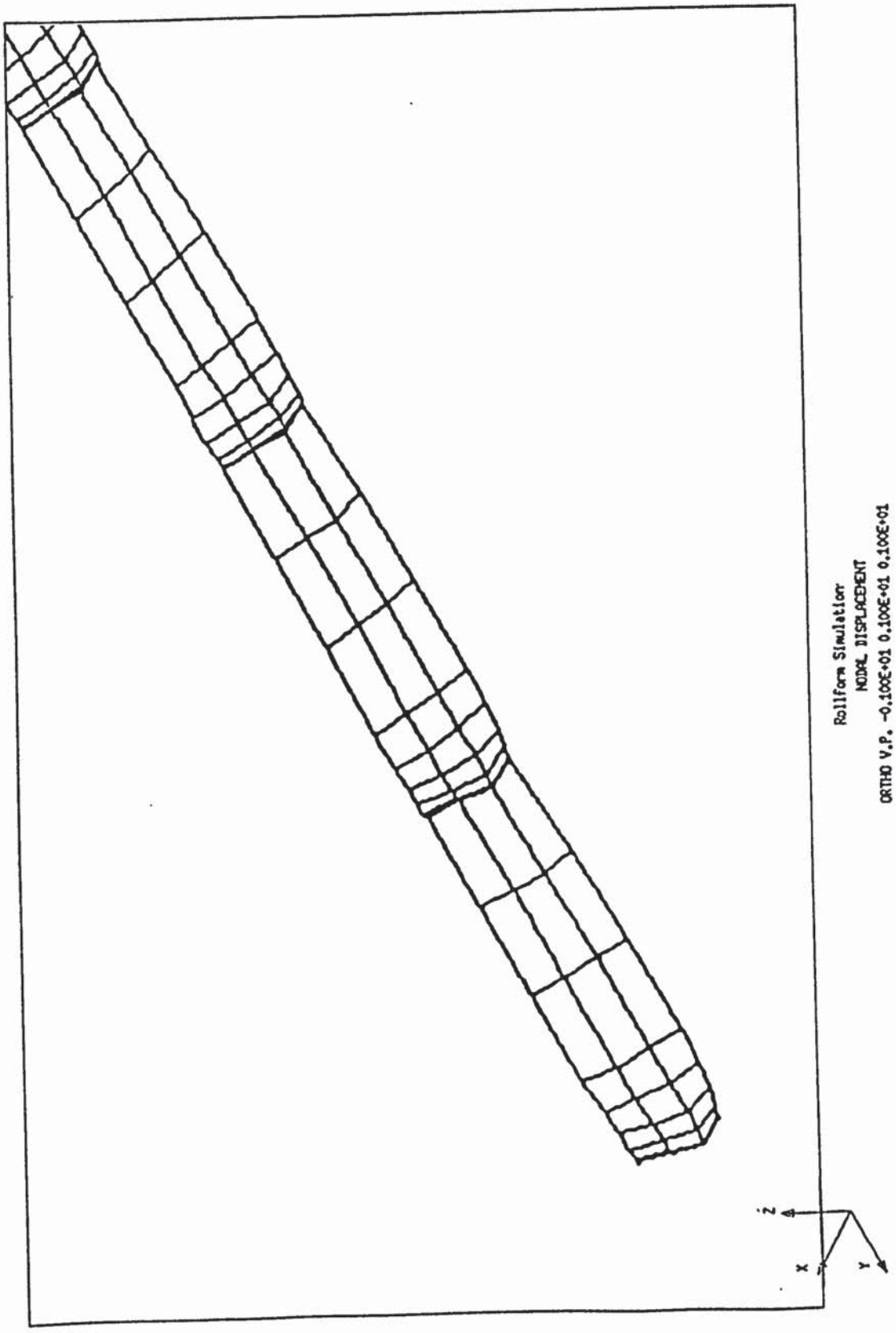

Figure 6.17. Plot of Deformed Specimen (Sheet 2)

CHAPTER 7

INTRODUCTION TO COMPUTER VISION TECHNIQUES

The manual measurement of the grids on roll formed specimens for calculating plastic strains was described in the Chapter 5. This method is time-consuming. Hence a technique was developed for the measurement of plastic strains induced in the material during the cold roll forming process using digital image processing methods. A grid is marked on the sheet metal. The points of intersection of the grid are marked prominently so that the grey level of these points is substantially different from the background. The video images of the undeformed and deformed grids are processed by the imaging system and the co-ordinates of these grid points are calculated automatically. Once the two sets of co-ordinates are known, plastic strains are calculated by a separate program.

7.1 Basics of Digital Image Processing

A video camera produces an analogue video signal (RS-170 format) containing image data if the camera is of the tube type (Figure 7.1). The analogue signal is transmitted to the image processor which, in turn, is converted to a digital signal containing the image data in the form of digital picture elements or pixels. Once the image is stored in the memory, it is accessed for display or additional computer processing. Display circuitry transforms the pixels stored in the memory back in-to an analogue signal for display on a video monitor.

In the case of a solid state camera, separate photo diodes located at each pixel area detect the illumination from the object (Figure 7.1). The elements of the solid state Charged Coupled Device (CCD) are usually arranged in either a linear or a rectangular array. The output signal of the camera is obtained by sensing each diode in an ordered sequence to obtain a series of voltage pulses representing the value of light intensity on the pixel being sensed at the respective location. The output of the sensor is a series of

voltage pulses representing the light intensity at the pixel location. The voltage pulses must be converted into RS-170 format for viewing the image on a standard television monitor or digitised if it is desired to enter the data in computer memory.

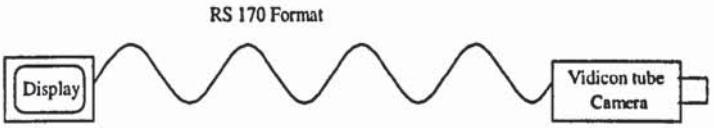

(a) Signal conversion for display on standard TV monitor

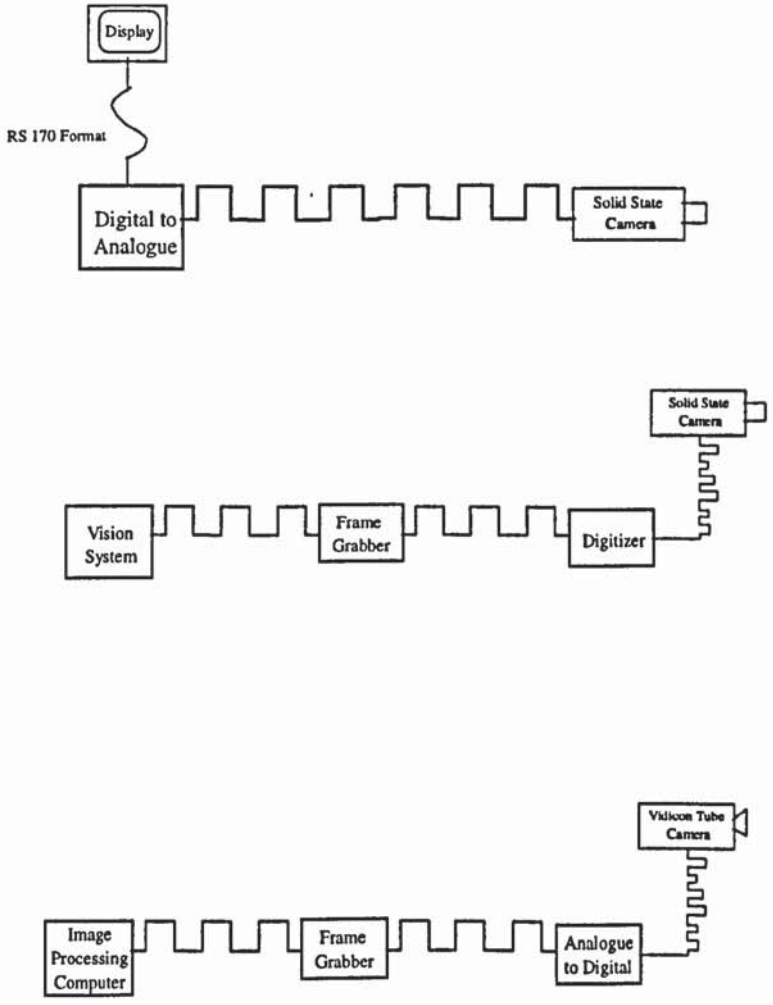

(b) Signal conversion for image processor use

Figure 7.1 Conversion of an Analogue Video Signal

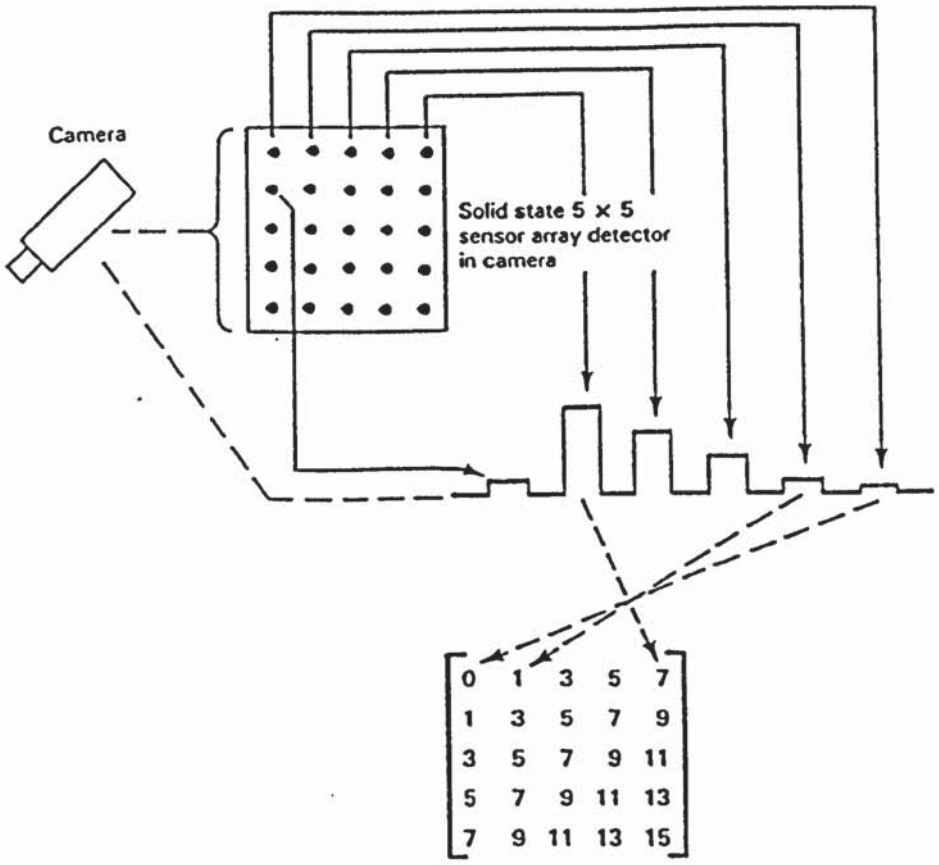

Fig 7.2a Voltage pulse train from (5 x 5 array) solid state camera and resultant pixel values in image array

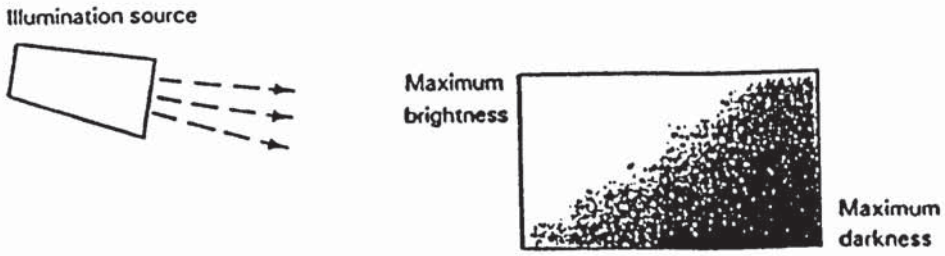

Fig 7.2b An image with brightness gradient

The number of pixels that are displayable on a Video Display Unit (VDU) defines the display resolution of the VDU. The frame grabber to be used has a resolution of 512 x 512. The software development package used to access the frame grabber is a software shell usually written in C language or another appropriate high level programming language. A specific pixel in its most elementary form is identified by its co-ordinates in the N x M array representing the picture (Figure 7.3). The pixel at the (m,n) location also has a numerical value associated with it, which represents the average value of illumination impinging on the area of the picture represented by the pixel. If a binary system is used to represent the intensity of illuminations; regions with no light will be indicated by zero and those with brightest illumination by one. There will be no information concerning the pixel having intermediate values of illumination under this system. In order to provide information on intervening values of illumination, eight bits are used to represent the pixel value giving a grey scale of 256 levels (0-255).

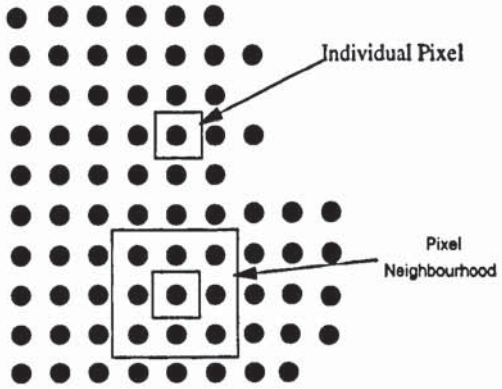

Figure 7.3 Pixel Arrangement

The points of intersection of the grid lines may occupy one or more pixel spaces with grey scale values between 0 and 256 (as close to zero as possible) depending on the method of marking the grid. By using the image processing software package, the process of digitisation of these pixels, before and after distortion has been automated. Once the two sets of grid co-ordinates are determined, another software routine was written to calculate the strains. The entire process of strain measurement has therefore been automated.

7.2 Imaging Software Package MATROX ITOOLS® and Matrox Imaging Library Software

The Digital Image Processing package used in this project is a highly versatile imaging software package called MATROX ITOOLS® together with an imaging library software.

The Matrox Imaging Library (MIL) package is a hardware independent modular imaging library.

It supports:

- Image processing
- Blob Analysis
- Pattern Recognition
- A basic graphics set

In general, MIL can manipulate either grayscale or colour images. However statistical, blob analysis and pattern recognition operations are done on grayscale images only. A MIL application can run on any VESA compatible Video Graphics Adapter (VGA) board or the MATROX imaging boards. MIL is capable of running solely with the Host CPU, but can take advantage of any specialised accelerated Matrox hardware that is also present in this system and is more efficient.

7.2.1 Image processing capabilities

Images can also be loaded to the system from previously saved data files. Once loaded, it is possible to smooth, accentuate, qualify or modify specifically selected features of an image using the MIL image processing capabilities. These capabilities include point-to-point, statistical, spatial filtering and morphological operations.

7.2.2 Graphics capabilities

Basic graphics tools for annotating images are provided by MIL. These are writing text, drawing rectangles, arcs, lines and dots.

7.2.3 Blob analysis capabilities

This capability allows identification and measurement of connected regions (commonly known as blobs or objects) within an image. The blob analysis module can measure a wide assortment of blob features such as blob area, perimeter, Feret diameter (Figure 7.9) at a given angle, the minimum bounding box and compactness.

7.2.4 Pattern recognition capabilities

The MIL pattern recognition capabilities can be used to solve machine vision problems such as alignment, measurement and inspection of objects. These capabilities include finding:

- The co-ordinates of a model in a target image
- The number of occurrences of a model in a target image

7.2.5 MIL objects

MIL operates on virtual objects, such as data buffers and input devices, rather than physical ones. These virtual objects must be allocated before their data can be manipulated and must be released when they are no longer required. Objects that need to be allocated are: system devices, digitisers, displays and data buffers. For simpler applications, those set up by default will generally meet the application needs.

7.2.6 Image pixel depth

The MIL package can:

- Grab 8, 16-bit or colour (RGB 8:8:8) images
- Process 8 or 16 -bit grayscale images.
- Process colour images depending on the operation. Each 8 or 16-bit band of a colour image is processed individually one at a time.
- Display 8-bit grayscale or colour (RGB 8:8:8) images

7.2.7 The library

MIL is available as a C library and as a DLL under Microsoft Windows Operating System Version 3.1.

7.2.8 Matrox Imaging library interpreter (MILINTER)

MILINTER is an interactive interpreter that accesses all the functions supplied with the MIL package. It enables experimenting with MIL functions without having to recompile every time a change is made. The syntax of MILINTER is similar to C Language. This similarity of programming syntax means that C programs based on command lists can be developed. MILINTER exists for both DOS and Windows environments.

7. 3 Image Processing

Pictures or images are important sources of information for interpretation and analysis. Human analysis of these images or objects has inherent difficulties: the visual inspection process is time consuming and is subjected to inconsistent interpretations and assessments. Image processing solves these problems by making it possible to automate the extraction of useful information from image data. Image processing can perform various types of image enhancements, distortion corrections and measurements.

There are two main types of image processing applications:

- Those that enhance or reconstruct an image
- Those that generate a numeric or graphic report which relates specific image information.

The MIL package provides a comprehensive image processing module. It supports the following operations:

- Point-to-point operations
- These include operations such as contrast thresholding, image comparisons, image subtraction, and image mapping which compute each pixel result as a function of the pixel value at a corresponding location in either one or two source images.
- Statistical operations which extract statistical information from a given image
- Spatial filtering operations include operations which can enhance and smooth images and remove noise from an image.
- Morphological operations include such operations as erosion, dilation, opening and closing of figures. These compute new values according to geometrical relationships and matches to known patterns in the input image.

However the application of image processing to the problem of strain measurement does not require all of the above operations.

7.3.1 Improving the image quality

Prior to manipulating and extracting information from an image, many applications require that the best possible digital representation is obtained. Several factors affect the quality of an image.

These include:

(i) Random noise.

There are two main types of noise:

(a) *Gaussian noise.* The exact value of any given pixel is different for each grabbed image when this kind of noise is present. This type of noise adds or subtracts from the actual pixel value.

(b) *"Salt and Pepper" noise.* Arbitrary values of high frequency noise which are completely unrelated to the pixel values are sometimes introduced.

Random noise can be caused either by the camera or by the digitiser. This is because electronic devices in general tend to generate a certain amount of noise.

(ii) ***Systematic Noise*** appears as a regular pattern that is not part of the actual image which can be caused by either the camera or the digitiser or lighting. If the image is magnified, microscopic dust particles either on the object or the camera lens can appear to be part of the image.

(iii) ***Distortions*** appear as geometric transforms of the actual image generally caused by the curvature of the lenses or an inequality in the aspect ratio of an image acquisition device.

7.3.2 Techniques to improve images

As most interference problems cannot be corrected at source very easily, the image can be improved as much as possible by pre-processing without affecting the information which is being sought.

The procedure used to improve an image is:

- Grab the image of the object of interest several times, averaging each image frame with the previous. This method is effective on Gaussian random noise.
- Apply a median filter to the image. This technique replaces each pixel with the median value of its neighbourhood. This method is good for salt-and-pepper noise.

- Apply a low-pass spatial filter to the image. This technique replaces each pixel with a weighted-sum of its neighbourhood which is suitable for reducing Gaussian random noise and systematic noise.
- Performing an opening operation to remove small particles.
- Performing a closing operation to remove small holes in objects.
- Using a camera that digitises the image with square pixels (that is a 1:1 aspect ratio). This is specially important if the image is to be rotated. The aspect ratio may also affect other operations like blob analysis. If the aspect ratio of a grabbed image needs to be changed, a MIL command- MimResize( ) is available.

7.3.3 Thresholding images

Once the image has been improved as much as possible, the image can be manipulated in order to extract information from it. The MIL image processing module offers several image manipulating operations. Thresholding images implies reducing each pixel to a certain range of values. Sometimes an operation can be performed more efficiently if the only information required is present in the image. Images with full grayscale levels are useful for some tasks, but have a redundant amount of information for others. For the application of strain measurement, the following two methods are useful:

7.3.4 Binarizing

When performing a binarizing operation, the image is reduced to two grayscale values: zero and the maximum value for the buffer. For example, the maximum value of an 8-bit buffer is 255. Pixels with 0(zero) values are seen as black, whereas those set to the maximum buffer value are seen as white. Pixels that meet a specified condition are changed to the maximum value and those which do are not changed to 0(zero). Binary images are useful when trying to identify geometrical patterns and objects in the image since they are not cluttered with shading information. When binarizing, it is important to select an appropriate thresholding condition that preserves the required information.

7.3.5 Clipping

Clipping changes the image data less dramatically than binarizing. It changes the data to include only the range of pixel values of interest. Clipping takes a condition with at most two threshold points and replaces only those pixels that meet the condition with given values. Pixels that do not meet the condition are unaffected.

7.3.6 Advanced image manipulation

MIL also has advanced image processing capabilities. It supports neighbourhood operations that can be customised to suit the application. These operations include:

- *Custom spatial filtering operations*
  Special filtering operations include operations which can enhance and smooth images, accentuate image edges and remove noise from the image.

- *Custom morphological operations*

  Morphological operations are neighbourhood operations which compute new values according to geometric relationships and matches of known patterns in the input image. Different geometric relationships for these operations are specified using a structuring element.

MIL supports the following morphological operations:

Erosion / Dilation

These functions allow the possible growth stages of an object in the foreground (non-zero pixels) of an image to be viewed.

Thinning / Thickening

Objects can be reduced or enlarged in the foreground (non-zero pixels) of an image based on a more rigid match of the pixel's neighbourhood and the structuring element. Using a thickening operation an object can be enlarged. Using a thinning operation an object can be reduced and perform operations such as finding their skeleton.

Pattern Matching

This allows the determination of how similar certain areas of the image are to a pattern (specified by a structuring element). Pattern matching takes a binary or grayscale source image and produces a grayscale image whereby each pixel is the count of the number of matches between the neighbourhood and structuring element values.

Hit or Miss Transformation

MIL can determine which pixels have neighbourhoods that match the template exactly by performing a 'hit or miss' operation. When a pixel's neighbourhood matches the template exactly the pixel is replaced with the maximum value of the buffer (for example, 0xff for an 8-bit buffer). When the neighbourhood does not match exactly, the pixel is replaced with the value zero.

7.4 Blob Analysis

Blob analysis is a branch of image analysis where many areas of interest within an image are measured and classified. These areas of interest are commonly known as blobs or objects.

Blobs are areas of touching pixels which are in the same logical pixel state called the foreground state. The alternate state is called the background state. Typically, the background has the value zero and the foreground is everything else although some control is generally provided to reverse the sense. In most applications, the interest lies only in blobs whose measurements or features satisfy given criteria. Blob analysis is

often performed as an elimination process whereby only blobs of interest are considered in further analysis. This is to reduce the computation time.

The steps involved in blob analysis are:

- Exclusion or deletion of blobs that do not meet given criteria
- Analysing the remaining blobs to extract further information

Once the raw data is reduced to a few measurements, results are generally more comprehensible and useful.

7.4.1 MIL and blob analysis

MIL package includes a blob analysis module which can measure blob features such as

- Blob area
- Perimeter
- Feret diameter at a given angle
- Minimum bounding box
- Compactness

MIL uses a user specified blob identifier to discriminate between blobs and background. Controls are provided to allow this identifier image to be interpreted (which pixels are part of which blob). Blobs are considered to consist of either zero or non-zero pixels, depending on the foreground control setting. The non-zero pixels can either have any value or must be set to the maximum value of the buffer, depending on the identifier type (grayscale or binary).

7.4.2 Typical steps to performing blob analysis

1. Acquire or load an image which was captured under the best possible conditions to minimise the amount of pre-processing required.
2. Reduce the noise if necessary
3. Binarize the image so that the background is in one state (zero or non-zero) and the blob pixels are in the other state. This image is known as the blob identifier image.
4. Pre-process the image if necessary. If there are too many noise particles, calculation time will be increased or the number of blobs might exceed the maximum number that can be handled by MIL.
5. Allocate a buffer for blob analysis results.
6. Adjust blob analysis controls to fit the application. These include the pixel aspect ratio, when to consider two pixels touching - along horizontal and vertical only or along the diagonal, which values in the identifier image represent a blob- zero or non-zero.
7. Allocate a list of features which should be calculated. By default this list is empty.
8. Calculate the required features and analyse the results.

7.4.3 Setting up for blob analysis

The MIL blob analysis capabilities allow the measurement of connected regions within an image. MIL requires a user-specified blob identifier image in order to determine which pixels belong to which blob in the original image being analysed. Blob features, which involve overall shape, are measured directly from this image.

The MIL blob analysis module always considers touching foreground pixels in the blob identifier image to be part of the same blob. If part of a blob is in the background pixel state because of lighting or reflection, it will be considered as part of the background during analysis.

Once the best possible image has been acquired and most noise has been filtered out of the image, different blobs must be separated from the background.

Segmentation can be done in two ways:

- Binarize the image so that background pixels are represented as zero values and blob pixels are represented as a different value.
- Clip all background pixels to zero while retaining the original values of blob pixels. This method has the advantage that a separate buffer is not needed to hold the binary image. Clarity of the image after clipping may be inferior to the quality of the image after binarization.

7.4.4 Adjusting blob analysis processing controls

Prior to any blob analysis calculations, it must be ensured that the interpretation of the blob identifier image is correct. Certain aspects of the blob identifier image listed below can be controlled:

- Which pixel values are considered to be in the foreground
- Whether two pixels that touch at their corners are considered part of the same blob by appropriately defining the image lattice.
- Whether non-zero pixels can have any value or must be set to the maximum value of the buffer.
- The pixel aspect ratio of the image.

7.4.5 Controlling the image lattice

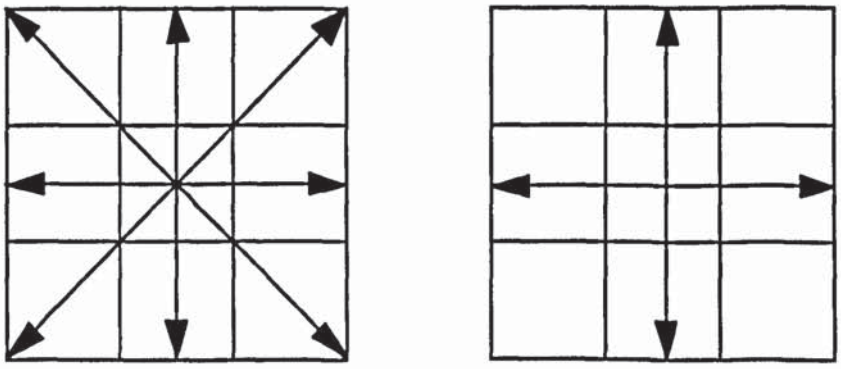

(a) 8 connections (b) 4 connections

Figure 7.4 Lattice with neighbour connections

In MIL images are represented using a square lattice (Figure 7.4), and it considers adjacent pixels along the vertical or horizontal axis as to be touching each other. However, whether two diagonally adjacent pixels are considered touching can be controlled.

7.4.6 The pixel aspect ratio

When acquiring an image of an object, each pixel represents some real distance both in height and width. Ideally, this distance is the same in both directions, producing square pixels and allowing for simple measurement calculations. However it is quite common that after digitisation, a pixel might represent a different distance in each direction. The ratio of the pixel's width to height is called the pixel aspect ratio. Hence , if the pixel width and height are equal, the pixel aspect ratio is 1.0.

In blob analysis, the pixel aspect ratio directly affects measurements. There are alternatives to rectify this situation.

- The image can be adjusted and the required blob analysis measurements can be made.
- Calculations can be done by taking the actual aspect ratio into consideration without modifying the image.

However, any feature derived from multiple Feret diameters cannot take into account the pixel aspect ratio accurately, and better results are obtained by resizing the image. All results including those which are just positions within the image are affected by aspect ratio (Figure 7.5).

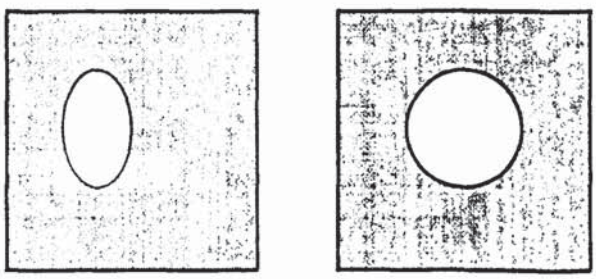

aspect ratio =1.3 aspect ratio = 1.0

Figure 7.5 Circle with aspect ratio

7.4.7 Analysing the blobs

The MIL blob analysis module can calculate a number of different blob features such as the area, perimeter, Feret diameter, the centroid of each selected blob.

7.4.8 The area and perimeter

Each pixel in the image represents a real width and height. However, all results from the blob analysis commands representing distance or area are expressed in raw uncalibrated pixel units. These results must be converted to real physical units. This process is much easier if the pixel aspect ratio is 1.

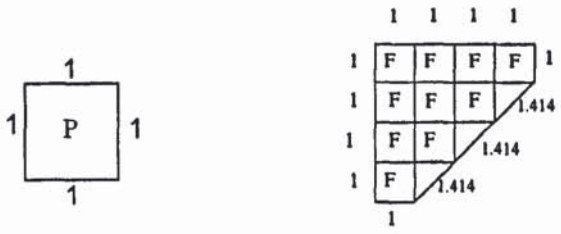

Figure 7.6 Area and perimeter of a pixel

Each pixel P is represented as shown. Hence the area of a single pixel blob is equal to 1 and the perimeter is equal to 4. The area of a larger blob excluding that of holes is equal to the number of pixels in the blob. The perimeter of a blob is equal to the total number of pixel sides along the blob edges including the edges of holes. An allowance has to be made for the staircase effect in a digital image which occurs when representing diagonals and curves. Figure 7.6 shows a blob F whose area is equal to 10 and the perimeter is equal to 14.242.

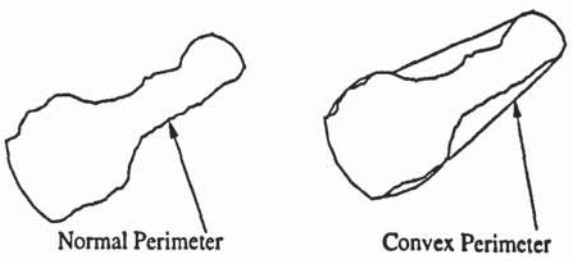

Figure 7.7 Convex perimeter of a blob

In addition to the normal perimeter, it is also possible to calculate an approximation of the convex perimeter (Figure 7.7) of the blobs which is the perimeter of the convex hull. This measurement is derived from taking the Feret diameter at different angles.

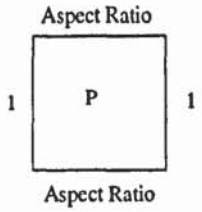

Figure 7.8 Pixel Aspect Ratio

When a pixel aspect ratio has been set to anything other than 1, the aspect ratio is applied to the pixel width during measurements. After the application of the aspect ratio, it can be represented as shown in Figure 7.8. All the calculated features are affected in the horizontal direction by a factor equal to the pixel aspect ratio. The results are no longer in 'pixel' units. Since blobs may not be rectangular, the length of the blob at different angles from the horizontal may have to be taken.

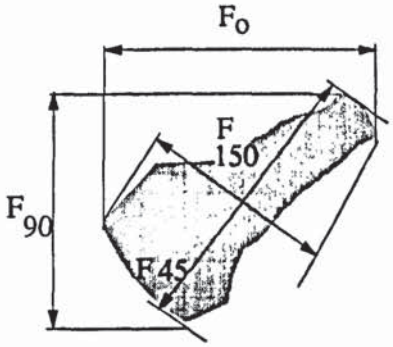

Figure 7.9 Feret Diameter

Since blobs may not be rectangular, the length of the blob at different angles from the horizontal may have to be taken. One of the many definitions of the blob length is the Feret diameter as shown in the Figure 7.9. With MIL, the Feret diameter at a specified angle can be calculated. It is also possible to determine the maximum, minimum and average Feret diameters automatically. Finding the location of a blob is very useful in some applications. The centroid can be calculated by MIL either in binary or grayscale mode.

7.5 Pattern Recognition

The MIL package includes a pattern recognition module which is capable of searching for a user-specified model in a target image.

The basic steps involved in performing a search are:

- Defining the model from a model image
- Specification of parameters and constraints
- Allocation of a result buffer
- Finding the model in the target image
- Reading the search results

7.5.1 Defining the model

To define a model there are two options available

1. Allocating a new model:
   In this option an image containing the pattern of interest must first be acquired or loaded into an image buffer.
2. Loading a previously stored model from a disk file into system memory.

7.5.2 Image alignment

Many applications perform some type of alignment operation which either physically or logically moves a target to an expected position. The MIL package provides techniques to find horizontal and vertical displacements of images by comparing the location of a unique model taken from an aligned image, with its actual location in the target image. The model can be chosen from any location in the aligned image provided that the model is unique.

7.5.3 Searches, models and model search parameters

MIL pattern recognition routines are capable of finding occurrences of a model in a target image.

7.5.4 Positional Accuracy

The positional accuracy can be set to:

(a) ± 0.5 pixel (Low)

(b) ±0.25 pixels (Medium)

(c) ±0.125 pixels (High)

The acceptance level for the specified model can be set using a MIL command. If the correspondence between the image and the model or the match score is below this level, they are not considered as an acceptable match. A perfect match is 100%, a typical match is 80% or higher. If the noise level is high, the threshold level may have to be set below a default value of 70%. Poor quality images increase the chance of false matches and increase the search time. Perfect matches are generally unobtainable because of the noise. A certainty threshold is very important because it can greatly affect the speed of the search. A good understanding of the search algorithm is necessary in order to obtain the optimum use of the search function. A brute force correlation of the entire model at every point in the model is not practical as the time taken could be considerable. The search algorithm must therefore be intelligent to overcome these problems.

It first performs a rough but quick search to find likely match candidates and then checks out these candidates in more detail to see which are acceptable. A certainty threshold is the correlation value above which the algorithm can assume that it has found a match without continuing to search the rest of the image for a better one. The certainty threshold can be set to 100% if it is absolutely necessary to have the best match. In this application of strain measurement, the threshold is set to 100%. Pre-processing of a search model can be skipped if the search speed is not too important.

7.5.5 Sub-Pixel accuracy

The highest match score occurs at only one pixel position, and drops off around this peak. The exact sub-pixel position of the model can be estimated from the match scores found at either side of the peak. A curve is fitted to the match scores found at either side of the peak, and the exact peak position is calculated using the equation of the curve. The curve is also used to improve the estimate the match score itself. The absolute limit on accuracy imposed by the algorithm itself and by the number of bits and precision used to hold the correlation result is about 0.05 pixels. This is the worst case error measured in X or Y when an image is artificially shifted by fractions of a pixel. In a real application, accuracy better than 0.1 pixels might be achieved in practice for low noise images, although in general it is better not to rely on more than 0.125 pixels.

7.6 Specifying and Managing Data Buffers

The MIL package allocates data buffers for various purposes such as for image data, look up table (LUT) data or results buffers. Data buffers can have different data depths and up to three dimensions: x, y co-ordinates and colour band dimension. The x and y dimensions generally specify the surface of the data buffer, while the colour band specifies the number of such surfaces required to represent an object in colour.

7.6.1 Allocation of data buffers

All data buffers must be allocated with memory before a function attempts to access them. When allocating a data buffer, the following must be specified:

- target system
- data type
- attribute
- dimensions

7.6.2 Managing Data Buffers

Mil provides several data buffer management commands.

These allows the following operations:

- Put data in
- Get data from
- Load from disk
- Save to disk
- Copy specific regions of a data buffer

7.7 MIL Program Structure

The structure of the MIL program is illustrated in figure 7.10.

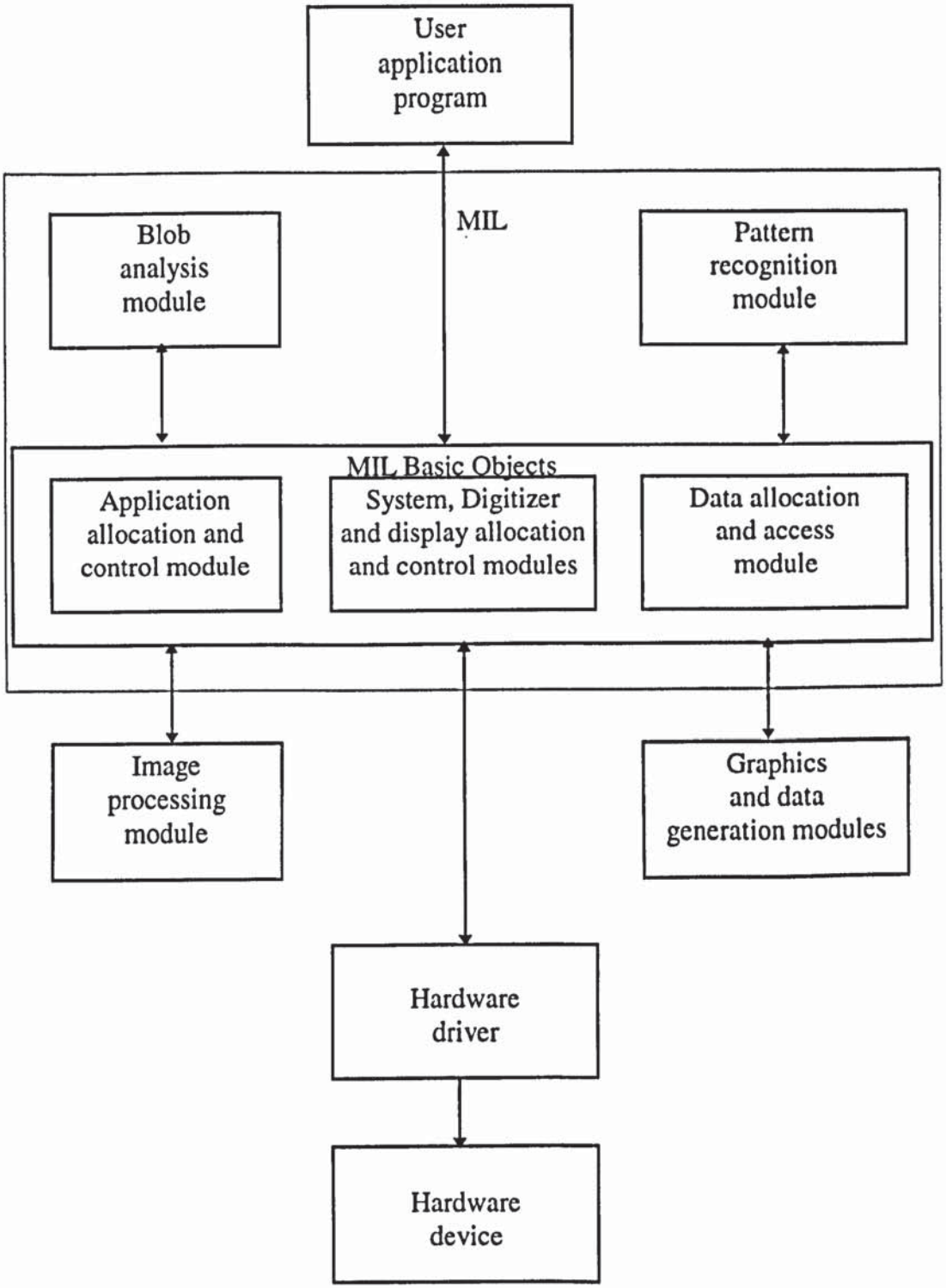

Figure 7.10 MIL Program Structure

CHAPTER 8

STRAIN MEASUREMENT USING COMPUTER VISION

The strains induced in the material during roll forming are both elastic and plastic. Residual plastic strains can be measured by the well known grid method [Noble]. An inscribed grid can be measured after deformation and the plastic strains calculated. This can be done after removing the material from the cold roll forming machine. The strains induced in the workpiece during forming are measured using strain gauges and this has been described in Chapter 5.

In this research residual plastic strains are measured
(1) manually, using an optical measurement system OMIS II (Chapter 5) and
(2) using machine vision and digital imaging technology.

The latter process can be subdivided into the following three activities.

1. Obtaining the digital representation of the deformed grid
2. Employing computational techniques to process the image data
3. Analysing and using the results of the processing for the purpose of evaluating the strains in the material.

Image acquisition transforms the visual image of a physical object and its intrinsic characteristics into a set of digitised data which can be used by the processing unit of the system. This image acquisition is to be done with a video camera and a frame grabber. When used with a host computer driven by Matrox software, the frame grabber is capable of performing complex image processing functions in real time. Images of the grid are captured before and after deformation. Matrox software is programmed to calculate the centroid of each grid point. Once the two sets of grid co-ordinates are determined, another software routine was written to calculate the strains. The entire process of strain measurement has therefore been automated.

8.1 Description of the Image Grabbing Procedure

In this application, grabbing the images of the reference axes and the grids marked on the specimens is the preliminary operation before processing the image. It is done by a set of programs mfocus1.cl , mfocus2.cl, mfocus3.cl, mfocus4.cl listed in Appendix H

.

The first stage in grabbing images is the allocation of an image buffer; *Milinter* works only with buffers. Image buffers are storage areas which can hold image data so that it can be displayed, manipulated, grabbed, and/or analysed. For this application it is sufficient to use the default image buffer which can be allocated during application initialisation with the *MappAllocDefault( )* macro. This macro can allocate and initialise a MIL application, allocate the system which receives the MIL commands, allocate the digitise and display, and allocate and clear a displayable image buffer on this target system, depending on what is requested.

An image can be grabbed using an allocated digital input device (camera), by issuing a single command call to *MdigGrabContinuous( )*. This function grabs an image frame into the specified buffer until the halt command *MdigHalt( )* is issued. When this function is called it stops the specified digitizer from grabbing data. The resultant image has to be saved for later processing. The function *MbufSave( ) is used,* to save the data buffer into a file using the MIL output format. The name of the file is specified at the beginning of the program and declared.

To quit the program, the MIL application defaults are freed, which could be allocated using the *MappAllocDefault( )*, together with the macro *MappFreeDefault( )*.

8.2 Procedure involved in Measuring the co-ordinates of the Grid Points

In analysing the image, the grid points are represented as blobs. It is necessary to determine the number of these blobs which are smaller than a certain size and the position of the centroid of each of these blobs.

This involves the following image processing steps:

- Load an image with some blobs (each blob representing one grid point).
- Binarize the image so that the blobs have a different greyscale value from the background: represent blobs in white and the background in black.
- Perform an opening operation to remove small particles from the image.
- Change the foreground value. Now, blobs are in black and the background in white.
- Allocate a list of features which should be calculated - the number of grid points and the centre of gravity of each blob).
- Calculate the required features.
- Save these values into the files for the calculation of strains.

The system was validated using a computer generated grid with known co-ordinates. The grid points were generated using a CAD system and plotted using a laser printer. The co-ordinates measured by the image processing system and the actual values were in close agreement.

Step 1: Load an image

For loading an image it is necessary to have an image previously saved into a file. This file is a data file and can be loaded using one of two methods:

- Load data file into an automatically allocated MIL data buffer
- Load data file into a previously allocated MIL data buffer.

Step 2: Binarize an image

When performing a binarizing operation, the image is reduced to two grayscale values: zero and the maximum value of the buffer (for example, the maximum value of an 8-bit buffer is 255). Pixels with zero values are seen as black, whereas those set to the maximum buffer value are seen as white. Pixels that meet a specified condition are changed to the maximum value and those which do not are changed to zero. Binary images are useful when trying to identify geometrical patterns and objects in the image

since they are not cluttered with shading information. When binarizing, it is important to select an appropriate thresholding condition that preserves the required information. (See Figures 8.1, 8.2, 8.3 and 8.4)

Step 3: Opening operation:

A way of improving the image might be to remove small particles which, for example, have been introduced by dust, or by removing holes in objects. These tasks can generally be resolved with an opening or closing operation, respectively. Opening and closing operations determine each pixel's value according to its geometric relationship with neighbourhood pixels. Besides removing small particles, opening operations also break connections between touching objects. Closing operations are very useful in filling holes in objects.

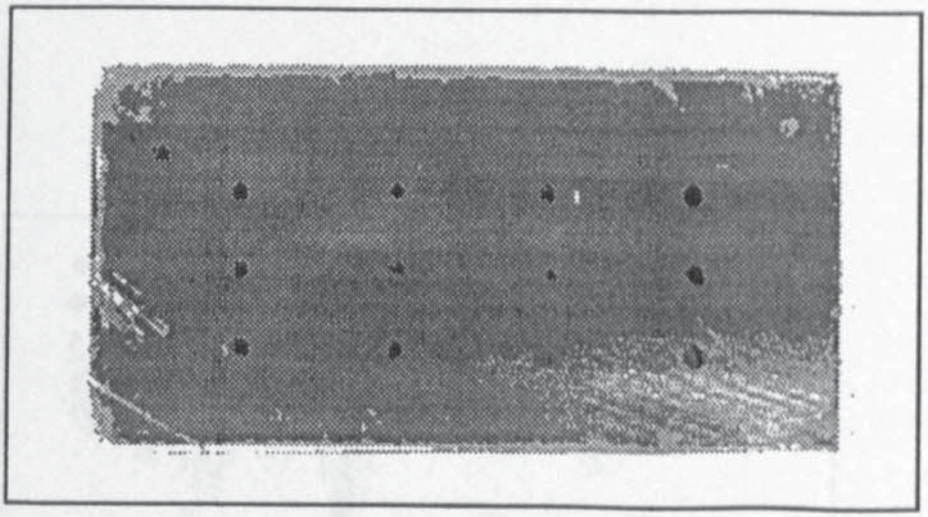

Figure 8.1: Image of a sheet of metal before deformation without sufficient illumination.

Figure 8.2: Binarization of the image (thresholding value:130)

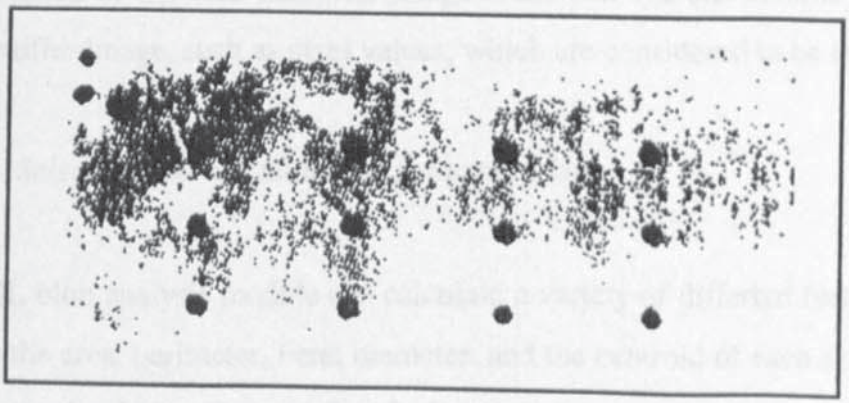

Figure 8.3: Binarization of the image (thresholding value:120)

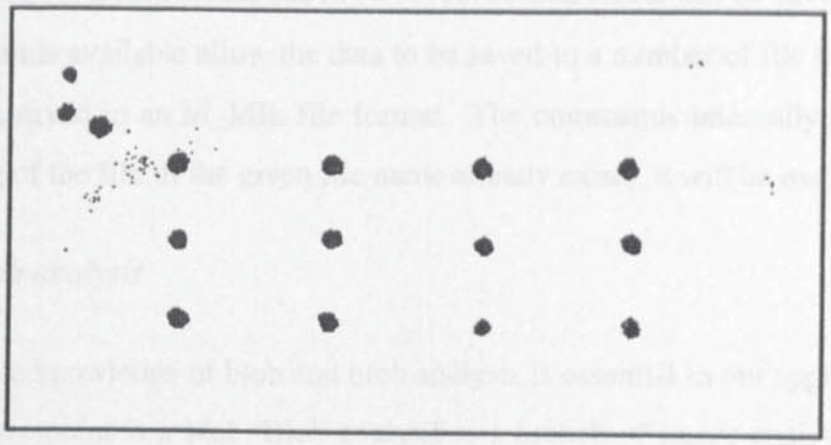

Figure 8.4: Binarization of the image (thresholding value:100)

Step 4: Change the foreground value

Before performing any blob analysis calculations, we should ensure that the interpretation of the blob identifier image is correct. We can control certain aspects of the identifier image, such as pixel values, which are considered to be in the foreground.

Step 5: Selection and calculation of features of blobs

The MIL blob analysis module can calculate a variety of different features of the blobs, such as the area, perimeter, Feret diameter, and the centroid of each selected blob. A list of features should be allocated first. In fact, it is the specified feature list that determines which of the calculations will be performed. The identifier image is scanned to locate blobs, and any selected features are calculated after calling the calculation function.

Step 6: Saving data

In this operation, a data buffer has to be saved. A data buffer can be saved to a disk file. The commands available allow the data to be saved in a number of file format. The data can also be saved in an M_MIL file format. The commands internally handle opening and closing of the file. If the given file name already exists, it will be overwritten.

Step 7: Blob analysis

A reasonable knowledge of blob and blob analysis is essential in our application because each measure point is a blob. Blob analysis is a branch of image analysis where many areas of interest within an image are measured and classified. These areas of interest are commonly known as blobs or objects.

Blobs are areas of adjacent pixels which are in the same logical pixel state called the foreground state. The alternate state is called the background state. Typically, the background has the value zero and the foreground is everything else, although some control is generally provided to reverse the sense. In most applications, the interest lies only in blobs whose measurements or features satisfy given criteria. Blob analysis is often performed as an elimination process whereby only blobs of interest are considered in further analysis; this is to minimise the computation time involved.

The steps involved in blob analysis are:

- Exclusion or deletion of blobs that do not meet given criteria.
- Analysing the remaining blobs to extract further information.

Once the raw data is reduced to a few measurements, results are generally more comprehensive and useful.

MIL package includes a blob analysis module which can measure blob features such as:

- Blob area
- Perimeter
- Centroid
- Feret diameter at a given angle

MIL utilises a user specified blob identifier to discriminate between blobs and background. Controls are provided to allow this identifier image to be interpreted to determine which pixels are part of which blob. Blobs are considered to consist of either zero or non-zero pixels, depending on the foreground control setting. The non-zero pixels can either have any value or must be set to the maximum value of the buffer, depending on the identifier type which is either grayscale or binary.

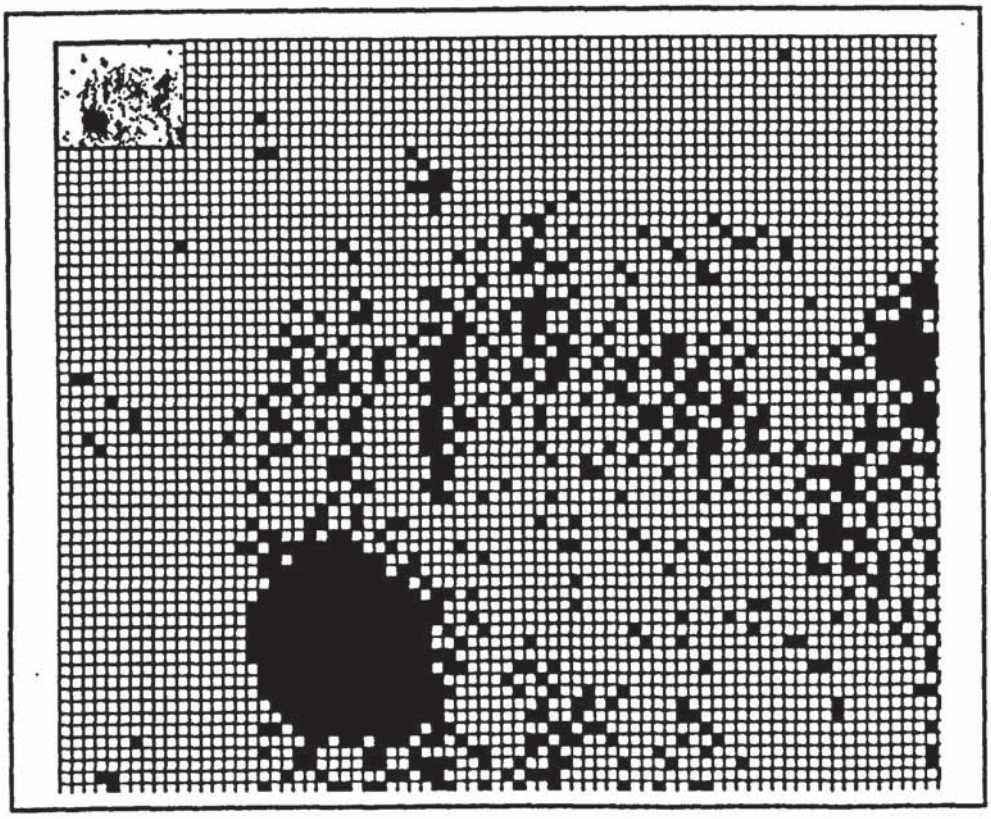

Figure 8.5: Image of a blob and the noise around it.

8.3 Description of the Procedure

After grabbing images, the images are processed to obtain the co-ordinates of each blob. The programs cogimag.cl (1 and 2) or cogmark.cl (1 and 2) (Appendix F) perform these operations and the co-ordinates are saved into data files.

This procedure is described below.

Step one: Declaration

The first part of the programs is a declaration of constants. These usually include:

(a) The name of the image to process
(b) The width and the height of the screen, in pixels
(c) The default value of thresholding binarization
(d) The name of the result files
(e) Size of one dimension (1D) data buffer
(f) Maximum number of blobs
(g) Maximum area for a blob, in pixel
(h) Radius of the smallest particles to keep, in pixels.

All of these constants will be used later in the program.

Step two: Processing

After allocating the system a 2D data buffer is created. The size of the buffer is defined by IMAGE_WIDTH and IMAGE_HEIGHT. The image is loaded into this previously allocated data buffer with the *MbufLoad( )* function.

The binarization gives a choice of the thresholding value of 128 in the default case or any value between 0 to 255. The user can change the value and the resulting binarized image can be viewed. The binarization is following by an opening and a closing operations which remove noise. Figure 8.5 shows a typical image of a blob and the noise around it.

Step three: Calculation

The following require special consideration in the process of calculation:

(a) The number of blobs

(b) The co-ordinates of the centroid of each blob

The MIL software cannot determine the number of blobs directly. By using the feature, *area*, blobs whose area is either smaller or bigger than a certain value can be excluded. The result is stored in the previously allocated result buffer (BlobResult).The change of foreground value is made before recognising the blobs (black) and the background (white).

MIL can calculate the co-ordinates of the centroid directly. The features M_CENTER_OF_GRAVITY_X, M_CENTER_OF_GRAVITY_Y are selected first and then the function *MBlobCalculate( )*. The results are written in to the same result buffer (BlobResult). The results from BlobResult are put it into the arrays (CogX and CogY). Cross-hairs are drawn at the centroid of each blob (Figures 8.6 and 8.7).

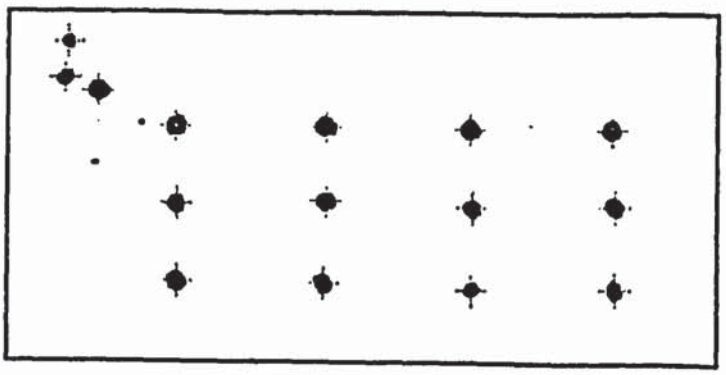

Figure 8.6 : The centroids are marked with cross hairs.

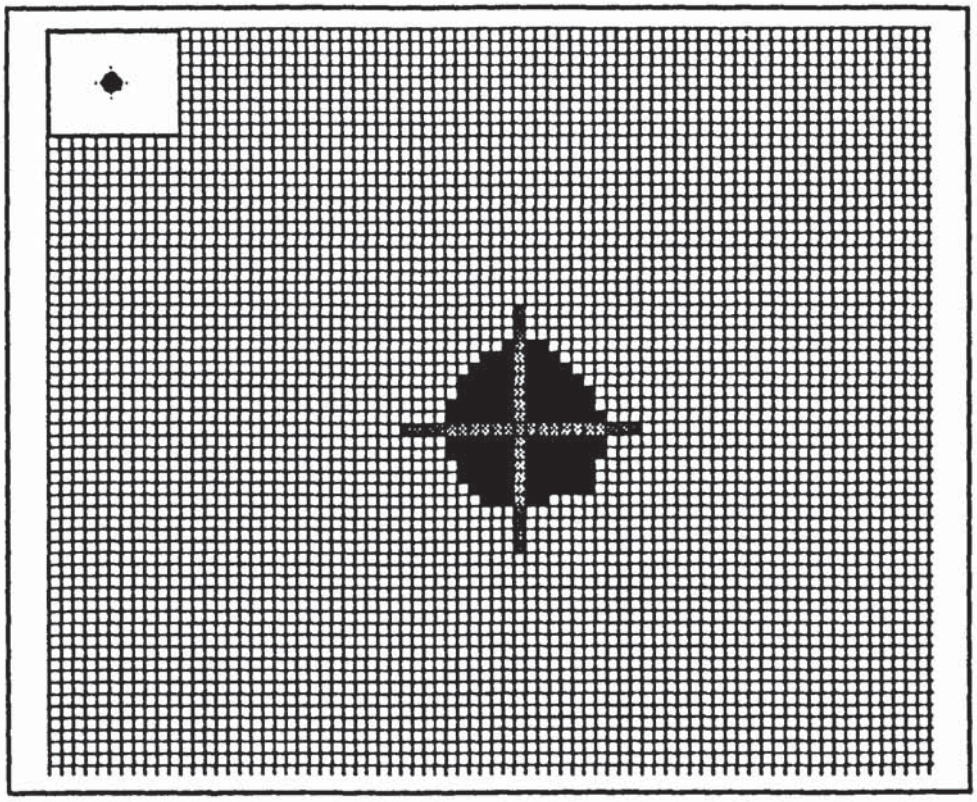

Figure 8.7: Image of a blob, and its centroid (marked by a cross hair)

Step four: Saving data

The MIL package and the Milinterpreter are not able to make the calculations such as strains. The MIL package is made specially for processing images and is not intended for mechanical calculations (stress, strains etc.). It does not support any floating point calculations and works only with integers. These co-ordinates are saved first for use in other programs later.

The co-ordinates of the centroid are in two arrays and MIL is able to save only data buffers; It is not able to save arrays. Therefore buffers (StructElemx, StructElemy), are allocated to store values and later save buffers into files (Resultx_file, Resulty_file). In order to conclude the operation of the program all of the MIL applications which were allocated earlier are made free.

Step Five: Linking of the different programs

The Link.cl program links the different MIL programs. It prompts the user to select the following options:

(a) grabbing

(b) processing images

(c) the image before deformation.

(d) the image after deformation.

For each choice the appropriate program is executed:

	Before Deformation	After Deformation
Grabbing the images	MFocus1.cl & MFocus2.cl	MFocus3.cl & MFocus4.cl
Processing the images	CogMark1.cl & CogImag1.cl	CogMark2.cl & CogImag2.cl

8.4 Measurement of Strains

Strain calculations are carried out with a program written in Microsoft Quick C Version 2.5.

The program consists of three main modules

(a) Retrieving the centroids of the grid points.

(b) Organisation of the co-ordinates of the grid point centroids.

(c) Calculations of strains.

8.4.1 Special Considerations

Measuring the co-ordinates of the rectangular array of 12 grid points before (Figure 8.8) and after deformation (Figure 8.9), presents a special problem. The position of the specimen before and after deformation can never be the same but the calculations have to be done in the same co-ordinate system.

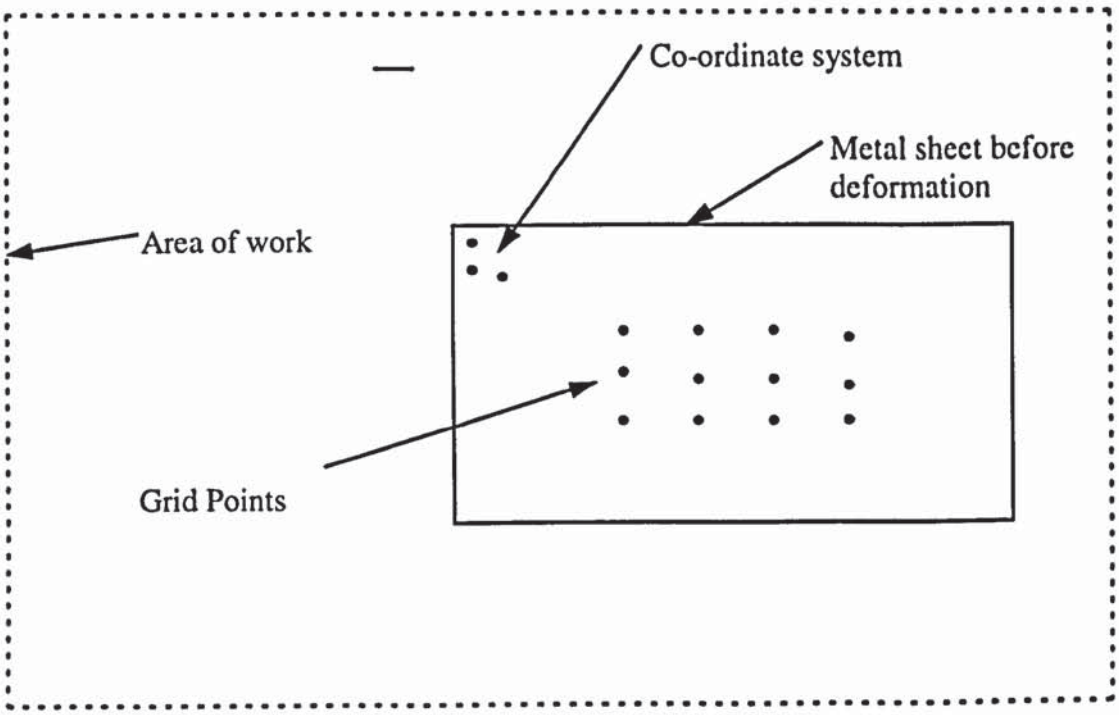

Figure 8.8 Position of the specimen before deformation.

8.4.2 Retrieving the co-ordinates of the grid points

The function "Fileopen" opens the MIL file, reads the values of the centroid, and saves it in an array.

These values have to be saved into the data files. MIL is capable of saving only buffers and the values have to be extracted from the buffer. MIL saves these values at the same address. Files are read only from this address. In addition, only a number of sets of values equal to the number of grid points is read from the file. These values are loaded into an array. This function is called each time the grid co-ordinates are required for the MIL processing.

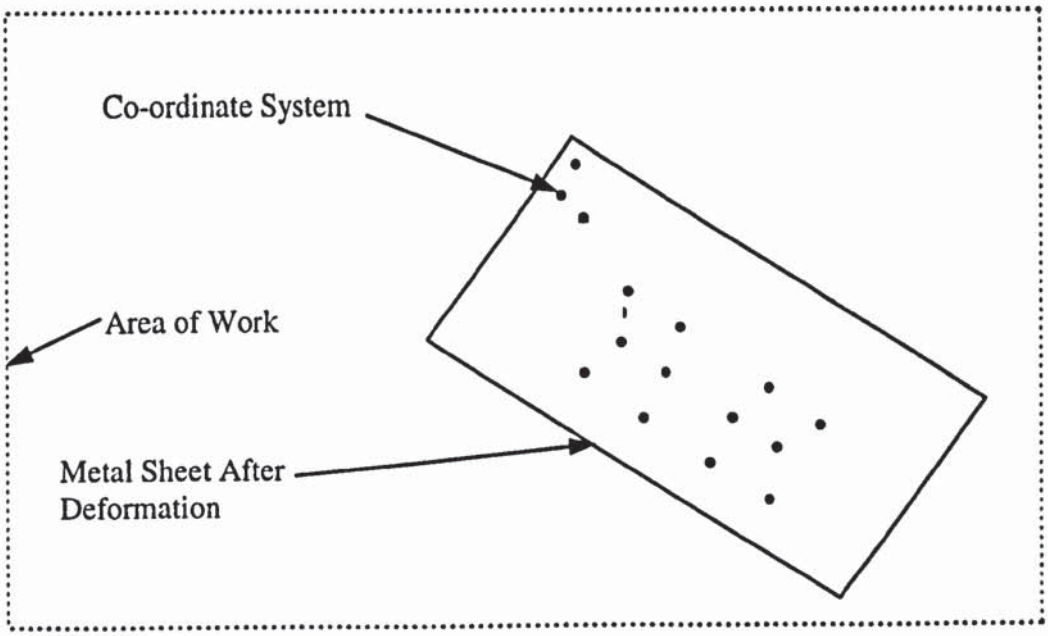

Figure 8.9 Position of the specimen after deformation.

8.4.3 Organisation of the grid point co-ordinates

It has to be ensured that the same reference co-ordinate system is used with the grid point co-ordinates before and after deformation. This is achieved with a transformation of co-ordinates - one rotation and one translation.

Two co-ordinates systems are required:

(a) one for the sheet metal specimen before deformation
(b) one for the sheet metal specimen after deformation

These two reference co-ordinate systems should be remote from the zone where strains are experienced. A co-ordinate system is represented by three points, two in two different directions as shown in figure 8.10. It is not necessary that they are perpendicular.

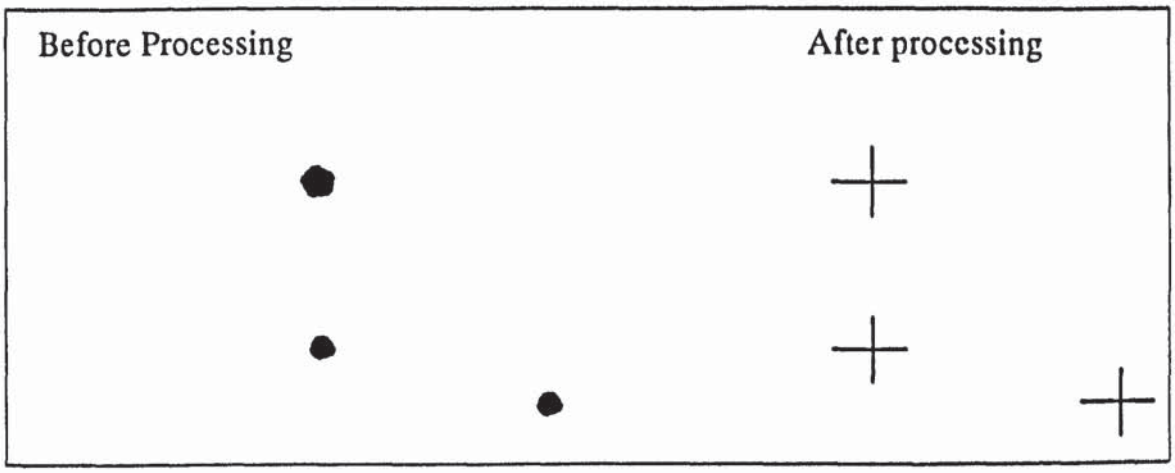

Figure 8.10 Example of a coordinate system

Each point of the co-ordinate system is considered a blob. The three points representing the co-ordinate system before and after deformation are processed. The co-ordinates of the centroid of each blob is determined. The function "change" transforms the co-ordinates from the deformed system to the undeformed system.

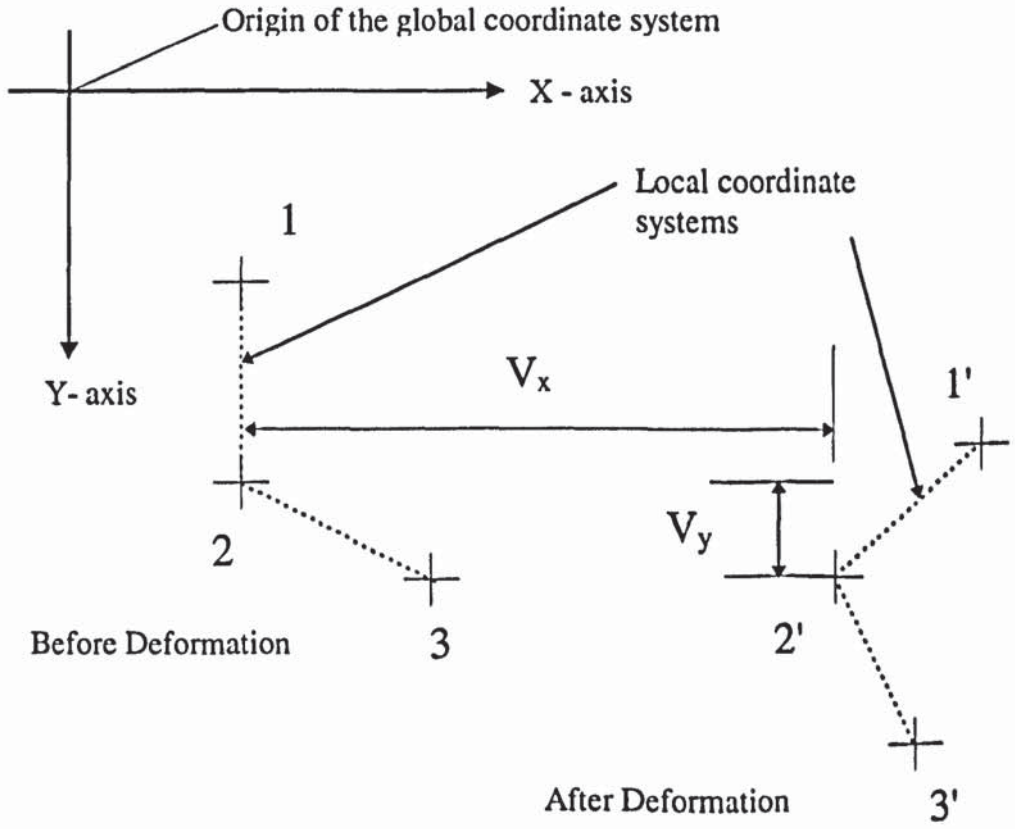

Figure 8.11 Translation Vector

First, the function calculates the translation vector as shown in figure 8.11. This vector is determined by the co-ordinates of the origins of the local co-ordinate systems. Its value is (Vx,Vy) for a translation from "before" to "after" deformation. Secondly, the function calculates the rotation angle (Figure 8.12).

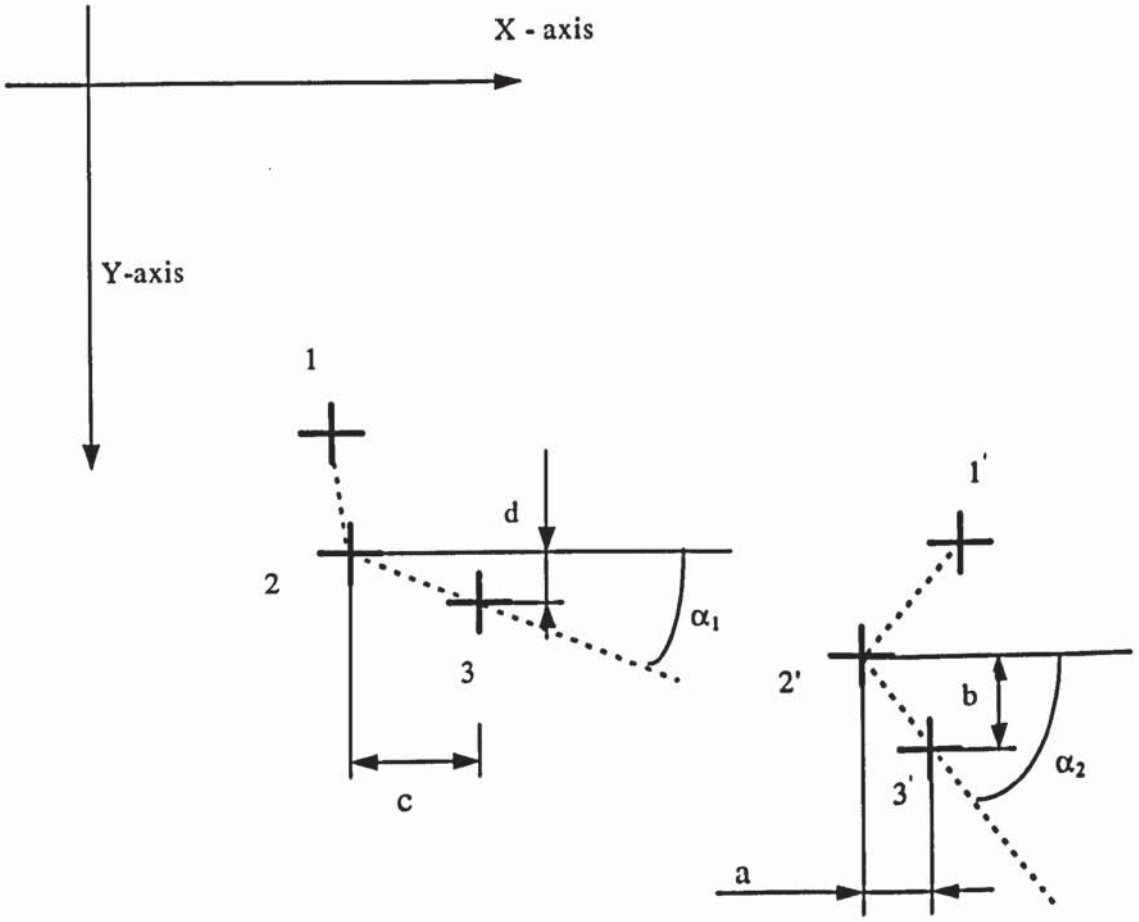

Figure 8.12 Determination of the rotation angle.

Each grid point after deformation can be transformed to the undeformed local co-ordinate system as shown in figure 8.13 and figure 8.14.

Once all the grid points are in the same co-ordinate system, then their co-ordinates can be determined as follows:

arctan (d/c) = α_1 angle between the horizontal direction and 2-3 direction

arctan(b/a) = α_2 angle between the horizontal direction and 2' - 3' direction

Rotation angle = $\alpha_2 - \alpha_1$

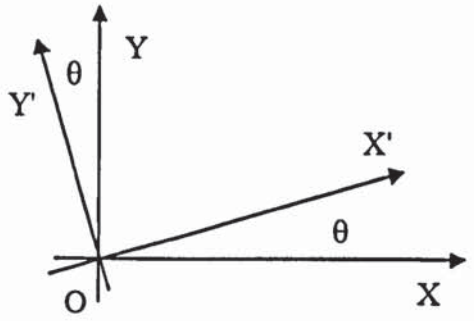

Figure 8.13 Transformation of the co-ordinates system

Let (x, y) be the reference co-ordinate system before rotation and

(x', y') be the co-ordinate system of after rotation

Then

$$x' = x\cos\theta + y\sin\theta$$

$$y' = -x\sin\theta + y\cos\theta$$

This can also be expressed as

$$\begin{bmatrix} x \\ y \end{bmatrix} = [K] \begin{bmatrix} x' \\ y' \end{bmatrix} \qquad [K] = \begin{bmatrix} \cos\theta & -\sin\theta \\ \sin\theta & \cos\theta \end{bmatrix}$$

$$\begin{bmatrix} x' \\ y' \end{bmatrix} = [K]^{-1} \begin{bmatrix} x \\ y \end{bmatrix} \qquad [K]^{-1} = \begin{bmatrix} \cos\theta & \sin\theta \\ -\sin\theta & \cos\theta \end{bmatrix}$$

The transformation of co-ordinates system is made with respect to the origin O (0,0) of the global co-ordinate system. In this application, the origin of the image is not the same as the origin of the first local co-ordinate system (undeformed). Hence the centre of rotation is not the origin O(0,0) of the global co-ordinate system.

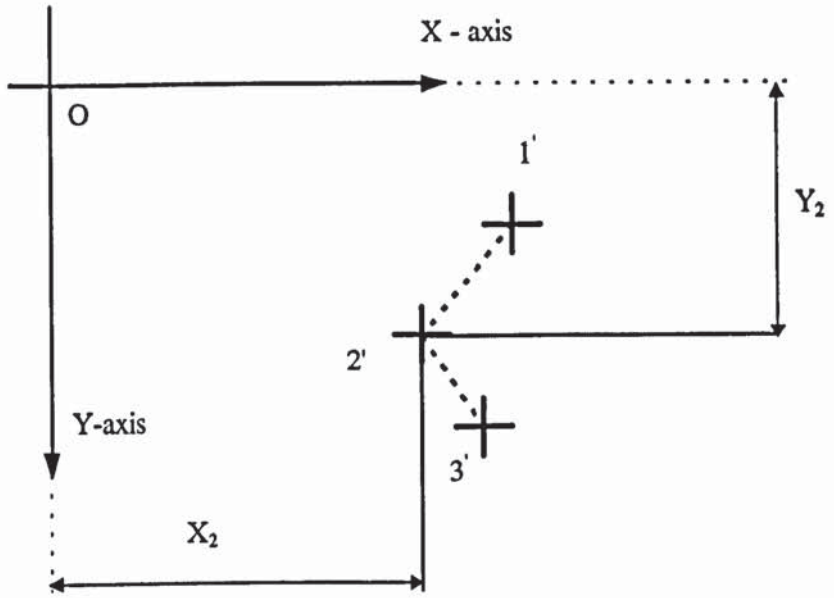

Figure 8.14: Rotation in the co-ordinates system after deformation

The co-ordinates of the points after deformation are given by

$$\begin{bmatrix} X' \\ Y' \end{bmatrix} = \begin{bmatrix} (X - X_2)\cos\theta + (Y - Y_2)\sin\theta \\ -(X - X_2)\sin\theta + (Y - Y_2)\cos\theta \end{bmatrix} - \begin{bmatrix} V_X \\ V_Y \end{bmatrix} + \begin{bmatrix} X_2 \\ Y_2 \end{bmatrix}$$

where

$\begin{bmatrix} X' \\ Y' \end{bmatrix}$ = Co-ordinates of the points after deformation in the co-ordinate system of the image before deformation.

$\begin{bmatrix} V_X \\ V_Y \end{bmatrix}$ = Vector translation

$\begin{bmatrix} X_2 \\ Y_2 \end{bmatrix}$ = Centre of Rotation

8.5 Algorithm for the Organisation of Grid Points

The aim of this algorithm is to order the grid point co-ordinates in a manner suitable for the calculation of strains. It is necessary to classify and number every grid point. (Figure 8.15)

8.5.1 The choice of the origin of the local co-ordinate system of the grid points

The base or origin of all points in the grid is the point located at the top left of the grid. This is actually the origin of the local co-ordinate system of the grid points. To locate this point, the program will search for the grid point with the smallest x and y values with respect to the global co-ordinate system.

8.5.2 Columns of grid points

The points that belong to each column are determined for the purpose of arranging them in sequence. These points have the same x-axis co-ordinate of the base or origin ($\pm \Delta x$) but different y-axis co-ordinates.

8.5.3 Classification of the columns of grid points

The grid points in each column are classified from the smallest to the biggest y value.

8.5.4 Calculation Procedure

The calculations are performed in the sequence shown in the figure 8.15 and in the following order

(a) points 1,4,5 and 2

(b) points 4,7,8 and 5

(c) points 2,5,6 and 3

-etc...

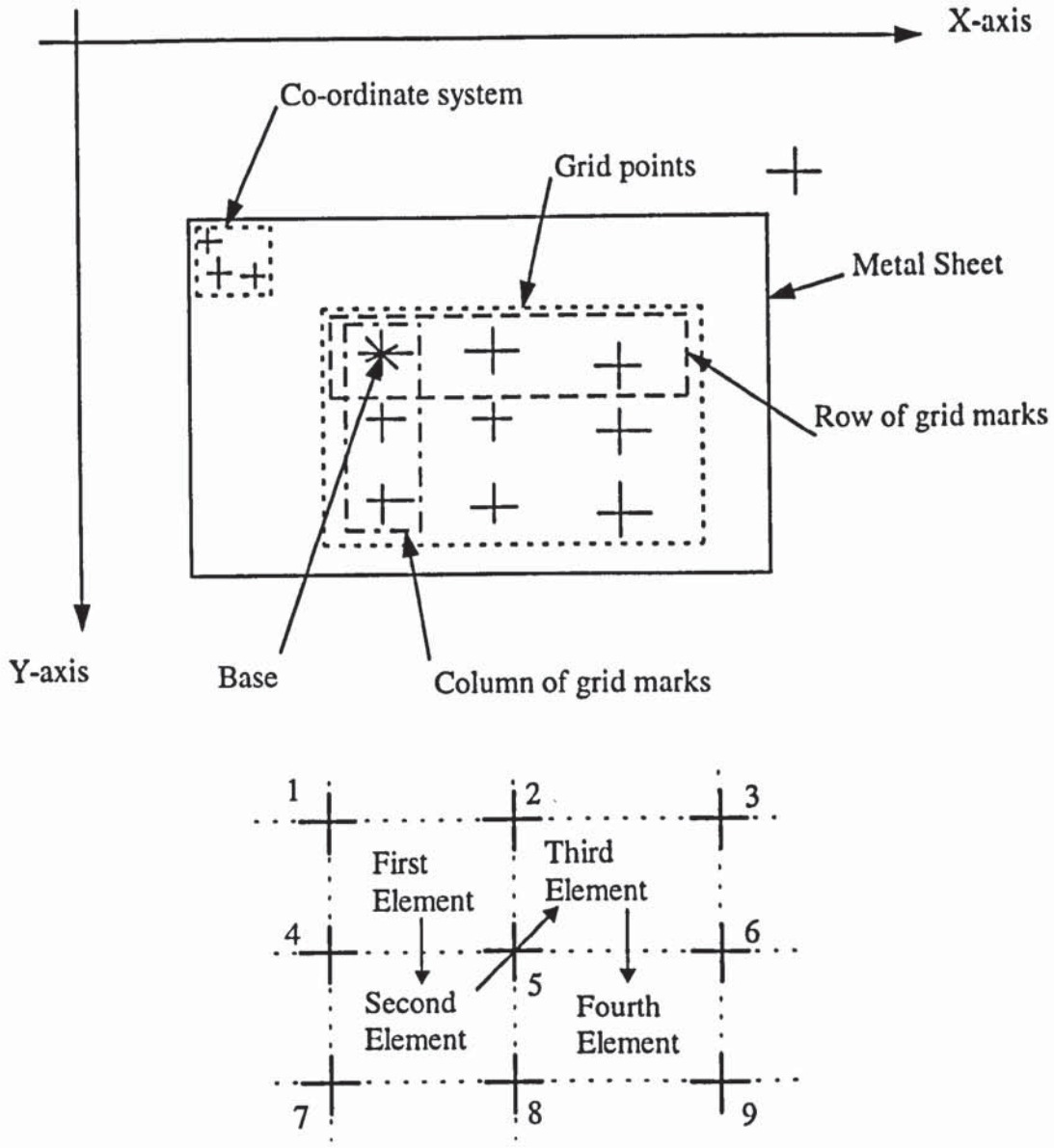

Figure 8.15 Classification of grid points

8.5.5 Calculation of strains

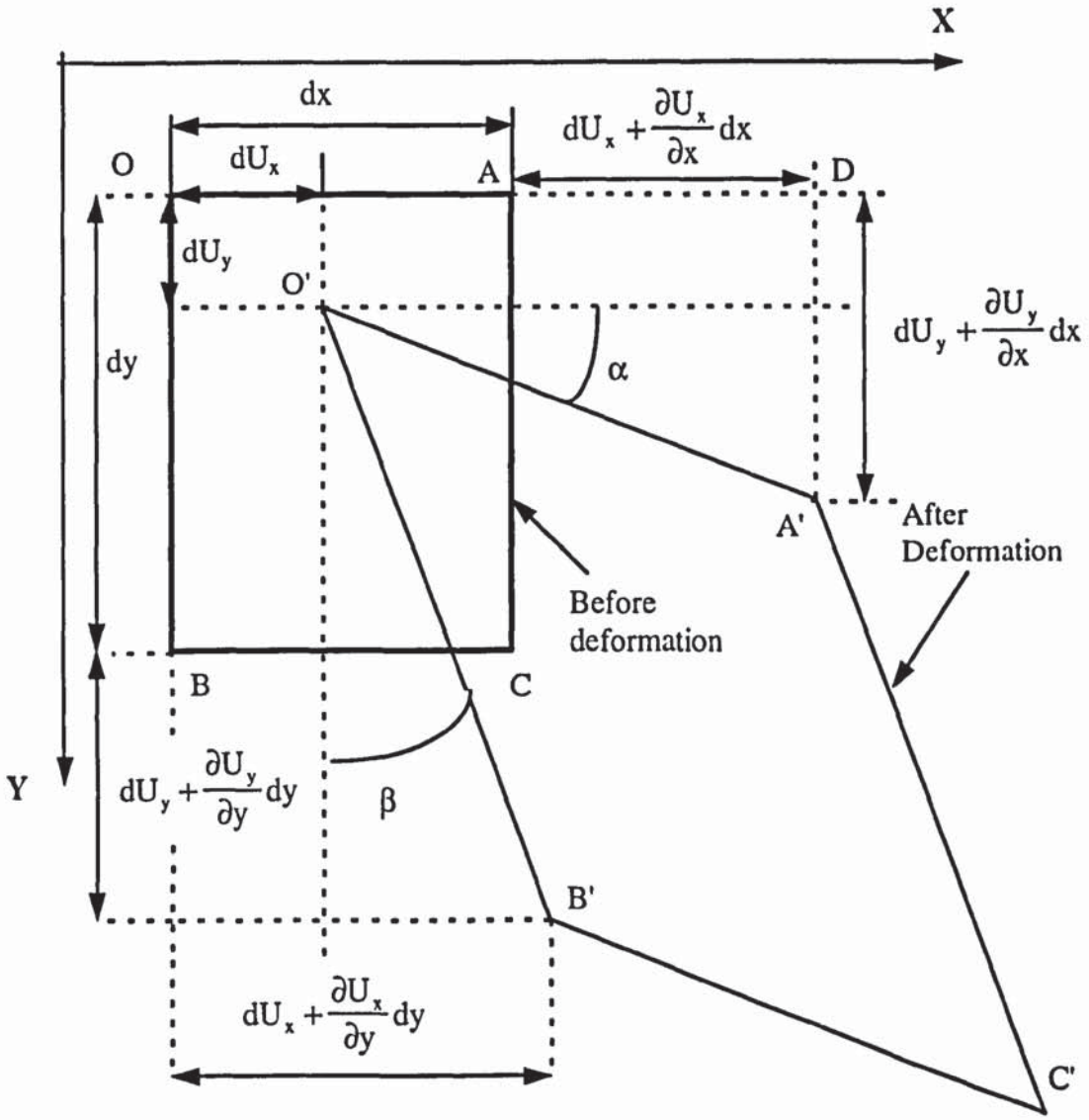

Figure 8.16 Deformation of a plane element.

Consider the Cartesian plane of two dimensions with a (x, y) co-ordinate system. The rectangle (OACB) before deformation (dx and dy each side) becomes the quadrilateral (O'A'C'B') after deformation.

The formulas used for the calculations of strains in the *Strains.C* program are:

$$\varepsilon_{xx} = \frac{x_{A'} - x_{O'} - (x_A - x_O)}{x_A - x_O}$$

$$\varepsilon_{yy} = \frac{y_{B'} - y_{O'} - (y_B - y_O)}{y_B - y_O}$$

$$2\varepsilon_{xy} = \gamma_{xy} = \frac{y_{A'} - y_{O'}}{x_A - x_O} + \frac{x_{B'} - x_{O'}}{y_B - y_O}$$

8.5.6 Printing of the results

The printing of the results includes:

(a) The number of points for calculations (four).

(b) The value of Eps1 (longitudinal strain).

(c) The value of Eps2 (transverse strain).

(d) The value of Eps12 (angular distortion).

8.5.7 Comparative tests

To evaluate the accuracy of the vision system, the strains measured with the vision system were compared with the strains measured with conventional methods.

First, three tensile tests were carried out on Aluminium Alloy specimens (Figure 8.17a) and the strains were recorded at the peak stress. The yield stress of the material was established during these tests. A second series of tests were carried out with four specimens made of sheet metal from the same stock. A grid was marked on the specimen as shown (Figure 8.17b). A tensile force of 15kN was applied in the longitudinal direction to subject the specimen to the same stress peak. An image of the grid was captured before and after the application of the load and the strains were calculated using the computer vision software developed.

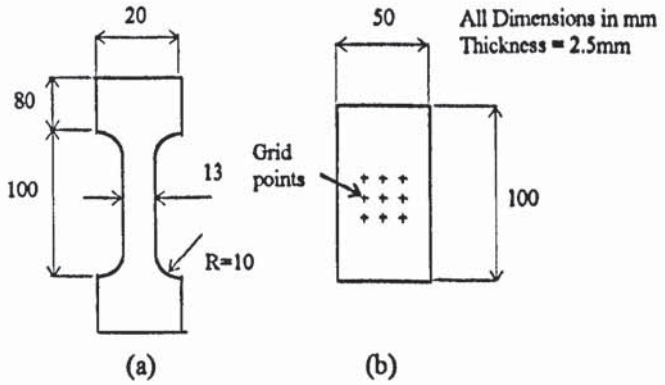

Figure 8.17. Test Specimens for strain measurement using computer vision techniques.

Strains Measured using Conventional Methods

	Peak Stress (MPa)	Yield Stress (MPa)	Max Strain
Test 1	122.5	119	0.0175
Test 2	121.5	118	0.0176
Test 3	123.3	117	0.0179

Strains Measured using the Vision System

	Eps1	Eps2	2Esp12
Test 1	0.0197	-0.0032	variable
Test 2	0.0149	0	variable
Test 3	0.0156	0	variable
Test 4	0.0153	-0.006	variable

The results obtained for Eps1 using the vision system agree well with the results obtained by conventional means.

8.5.8 Conclusion

The objectives of providing a basic framework for the measurement of strains using a vision system has been achieved. At present, the system is able to grab an image and process it, as well as calculate the corresponding strains.

The algorithm developed for the calculation of strains is quite restrictive in the sense that the program works only for planar case with no holes. In addition, the grid is assumed to be nearly perfect and evenly spaced .

CHAPTER 9

DISCUSSION AND CONCLUSION

The strains in the specimens measured during the experiments can be classified as (a) Longitudinal and (b) Lateral. These strains were measured both in the web and the flanges of the specimens. Both Steel and Aluminium specimens were used during the experiments. Strains were measured for different interpass distances and numbers of roll stations to study the possible effect of these parameters on the strains measured.

Experimental strain values are compared with the values predicted by theory and finite element analysis. Finally, plastic strains measured using the grid method and computer vision techniques are compared to validate the software developed for strain measurement.

9.1 Elastic-Plastic Strain Analysis

9.1.1 Longitudinal strains in the web

(a) Longitudinal strains in the web (CRF Mill No:2) Steel Specimen

The longitudinal strains in the web measured on specimens formed on the CRF mill No:2 are shown in Figure 9.1. They show a compressive maximum at a distance of about 20 mm from the central position of the roll, and then turn in to a tensile maximum near the roll. A rapid strain recovery then follows. As the interpasss distance decreases, the maximum compressive strain become more severe. It can be seen that the maximum compressive strain is highest when the interpass distance is lowest.

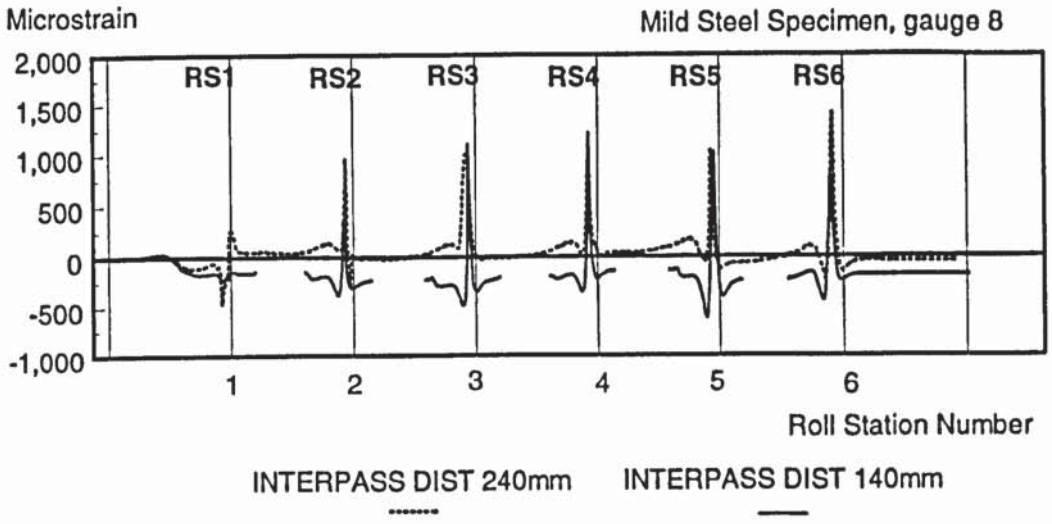

Figure 9.1 Longitudinal strain distribution in the web (CRF Mill No: 2)

(b) Longitudinal Strain in the web (CRF Mill No: 1) Aluminium Specimen

The longitudinal strains in the web of an Aluminium specimen are shown in Fig 9.2. The strains in the specimen are compressive except near the roll stations. The strains undergo a compressive maximum at a distance of about 15 mm from the roll station centre lines, and then turns into tensile maxima near the roll centre lines. A rapid strain recovery then follows.

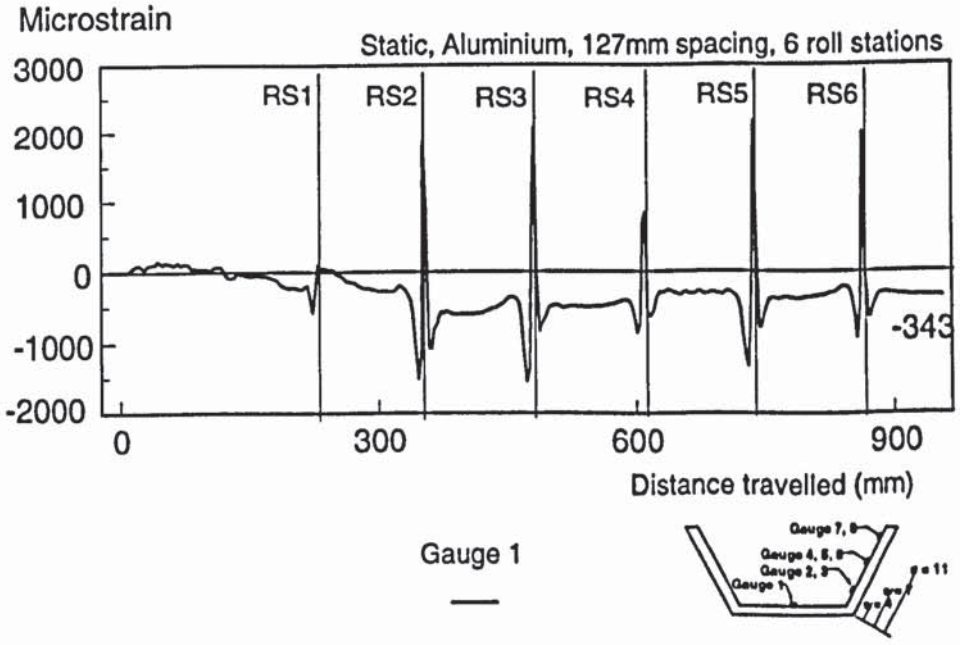

Figure 9.2 Longitudinal strain distribution in the web (CRF Mill No:1)

9.1.2 Longitudinal strain in the flange

(a) Longitudinal strain in the outer edge of the flange (CRF Mill No:2)

The longitudinal strains in the flange measured for different interpass distances are shown in Figure 9.3. The strains reach a compressive maximum before a tensile maximum. The maximum tensile strain is observed some distance before the centre-line of the roll. This maximum tensile strain is affected by the interpass distance between the roll stations. As the interpass distance between the roll stations increases from 140 mm to 240 mm the tensile maximum strain as well as the residual strain increases. This increase in the residual strain in the outer edge is undesirable since the straightness of the flange will be affected. The maximum compressive strain increases when the interpass distance changes from 240 mm to 140 mm.

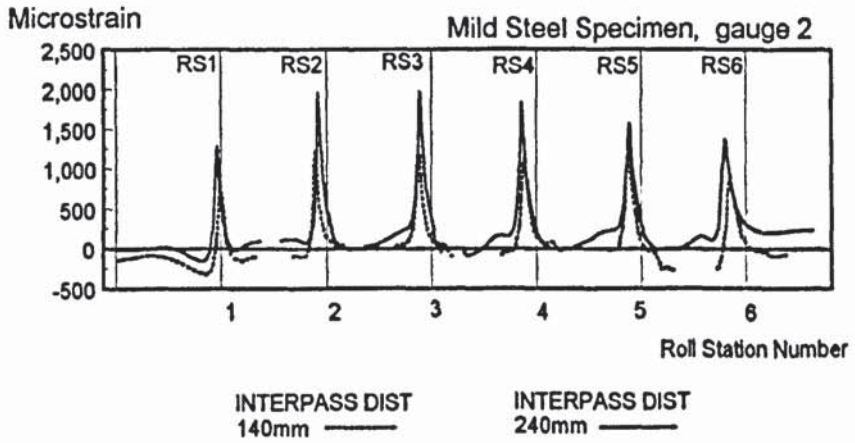

Fig 9.3 Longitudinal strain in the outer edge of the flange

(b) Longitudinal strain near the bend line of the flange (CRF Mill No:2)

The graphs of the longitudinal strains near the bend line of the flange are shown in the Figure 9.4. Unlike the longitudinal strains at the edge, the longitudinal strain at the bend line are mostly compressive. The compressive residual longitudinal strain between the roll stations is highest when the interpass distance between each roll station is 140 mm and it was observed that this residual strain decreases as the distance between the roll stations is increased to 240 mm. Slight changes are observed in the compressive

longitudinal strain influences the bending stress in the lateral direction. The addition of such redundant strains gives rise to complex effects to the forming of the required cross-sectional profile and may decrease the intensity of springback deformation as shown in the springback tests. This leads us to expect that the larger the values of these redundant strains become in the process of cold roll forming, the more does the cross-sectional profile improve.

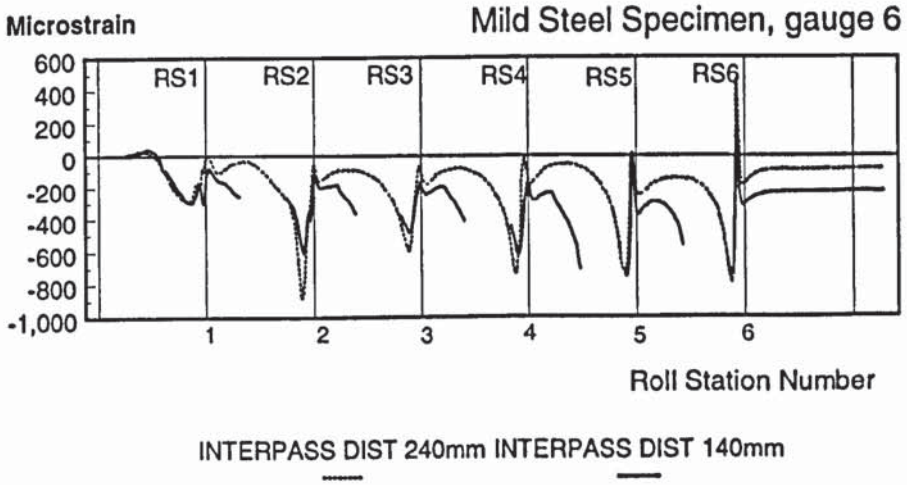

Fig 9.4 Longitudinal strain near the bend line of the flange (CRF Mill No: 2)

(c) Longitudinal strain variation across the flange (CRF Mill No: 1)

The longitudinal strains in the flange measured on Aluminium specimens formed on the CRF Mill No: 1 are shown in Figure 9.5. These strains follow the same general pattern as the specimens formed on mill No:2 (Figure 9.7).

By considering the position of the maximum value of $\frac{d\theta}{dz}$ on the bend angle curve [Panton3], the reason for this becomes apparent. As illustrated in Figure 9.6, the maximum value of $\frac{d\theta}{dz}$ will always occur at the boundary of regions II and III. So the maximum strain will occur before the centre line of the roll.

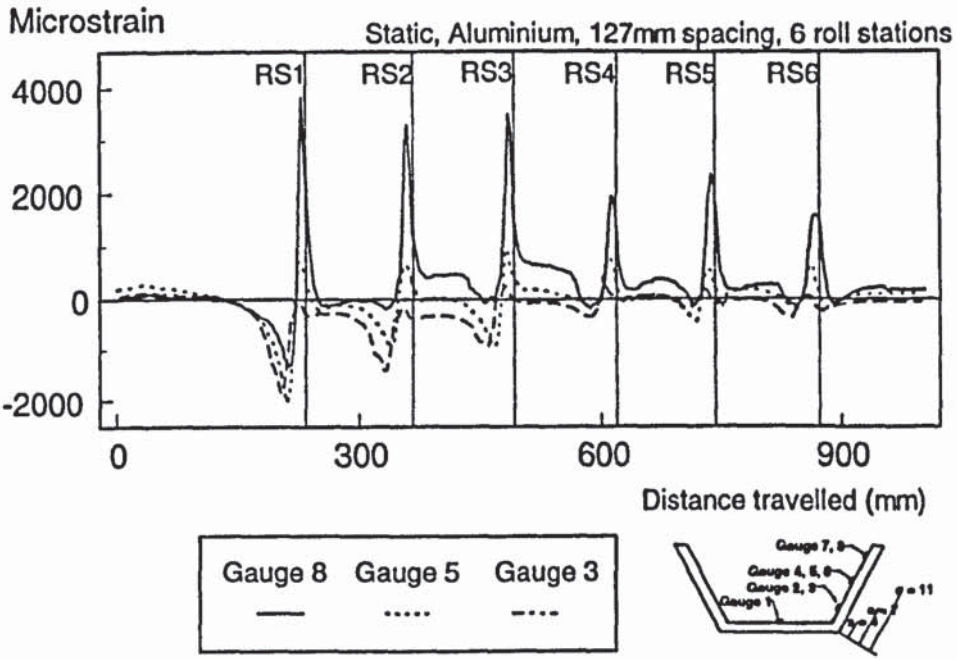

Figure 9.5. Longitudinal strain distributions in the flange (CRF Mill No:1).

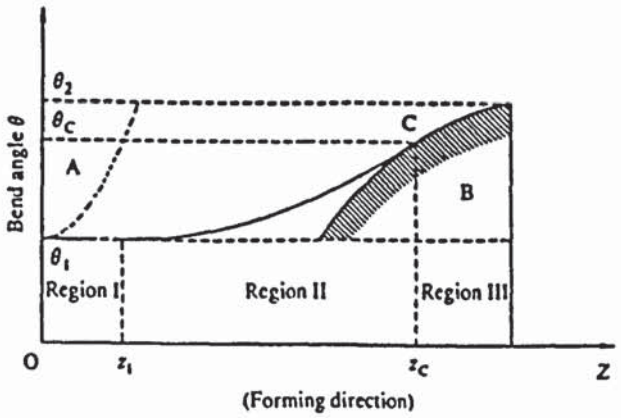

Figure 9.6. Bend angle curve [Panton3].

The "compressive-tensile" strain phenomenon can also be explained with Figure 9.8 (b) [Noble]. As the flange of the trapezoidal section being rolled into the mated rolls, Section A_i-B_i becomes compressive and section B_i-C_i becomes tensile. Deformation is more severe for the first three stations (Figure 9.5). This is due to the larger fold angles used for the first three roll stations (19.69°,15.9°,11.45°) than the last three stations (8.01°,5.74°,4.24°).

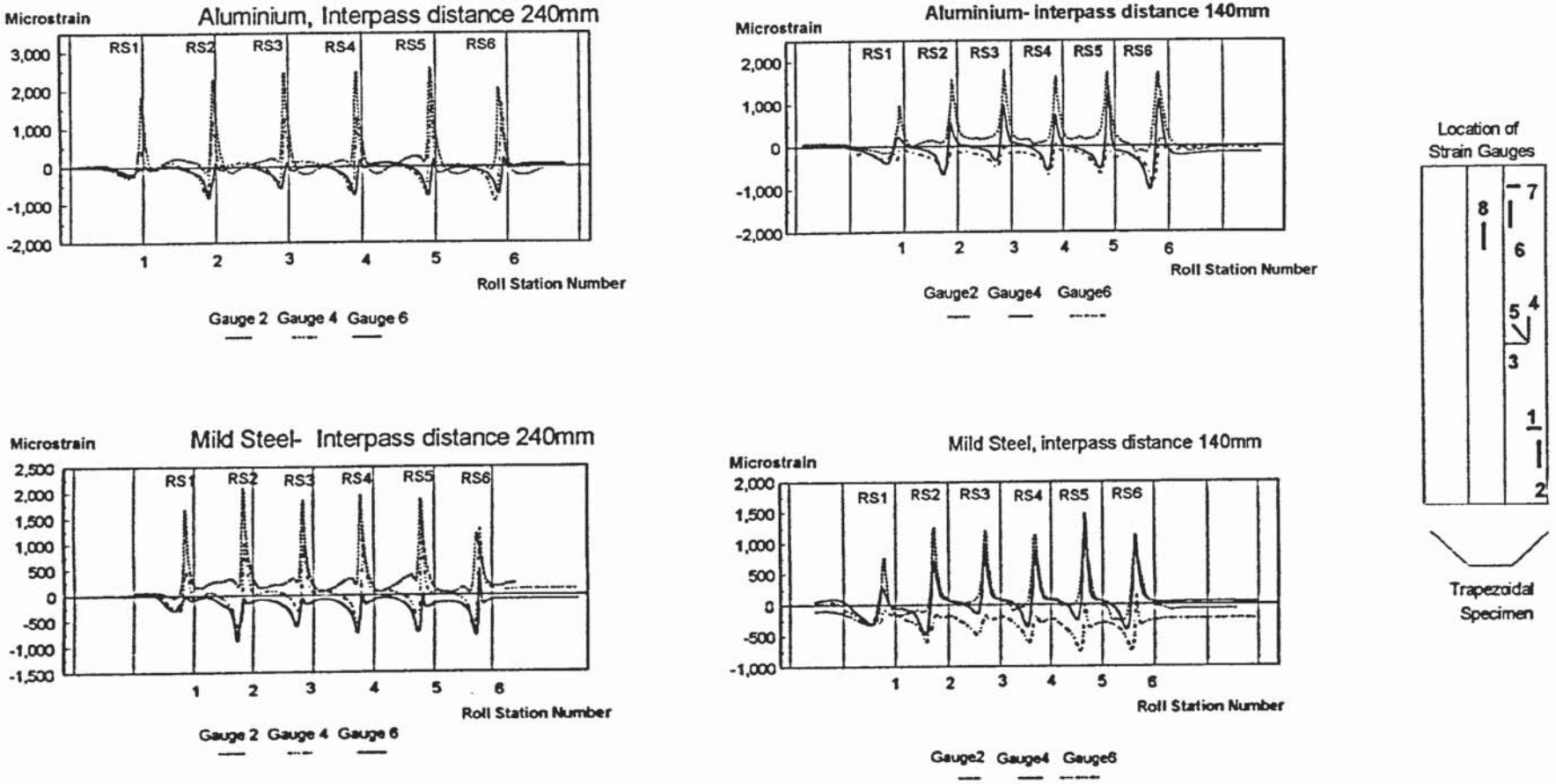

Figure 9.7. Comparison of Longitudinal Strain distributions at different locations of flange for Steel and Aluminium Specimens (CRF Mill No:2).

In general the longitudinal strain distribution increases from the fold line to the edge. This is explained with Figure 9.9 which shows a progressive elongation from the fold line to the edge of the strip. The residual strain is also higher near the edge. Large longitudinal strain results in a larger residual strain which in turn affect the straightness of a roll-formed product.

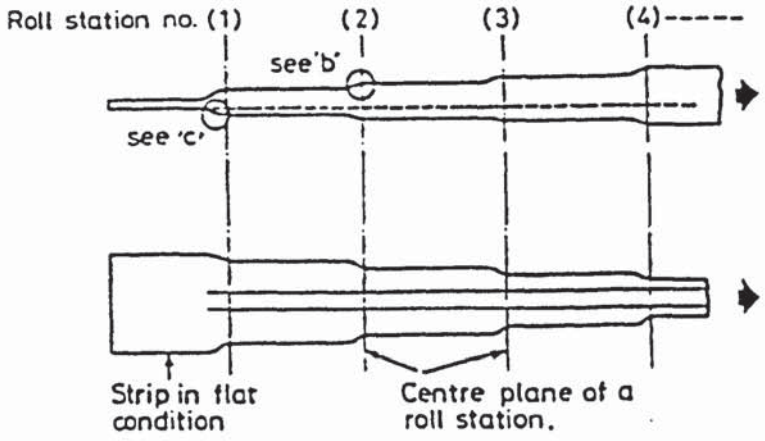

a)

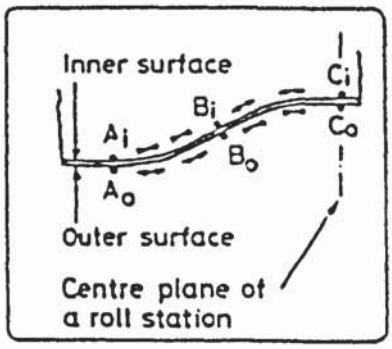

b)

Figure 9.8. Localised deformation during cold roll-forming [Noble].

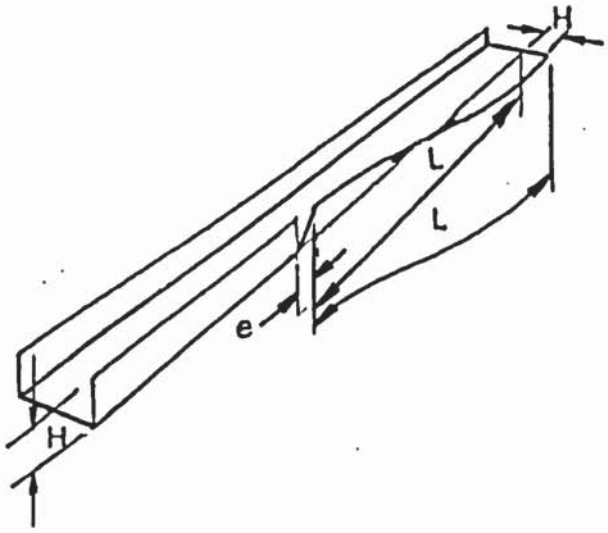

Figure 9.9. Edge of strip elongated during forming[Halmos4].

9.1.3 Lateral strains in the flange

(a) Lateral strains in the outer edge of the flange

Typical measured values of the lateral strain in the outer edge of the flange are shown in Figure 9.10. The compressive maxima occurs before the centre-line of the each roll station and the residual strain between the roll stations are the highest at the interpass distance of 140 mm.

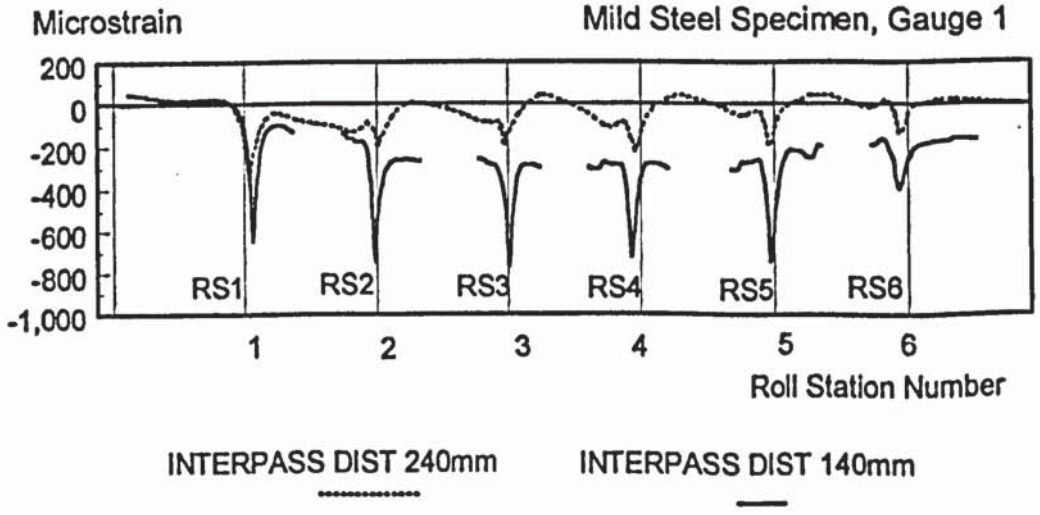

Fig 9.10 Lateral strain in the outer edge of the flange (CRF Mill No: 2)

The compressive maximum and the absolute residual strain is decreased as the distance between the roll stations increased to 240 mm. A lower lateral strain in the outer edge of the flange imply that the flange is also straighter.

(b) Lateral strain in the bend corner of the flange (CRF Mill No: 2)

The lateral strains in the bend corner of the flange are represented in Figure 9.11. These strains are always negative. The compressive maximum occurs just before the centre-line of each roll station. This is due to the fold line which developed the compressive strain. This compressive strain is at its highest when the interpass distance between the rolls station is 140 mm. As can be seen from Figure 9.11, there are slight changes in the compressive maximum before the centre-line of each roll station when the distance between rolls station increases from 140 mm to 240 mm. However, a gradual decrease in the absolute residual compressive strain is observed between the centre-line of the two rolls stations when the distance between the roll stations increases. A decrease in lateral residual compressive strain near the bend corner may increase the intensity of springback. On the other hand, an excessive increase in the lateral residual compressive strain may cause not only a decrease in springback deformation, but also a spring-forward tends to occur.

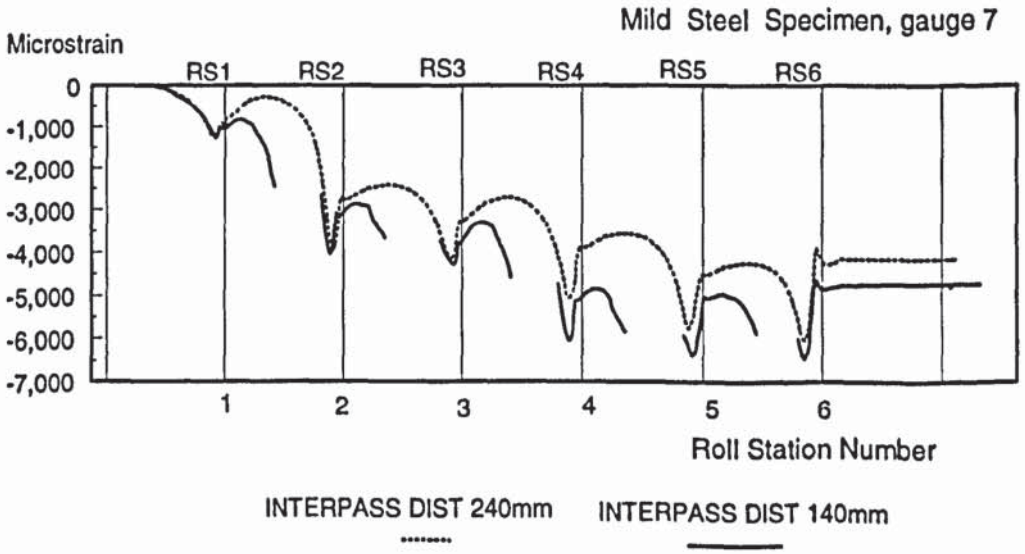

Figure 9.11 Lateral strain in the bend corner of the flange

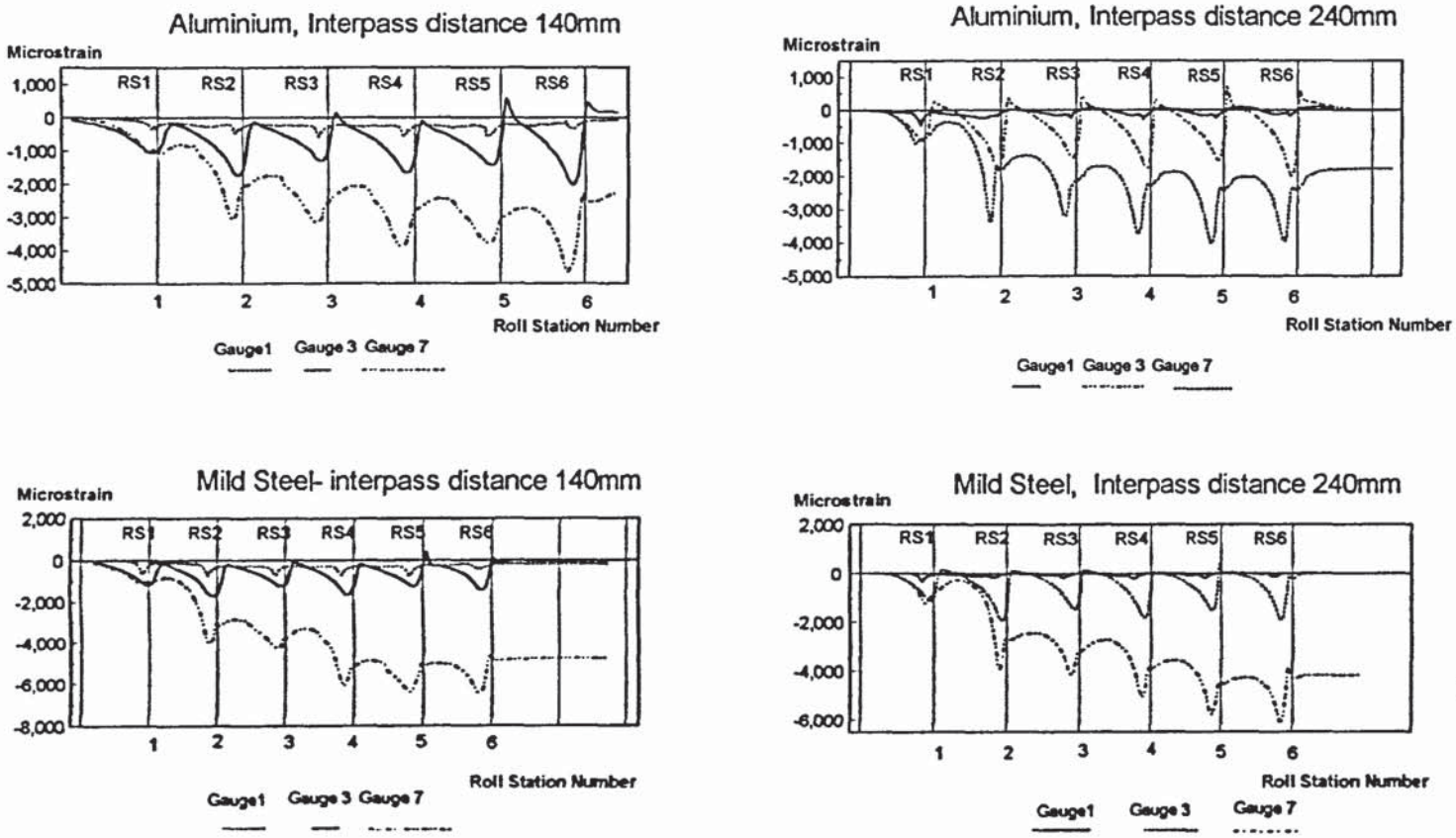

Figure 9.12. Comparison of Lateral Strain distributions at different locations of flange for Steel and Aluminium Specimens (CRF Mill No:2).

(c) Lateral strain variation in the flange

The lateral strains measured in the flange for specimens formed on the CRF mill No:1 are always negative as shown in Figure 9.13. A compressive maximum occurs just before the centre-line of each roll station. This is due to bending at the fold line which developed the compressive strain. Unlike the longitudinal strain, the absolute lateral strain distribution decreases from the fold line to the edge. Since Gauge 2 is near the fold line, naturally it will record the highest absolute lateral strain. The absolute residual strain is also the highest for gauge 2. Similar results were obtained for specimens formed on the CRF mill No:2 for different interpass distances (Figure 9.12).

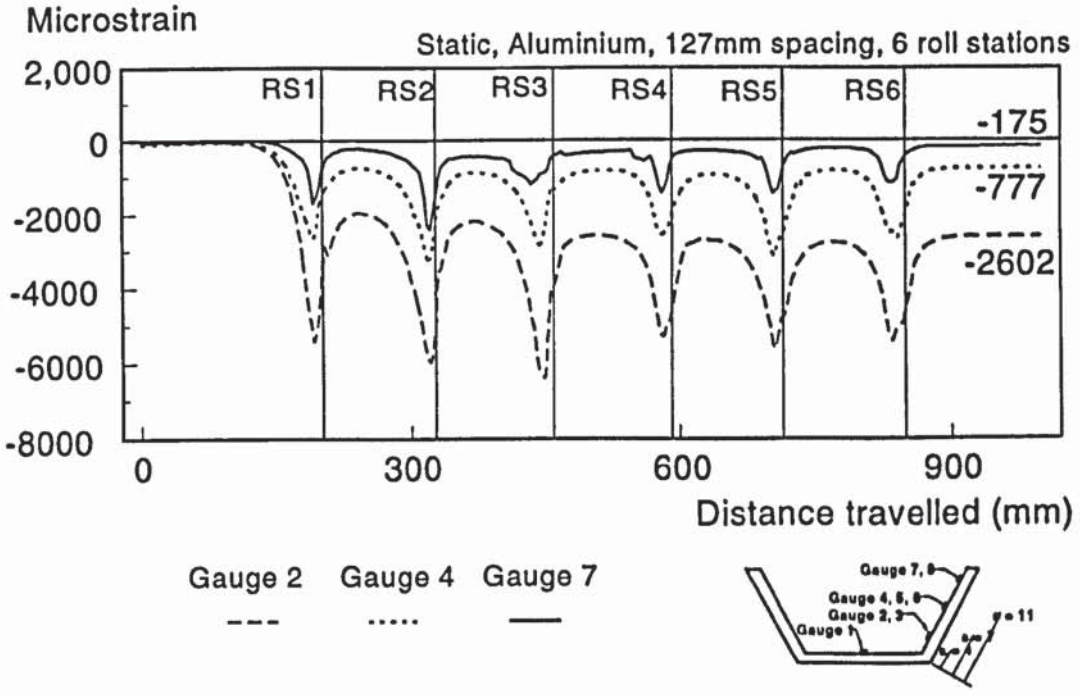

Figure 9.13 Lateral strain distributions in the flange (CRF Mill No:1)

9.1.4 Principal Strain Analysis

The maximum principal strains, measured with strain rosettes can be represented by Figure 9.14. Unlike the longitudinal strain distribution, the maximum principal strain does not have a compressive maximum before a tensile maximum. In fact, the maximum principal strains are always positive and keep close to the zero strain line before increasing to a tensile maximum. This tensile maximum is observed to occur some distance before the centre-line of the roll. The maximum principal strain shows no

significant difference for the two different interpass distances. This may be attributed to less dominant tensile strain on that particular region.

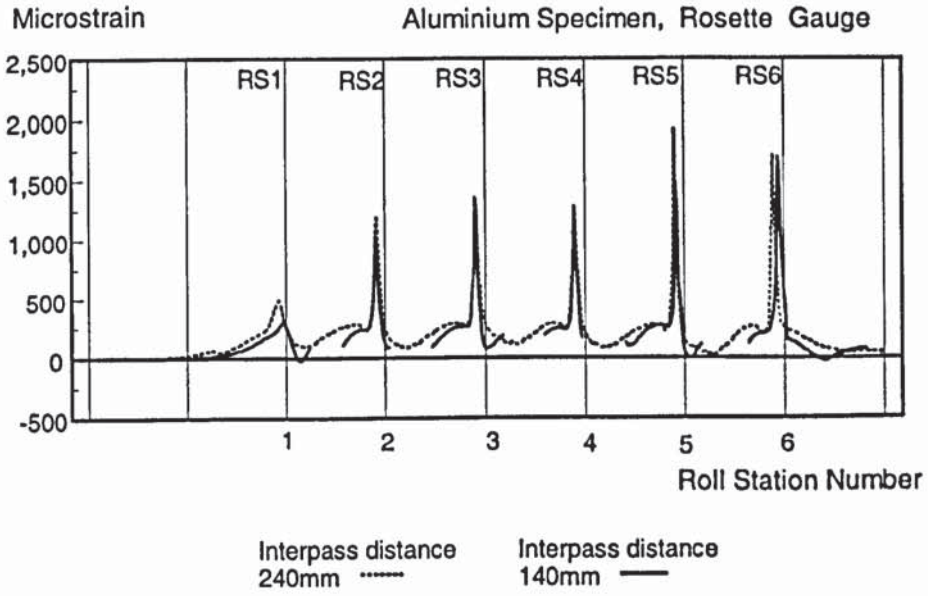

Figure 9.14 Maximum principal strain distribution (CRF Mill No:2).

The minimum principal strains are shown in figure 9.16. The minimum principal strains are always negative and a compressive maximum occurs some distance just before the centre-line of the roll. Slight changes are observed in the compressive maximum strain before the centre-line of the roll when the interpass distance of the roll increases. The residual principal strain distribution between the centre-line of each station increases as the interpass distance between each station changes from 240 mm to140 mm. This implies that the compressive strains are higher when the roll-stations are closed up during the forming operation.

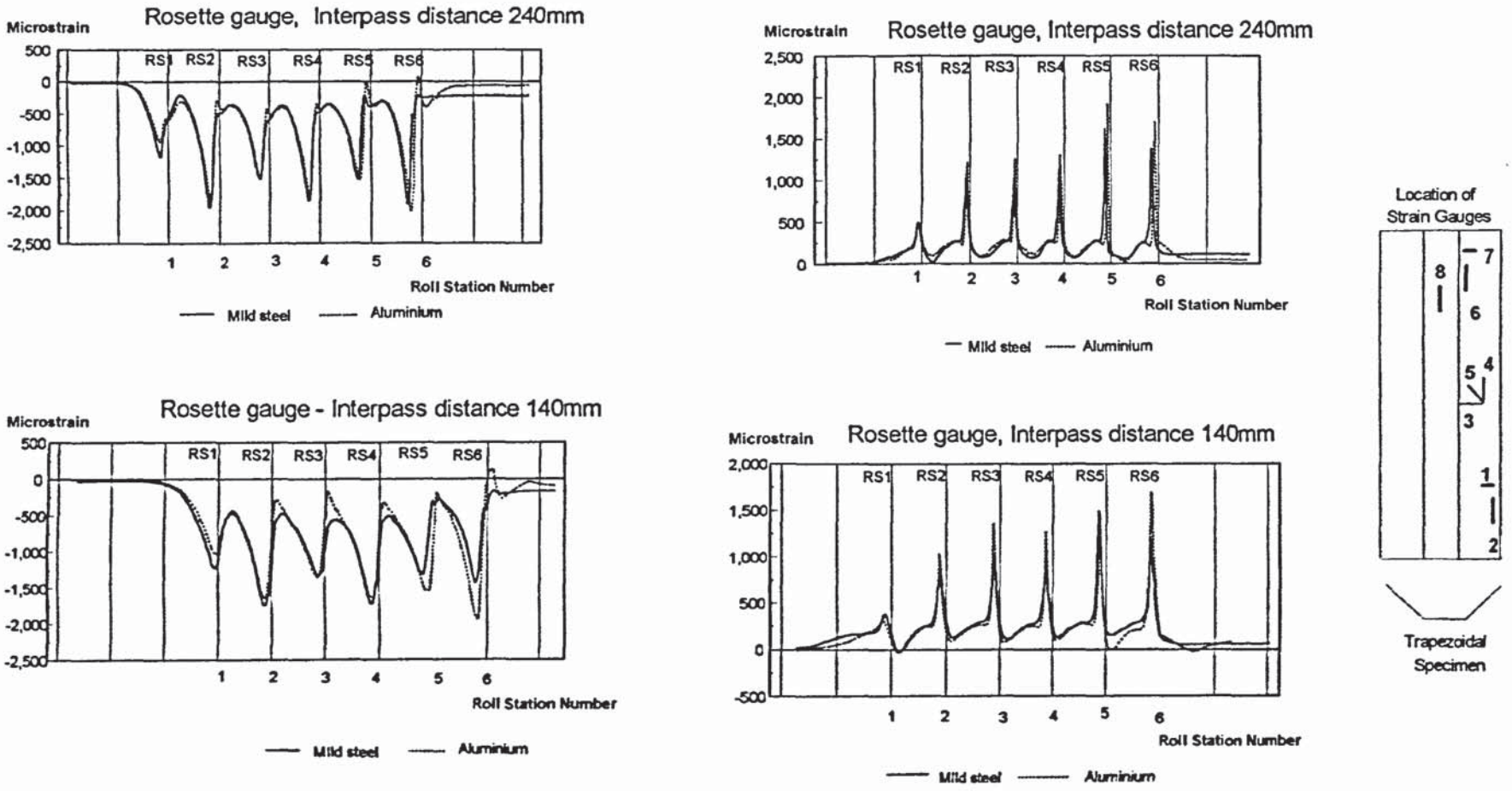

Figure 9.15. Comparison of maximum and minimum principle strain distributions for Steel and Aluminium Specimens (CRF Mill No:2).

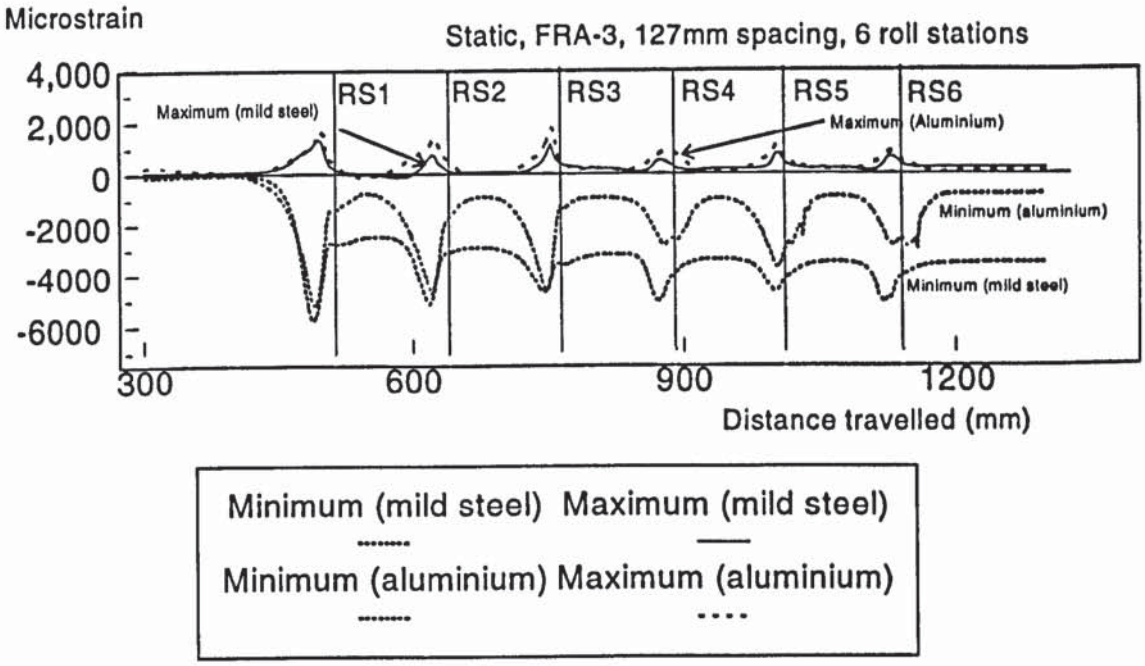

Figure 9.16 Comparison of maximum and minimum principal strain distributions (CRF Mill No:1)

The absolute minimum principal strain distribution is observed to be higher than the maximum principal strain distribution. This can be attributed to the dominant compressive lateral strain over lesser tensile longitudinal strain on the same region. Figure 9.15 shows the maximum and minimum principal strains in Steel and Aluminium specimens formed on the CRF Mill No:2.

9.1.5 Influence of material

The effect of different forming material can be seen by comparing the longitudinal strain distributions for Mild steel and Aluminium as shown in Figure 9.17. The longitudinal strain distribution for Aluminium is higher than that of the Mild steel due to higher ductility. On the contrary, under the same forming load, the lateral strain distribution is lower for Aluminium. (Figure 9.18)

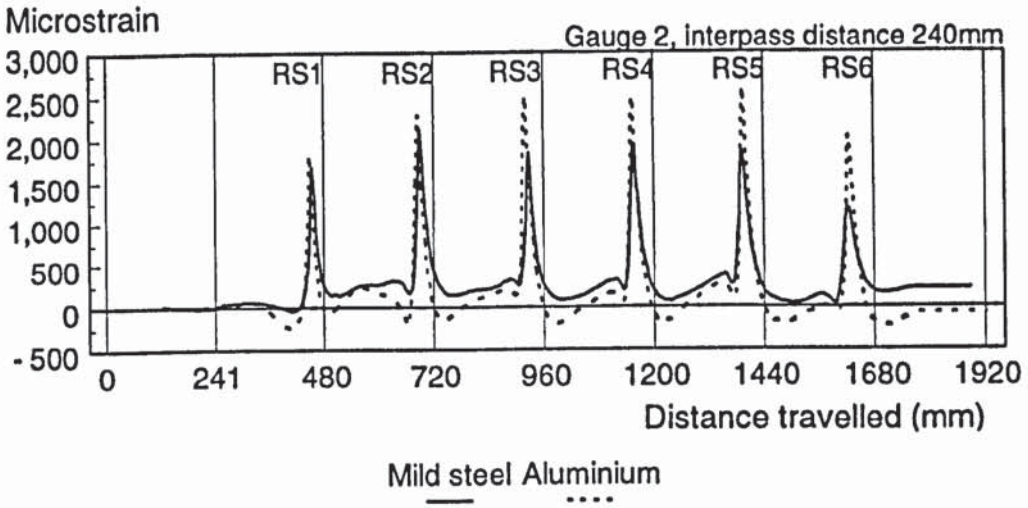

Figure 9.17 Influence of material on longitudinal strain (CRF Mill No:2)

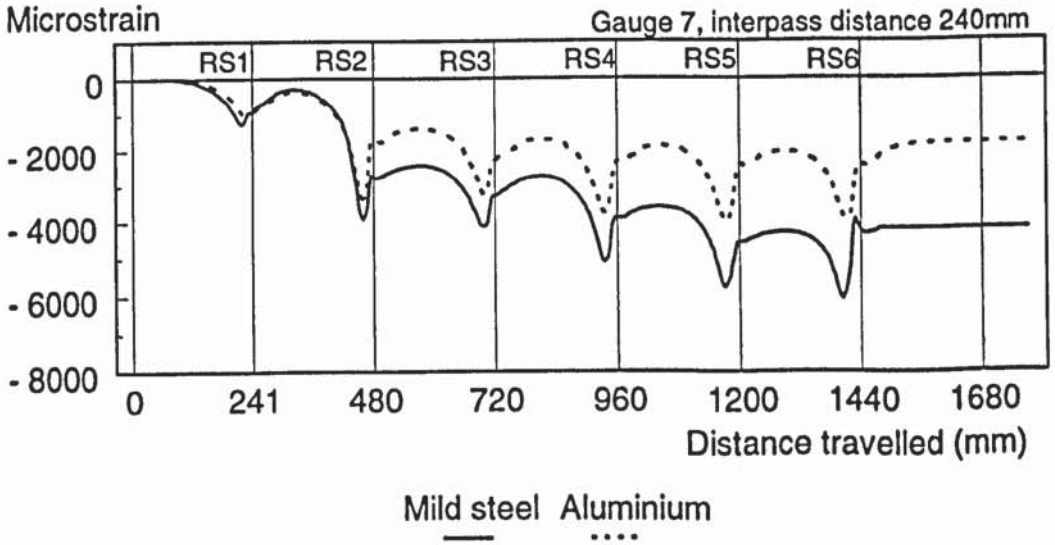

Figure 9.18 Influence of material on lateral strain (CRF Mill No:2)

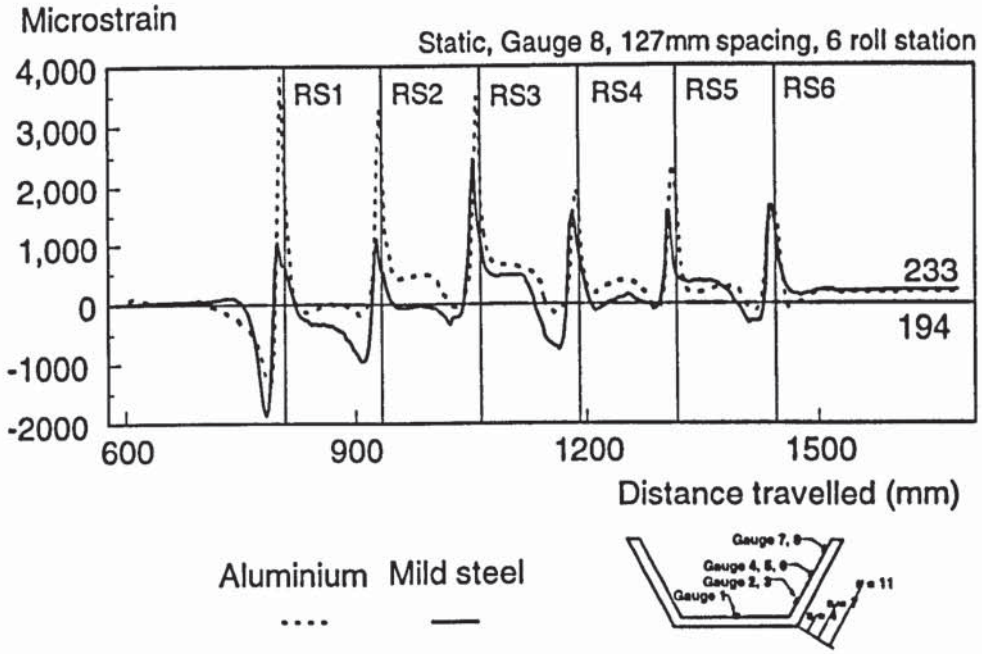

Figure 9.19 Influence of material on longitudinal strain (CRF Mill No:1)

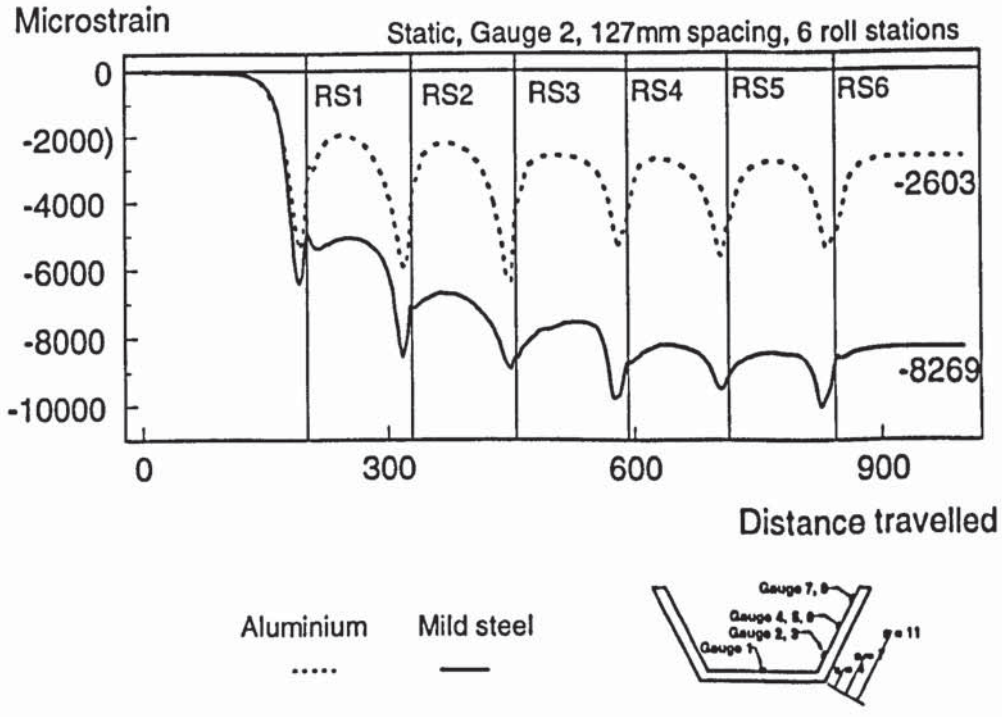

Figure 9.20 Influence of material on lateral strain (CRF Mill No:1)

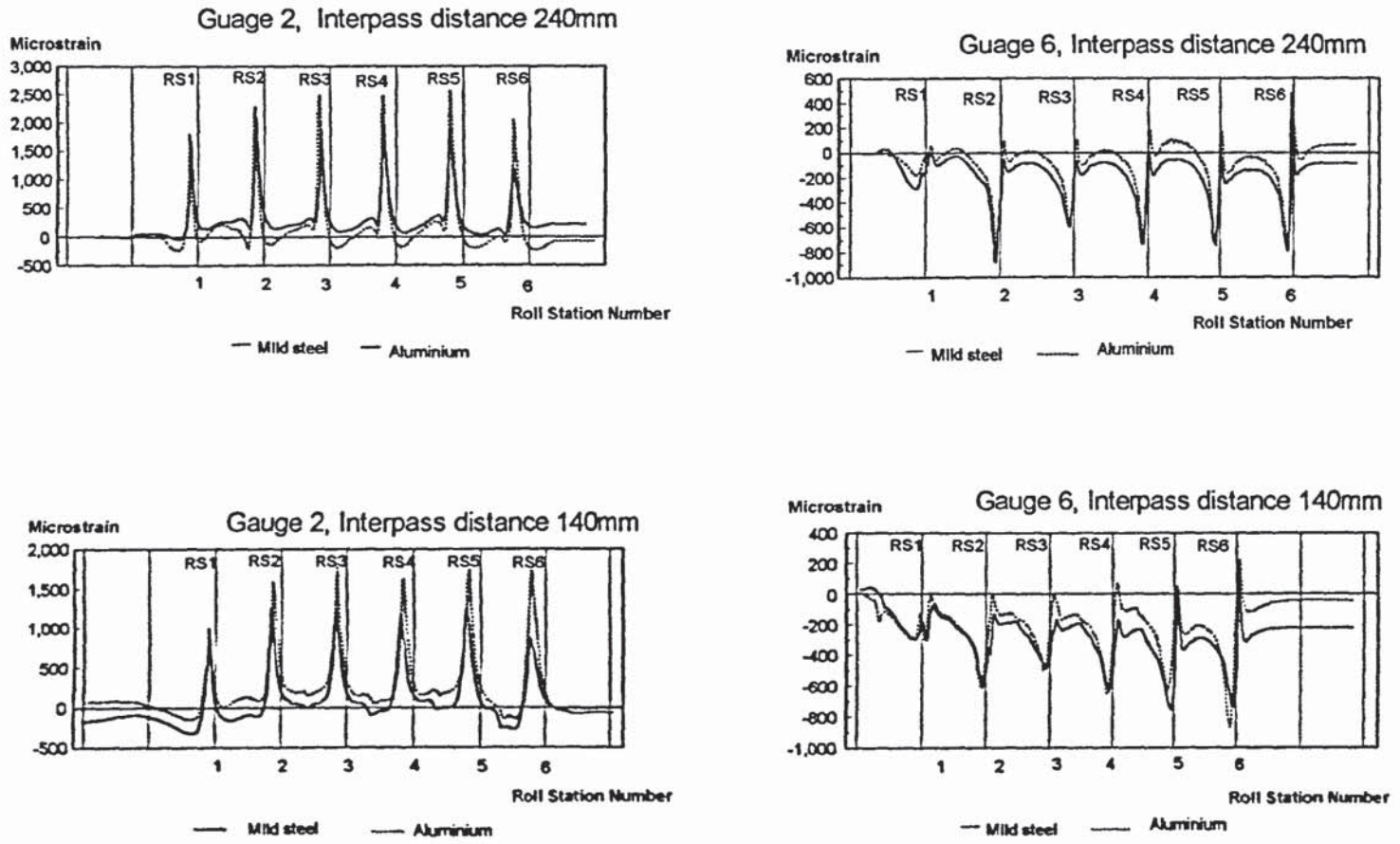

Figure 9.21(a). Comparison of strain distributions for Steel and Aluminium Specimens (CRF Mill No:2).

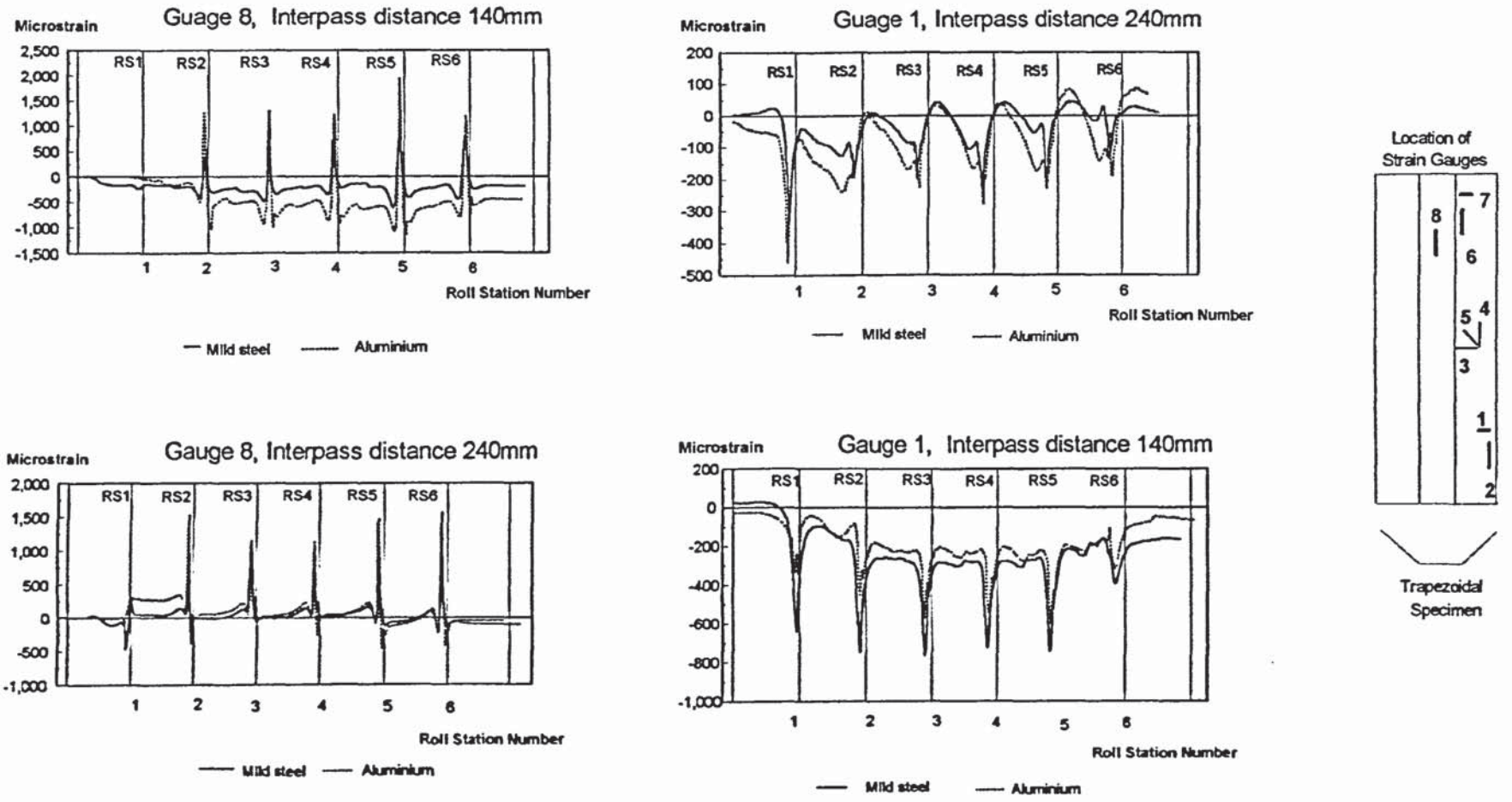

Figure 9.21(b). Comparison of strain distributions for Steel and Aluminium Specimens (CRF Mill No:2).

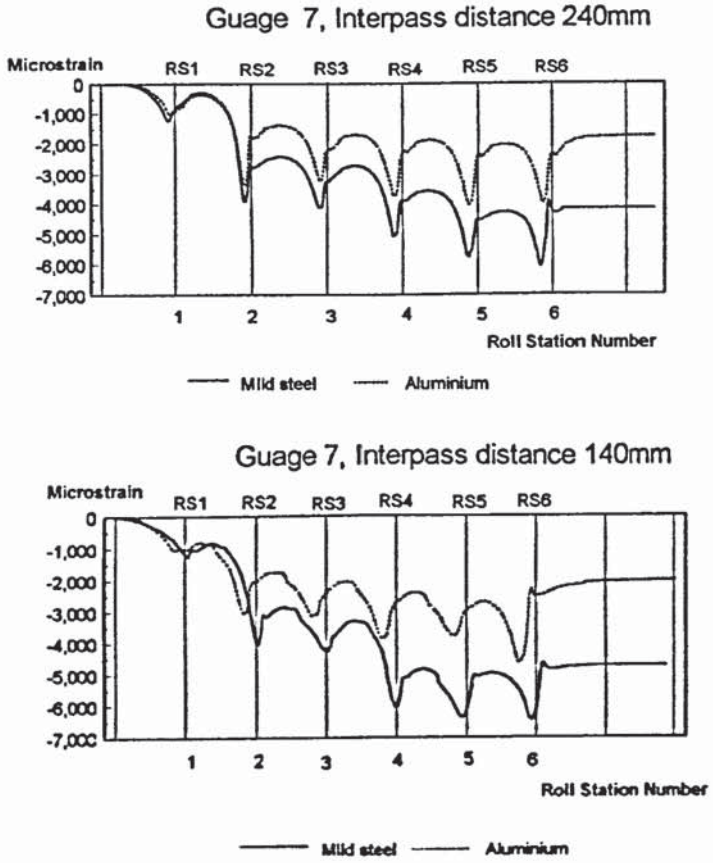

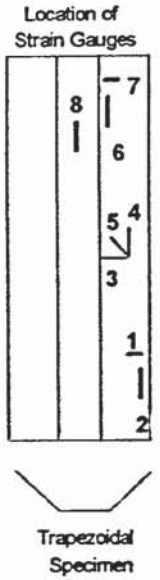

Figure 9.21(c). Comparison of strain distributions for Steel and Aluminium Specimens (CRF Mill No:2).

The effects of forming material can be seen by combining the longitudinal strain distributions of Gauge 8 for Mild steel and Aluminium, as shown in Figures 9.17 and 9.19. Aluminium has a higher longitudinal strain distribution compared with Mild steel due to higher ductility. On the contrary, under the same forming load, the lateral strains are lower for Aluminium (Figures 9.18 and 9.20). The lower residual longitudinal strain for Aluminium implies that it is more conducive for roll-forming since a straighter product can be obtained. Furthermore, the lower lateral strain for Aluminium implies that the flange is also straighter. Figure 9.21 shows the strains measured at different locations of Steel and Aluminium samples formed on the CRF mill No:2. The effect of interpass distance on the strains can also be seen.

9.1.6 Effect of the number of roll stations and interpass distance

(a) Effect of the number of roll stations

The effects of using 3 roll stations (RS1,3,6 spaced 2x127mm) instead of 6 roll stations (RS1-6 spaced 127mm) to roll-form the same trapezoidal section became apparent when considering the longitudinal strain and lateral strain for Aluminium. Deformation is more severe, with larger absolute longitudinal, lateral and residual strains, when roll-formed with 3 roll stations (Figure 9.22a & Figure 9.22b). This is due to larger forming angles between roll stations as shown in Table 9.1. The conclusion is to use the least fold angle in order to minimise the product curvature.

Roll station	Roll angle	Forming angle for 6 roll stations spaced 127mm	Forming angle for 3 roll stations spaced 127mm
RS1	19.69°	19.69°	19.69°
RS2	35.59°	15.9°	
RS3	47.04°	11.45°	27.35°
RS4	55.05°	8.01°	
RS5	60.79°	5.74°	
RS6	65.03°	4.24°	17.99°

Table 9.1 Forming angles with different roll stations

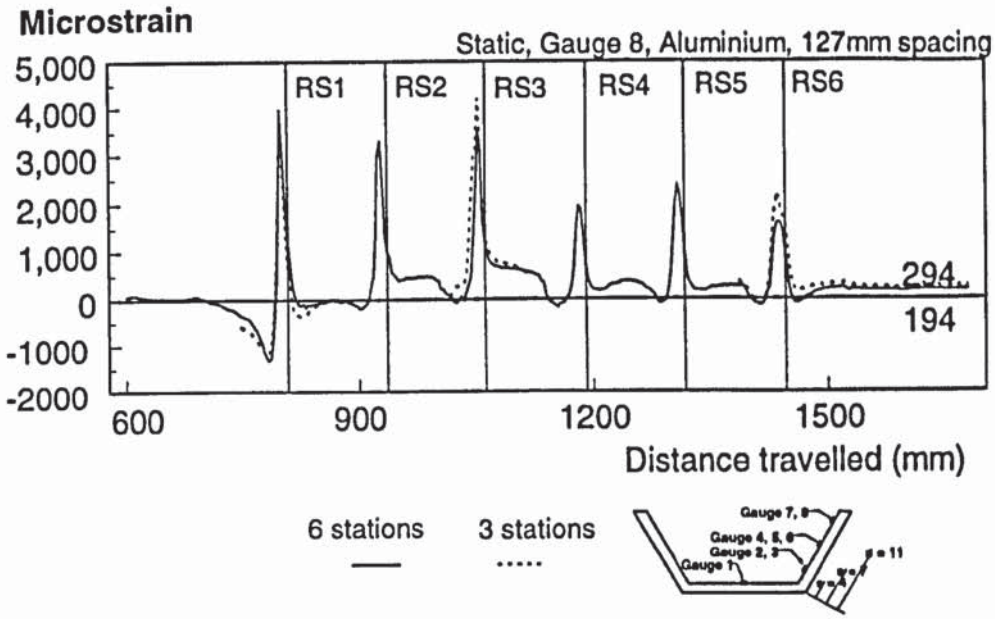

(a) Longitudinal strain (CRF Mill No:1)

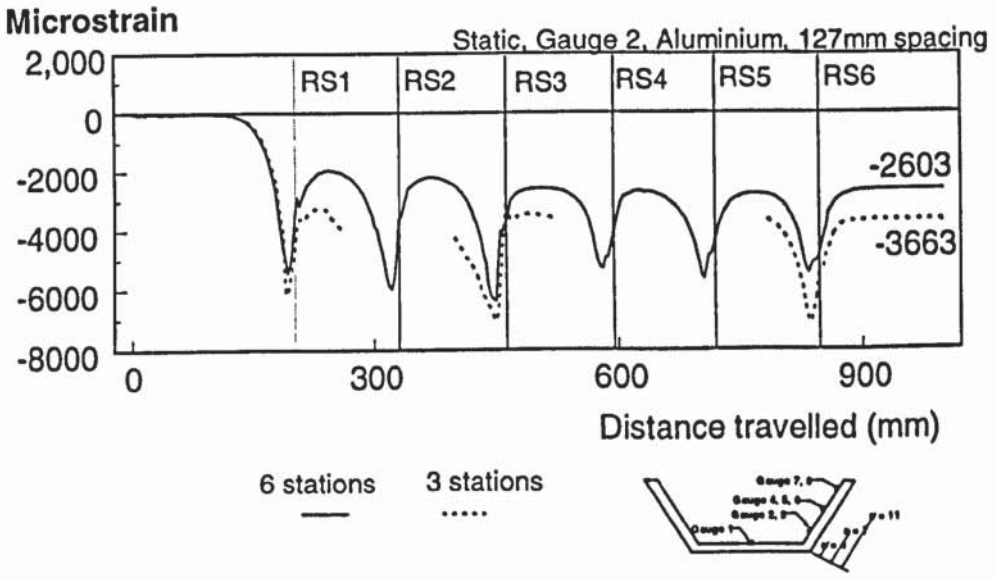

(b) Lateral strain

Figure 9.22 Comparison of 6 roll stations and 3 roll stations (CRF Mill No:1)

(b) Effect of roll station spacing

The effect of roll station spacing can be observed by studying the longitudinal strain distribution near the edge of the flange of Aluminium specimens . 3 roll stations (Figure 9.23) spaced 127 mm and 2x127 mm were used.

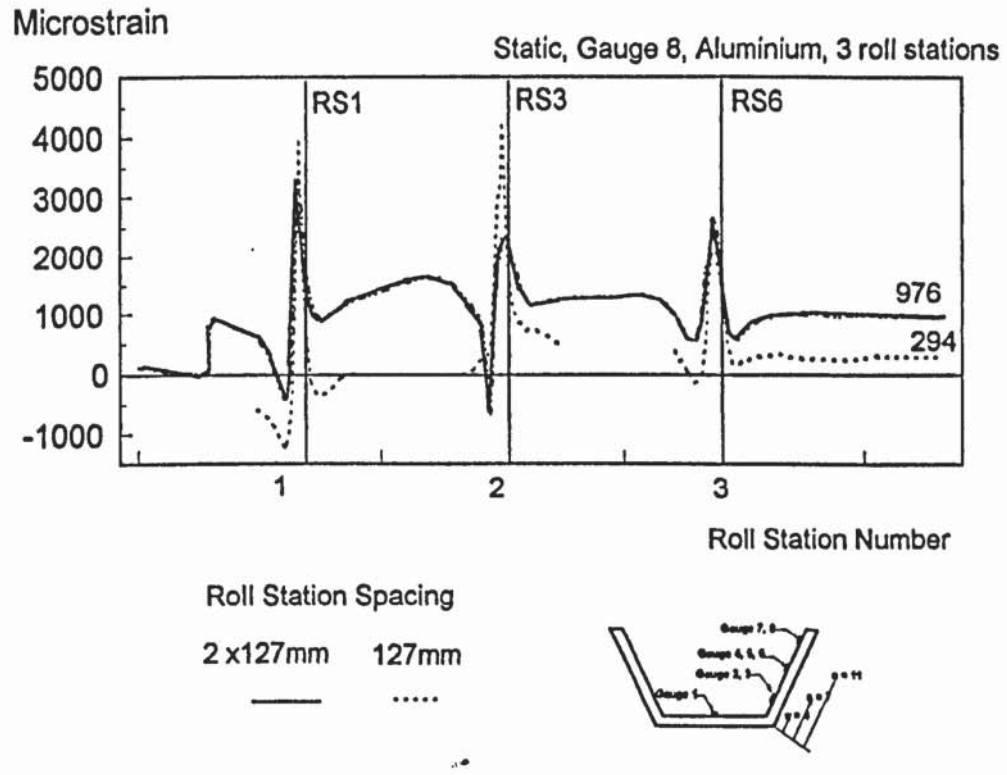

Figure 9.23 Comparison of longitudinal strains for 2x127 mm spacing and 127 mm spacing (CRF Mill No:1)

Peak longitudinal strain does not show much difference at RS1 and RS6, but a significant reduction in peak longitudinal strain is observed at RS3. Due to the increase in roll station spacing, the extended section is then less rigid. On the other hand, having larger roll station spacing is not encouraged as it results in a significant rise in residual strain. In fact, Bhattacharyya [Bhattacharyya2] had proposed that the roll station spacing should be greater than the deformation length, L, which is

$$L = \sqrt{\frac{8a^3\theta_p}{3t}} = 88 \text{ mm} \quad \text{in this application}$$

where a : Flange length of trapezoidal section

t : Thickness of forming strip

θ_p : Forming angle in one particular stage

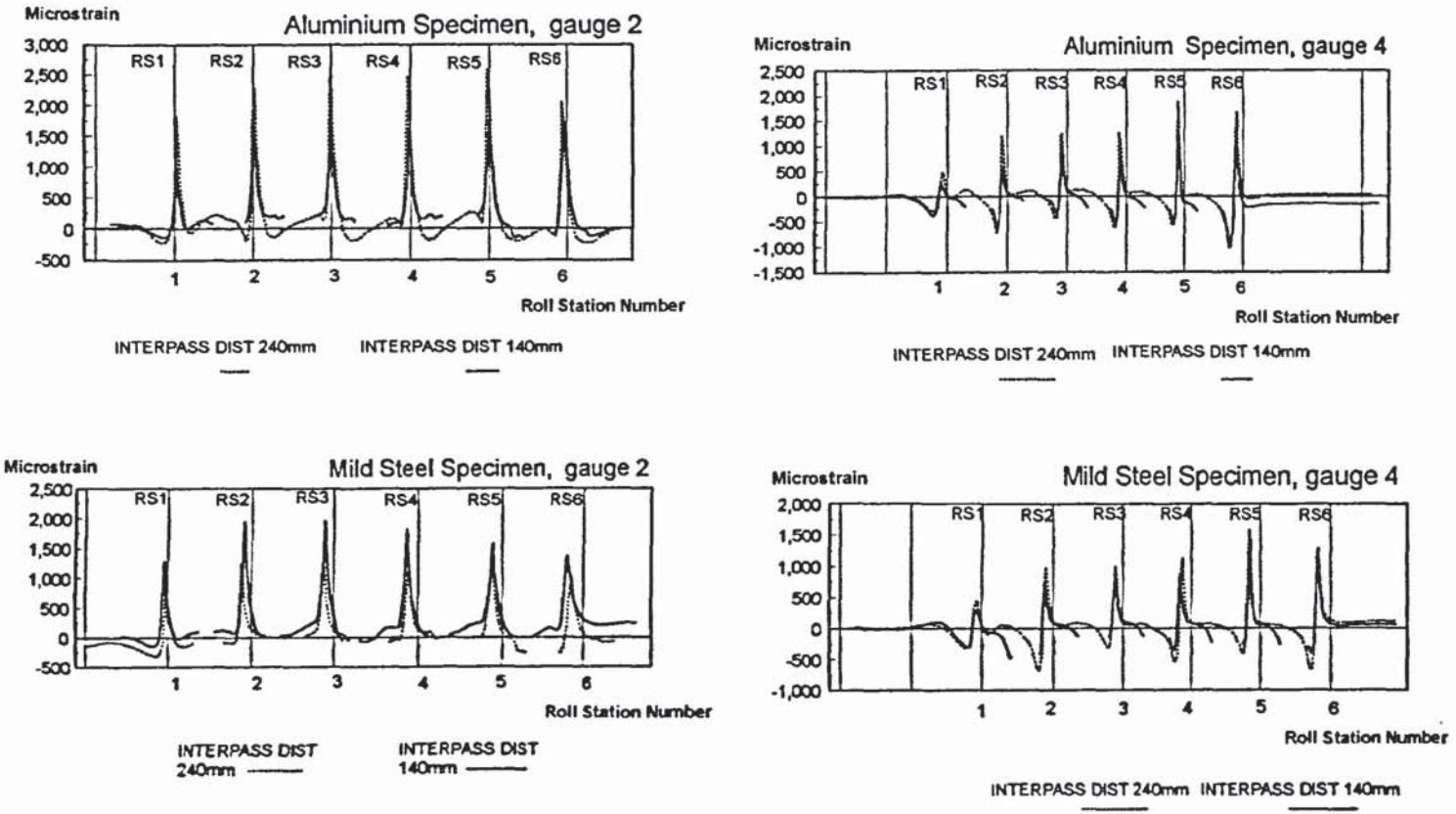

Figure 9.24(a). Comparison of Longitudinal and Lateral Strain distributions for different interpass distances (CRF Mill No:2, Steel and Aluminium Specimens).

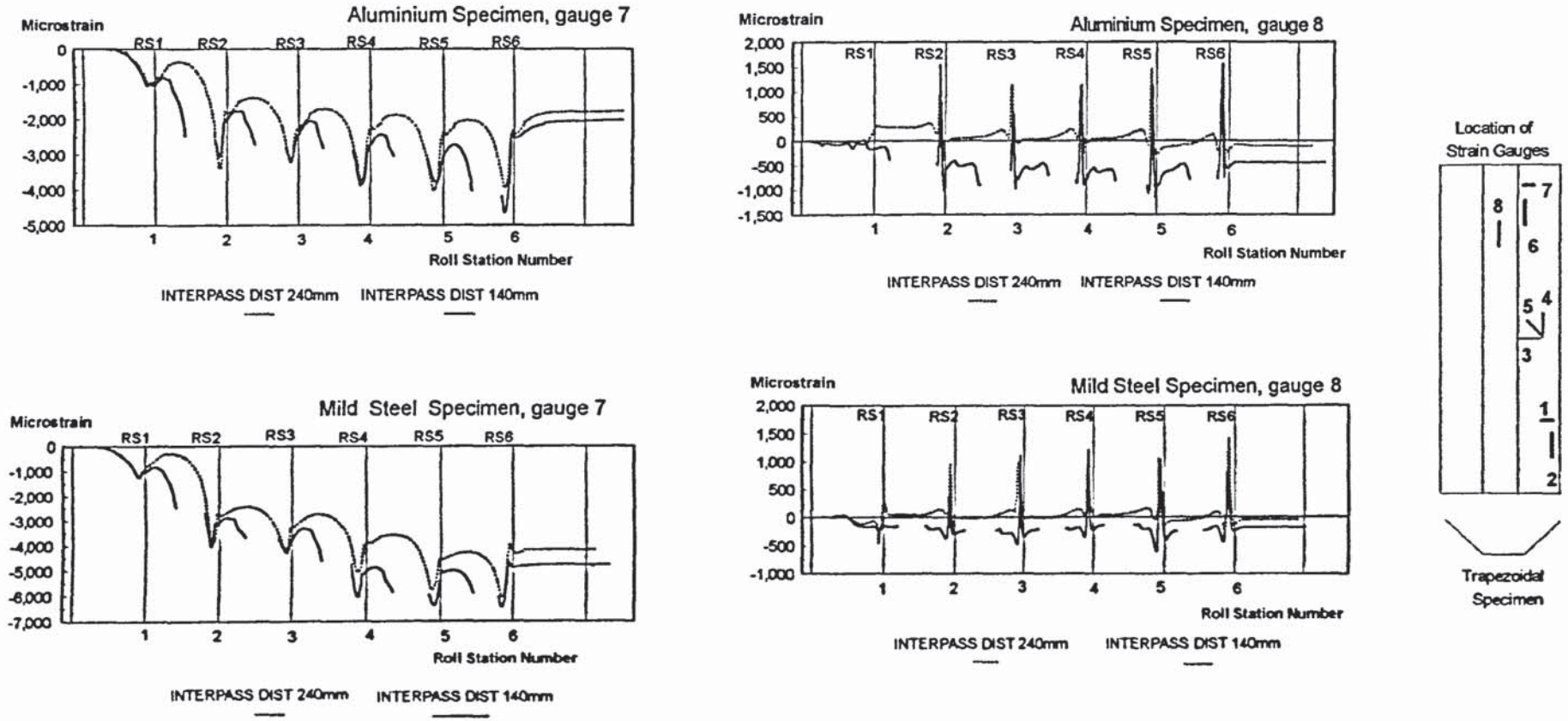

Figure 9.24(b). Comparison of Longitudinal and Lateral Strain distributions for different interpass distances (CRF Mill No:2, Steel and Aluminium Specimens).

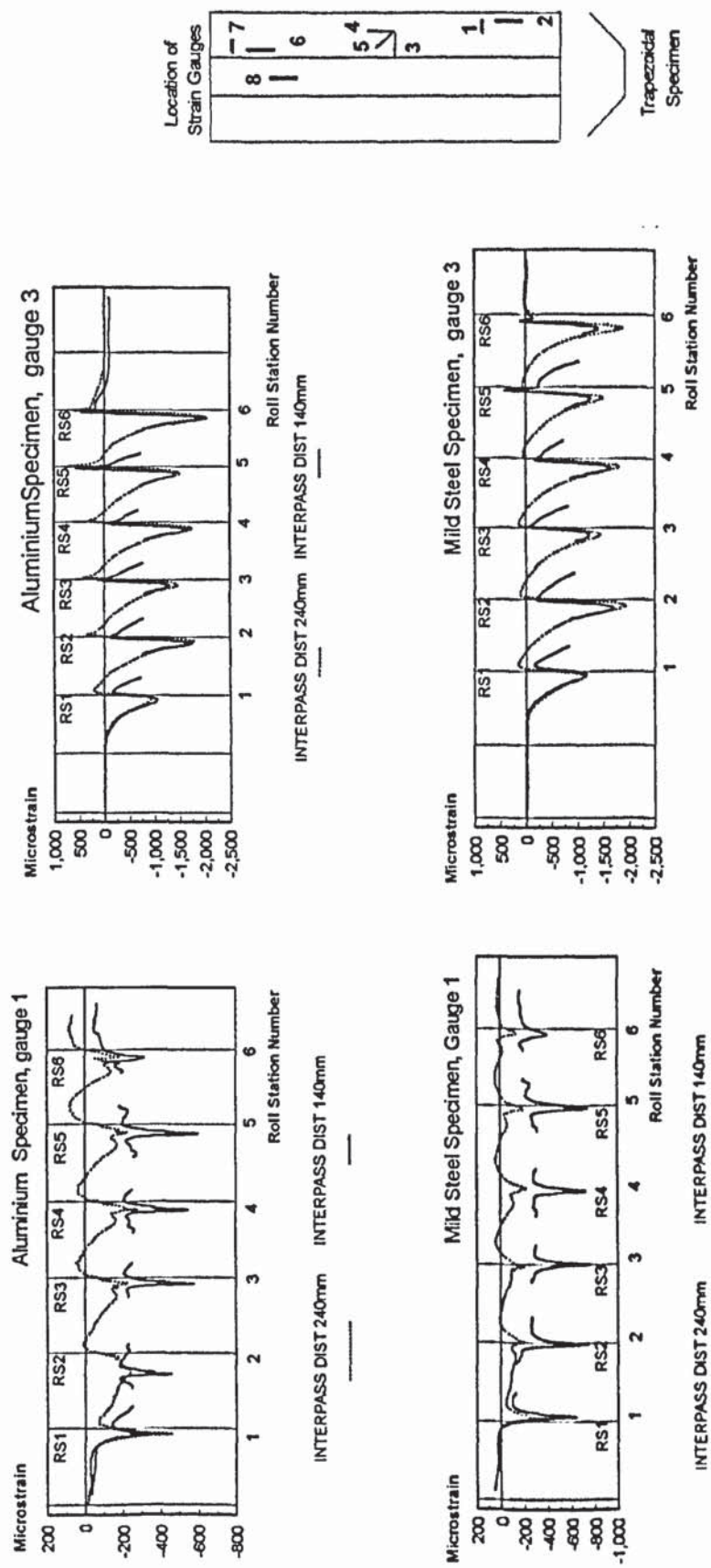

Figure 9.24(c). Comparison of Longitudinal and Lateral Strain distributions for different interpass distances (CRF Mill No:2, Steel and Aluminium Specimens).

Figure 9.24 compares the strains at various positions on the flange and the web for Steel and Aluminium specimens for varying interpass distances (CRF mill No:2). Two interpass distaces of 140mm and 240mm were used. In general the longitudinal strains are always greater for the larger interpass distance. Near the outer edge of the flange, the absolute value of the strains are greater for the smaller interpass distance. As the fold line is approached this difference is diminished.

Figure 9.25 shows the comparison of maximum and minimum principal strains for steel and aluminium specimens (CRF mill No:2) for interpass distances of 140mm and 240mm. For both types of specimens, the effect on the principal strains by the change of interpass distance is minimal.

9.2 Comparison of Experimental and Theoretical Strain Distribution.

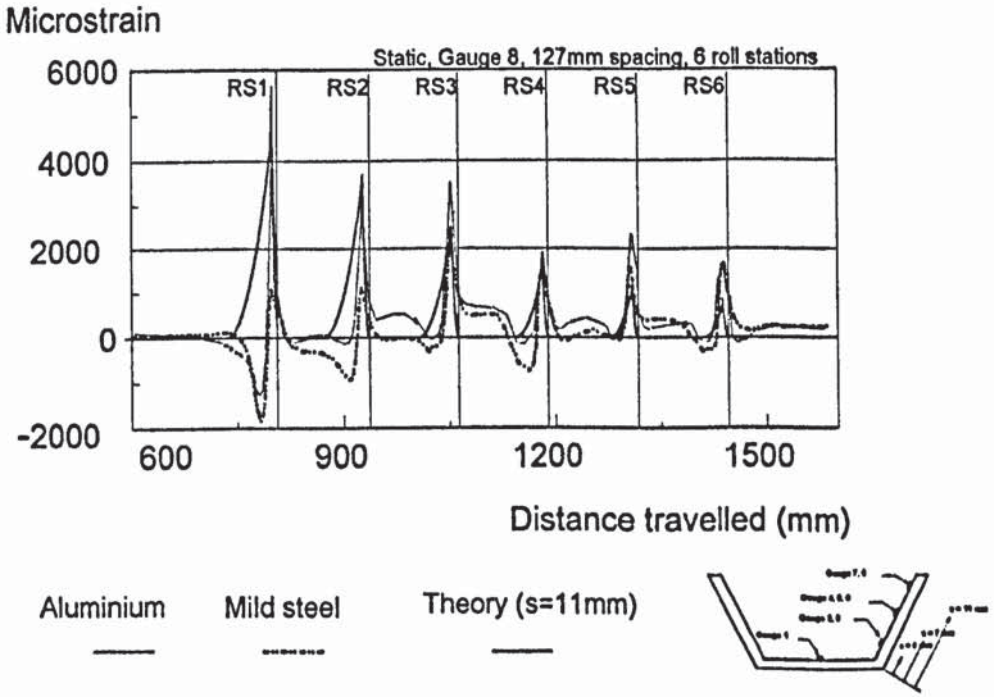

(a) 6 stations spaced 127 mm

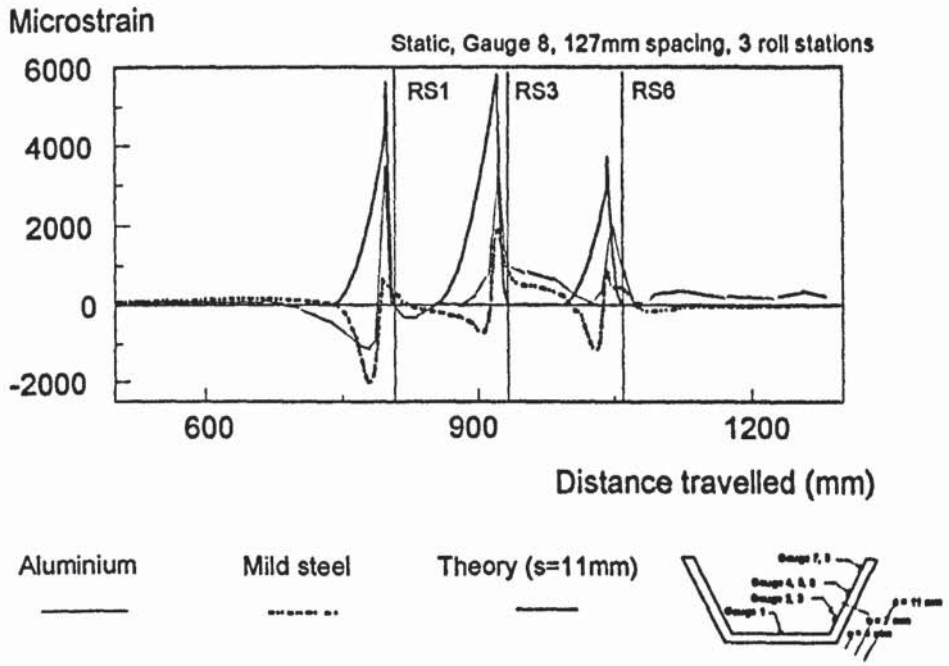

(b) 3 stations (RS1,3,6) spaced 127 mm

Figure 9.26 Comparison of experimental and theoretical strain distributions (CRF Mill No:1)

The theoretical longitudinal strain [Panton3] induced in the strip is a function of the slope $(\frac{d\theta}{dz})$ of the bend angle curve. Fig 9.26 shows a comparison of experimental and theoretical strain distributions. It can be seen that, in practice, some plastic deformation occurs so that the final strain does not return to zero. The theoretical values of the peak strain and the form of curve are in reasonable agreement for Aluminium but not for Mild steel. This discrepancy may be attributed to the fact that elastic springback is neglected in the analysis. Thus, the theoretical strain distributions are closer for Aluminium because of its lower yield strength. Unlike the experimental strain distribution, the theoretical strain distribution does not exhibit a compressive maximum before a tensile maximum since the effect of the folding of the flange (Figure 9.8) is not taken into account by Panton [Panton3] in his analysis. This is not a serious shortcoming in the theory as the most important factor is the maximum tensile strain, which is very much larger in magnitude than the compressive strain. In some instances the compressive strain might cause the flange to buckle.

9.3 Finite Element Analysis

The approximate method used to analyse the cold roll forming process and the various features available in the MARC finite element program were described in Chapter 6. The contour plots of strains, von Mises stresses, equivalent plastic strains and displacements from the analysis were also presented in Chapter 6.

In the following sections, the strains predicted by the finite element analysis are compared with experimental results and the difficulties encountered with the non-linear analysis are described.

9.3.1 Strains Predicted by the Finite Element Model

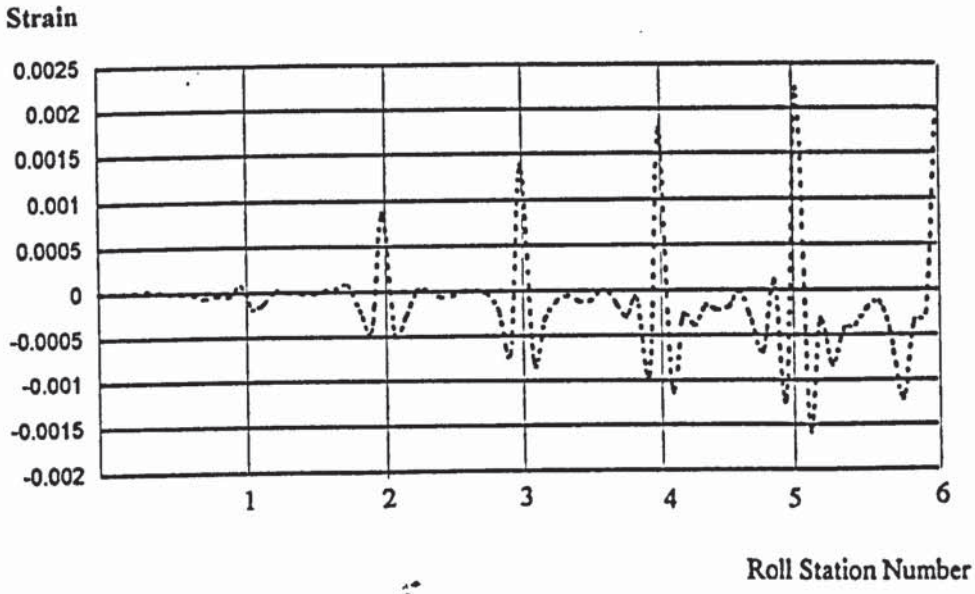

Figure 9.27 Longitudinal strain distribution in the flange of a steel specimen using MARC finite element simulation (CRF Mill No:1).

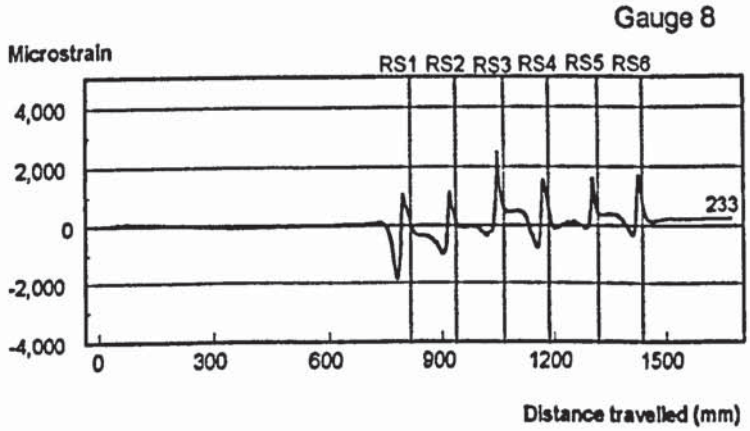

Figure 9.28 Longitudinal strain distribution in the flange of a steel specimen determined experimentally using the CRF Mill No:1

Figure 9.27 shows the calculated strain distribution in the flange of an Aluminium specimen using the MARC finite element software. This compares favourably with the actual strains recorded experimentally on an identical specimen using the CRF mill No:1, shown in figure 9.28. There is reasonable correlation of the strain maxima and the general pattern of the strain variation as shown in Figure 9.29 where the two strain traces are superimposed.

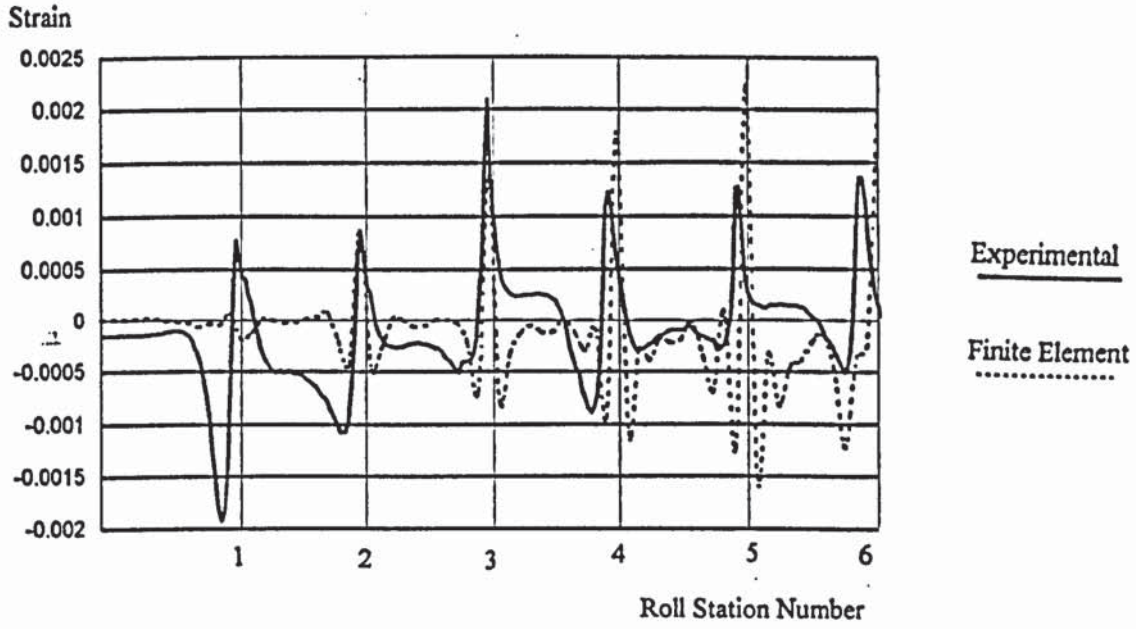

Figure 9.29 Comparison of experimental longitudinal strain distribution with strains predicted by finite element analysis.

9.3.2 Incremental - Iterative Solutions

The main objective in incremental-iterative solutions is to achieve a balance between the applied forces **f** and the internal resisting forces **p** by solving the equation

$$\mathbf{f} - \mathbf{p} = \mathbf{0}$$

Iterative techniques which estimate a solution for the above equation usually result in an imbalance resulting in a residual or an out-of-balance force. This iterative process is repeated until this residual force is small enough to satisfy a preset convergence tolerance. Setting the correct number of iterations, residual load and convergence tolerance requires a trial and error approach. Residual force criteria were difficult to satisfy even when iterative displacements are converging within tight tolerances. Some of the problems encountered during the solution using Newton-Raphson method and some potential problems are:

Linearisation expense

The operations performed in an iteration within a load increment are: computation of residual forces and tangent stiffness matrix, factorisation of the tangent matrix, backward/forward substitution and updating the solution and testing for convergence.

In problems of increasing size the most expensive step is the factorisation of the tangent matrix. The type of element used also has a direct influence on the problem size. The

number of elements used had to be kept to a reasonable figure to keep the problem size manageable. The finite element mesh was designed so that the areas of interest has a higher density of elements. The output had to be controlled rigorously to suppress unwanted results to conserve disk storage space.

Load increments

The size of the load increment was pre-determined. The tangent stiffness matrix varies throughout the analysis. Equal load increments were used in this analysis. This produces unequal residual forces and unequal displacements. A load increment which produces a reasonable displacement with rapid convergence at the beginning of the analysis may predict large displacement increments with low convergence as the structure yields and becomes more flexible. A considerable amount of trial and error was required to determine the appropriate load increment.

Step direction

Positive load increments were applied throughout the analysis as the section was a simple trapezoid. For sections with complicated shapes the equilibrium curve can reach a maximum and then decrease. In order to follow such a path, negative load increments must be applied.

Constant load iteration

In Newton-Raphson analysis, the load is kept constant during the iteration process. For certain roll formed sections with complicated shapes the equilibrium curve could reach a maximum and then decrease. In such cases it is possible for the applied load to be greater than the load which the structure can resist in which case convergence is impossible.

Sudden non-linearities

When analysing cold rolled formed sections with more complicated shapes where distinct events could occur which drastically alter the stiffness resulting in large residual forces, a 'hiatus' could be caused in the solution. When analysing simple trapezoidal sections there is no danger of such situations occurring.

Non-convergence

If the analysis fails to converge in a specified number of iterations then it is necessary to either terminate the solution or restart this load step with a smaller increment size. In the MARC program, the RESTART option allows this to be performed.

9.4 Plastic Strain Analysis

Plastic strains were measured using the grid method and computer vision techniques. A grid marked on the specimen was measured before and after partial deformation. Positions

of the roll stations were marked on the partially formed specimen before removing from the mill. Strain measurements were made on small areas (near the roll stations) in the flange using the OMIS II system (described in Chapter 5) and the computer vision system. Figure 9.30 shows a comparison of the plastic strain distributions measured with grid method and computer vision techniques. The peak tensile plastic strain is observed some distance before the centre-line of the roll. This strain increases from the fold line to the edge. On the contrary, compressive plastic strain decreases from the fold line to the edge. It is always negative or experienced a compression stress. Similarly, a compressive maximum occurs just before the centre-line of each roll station.

The strains measured using the software developed for measuring plastic strains is in reasonable agreement with the results obtained with the grid method. This software needs to be further developed and tested if it is to be used with confidence. The software can only be used with a planar surface with no discontinuities on the surface. Any out of plane bending will introduce errors in the calculation. Lighting is also critical in obtaining correct results. This has proved to be one of the biggest problems.

Also shown in Figure 9.30 are the longitudinal and lateral strains measured with the strain gauges near the edge of the flange. The gauge results are the most reliable. The strains measured by the grid method and the computer vision techniques are prone to errors and are less reliable.

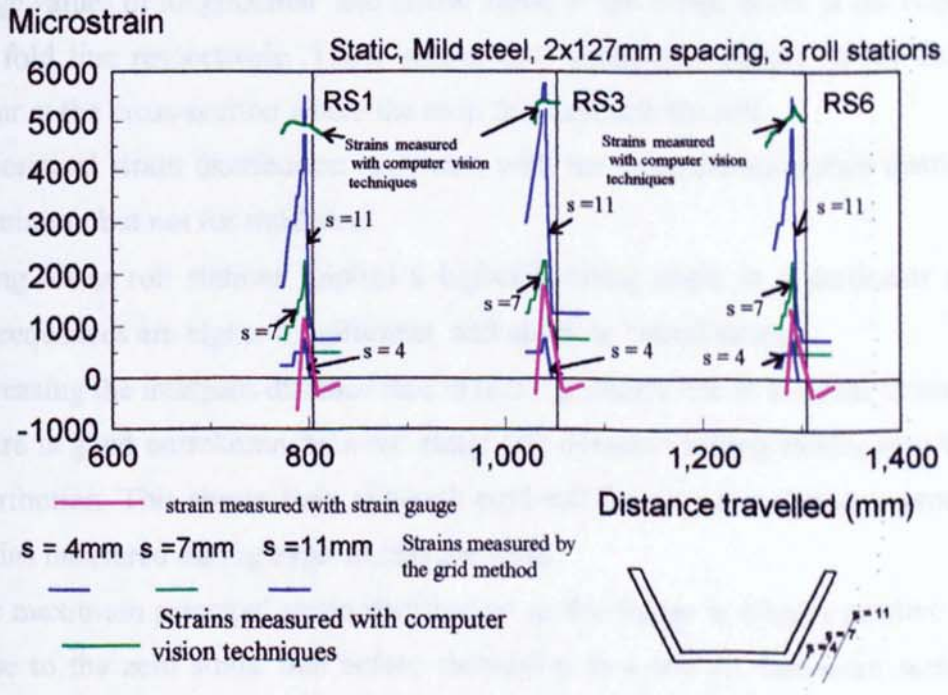

Figure 9.30 Plastic strain distributions (a) Longitudinal strains

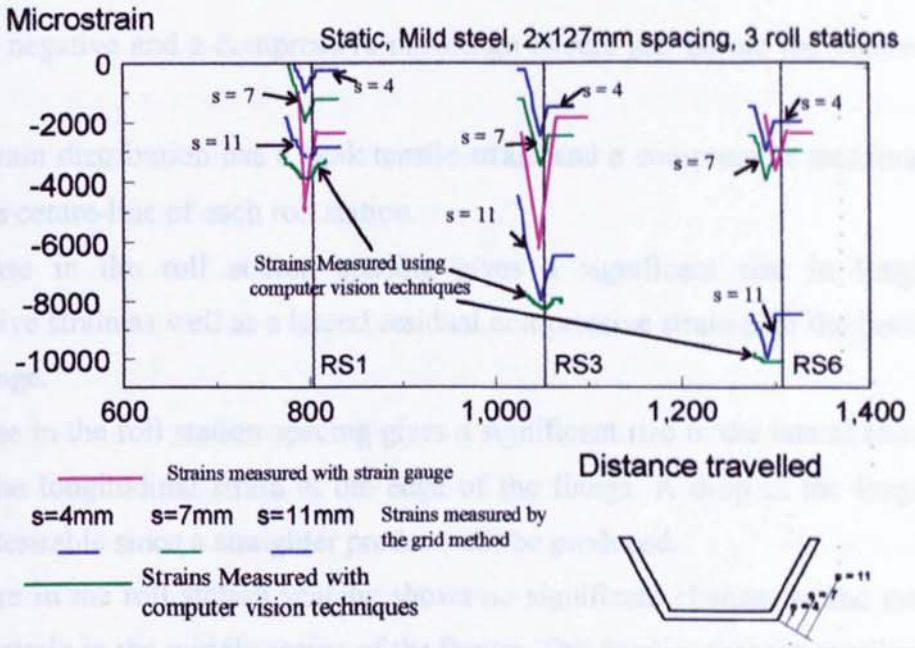

Figure 9.30 Plastic strain distributions (b) Lateral strains

9.5 Conclusions

The experimental investigation of strain distributions during the roll-forming of a trapezoidal section has revealed a number of useful findings listed below.

- Forming material with higher ductility produced a straighter product with less springback.
- Large values of longitudinal and lateral strain in the flange occur at the edge and near the fold line respectively. These strains are significant factors in roll-forming and occur at the cross-section where the strip first contacts the roll.
- Theoretical strain distribution correlates with the experimental strain distribution for aluminium but not for mild steel.
- Using fewer roll stations implies a higher forming angle in a particular stage. The consequences are higher longitudinal and absolute lateral strains.
- Increasing the interpass distance results in a significant rise in residual strain.
- There is good correlation between static and dynamic testing modes regarding strain distribution. This shows that, although cold roll forming is a dynamic process, static strains measured during experiments are valid.
- The maximum principal strain distribution in the flange is always positive and keeps close to the zero strain line before increasing to a tensile maximum some distance before the centre-line of the roll. However, the minimum principal strain distribution

is always negative and a compressive maximum occurs just before the centre-line of the roll.

- Plastic strain distribution has a peak tensile strain and a compressive maximum (just before the centre-line of each roll station.
- A decrease in the roll station spacing gives a significant rise in longitudinal compressive strain as well as a lateral residual compressive strain near the bend corner of the flange.
- A decrease in the roll station spacing gives a significant rise in the lateral strain but a drop in the longitudinal strain at the edge of the flange. A drop in the longitudinal strain is desirable since a straighter product will be produced.
- A decrease in the roll station spacing shows no significant changes in the maximum principal strain in the middle region of the flange. This implies that the tensile strain is less dominant on that particular region. However a decrease in the roll spacing gives a significant rise in the absolute minimum principal strain between the spacing of each station.
- The experimental technique developed to measure strains using computer vision has certain limitations. It can be considered as the basis for developing a useful tool for strain measurement. The results are encouraging but further work is necessary to realise its full potential. The results obtained under perfect conditions are satisfactory, but under practical situations the shortcomings become evident. The specimen may not be perfectly flat, lighting and reflections become problematic and it is difficult to align the camera exactly perpendicular to the workpiece.
- The finite element analysis is useful in predicting the maximum and minimum values of strains developed and their locations in the workpiece. This is very useful during the design of a mill and/or the tooling for cold roll forming.
- This research has provided a better understanding of the cold roll forming process and the various factors that affect the quality of the roll formed sections. It has also enabled the tooling and roll forming mill designer to predict the behaviour of the material using finite element analysis.

9.6 Recommendations for future work

All research in the area of cold roll forming should be eventually directed at the design of roll tooling and cold roll forming mills to produce roll formed sections. The key to this is the understanding of the material behaviour during forming. To control the quality of the

section that is being formed, the strain development during forming has to be fully understood. The approach taken during this research was to predict these strains using finite element analysis and measure the actual strains experimentally and compare them to get a better understanding of this forming process.

In this research a comprehensive set of experiments were performed to measure strains developed during cold roll forming using two cold roll forming mills with specimens of different materials at different interpass distances. Experimental work in cold roll forming is time consuming and expensive, as new tooling costs are considerable and the design of the mills do not allow various parameters to be changed. Most mills including one of the mills used in this work have fixed roll centres. The experimental work was performed on simple trapezoidal sections. For future research work experimental work should be carried out on more complicated shapes to study the strain development during forming. More experimental work to understand springback is also necessary. Both these areas are important for designing roll tooling and cold roll forming mills.

A commercially available Finite Element software package MARC® was used analyse the cold roll forming process. This was only an approximate method based on observation and traditional engineering practice and when compared with experimental results, it is able to predict strains with reasonable agreement.

A complete exact simulation of the process should be done to get a better understanding of the process. Use of a Finite Element scheme with explicit codes is also recommended. Explicit simulation is achieved without forming a stiffness matrix and does not involve the solution of equations. Solution failures are avoided and core storage requirements are reduced. Solution of a problem such as this which involve large displacements and contact is time consuming and prone to failure using implicit code.

According to currently available literature, computer vision has not been used by any other author for the purpose of measuring strains, at least in the area of cold roll forming. The software developed for the computer vision system could be developed further to make it a more useful general purpose tool in strain measurement. In this research the technique was used to measure plastic strains. Elastic strains under dynamic conditions could be measured by employing high speed image capturing cameras. The present system has been developed for measuring strains on a perfectly flat surface held perpendicular to the camera. An algorithm could be developed to make the system insensitive to the direction (within reasonable limits) of the camera.

References

[Angel1] Angel,R.T., Designing Tools for Cold Roll Forming, The Iron Age, Vol. 164, No. 18, Nov 1949, pp 83-88

[Angel2] Angel,R.T., Cold-Roll Forming, ASME Handbook, Metals Engineering Processes, McGraw Hill, 1958, pp 167-177

[Beecher] Beecher,D.J., Cold Roll Forming Profiles from Material Of non-Uniform Thickness, Proc. of the First International Conference on Rotary Metal Working Processes, London, UK., November 20-22, 1979, pp 445-454

[Bhattacharyya1] Bhattacharyya,D., Smith,P.D., The Development of Longitudinal Strain in Cold Roll Forming and its Influence on Product Straightness, Advanced Technology of Plasticity, 1984, Vol 1, pp 422-427

[Bhattacharyya2] Bhattacharyya,D., Smith,P.D., Yee, C.H., Collins,I.F., The prediction of Deformation Length in Cold roll-Forming, Journal of Metal Working Technology, Vol 9, March 1984, pp 181-191

[Cadney] Cadney,S., Cold Roll Forming. The art that could do with some science?, The Production Engineer, September 1981, pp 19-21

[Cookson] Cookson, W., The Cookson Method of Cold Roll-forming, Sheet Metal Industries, October 1966, pp 761- 769

[Dally] Dally, J.W., Riley,W.F., Experimental Stress Analysis, 2nd ed.1985: McGraw-Hill.

[data M] data M GmbH, Mehlbeerenstraβe 2, D-82024 Taufkirchen, Germany

[Doyle] Doyle,J.F., Phillips,J.W., Manual on Experimental Stress Analysis, 5th ed.1989, Society for Experimental Mechanics

[Duggal] Duggal, Nitin. Ahmetoglu., Mustafa, A., Kinzel, Gary L., Altan, Taylan., Computer aided simulation of cold roll forming - a computer program for simple section profiles, Journal of Materials Processing Technology, v 59, no: 1-2 ,May 15 1996, pp 41-48.

[Evans1] Evans, B., Advanced Techniques and Machines for Cold Roll Forming - Part 1, Sheet Metal Industries, July 1973, pp 389-396

[Evans2] Evans,B., Advanced Techniques and Machines for Cold Roll Forming - Part 2, Sheet Metal Industries, August 1973, pp 448-455

[Eyres] Eyres, P.K., The Development of Cold Roll Forming at the Machine Tool Industry Research Association, Proc. Second International Conference on Rotary Metal Working Processes, Stratford-upon-Avon, 1982, pp 175-186

[Griffin1] Griffin, E., Cold Roll-Forming and Manipulation of Light-Gauge Sections, Journal of Institute of Metals Vol 84, 1955-56, pp181-197

[Griffin2] Griffin,E., Cold Roll Forming of Strip and Sheet Materials- part II, Proceedings of the Second International Conference on Rotary Metalworking Processes, Stratford-upon-Avon, 1982, pp 227-246

[Halmos1] Halmos,G.T., Trends in Roll Forming, Sheet Metal Industries, January 1983, pp38-42.

[Halmos2] Halmos,G.T., Practical Design Guide for Brake and Roll Formed Products, The Fabricator, Vol 12, No.4, May/June 1982

[Halmos3] Halmos,G.T., Practical Design Guide for Brake and Roll Formed Products, The Fabricator, Vol 12, No.5, July/August 1982

[Halmos4] Halmos,G.T., High Production Roll Forming, Society of Manufacturing Engineers, First Edition,1983

[Haritos] Haritos, G. Ghosh, S K. Milner, D A . Computer algorithm to link a finite-element package to the CAD/CAM of cold roll-forming. Journal of Materials Processing Technology. v 31 n 1-2 May 1992 p 277-293.

[Jimma1] Jimma,T., Morimoto,H., Grid Strain Analysis of Cold Roll Forming Process of Channel, Journal of the Japanese Society of the Technology of Plasticity, Vol 25, November 1984, pp 1005-1013

[Jimma2] Jimma,T., Morimoto,H., Grid Stress Analysis of Cold Roll Forming Process of Channel, Journal of the Japanese Society of the Technology of Plasticity, Vol 26, January 1985, pp 45-52

[Jimma3] Jimma, T.,Ona,H., Optimum Roll Pass Schedules on the Cold Roll forming Process of Symmetrical Channels, Proceedings of the Twenty First International M.T.D.R Conference, Swansea, Wales, 1980, pp 63-68.

[Kato1] Kato,K., A Basic Study on Cold Roll Forming Techniques, Nihon Kokan Kubushiki Kaisha Technical Overseas, June 1963, pp 44-54

[Kato2] Kato,K., Saito,Y., Shinto,H., Effect of Metal Properties on shape of Roll Formed Product - Circular Arc Section, Technology Reports of the Osaka University, Vol 23, August 1982, pp 809-815

[King] King,T.E.E., Powell,I.J., Roll Forming Technology- The ORTIC design method, Sheet Metal Industries, March 1982, pp 210-212

[Kiuchi1] Kiuchi,M., Koudabashi,T., Sato,T., Computer Aided Design System of Optimized Rolls and Pass-Schedules for Cold-Roll-Forming Process, International Symposium of Metal Forming, Krakow, Poland, Vol 110, 16-18 September 1987, pp 24- 31

[Kiuchi2] Kiuchi,M., Koudabashi,T., Automated Design System of Optimal Roll Profiles for Cold Roll Forming, Proc. of the Third International Conference on Rotary Metalworking Processes, Kyoto, Japan, 1984, pp 423-436

[Kiuchi3] Kiuchi,M, Koudabashi, TSato, T., Automated Design System of Optimal Roll Profiles for Roll Forming of Welded Pipe and Tube, Proc. of the Third International Conference on Steel Rolling, Tokyo, Japan, September 1985, pp 335-342

[Kiuchi4] Kiuchi, Manabu., Abe, Kenji., Onodera, Ryu. Computerized numerical simulation of roll-forming process, Cirp Annals, V 44, no: 1, 1995, pp 239-242.

[Low] Low, Adrian., Introductory Computer Vision and Image Processing, McGraw-Hill, 1991

[MARC] MARC
User Information- Volume A
Element Library - Volume B
Program Input - Volume C
User Subroutines - Volume D
MARC Analysis Research Corporation, World Headquarters,
260 Sheridan Avenue, Palo Alto, California 94306

[McClure] McClure, Carl K., Li, Hanhui. Roll forming simulation using finite element analysis Manufacturing Review, Vol 8, no: 2, Jun 1995, pp 114-119.

[Masuda] Masuda,M., Murota,T., Jimma,T., Tamano,T., Amagai,T., Fundamental Research on Cold Roll Forming of Metals Strips, Bulletin of the Japanese Society of Mechanical Engineers, Vol 7, No. 28, 1964, pp 827-833

[Matrox] Matrox iTools Imaging Library User Guide
Matrox iTools MIL Interpreter User Guide

[Milner] Milner,D.A., CAD/CAM for Cold-Roll Forming Tools, The Production Engineer, November 1983, Vol 62, No. 11, pp 52-55

[Naidenov] Naidenov,A.A., Kaluzhskii,V.B., Roll Pass Design for Multiple Stand Piecework Cold Forming Mills, Stal in English, Vol. 7, January 1963, pp 57-61

[Nefussi] Nefussi, G., Gilormini, P., Simplified method for the simulation of cold-roll forming, International Journal of Mechanical Sciences, Vol35, no: 10, Oct 1993, pp 867-878.

[Noble] Noble,C.F., Sarantidis,T.M., A A A study Cold Roll Forming, First International Conference on Rotary Metal-Working Processes, London, UK, November 20-22, 1979, pp 411-424

[Oh] Oh,S.I, Kobayashi,S., Finite Element Analysis of Plane-Strain Sheet Bending, International journal of Mechanical Sciences, Vol.22, pp 583-594

[Ona1] Ona, H., Jimma,T., Prevention of Oil-Canning and Edge Buckling in the Cold Roll Forming Process of Wide Profiles, Proceedings of the Second International Conference on Rotary Metal Working Processes, Stratford-Upon-Avon, 1982, pp 247-256

[Ona2] Ona, H., Jimma,T., On Method of Roll Design for Cold Roll Forming of Light Gauge Steel Members, Journal of the Japanese Society of the Technology of Plasticity, Vol 24, July 1983, pp 707-714

[Ona3] Ona,H., Jimma,T., Fukaya, N., Experiments into the Cold Roll-Forming of Straight Asymmetrical Channels, Journal of Mechanical Working Technology, Vol 8, November 1983, pp 273-291

[Ona4] Ona,H., Jimma,T., Kozono,H., Nakako,T., Development in CAD for Cold Roll Forming, Proc. 26th International M.T.D.R Conference, Manchester, UK, 1986, pp 49-54

[Onoda] Onoda, Y., Recent Research Trends of Roll Forming in Japan, Proc. of the Third International Conference on Rotary Metal working processes, Kyoto, Japan, 1985

[Panton1] Panton, S.M., Computer Aided Form Roll Design, Ph.D Thesis, Aston University, April 1987

[Panton2] Panton, S.M., Milner, D.A., Thornley, R.H., Computer Aided Design of Form Rolls, Proc. 26th International M.T.D.R Conference, Manchester, UK, 1986, pp 417-424

[Panton3] Panton, S.M, Zhu, S.D, Duncan, J.L., Geometric Constraints on the Forming Path in Roll Forming Channel Sections, Proc Inst Mech Engrs, Vol 206, 1992, pp 113-118.

[Panton4] Panton, S.M, Zhu, S.D, Duncan, J.L., Fundamental Deformation Types and Sectional Properties in Roll Forming, International Journal of Mechanical Science, Vol 36, No.8, pp 725-735, 1994.

[Rhodes1] Rhodes,A., Boardman,A.S., McIntosh,D.H., Computer Aided Design and Manufacture of Rolls for Cold Roll Forming Machines, Proc. of the First International Conference on Rotary Metal Working Processes, London, UK, November 20-22, 1979, pp 425-444

[Rhodes2] Rhodes,A., Computer - Aided Design of Rolls for Cold Roll Forming- Part 1, Sheet Metal Industries, Vol 59, 1982, pp 643-651

[Rhodes3] Rhodes,A., Computer -Aided Design of Rolls for Cold Roll Forming- Part 2, Sheet Metal Industries, Vol 59, 1982, pp 789-792

[Rhodes4] Rhodes,A., Computer-Aided Roll Design for Cold Roll Forming, The Production Engineer, Vol 60, No 9, September 1981, pp32-34.

[Rhodes5] Rhodes,J, Design of Cold Formed Steel members, Elsevier Applied Science Publishers Ltd, Chapter 1, pp 6

[Russell] Russell,J.D., Kuhn, N.L., A Mathematical Model of Sheet Bending Applied To Corrugating, The Journal of the Australian Institute of Metals, Vol 11, No. 1, February 1966, pp 38-46

[Suzuki] Suzuki,H., Kiuchi,M., Nakajima,S., Ichidayama,M., Takada,K., Experimental Investigation on Cold Roll Forming Process II, Report of the Institute of Industrial Science, The University of Tokyo, Vol 26, No.8, Feb 1978

[Ubeco] UBECO GmbH, Postfach 2510, D-48595 Iserlohn, Germany

[Vander] Vanderploeg, E.J., Forming Metal Shapes by Cold-Rolling, Machinery, February 1948, pp 153-158

[Wright] Wright, J.R., Fundamentals of Roll Forming, Precision Metal, February1967, pp 23-25.

[Zhu] Zhu, S.D., Panton, S.M., Duncan, J.L., The Effects of Geometric Variables in Roll Forming a Channel Section, Proc Inst Mech Engrs, Vol 210, 1996, pp 127-134.

Appendix A

Theoretical Strain Distributions

Figure A1. Theoretical bend angle curve and strain distribution in folding from 0 to 19.69°

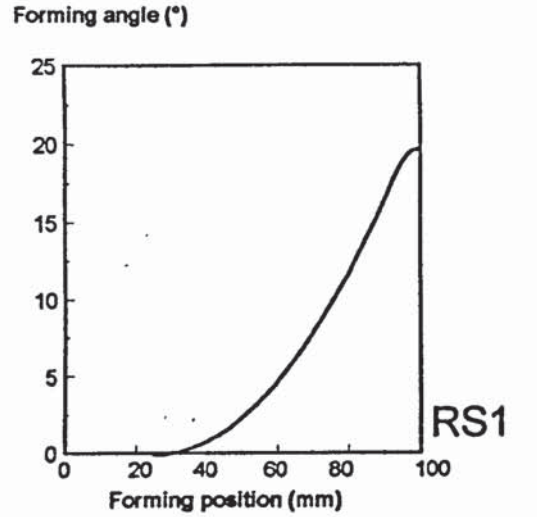

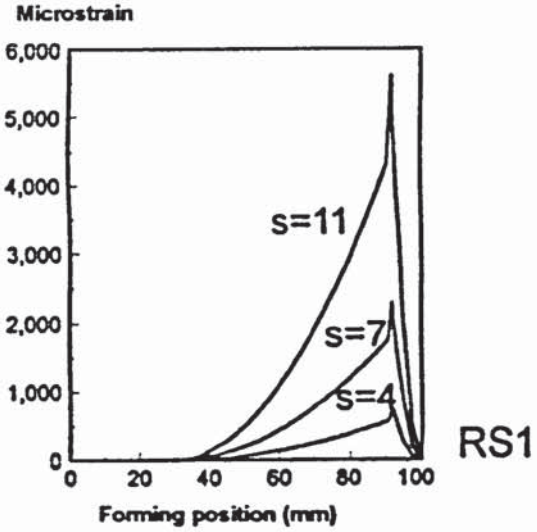

Figure A2. Theoretical bend angle curve and strain distribution in folding from 19.69° to 35.59°

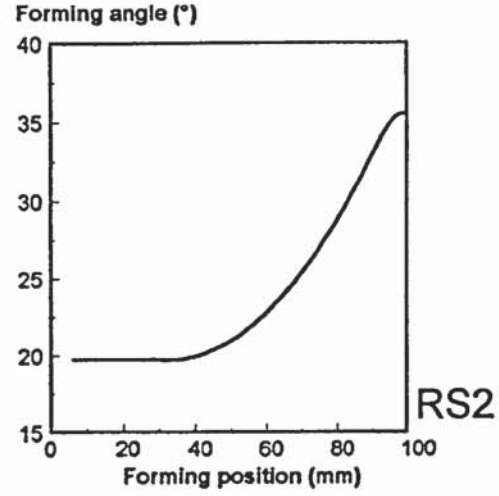

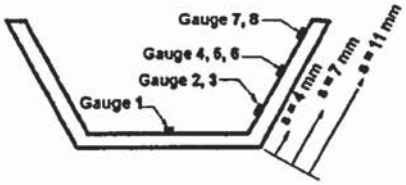

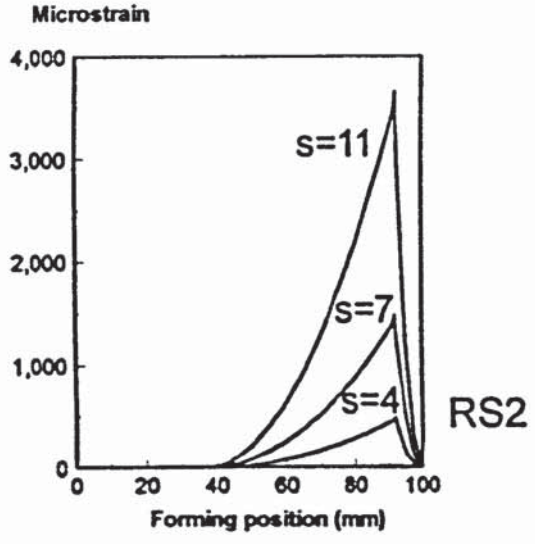

Figure A3. Theoretical bend angle curve and strain distribution in folding from 35.59° to 47.04°

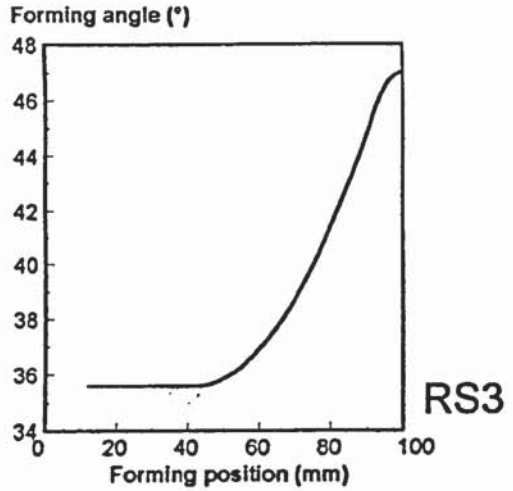

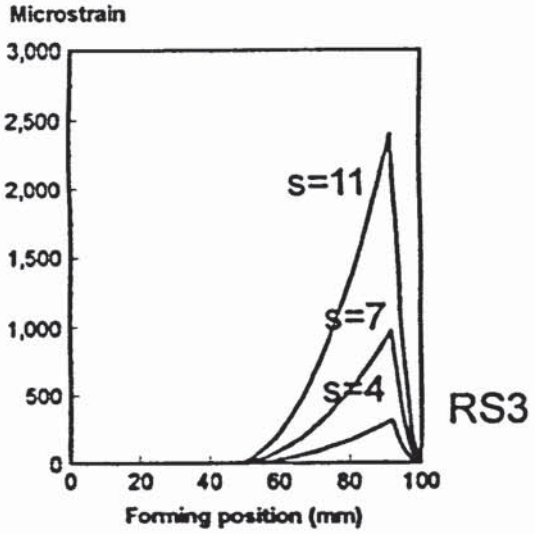

Figure A4. Theoretical bend angle curve and strain distribution in folding from 47.04° to 55.04°

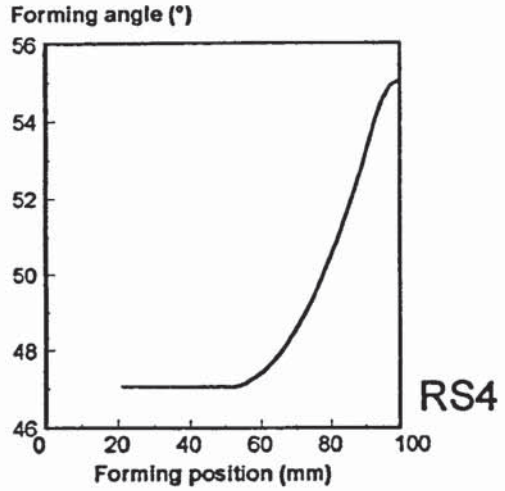

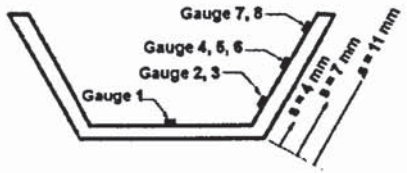

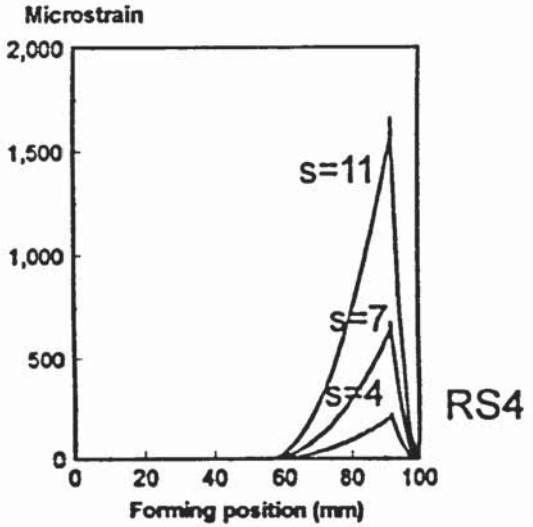

Figure A5. Theoretical bend angle curve and strain distribution in folding from 55.05° to 60.79°

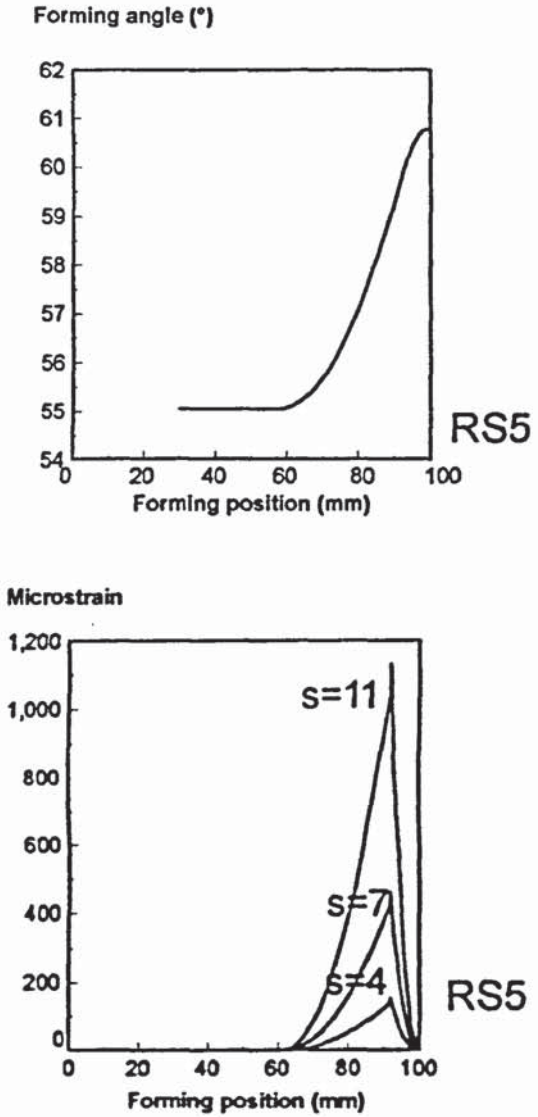

Figure A6. Theoretical bend angle curve and strain distribution in folding from 60.79° to 65.03°

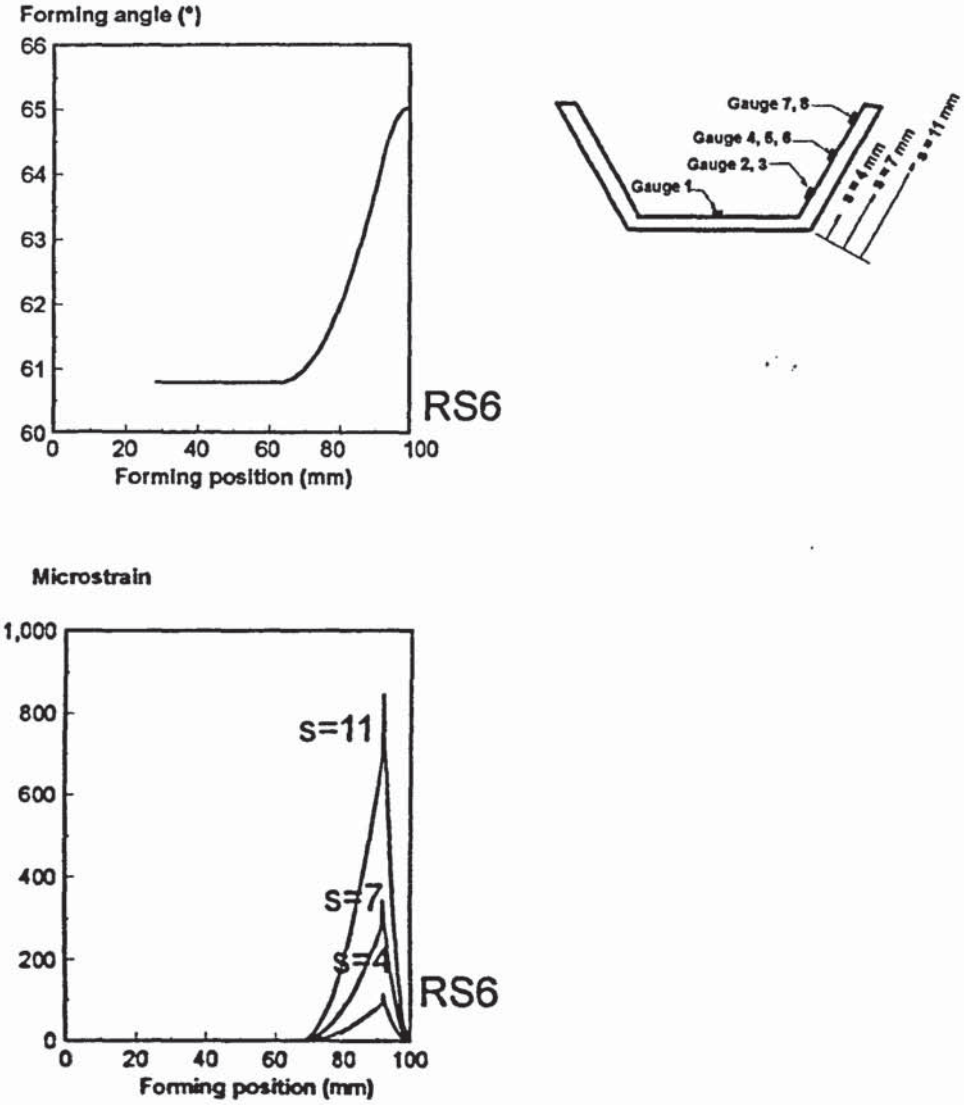

Figure A7. Theoretical bend angle curve and strain distribution in folding from 19.69° to 47.04°

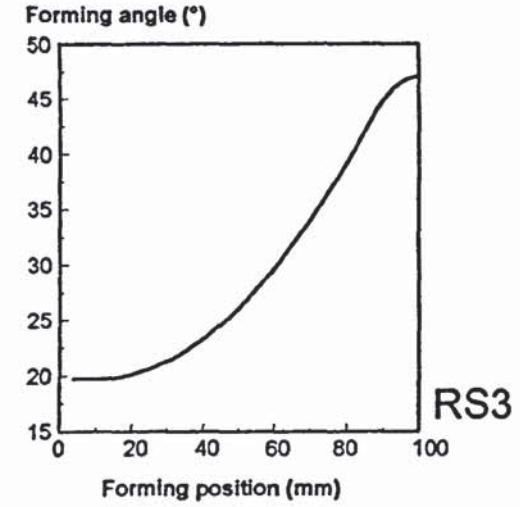

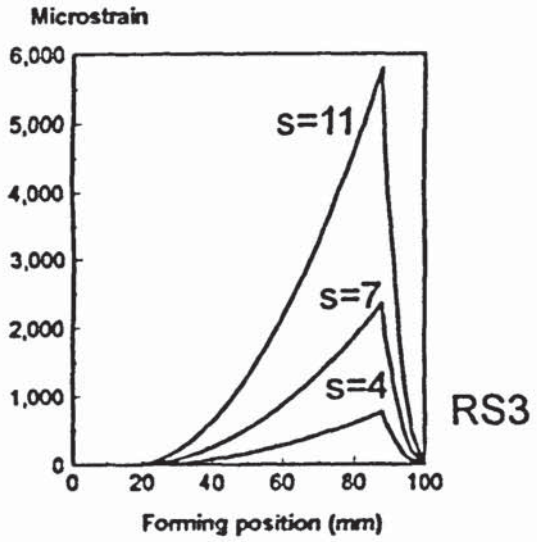

Figure A8. Theoretical bend angle curve and strain distribution in folding from 47.04° to 65.03°

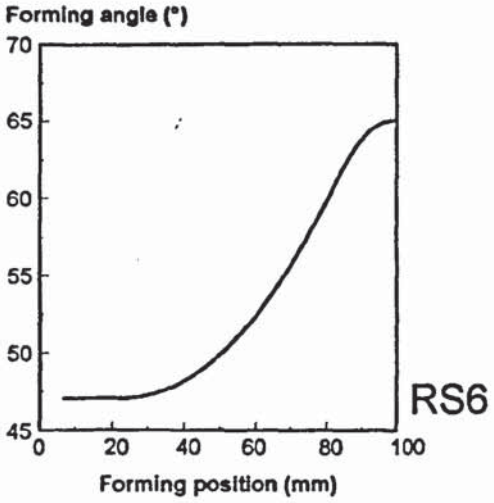

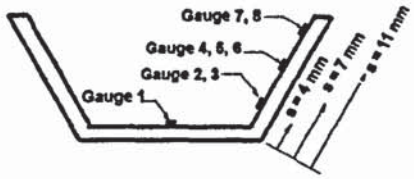

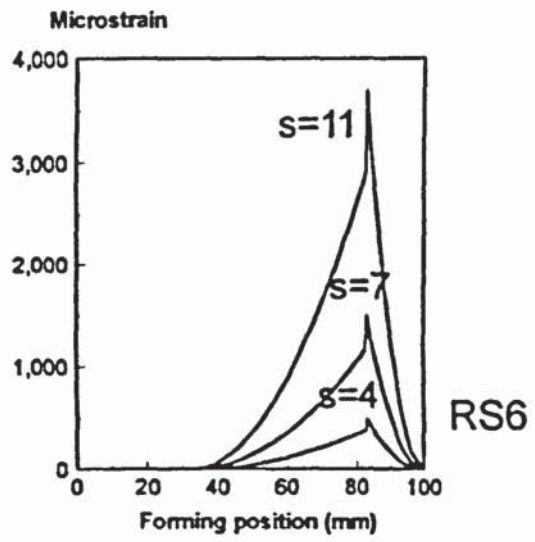

Appendix B

Experimental Strain Distributions

(a) CRF Mill No:1

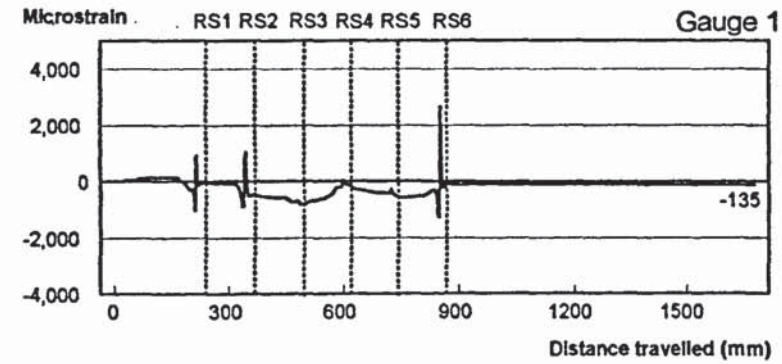

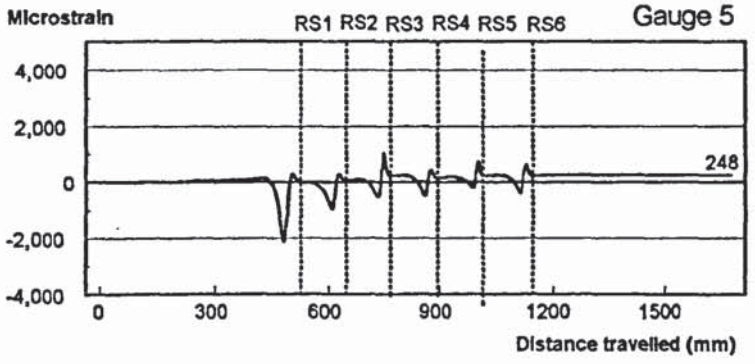

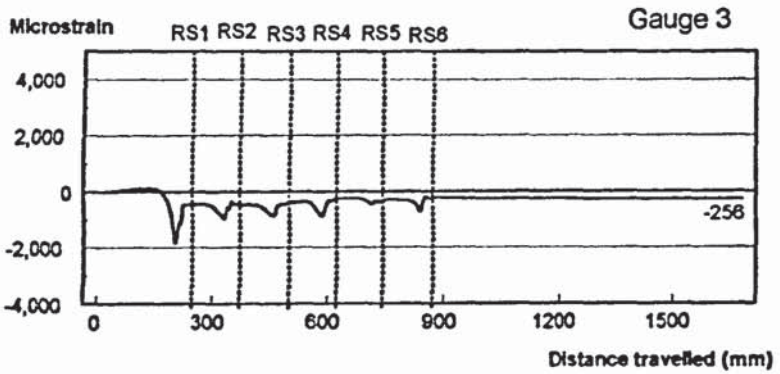

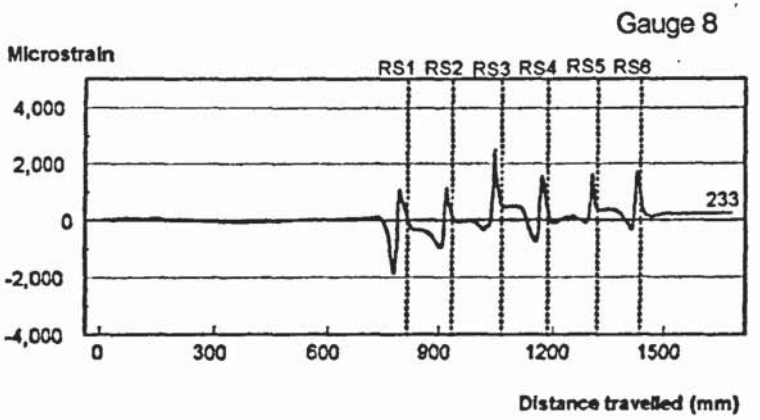

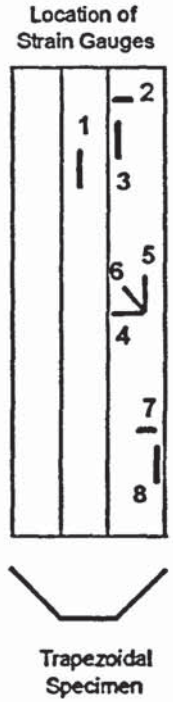

Figure B1. Graph of Strain Vs Distance travelled (CRF Mill No: 1, Mild steel Specimen, 6 rollers with 127mm spacing).

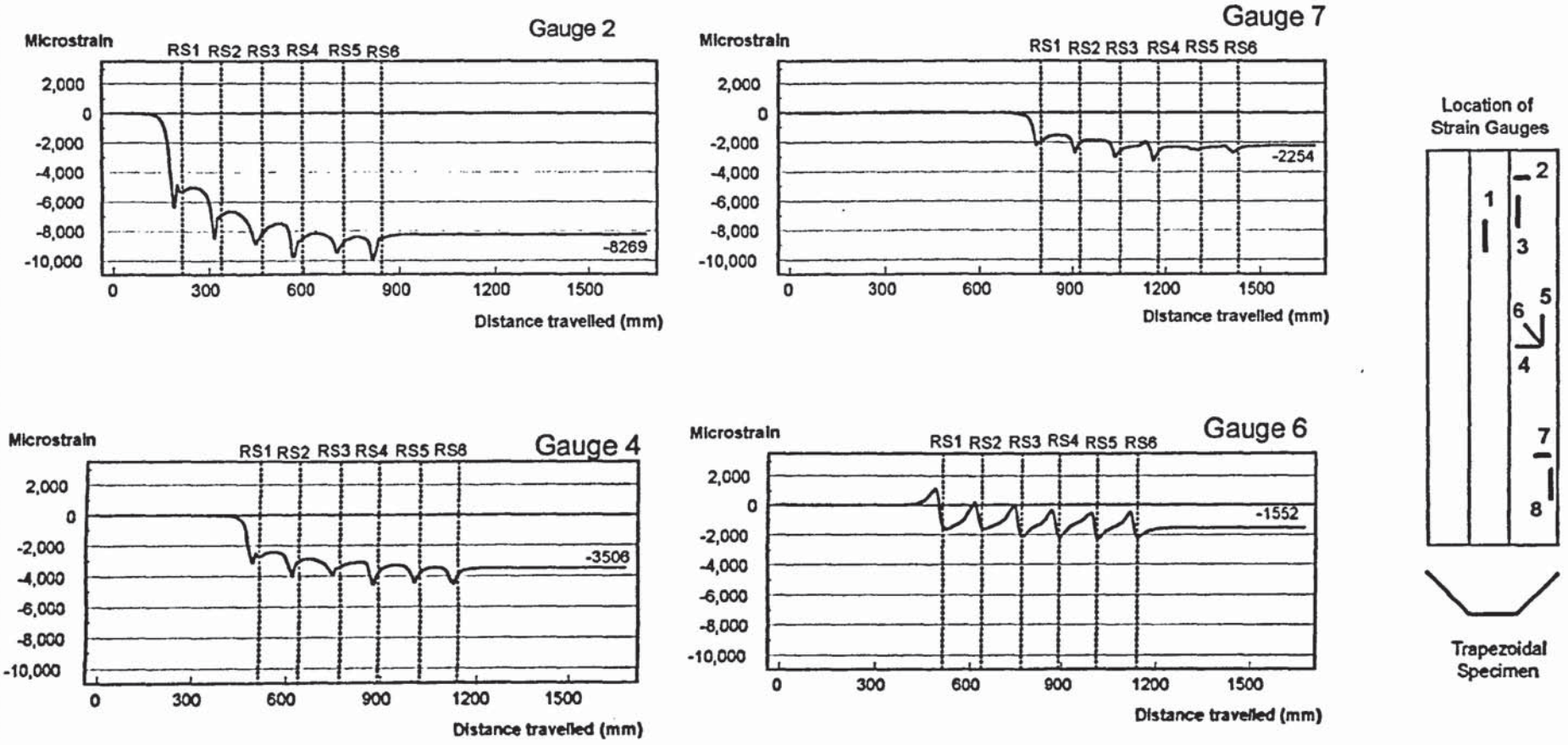

Figure B2. Graph of Strain Vs Distance travelled (CRF Mill No:1, Mild steel Specimen, 6 rollers with 127mm spacing).

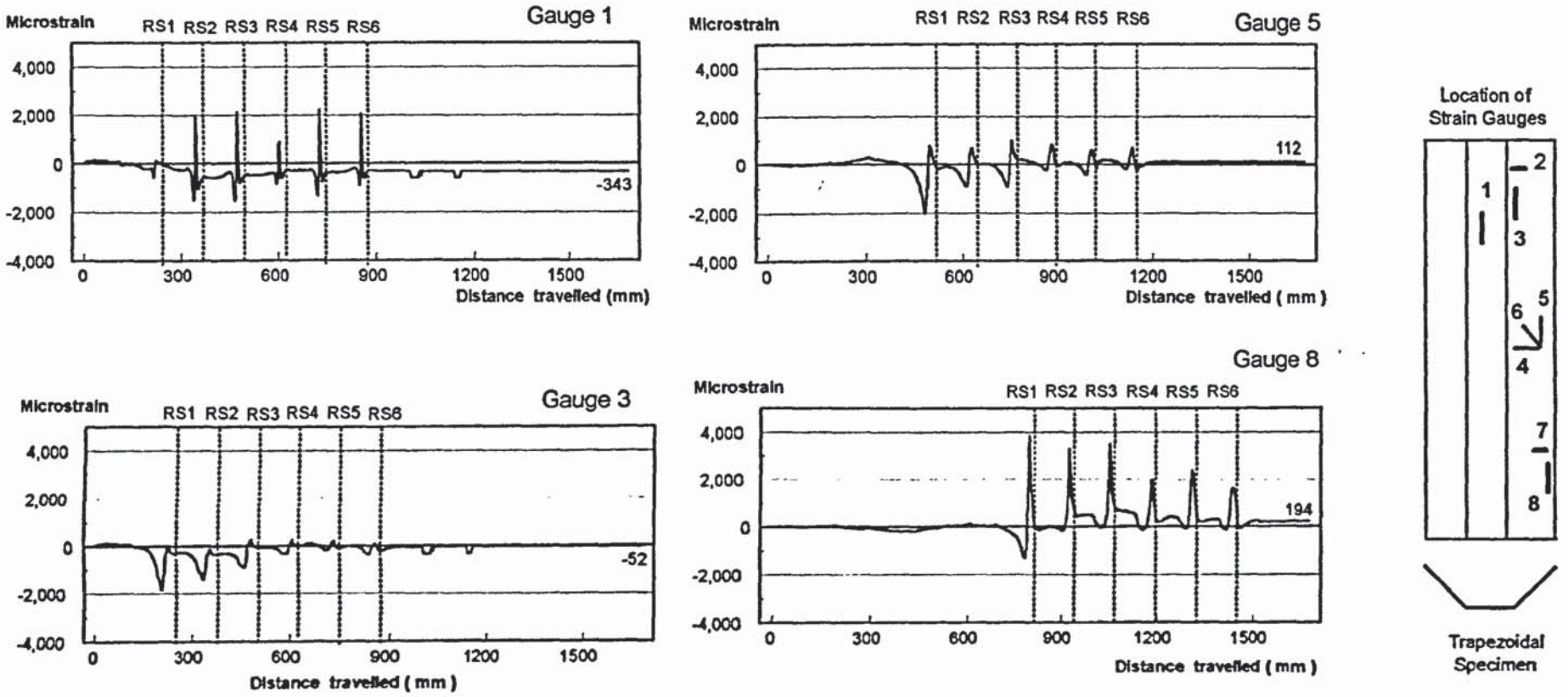

Figure B3. Graph of Strain Vs Distance travelled (CRF Mill No: 1, Aluminium Specimen, 6 rollers with 127mm spacing).

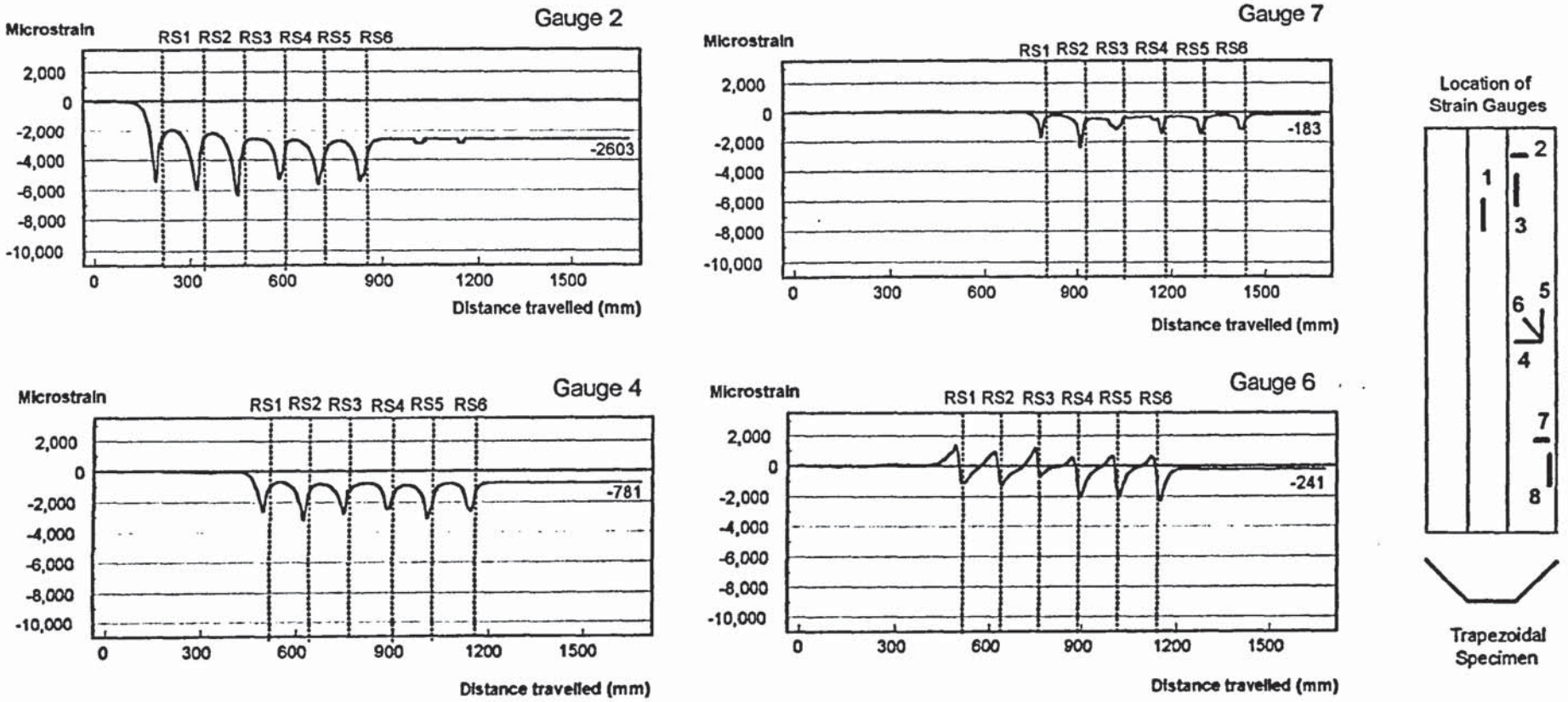

Figure B4. Graph of Strain Vs Distance travelled (CRF Mill No: 1, Aluminium Specimen, 6 rollers with 127mm spacing).

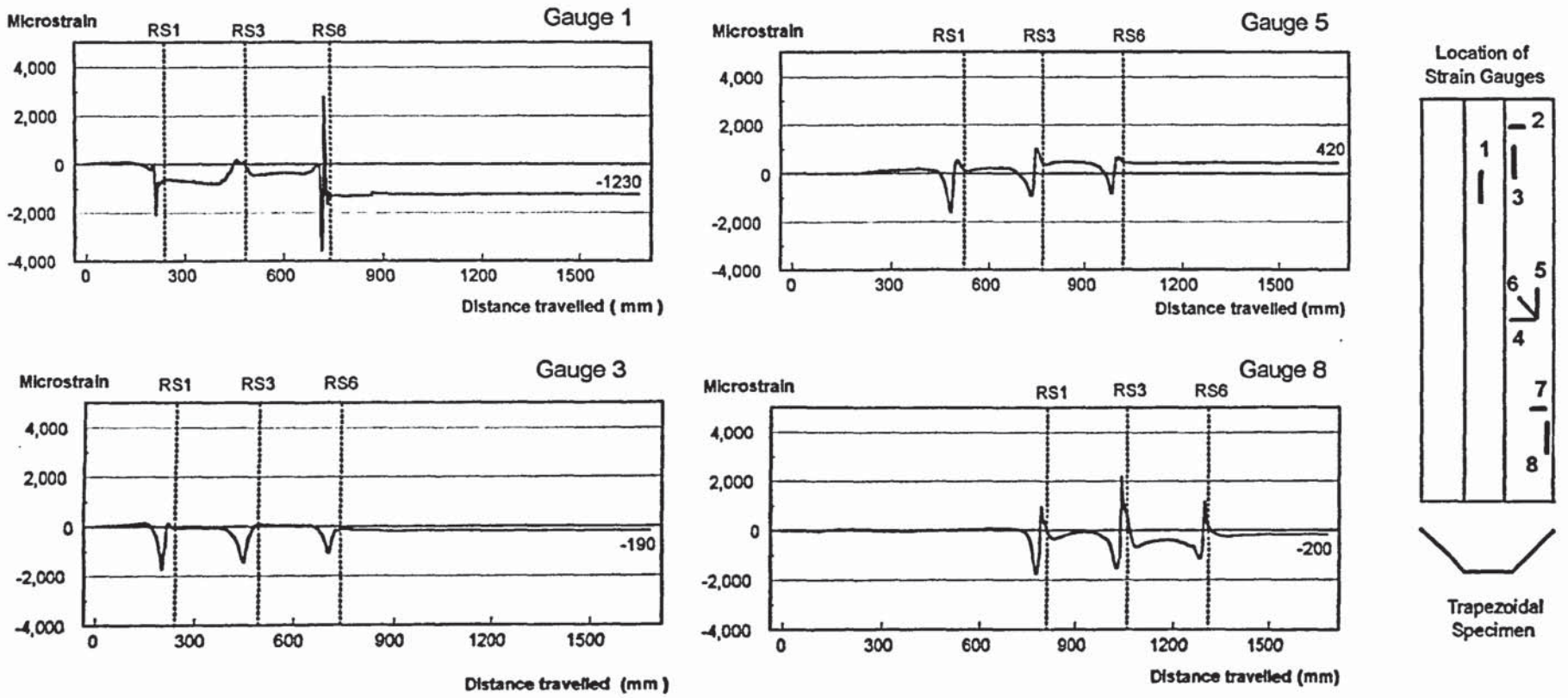

Figure B5. Graph of Strain Vs Distance travelled (CRF Mill No: 1, Mild steel Specimen, 3 rollers with 2x127mm spacing).

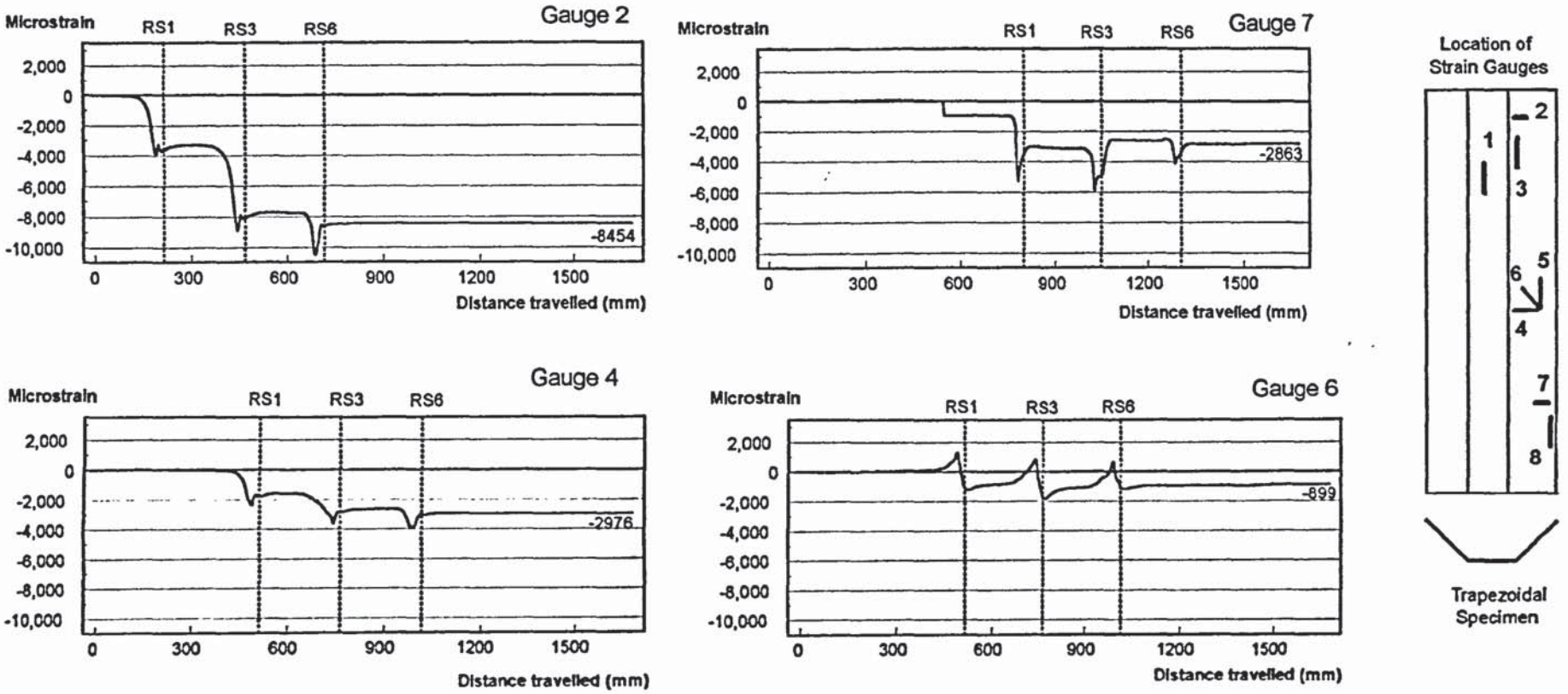

Figure B6. Graph of Strain Vs Distance travelled (CRF Mill No:1, Mild steel Specimen, 3 rollers with 2x127mm spacing).

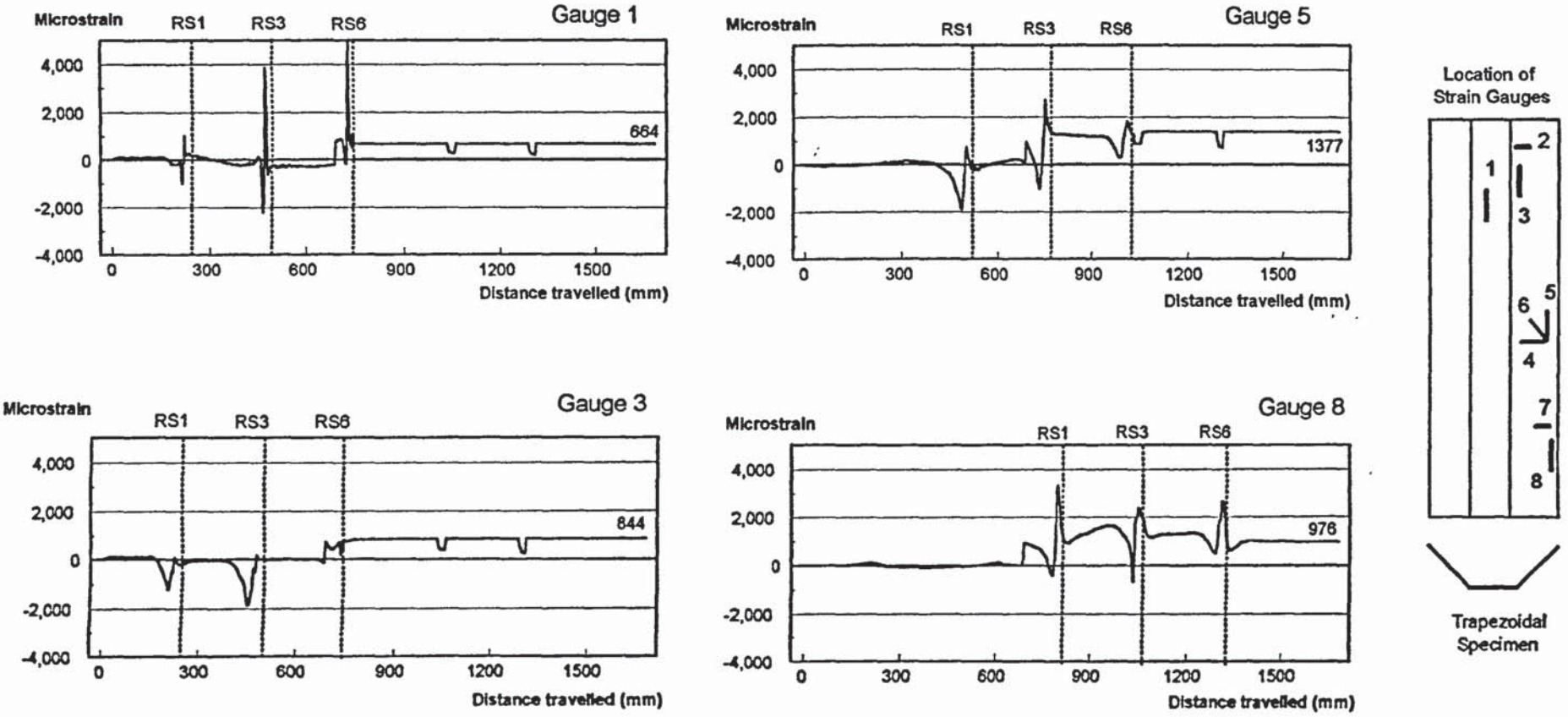

Figure B7. Graph of Strain Vs Distance travelled (CRF Mill No: 1, Aluminium Specimen, 3 rollers with 2x127mm spacing).

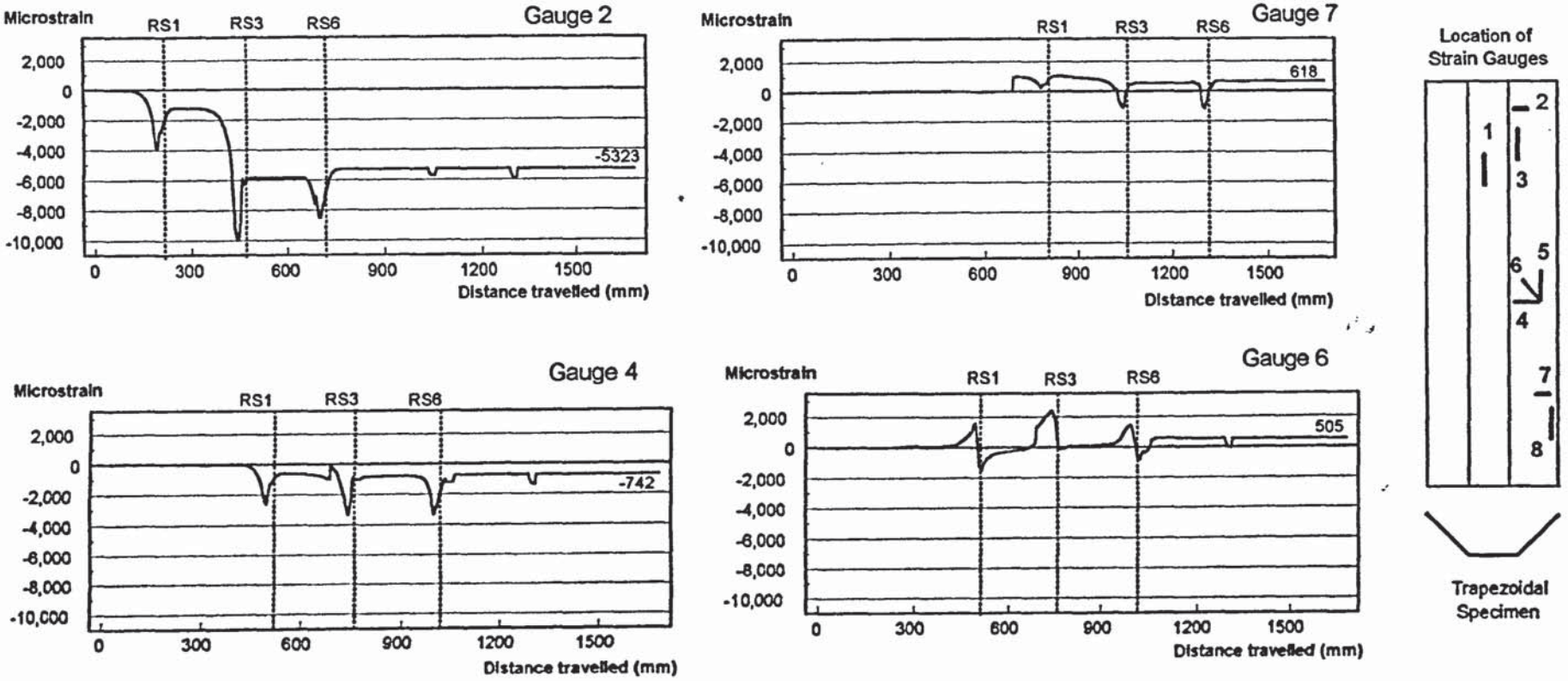

Figure B8. Graph of Strain Vs Distance travelled (CRF Mill No: 1, Aluminium Specimen, 3 rollers with 2x127mm spacing).

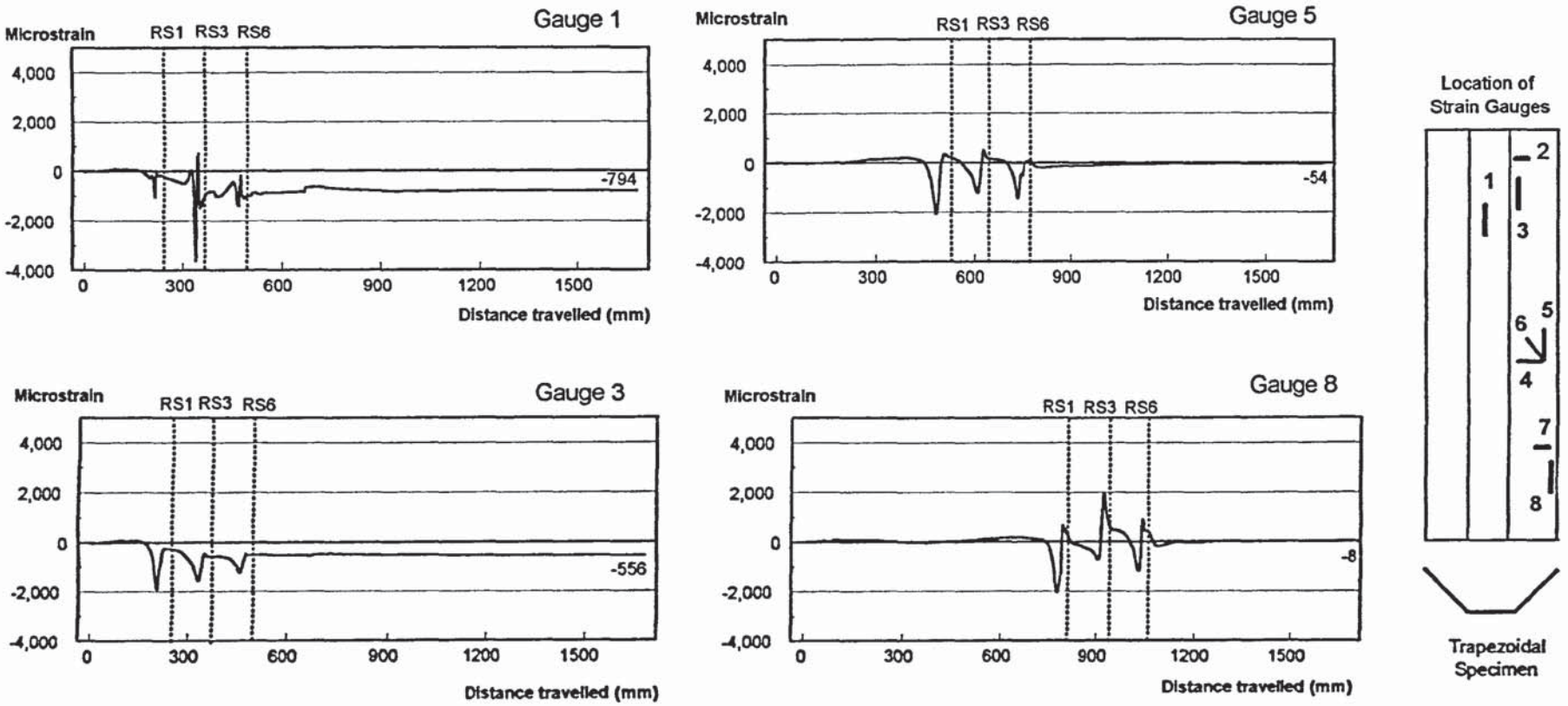

Figure B9. Graph of Strain Vs Distance travelled (CRF Mill No: 1, Mild steel Specimen, 3 rollers with 127mm spacing).

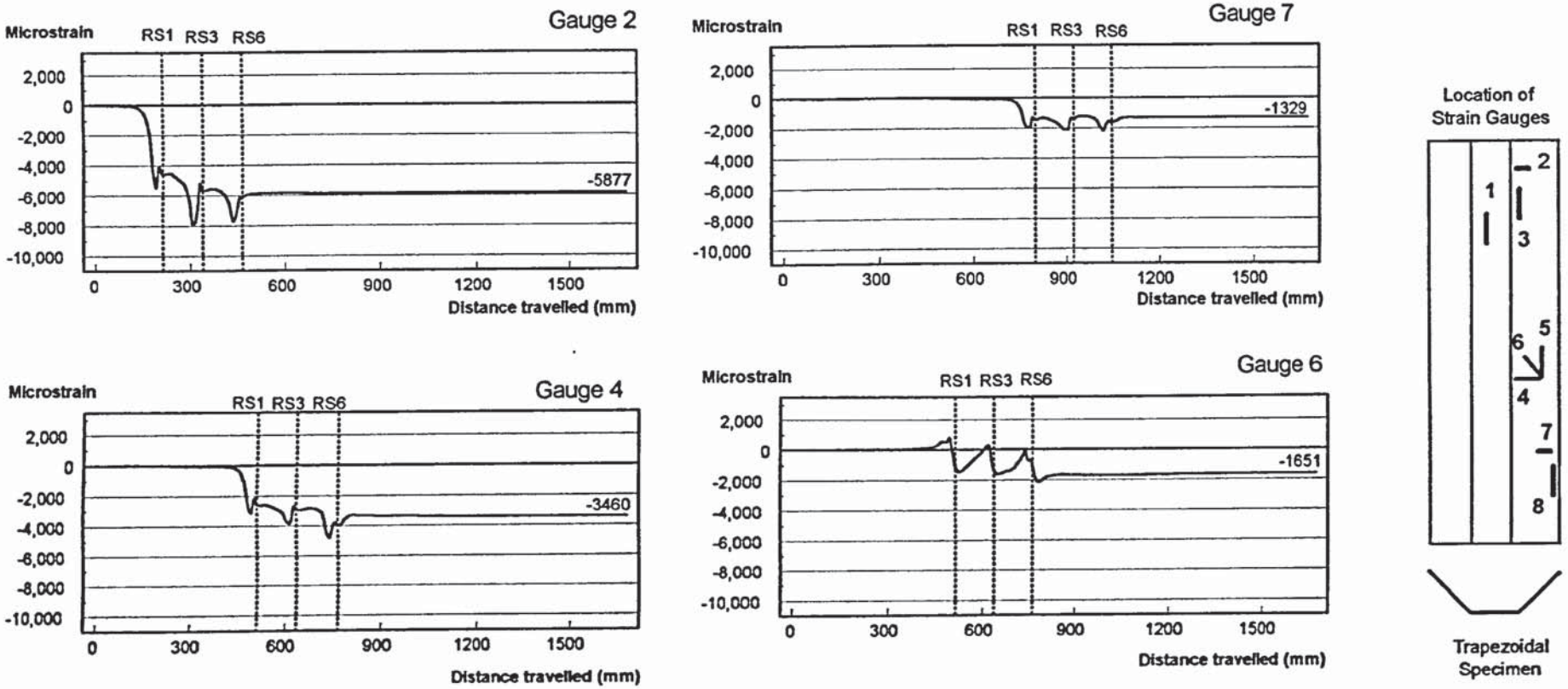

Figure B10. Graph of Strain Vs Distance travelled (CRF Mill No: 1, Mild steel Specimen, 3 rollers with 127mm spacing).

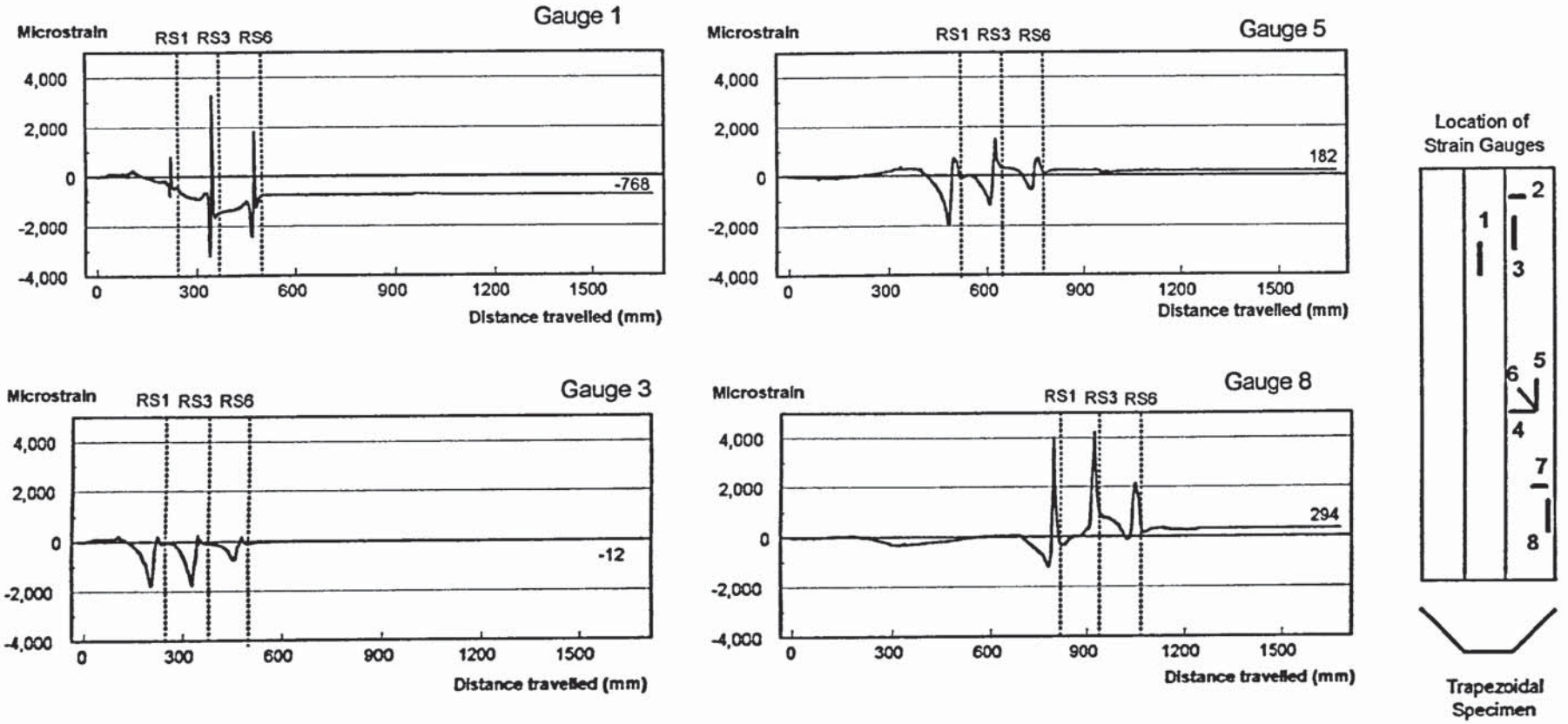

Figure B11. Graph of Strain Vs Distance travelled (CRF Mill No: 1, AluminiumSpecimen, 3 rollers with 127mm spacing).

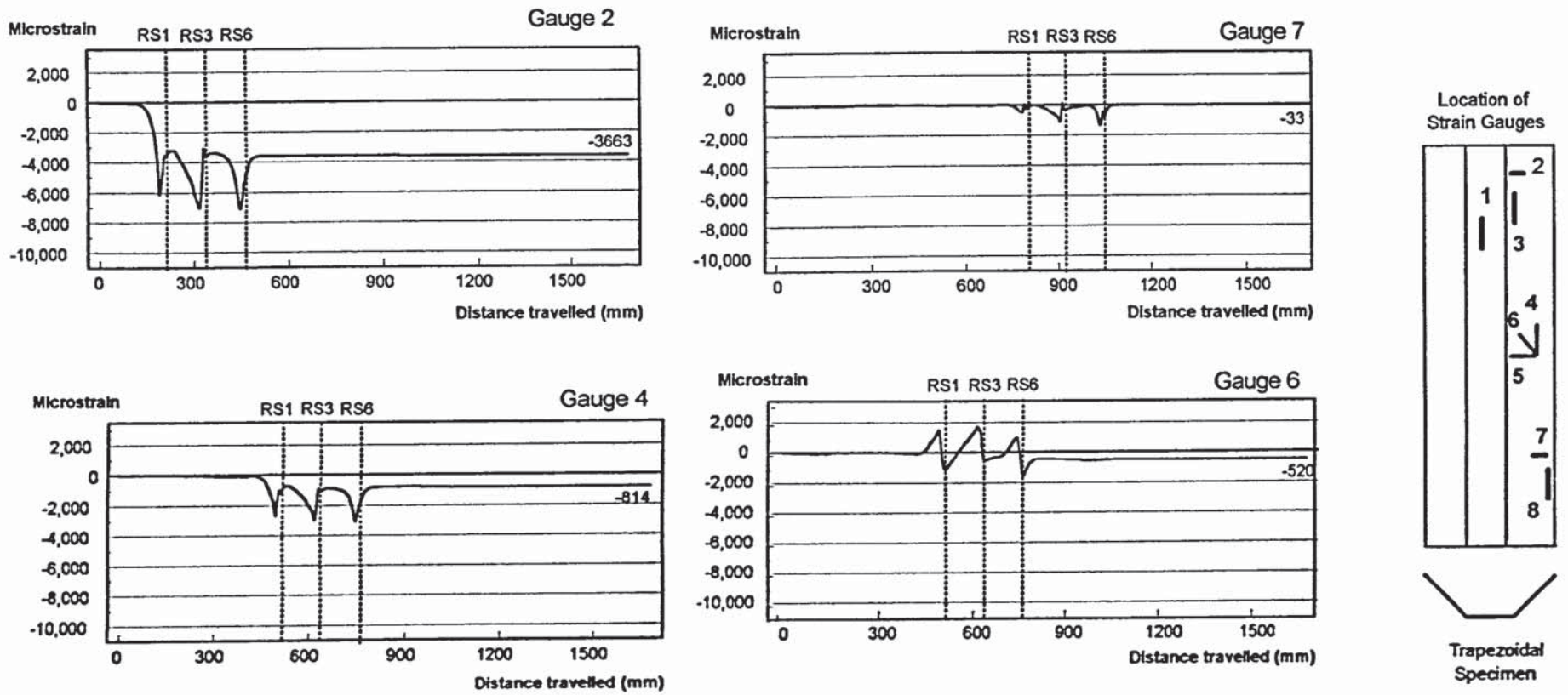

Figure B12. Graph of Strain Vs Distance travelled (CRF Mill No: 1, Aluminium Specimen, 3 rollers with 127mm spacing).

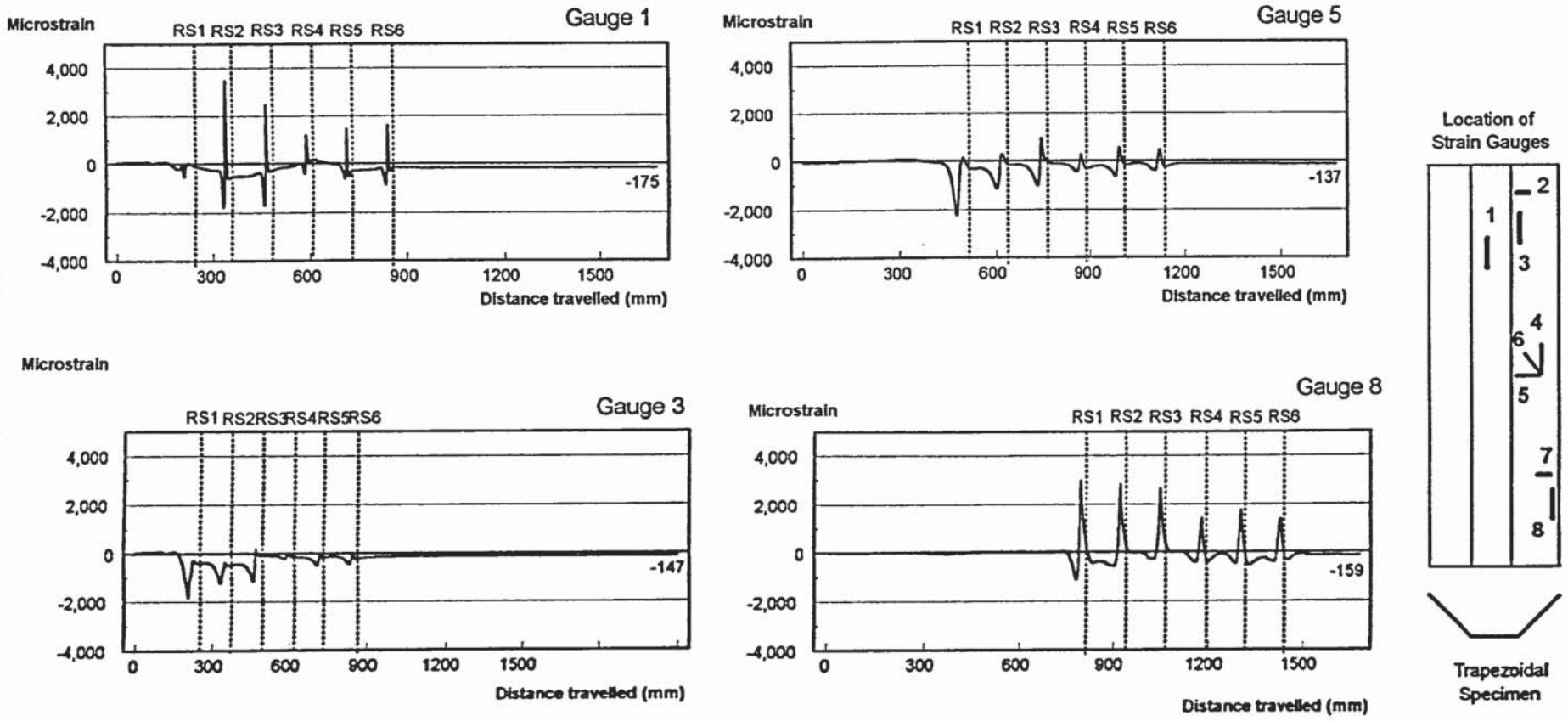

Figure B13. Graph of Strain(Dynamic) Vs Distance travelled (CRF Mill No: 1, Mild steel Specimen, 6 rollers with 127mm spacing).

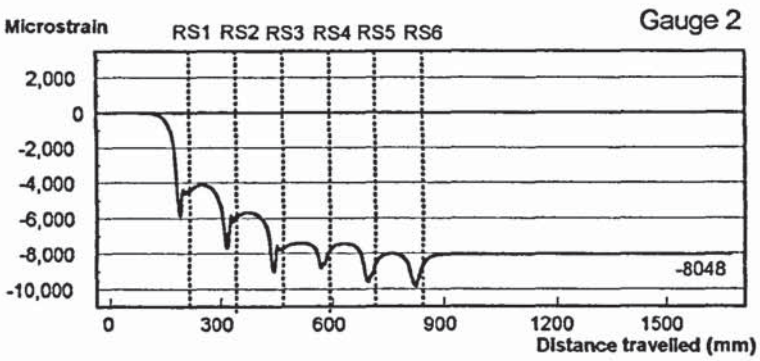

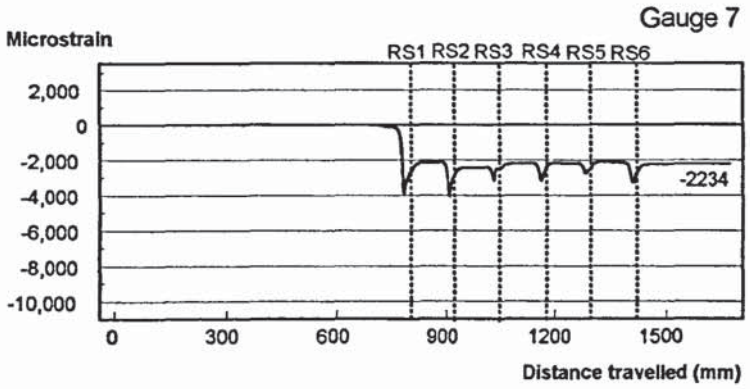

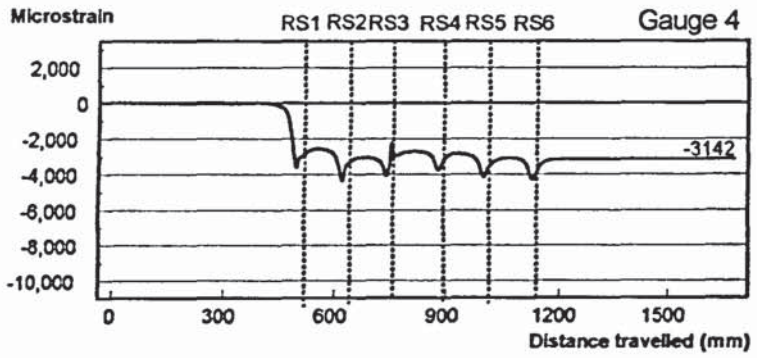

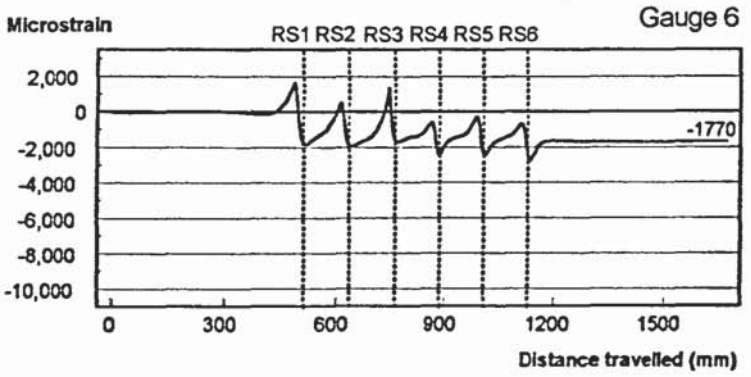

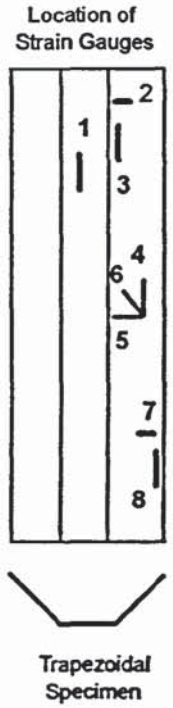

Figure B14. Graph of Strain(Dynamic) Vs Distance travelled (CRF Mill No: 1, Mild steel Specimen, 6 rollers with 127mm spacing)

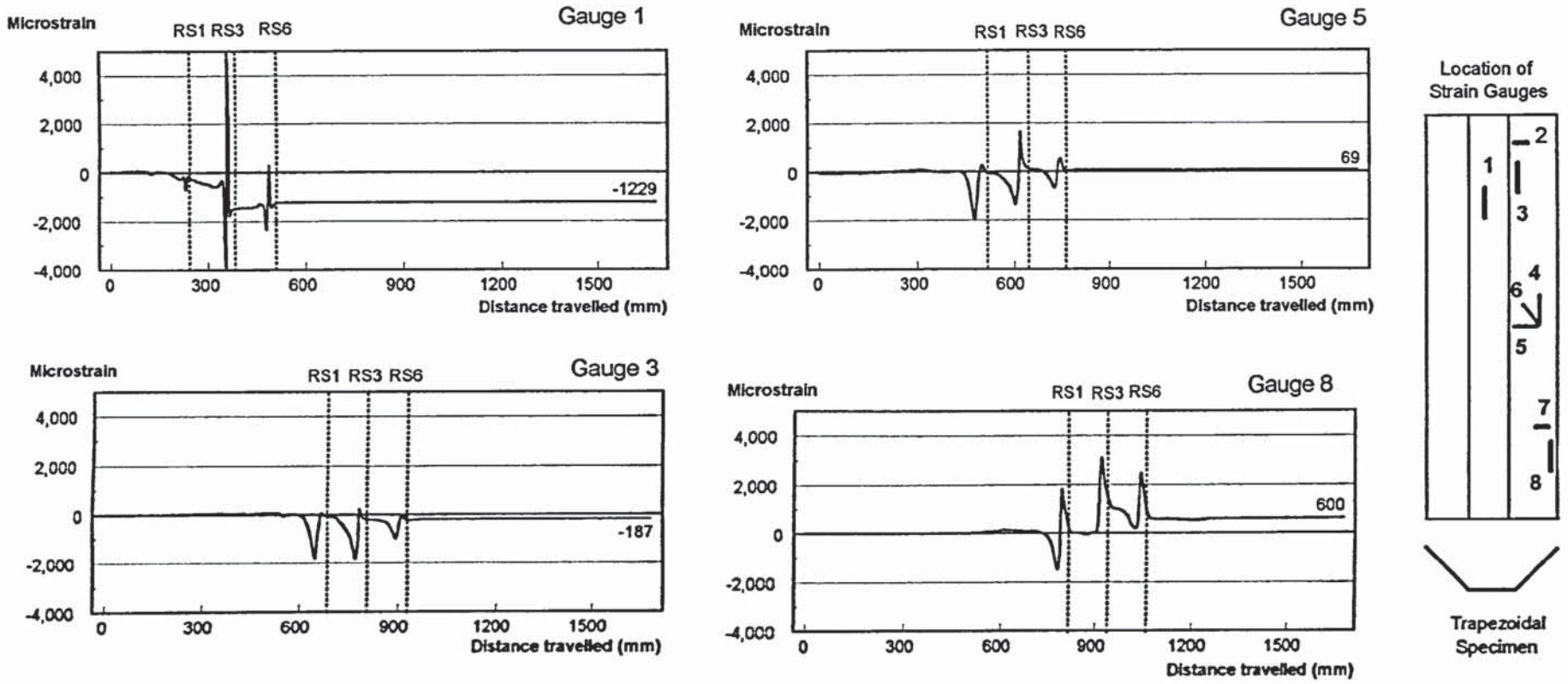

Figure B15. Graph of Strain (Dynamic) Vs Distance Travelled (CRF Mill No:1, Mild steel Specimen, 3 rollers with 127mm spacing)

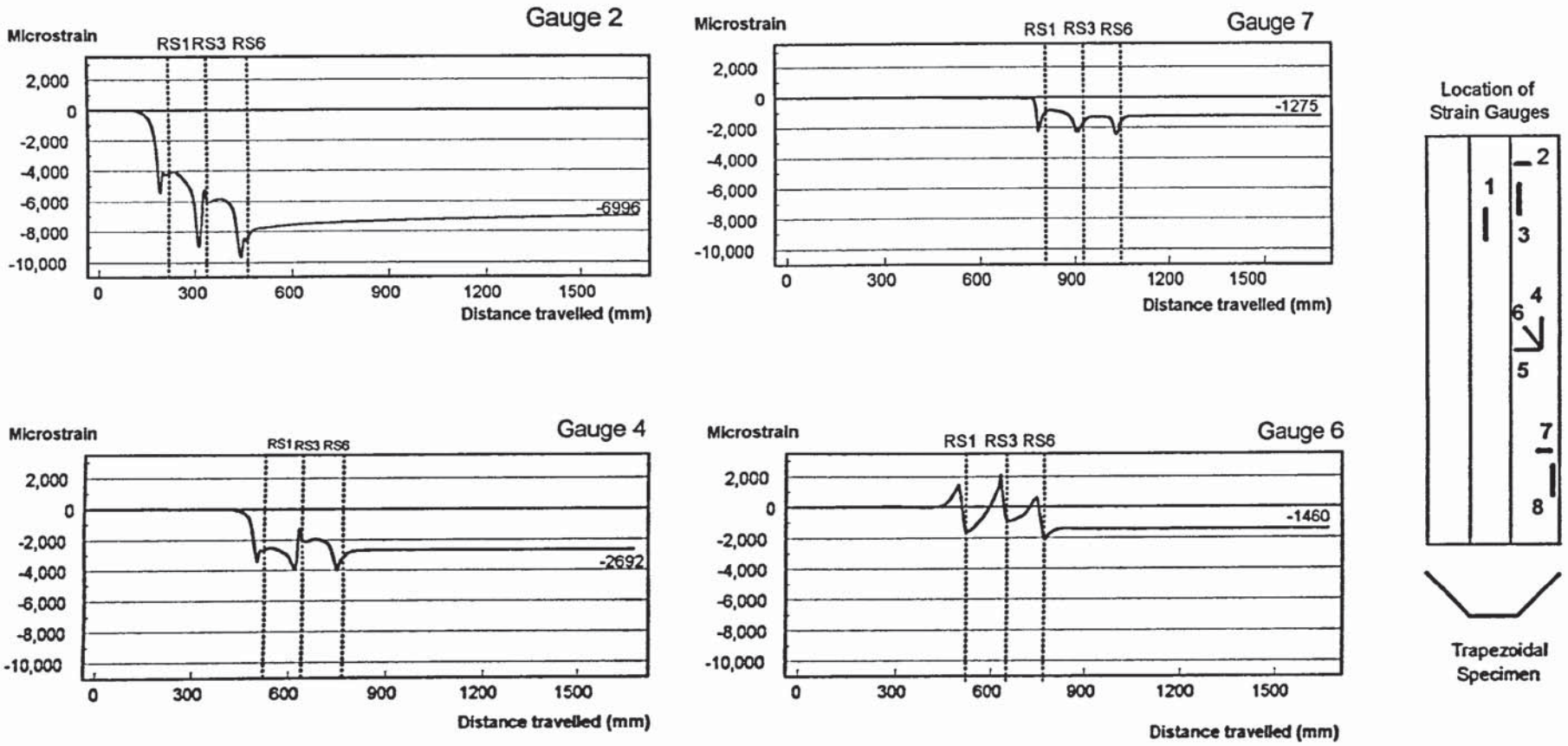

Figure B16. Graph of Strain (Dynamic) Vs Distance Travelled (CRF Mill No: 1, Mild steel Specimen, 3 rollers with 127mm spacing).

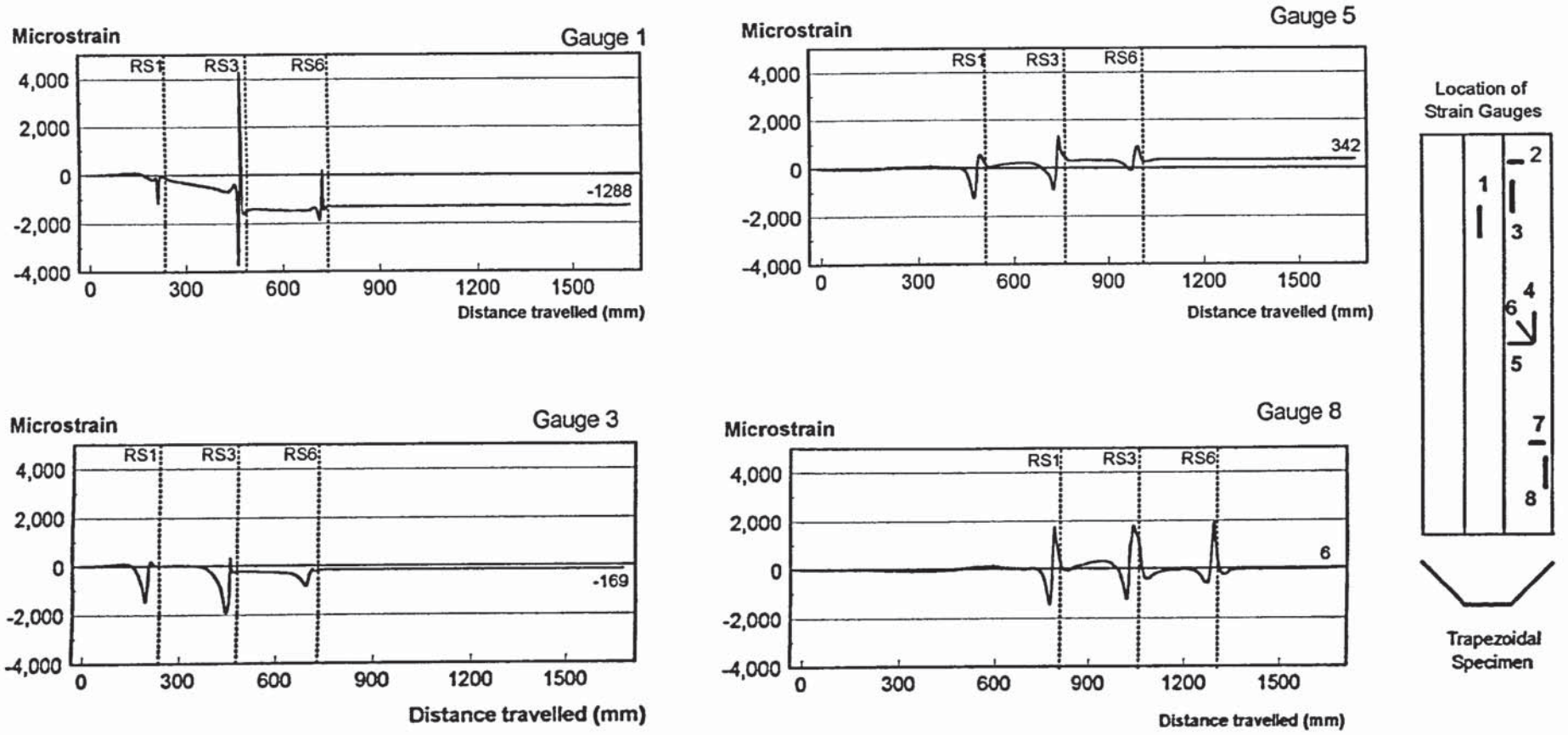

Figure B17. Graph of Strain (Dynamic) Vs Distance Travelled (CRF Mill No: 1, Mild steel Specimen, 3 rollers with 2x127mm spacing).

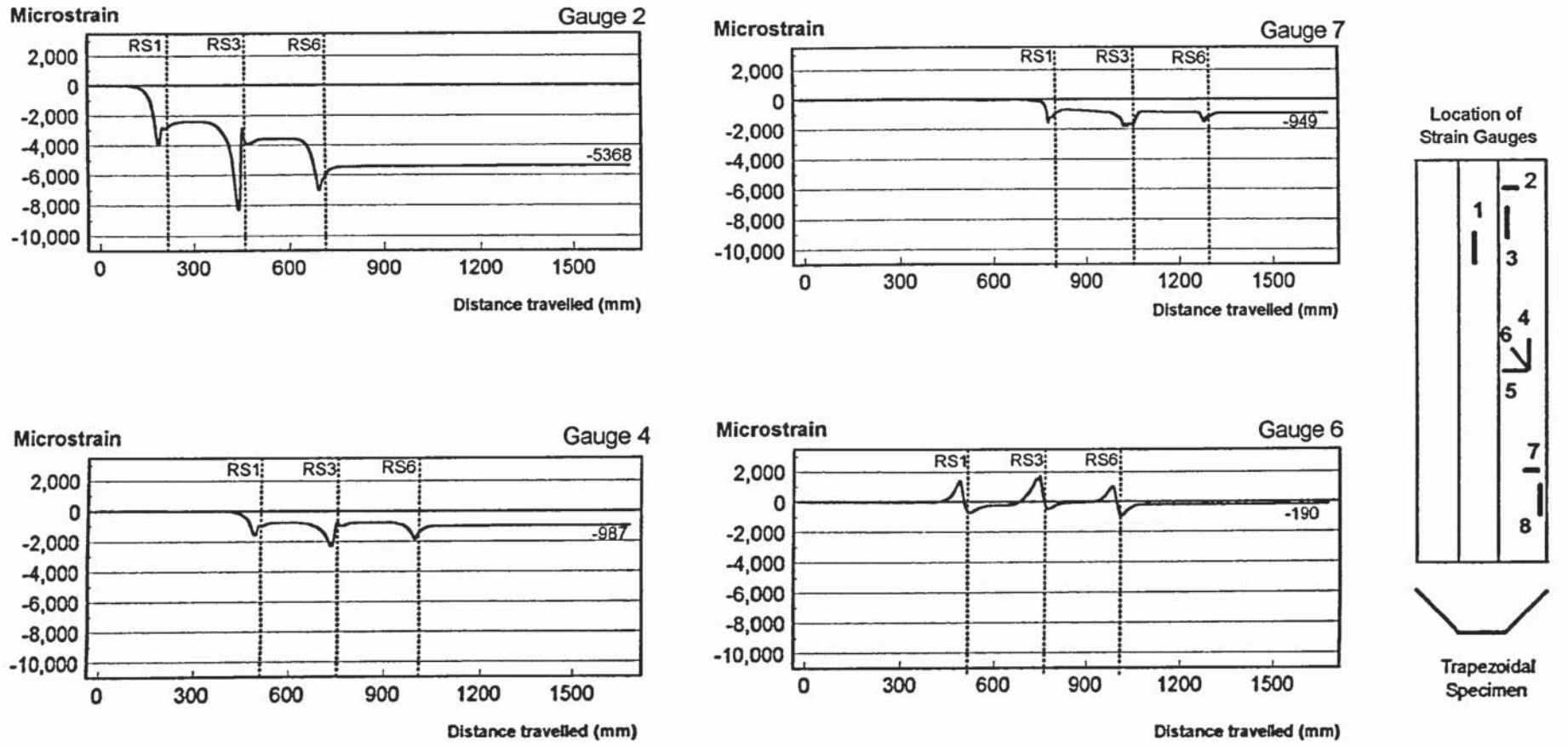

Figure B18. Graph of Strain (Dynamic) Vs Distance Travelled (CRF Mill No: 1,Mild steel Specimen, 3 rollers with 2x127mm spacing).

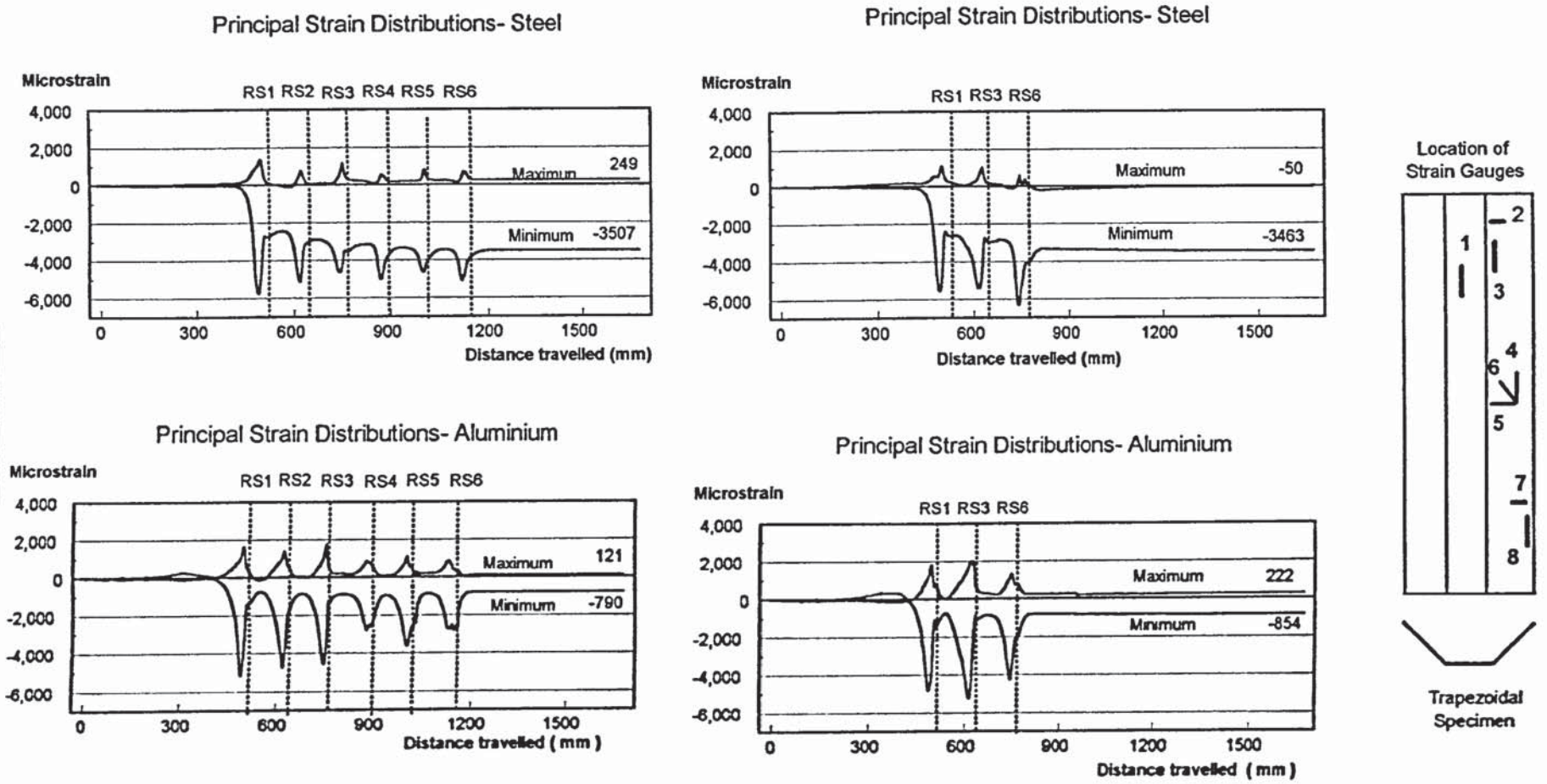

Figure B 19. Graph of Principal Strain Distribution Vs Distance Travelled (CRF Mill No:1, Steel and Aluminium Specimens, 6 and 3 Roll Stations).

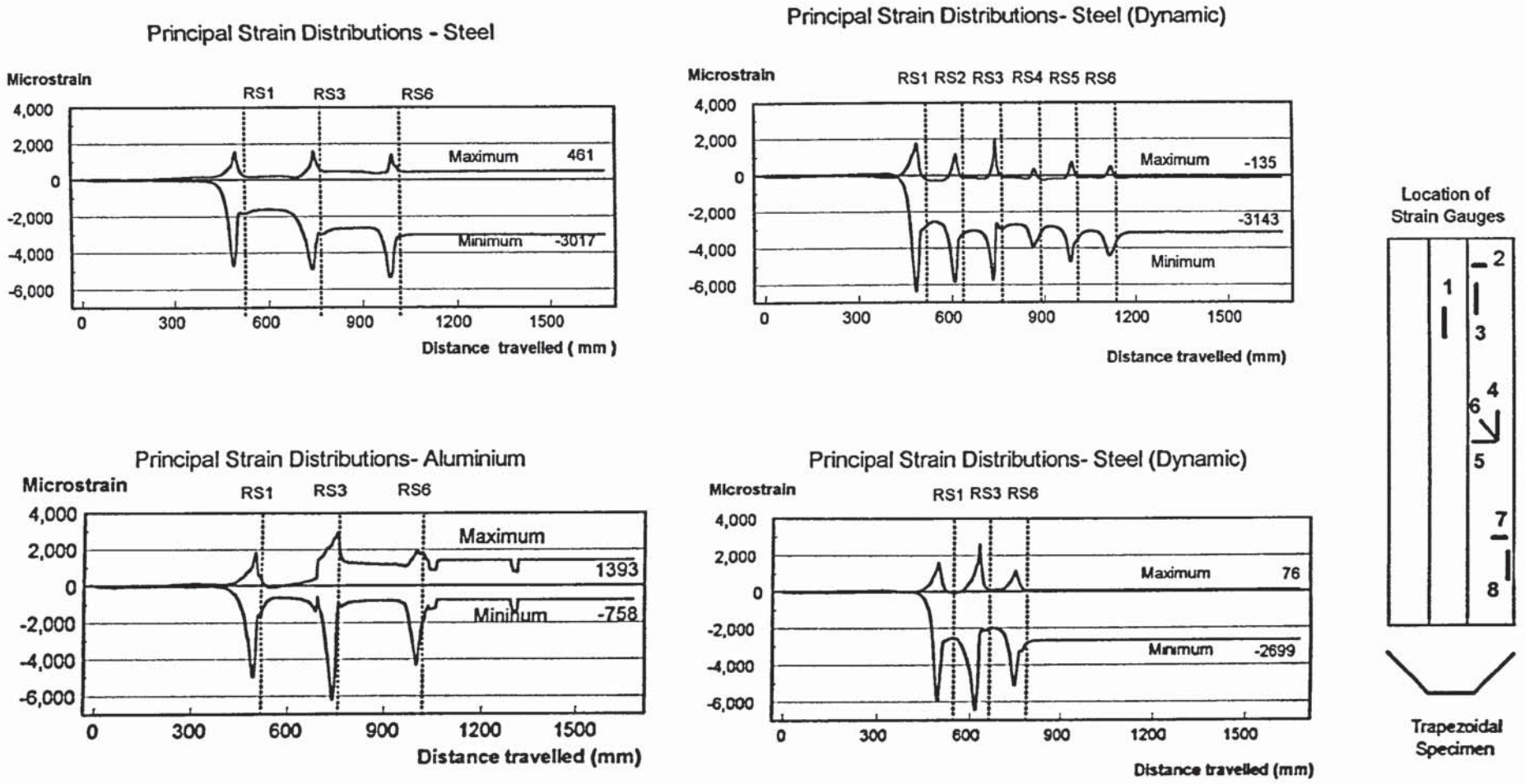

Figure B20. Graph of Principal Strain Distribution Vs Distance Travelled (CRF Mill No:1, Steel and Aluminium Specimens, 6 and 3 Roll Stations).

Appendix B

Experimental Strain Distributions

(b) CRF Mill No:2

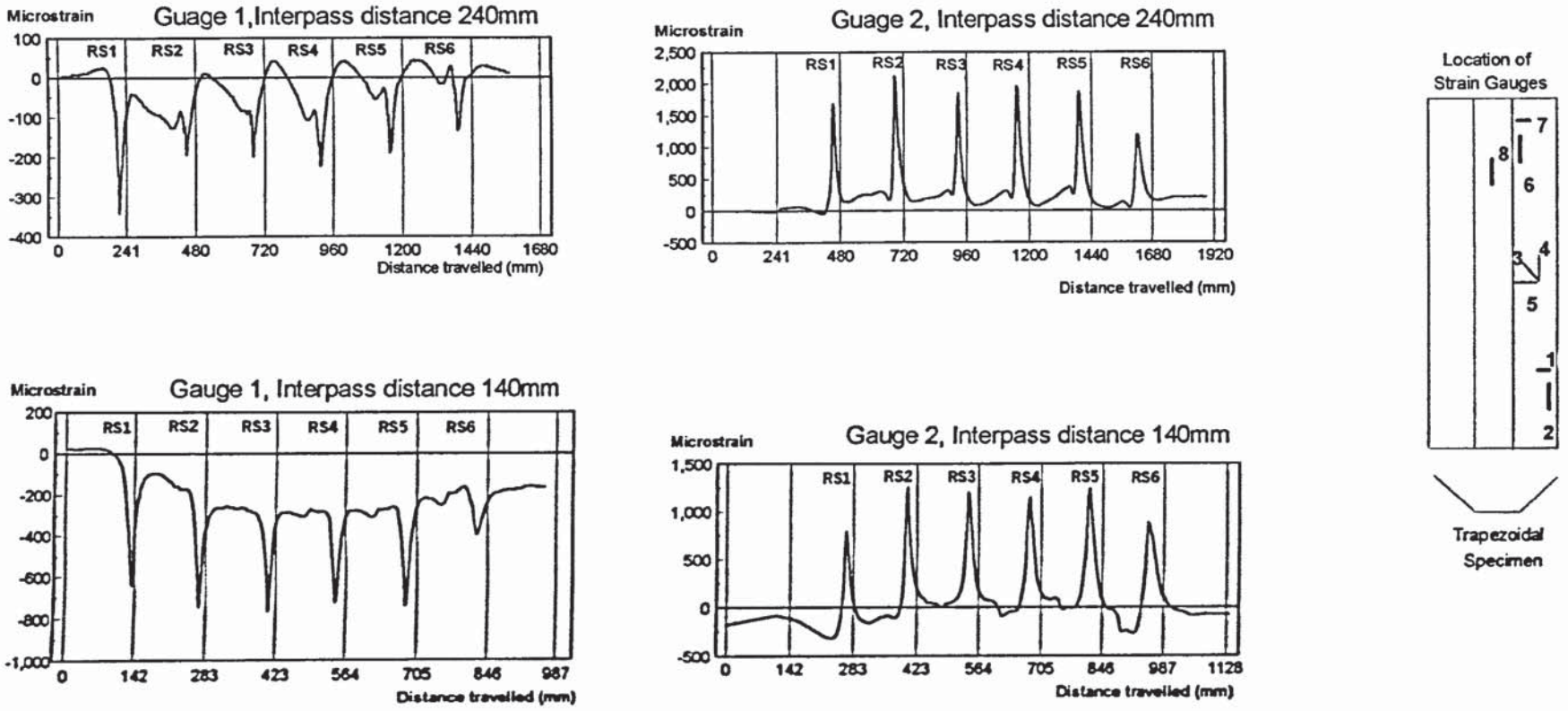

Figure B21. Graph of strain Vs Distance travelled for varying interpass distances(CRF Mill No:2, Mild Steel Specimens)

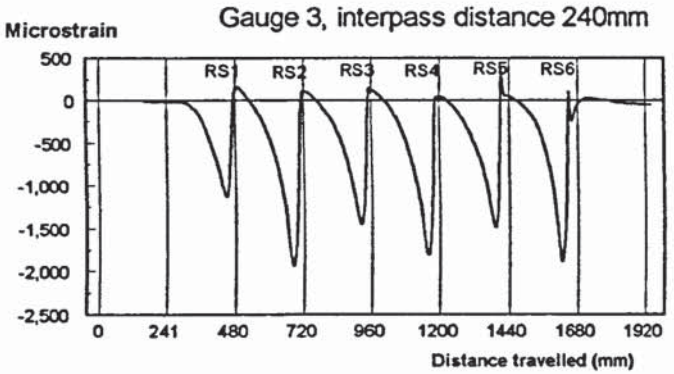

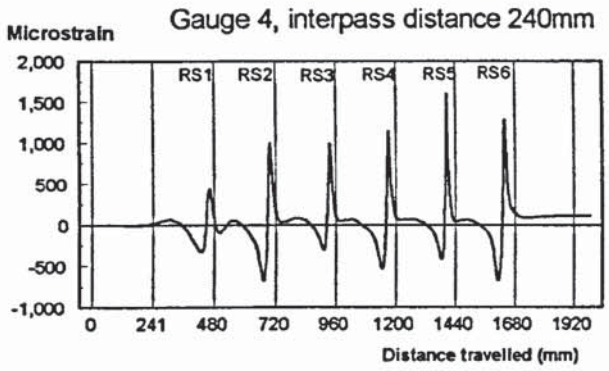

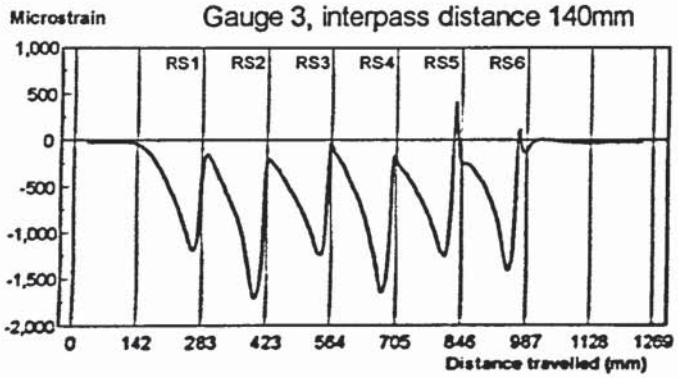

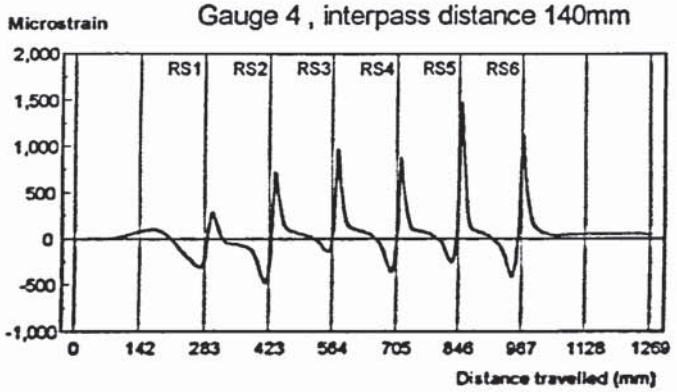

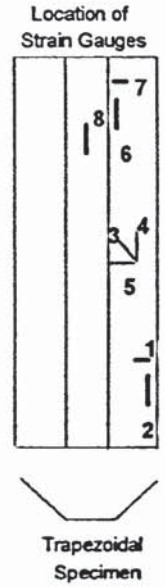

Figure B22. Graph of strain vs Distance travelled for varying interpass distances (CRF Mill No:2, Mild Steel Specimens).

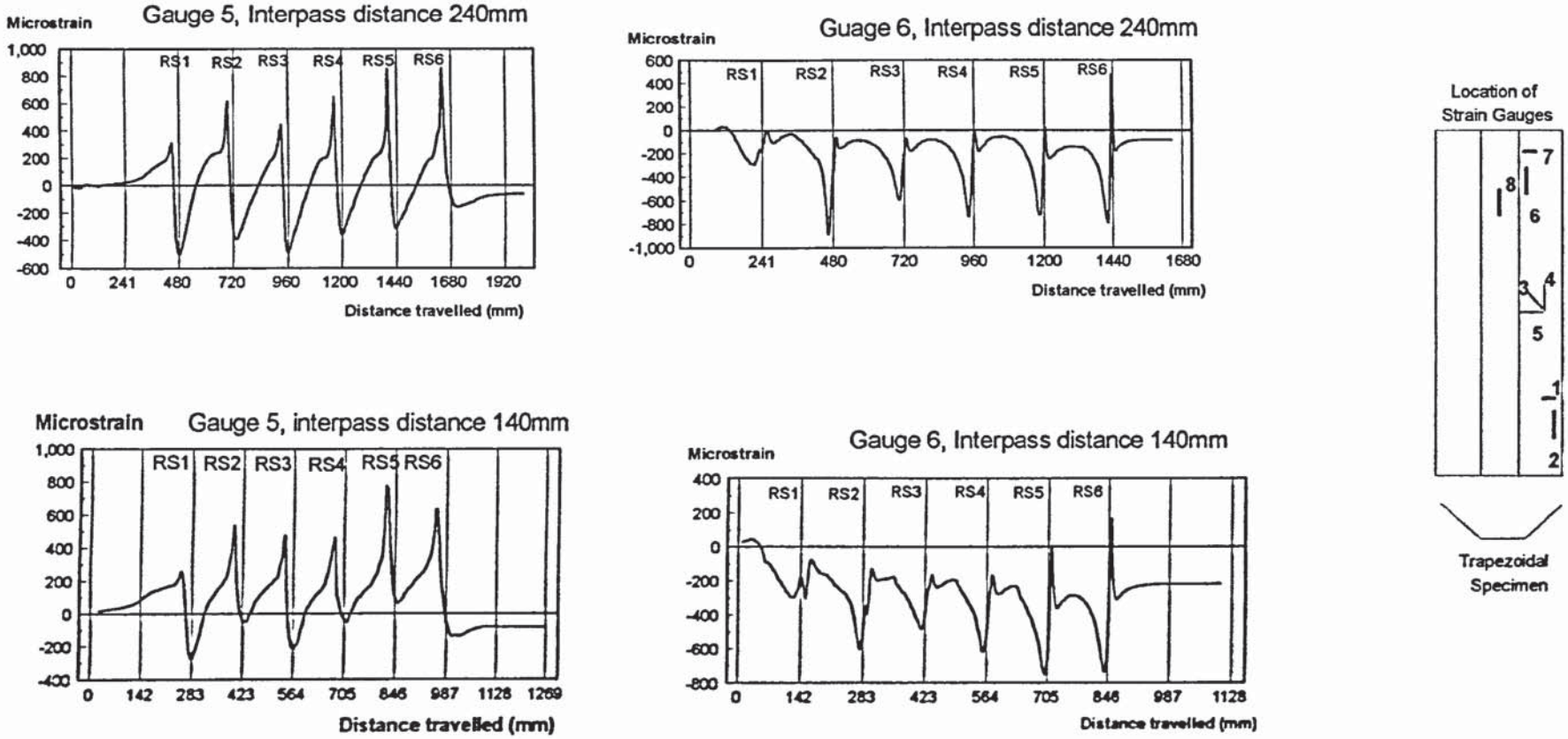

Figure B23. Graph of strain vs Distance travelled for varying interpass distances (CRF Mill No:2, Mild Steel Specimen).

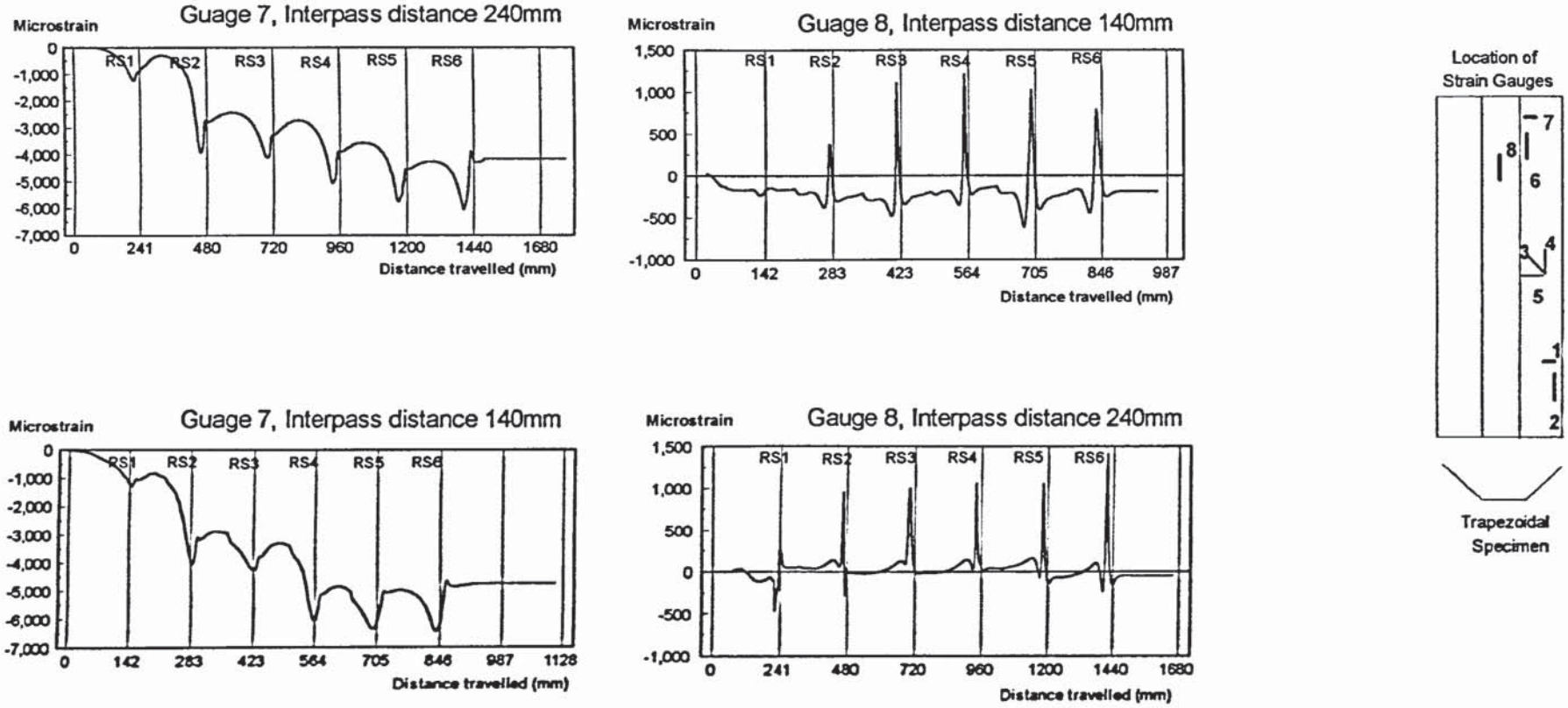

Figure B24. Graph of strain vs Distance travelled for varying interpass distances (CRF Mill No:2, Mild steel Specimen).

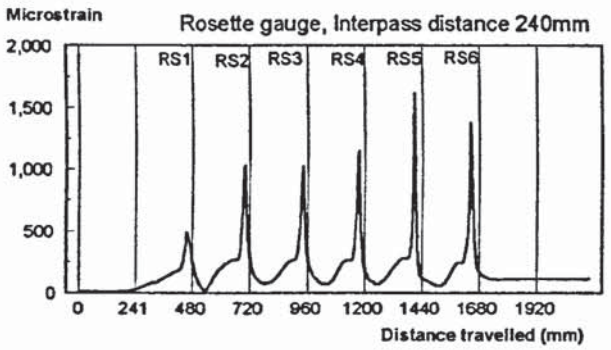

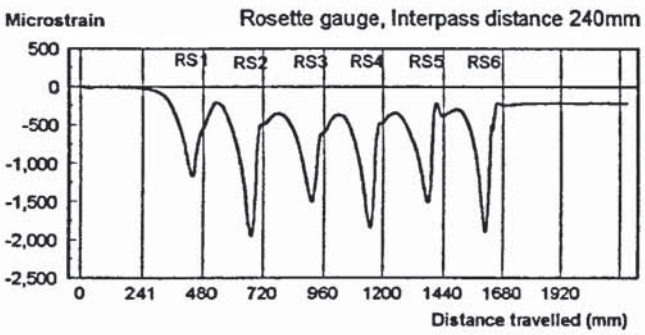

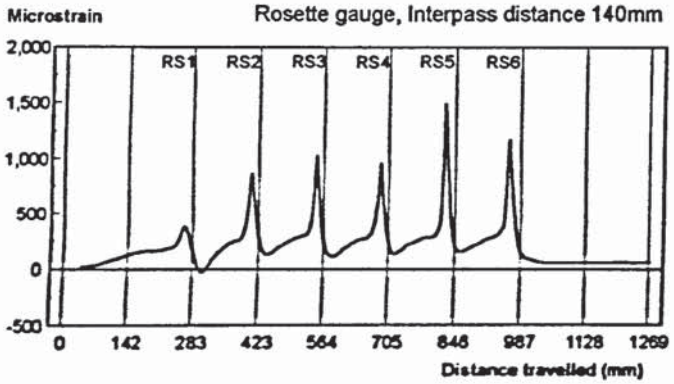

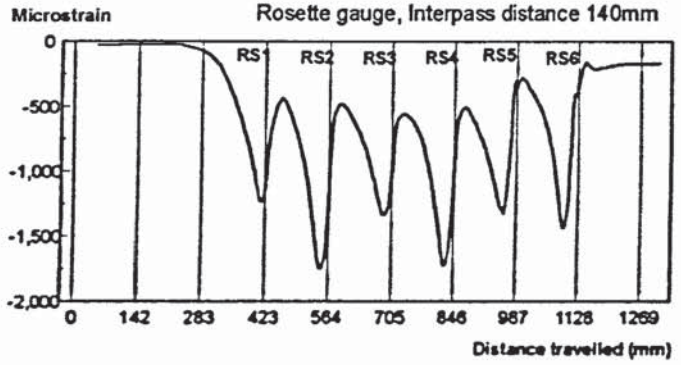

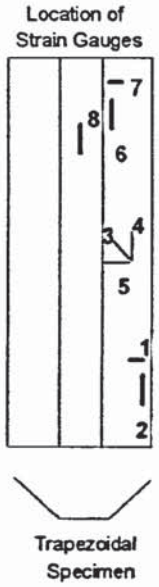

Figure B25. Graph of principal strain Vs Distance travelled for varying interpass distances (CRF Mill No:2, Mild Steel Specimen).

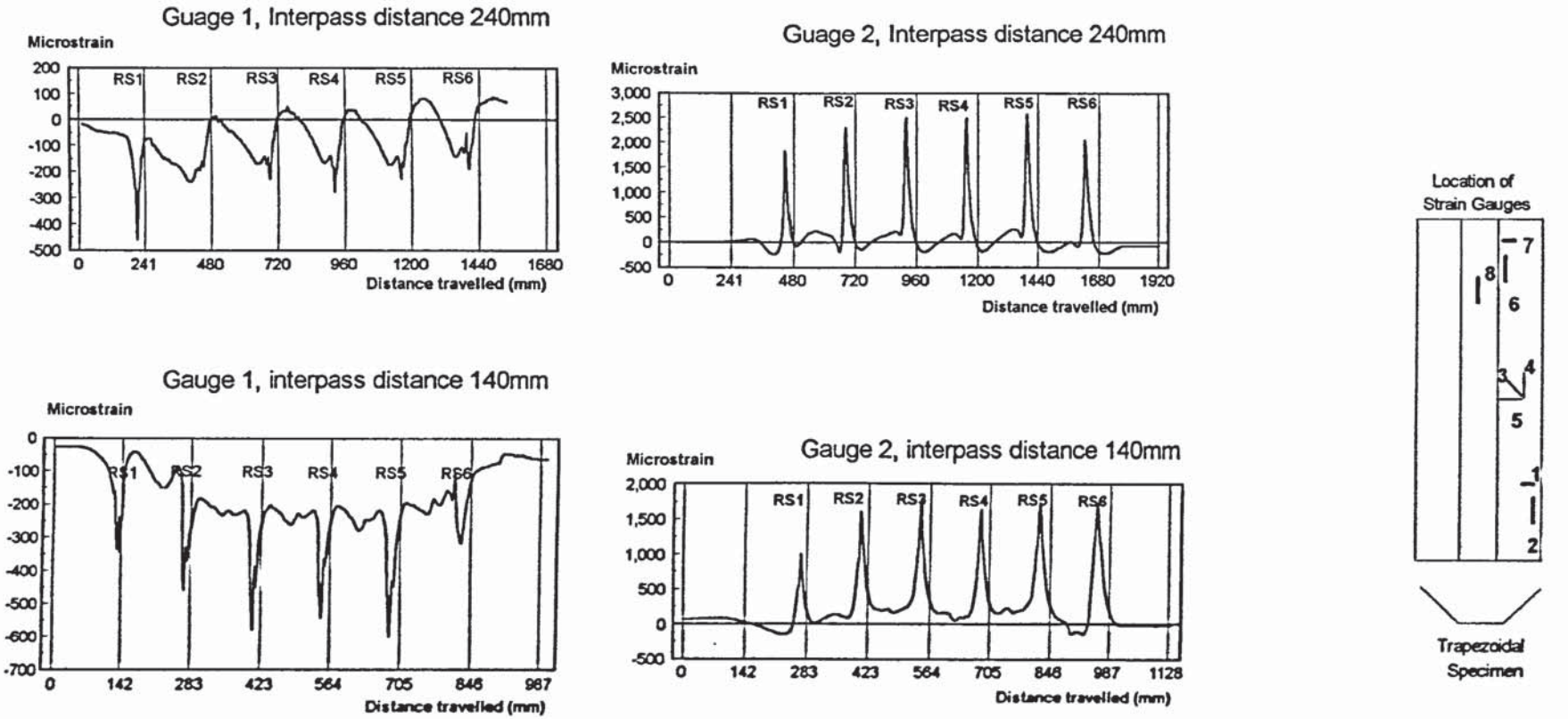

Figure B26. Graphs of strain Vs Distance travelled for varying interpass distances (CRF Mill No:2 , Aluminium Specimen).

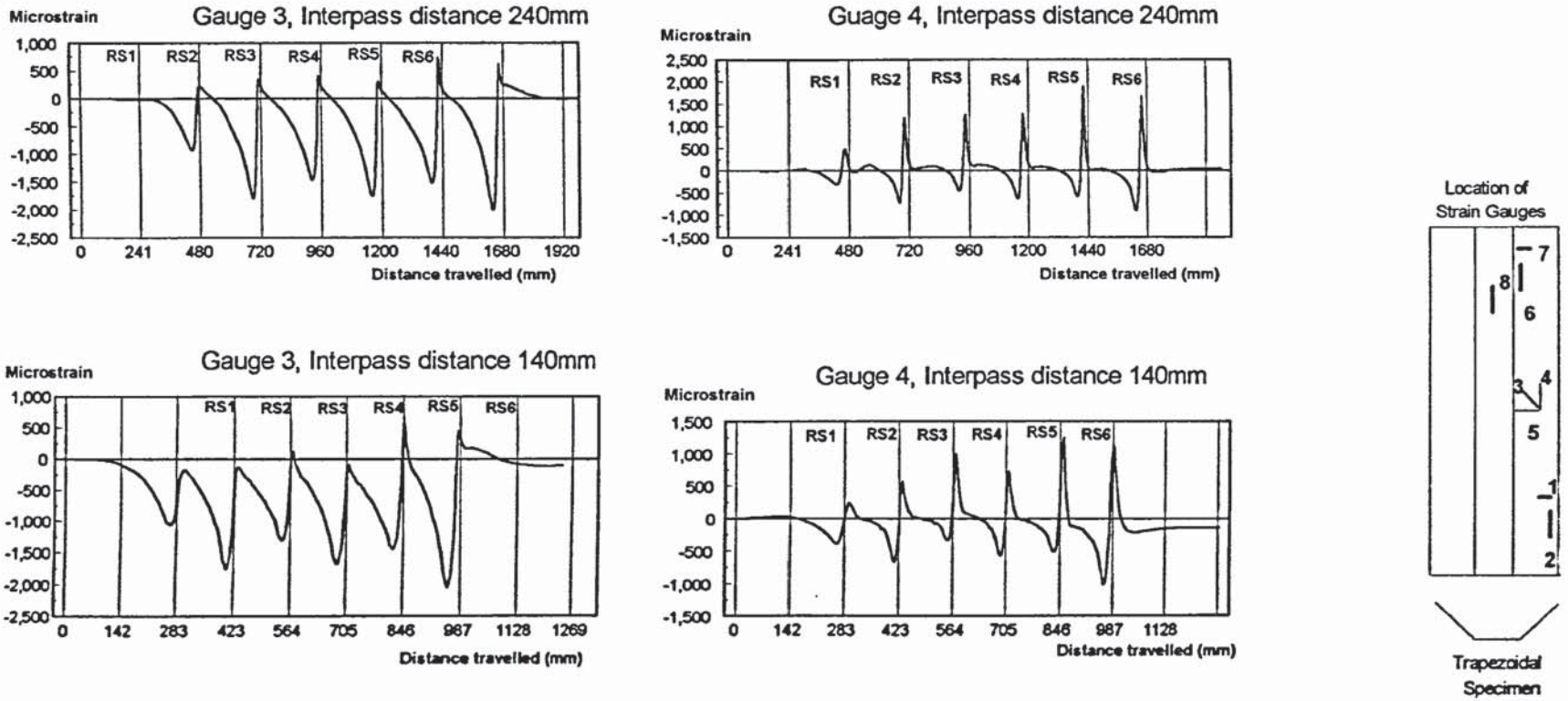

Figure B27. Graph of strain vs Distance travelled for varying interpass distances (CRF Mill No:2 , Aluminium Speimen)

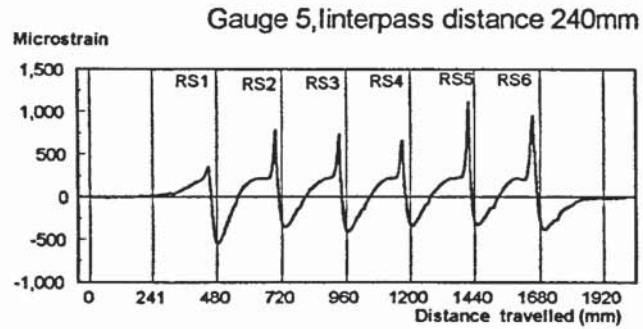

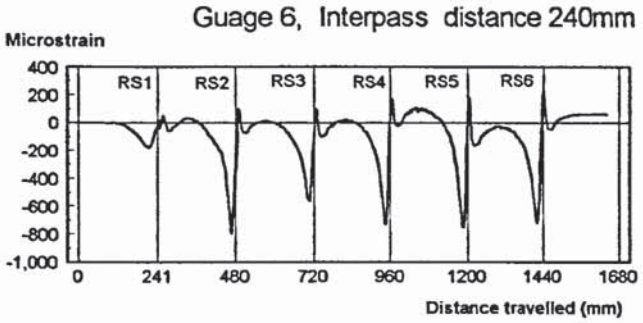

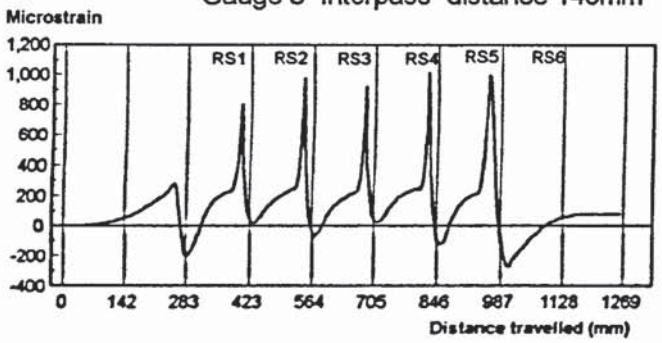

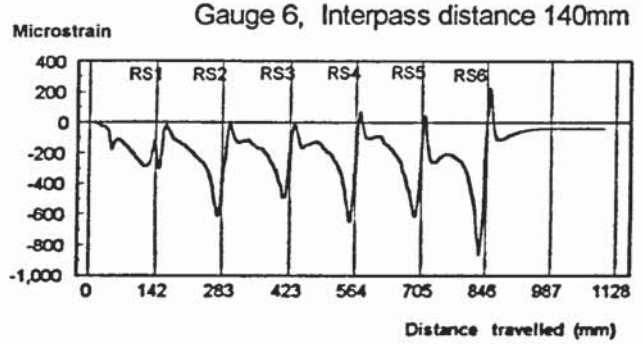

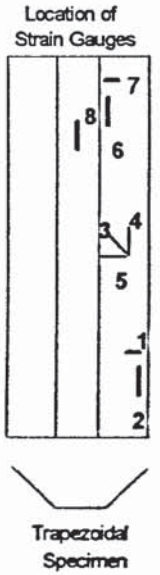

Figure B28. Graph of strain vs Distance travelled for varying interpass distances (CRF Mill No:2, Aluminium Specimen

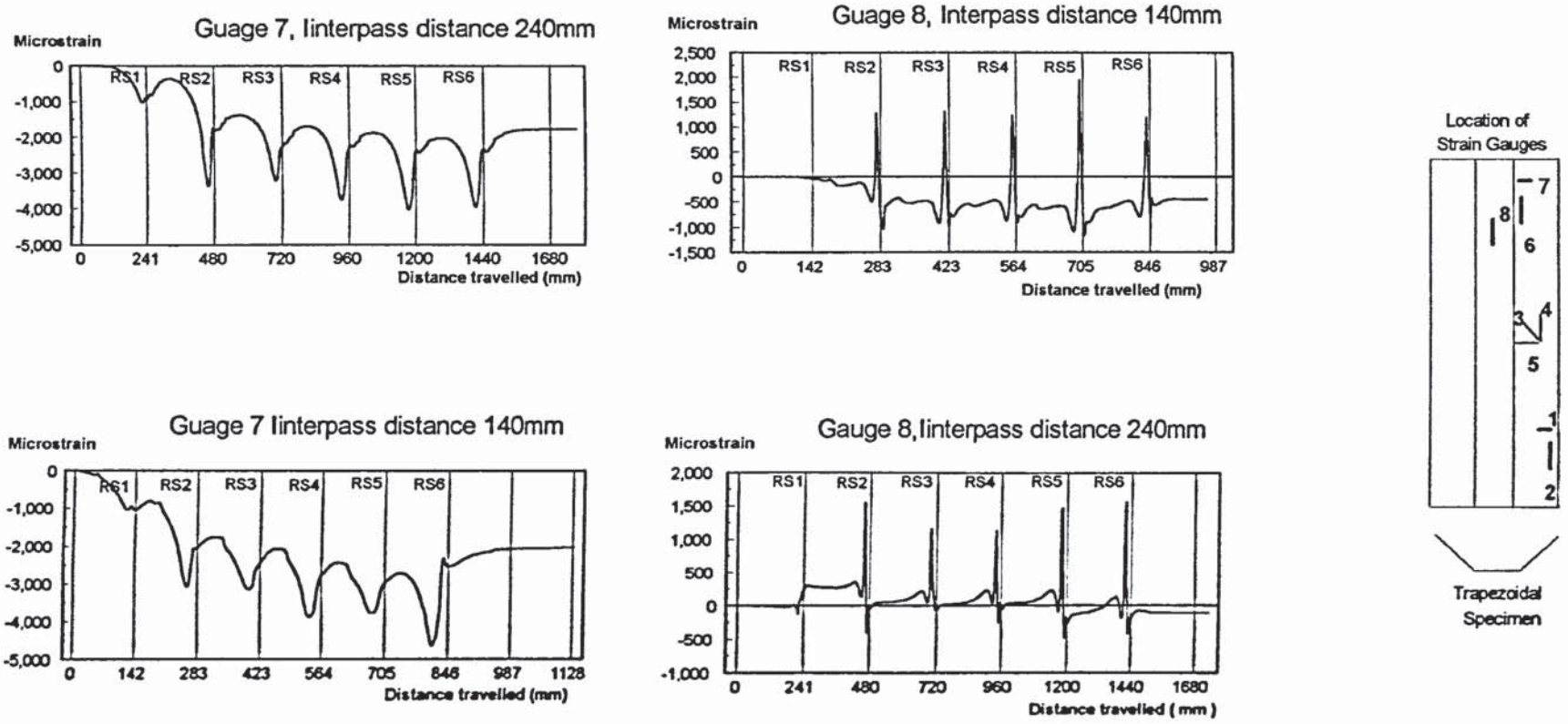

Figure B29. Graph of strain Vs Distance travelled for varying interpass distances (CRF Mill No:2, Aluminium Specimen).

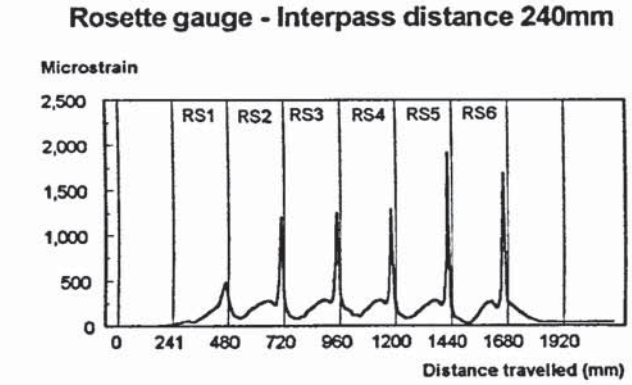

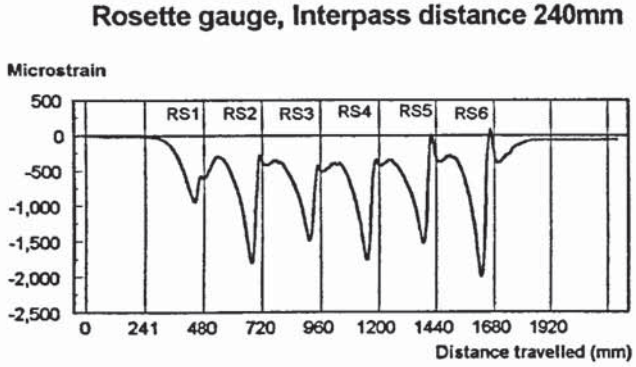

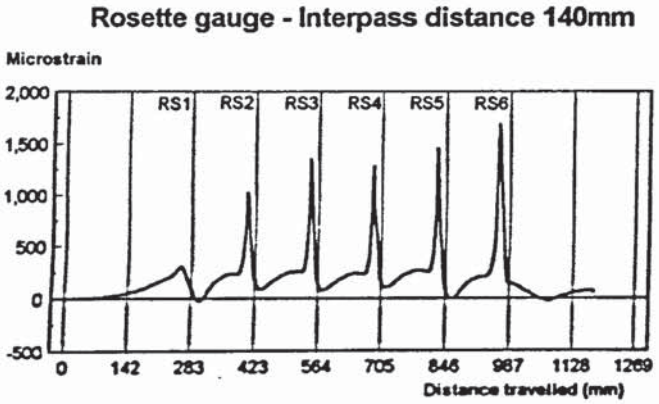

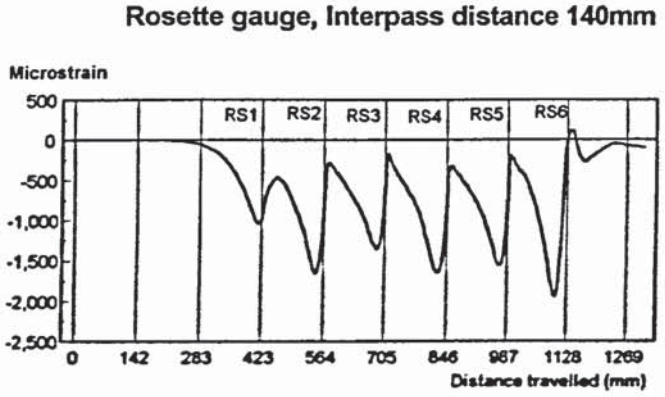

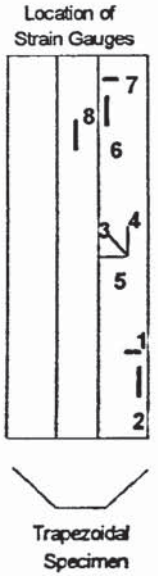

Figure B30. Graph of principal strain Vs Distance travelled for varying interpass distances (CRF Mill No:2, Aluminium Specimen)

Appendix C

Flowcharts for MIL Programs

Flowchart for the programs Cogimag1.cl, Cogimag2.cl, Cogmark1.cl and Cogmark2.cl

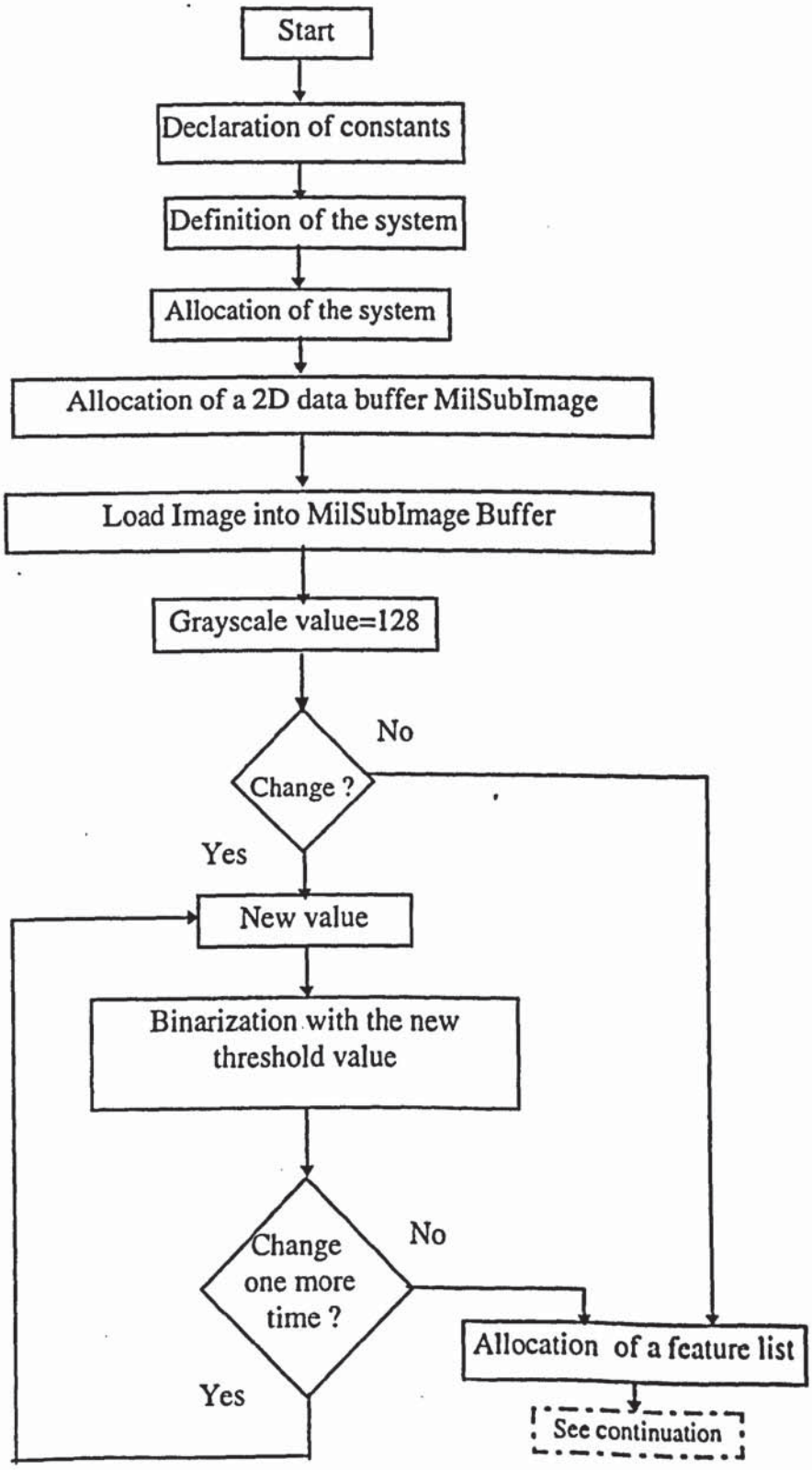

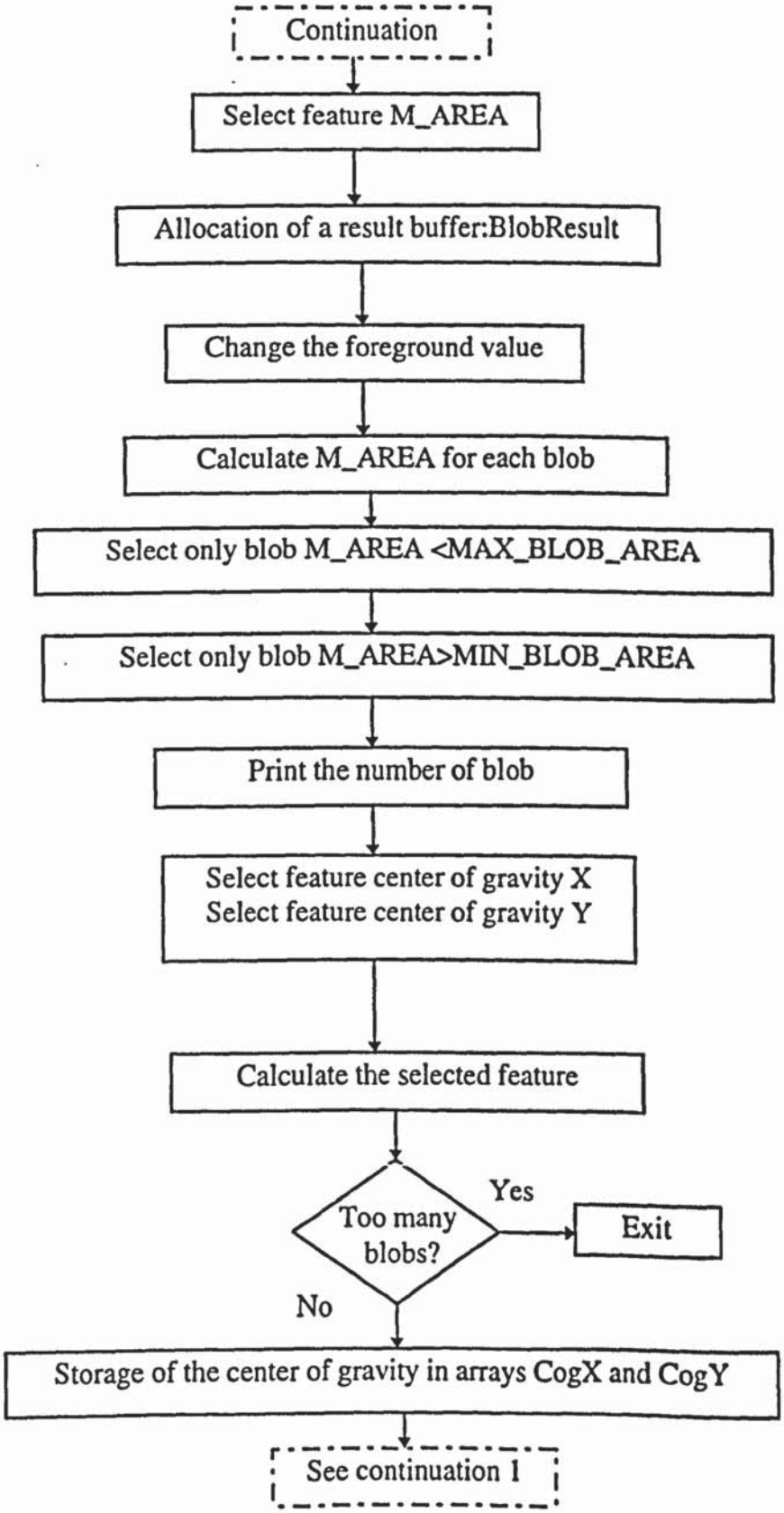
Continuation
Select feature M_AREA
Allocation of a result buffer:BlobResult
Change the foreground value
Calculate M_AREA for each blob
Select only blob M_AREA <MAX_BLOB_AREA
Select only blob M_AREA>MIN_BLOB_AREA
Print the number of blob
Select feature center of gravity X
Select feature center of gravity Y
Calculate the selected feature
Too many blobs?
Yes
Exit
No
Storage of the center of gravity in arrays CogX and CogY
See continuation 1

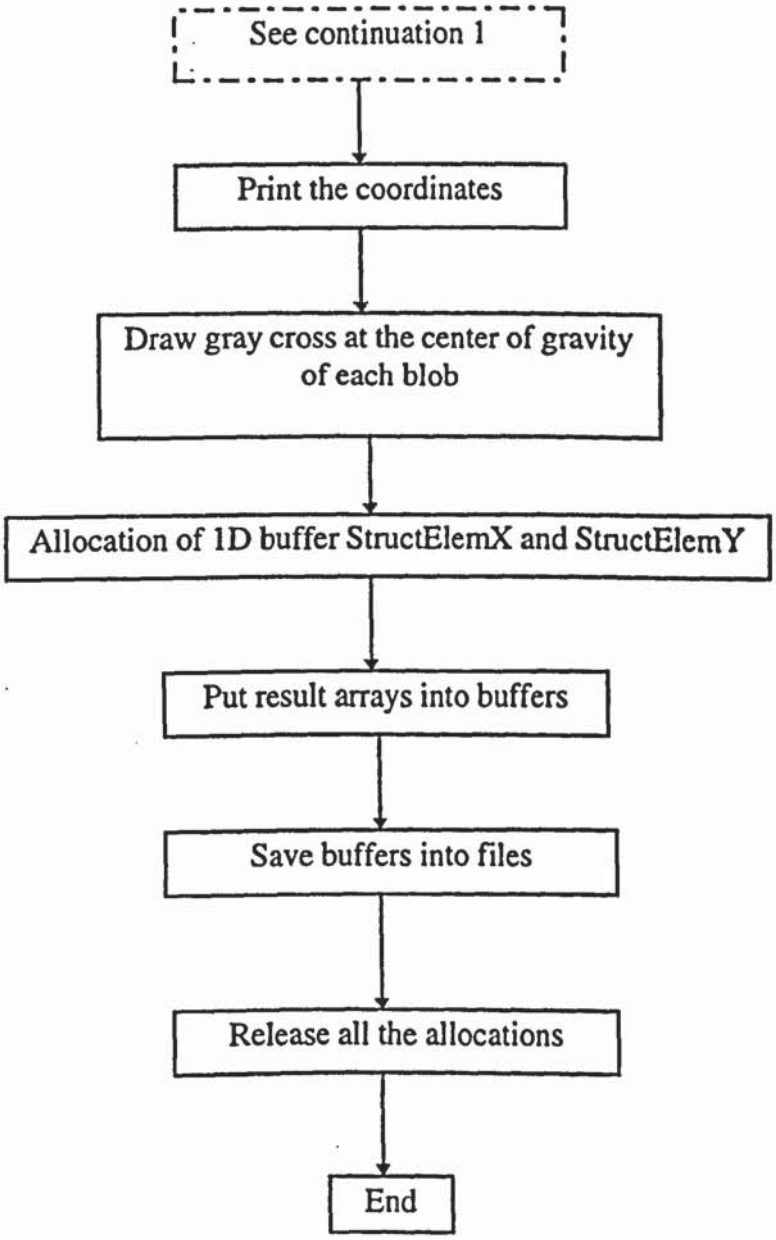
See continuation 1
Print the coordinates
Draw gray cross at the center of gravity of each blob
Allocation of 1D buffer StructElemX and StructElemY
Put result arrays into buffers
Save buffers into files
Release all the allocations
End

Appendix D

Flowcharts for C Programs

Main program

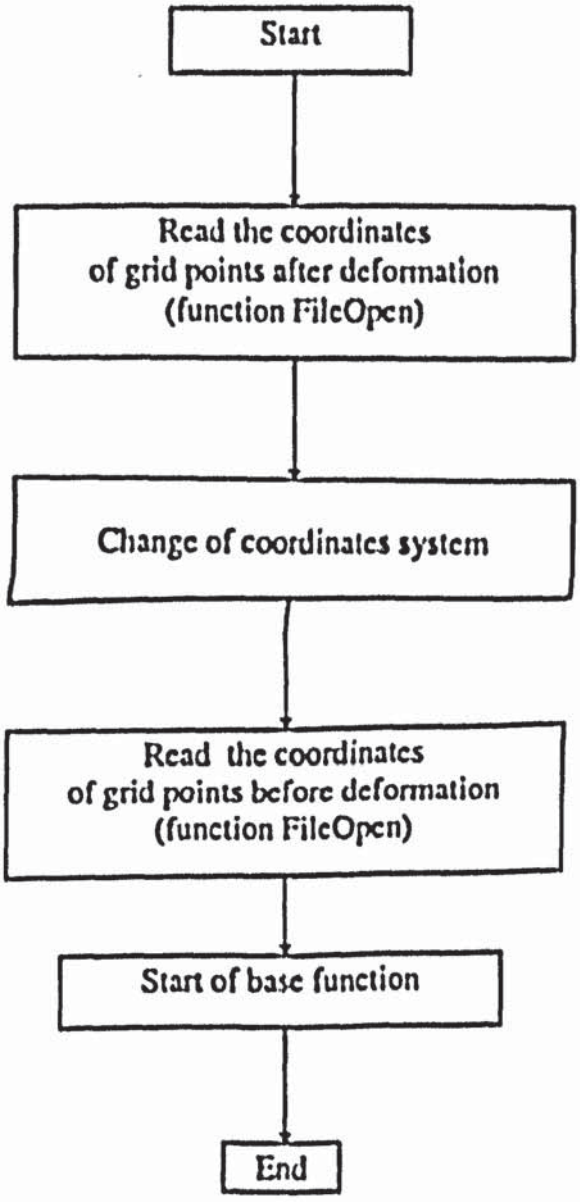

Function *FileOpen*

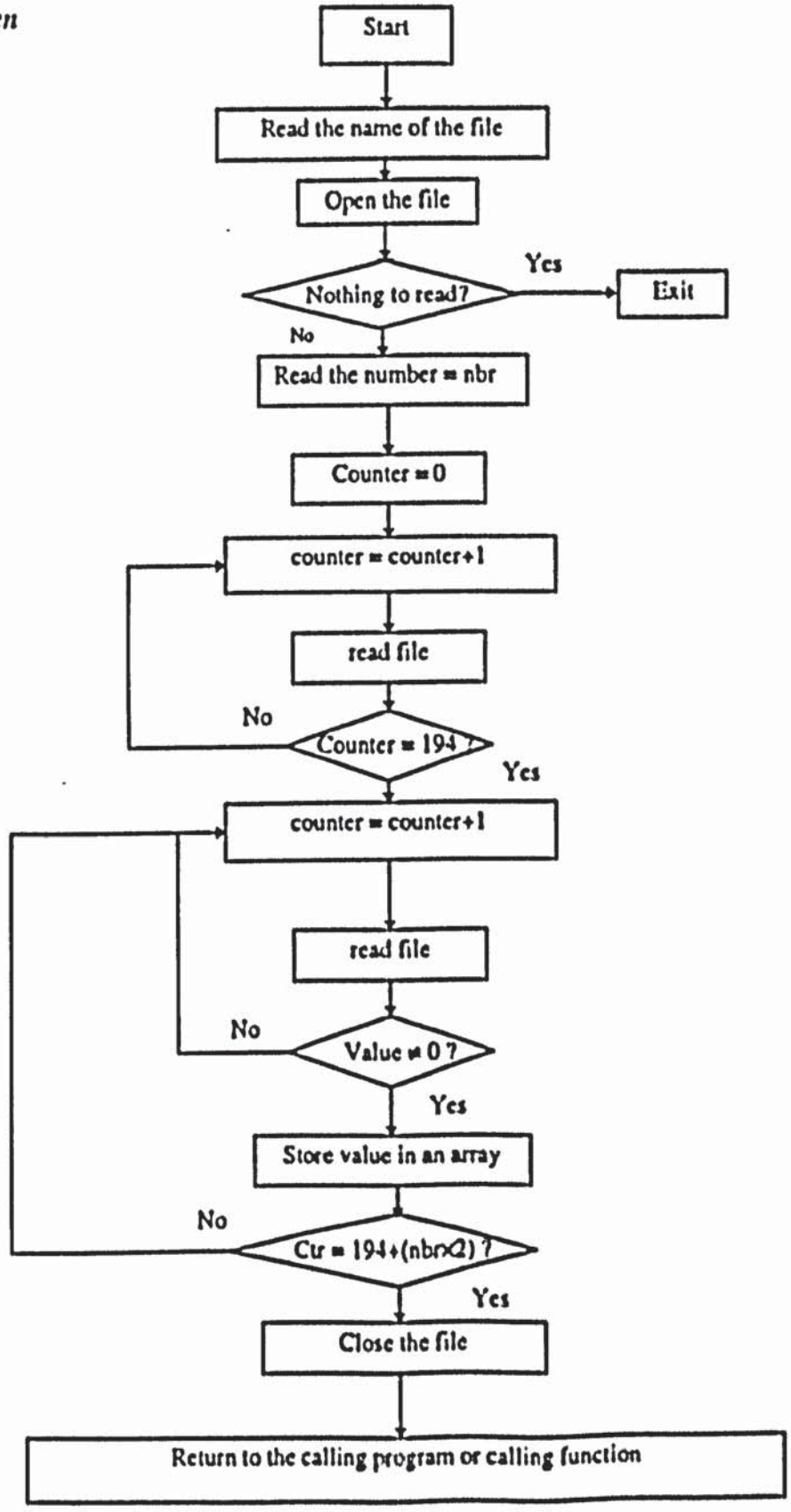

Change of Function

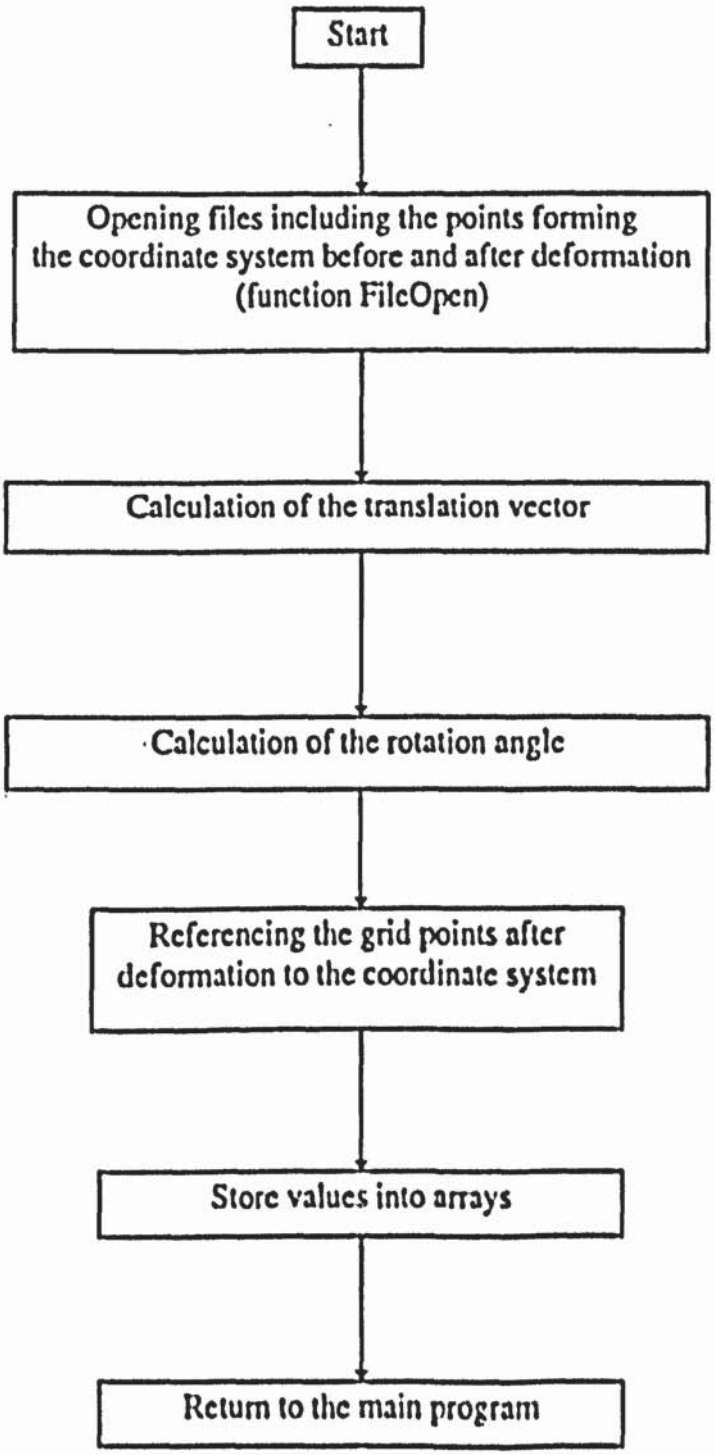

Translation vector

The translation vector is calculated with the origins of the two local coordinate systems (before and after deformation)

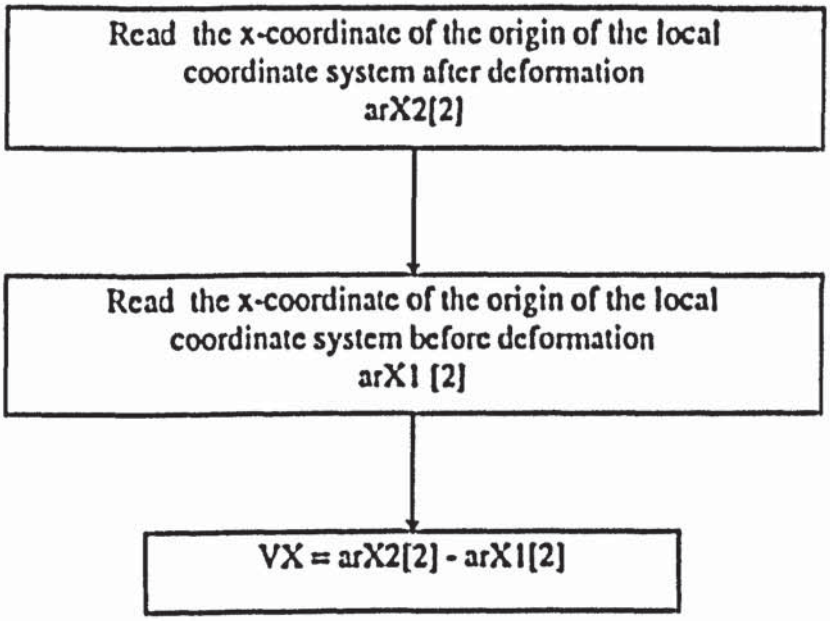

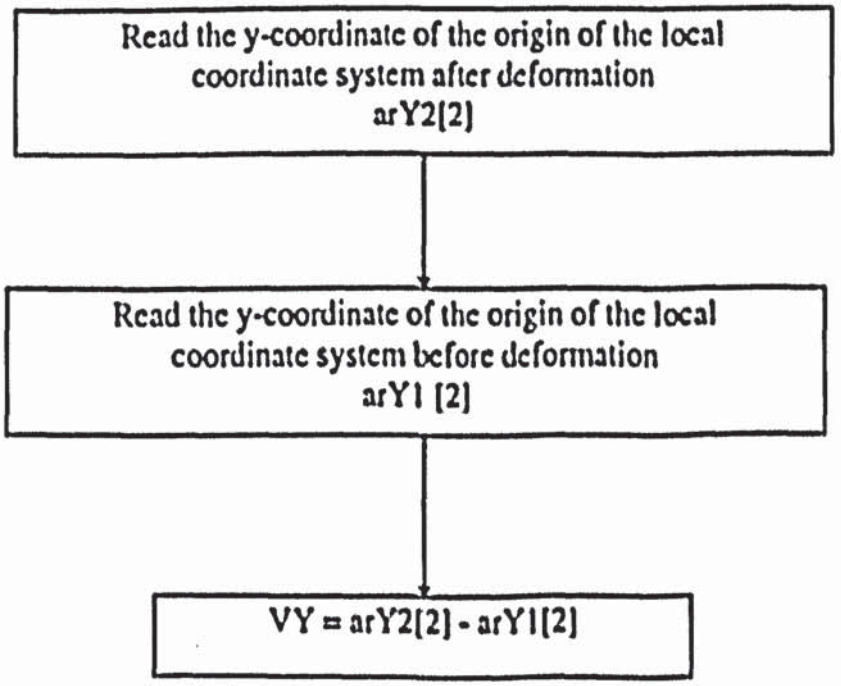

Rotation Angle

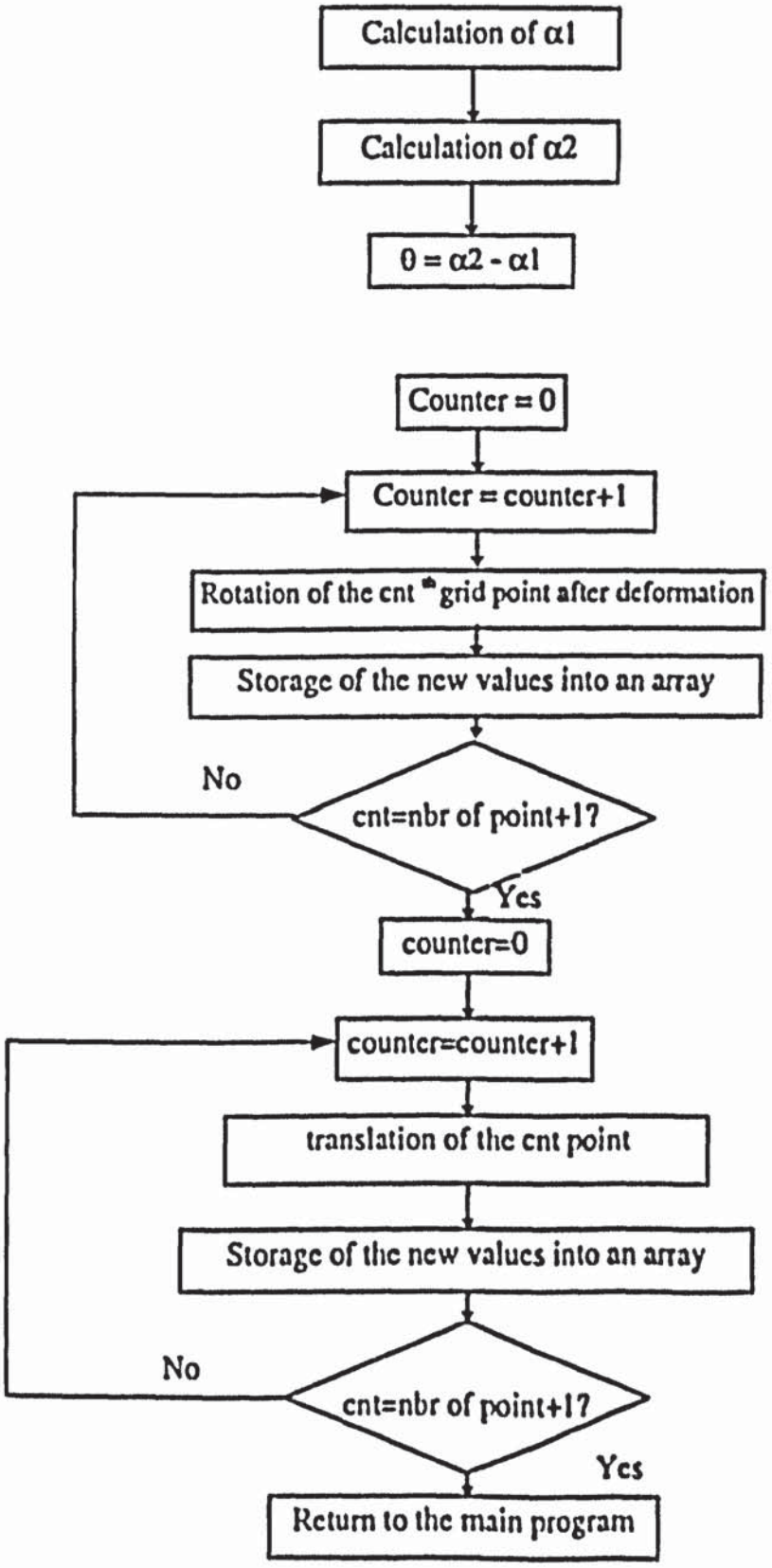

Rotation of the points

Translation of the points

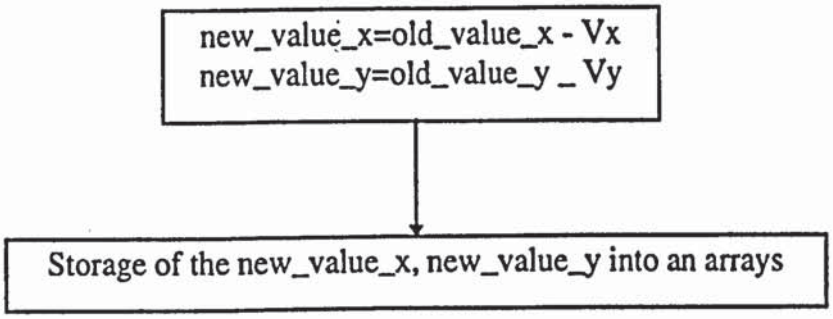

Function *base*

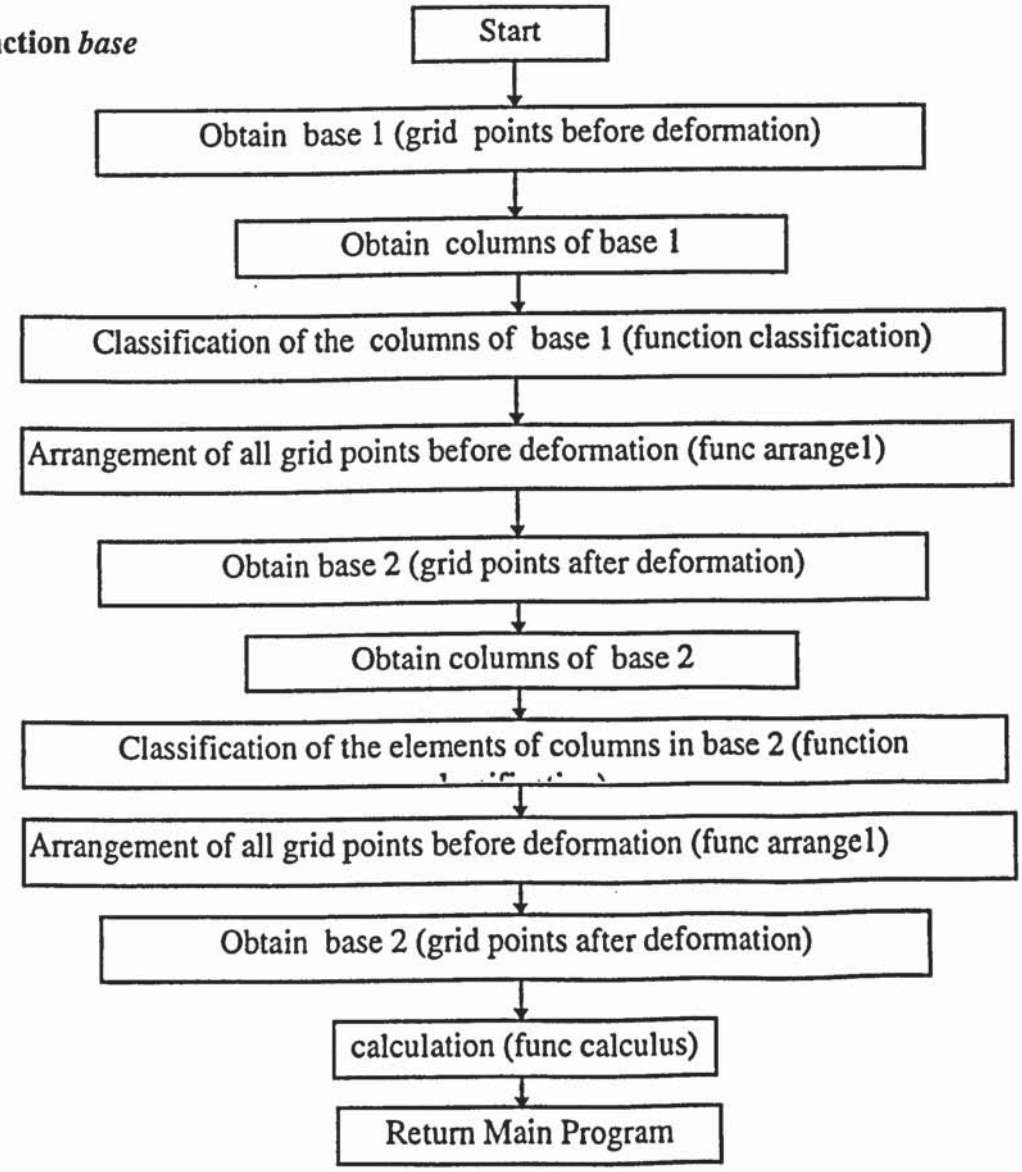

Determination of the base

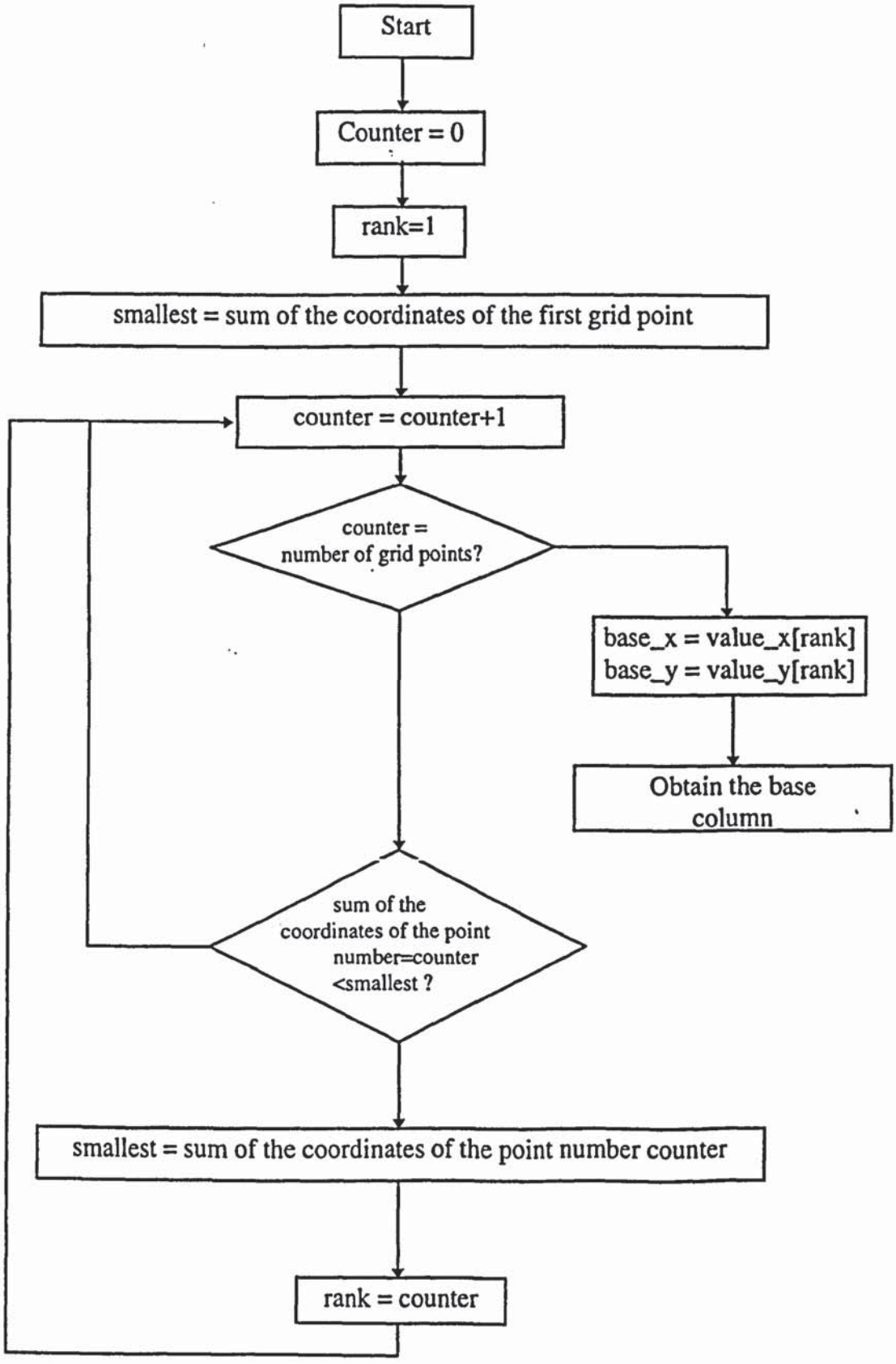

Obtaining the column of base

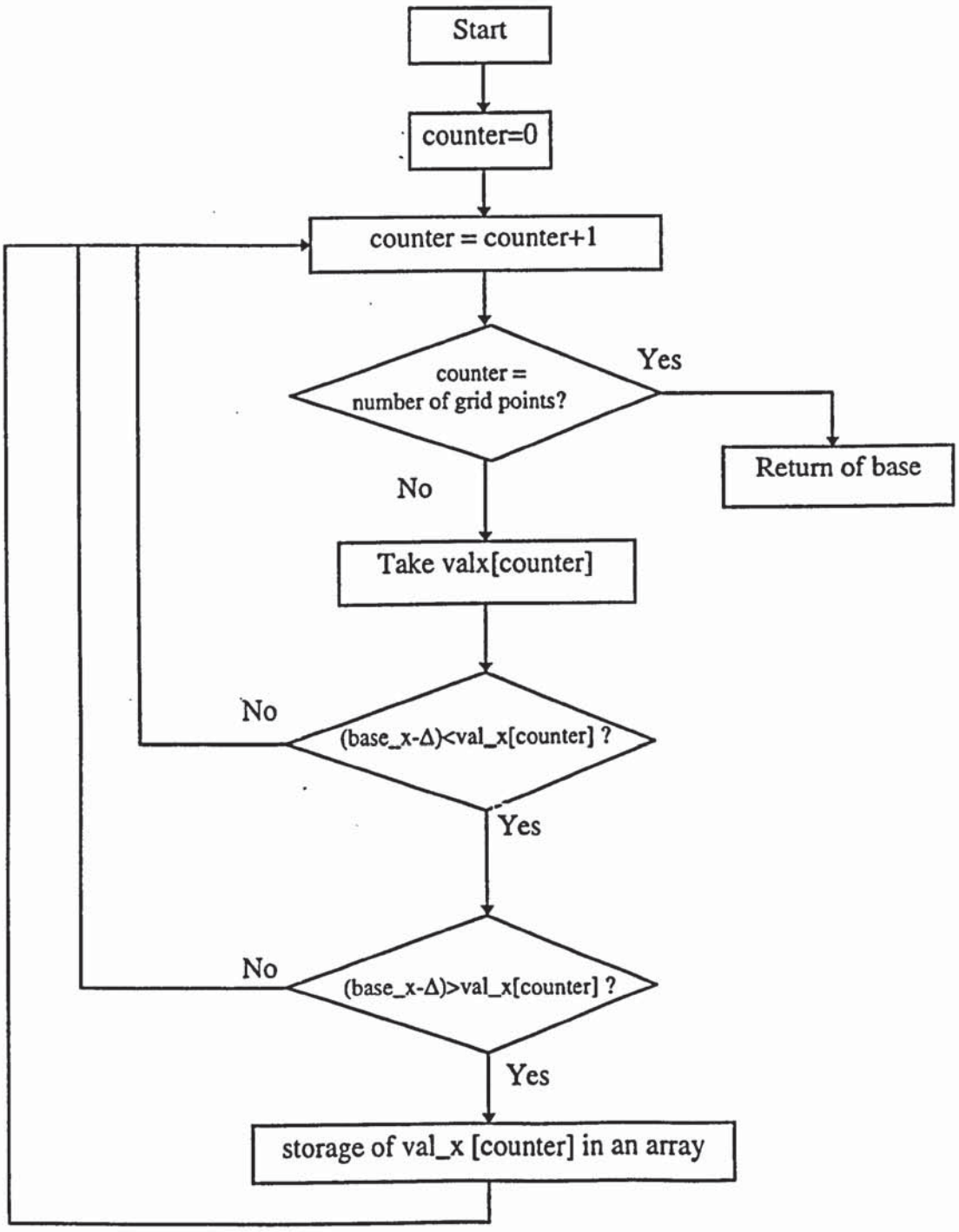

Classification of the elements of column base (function *classification*)

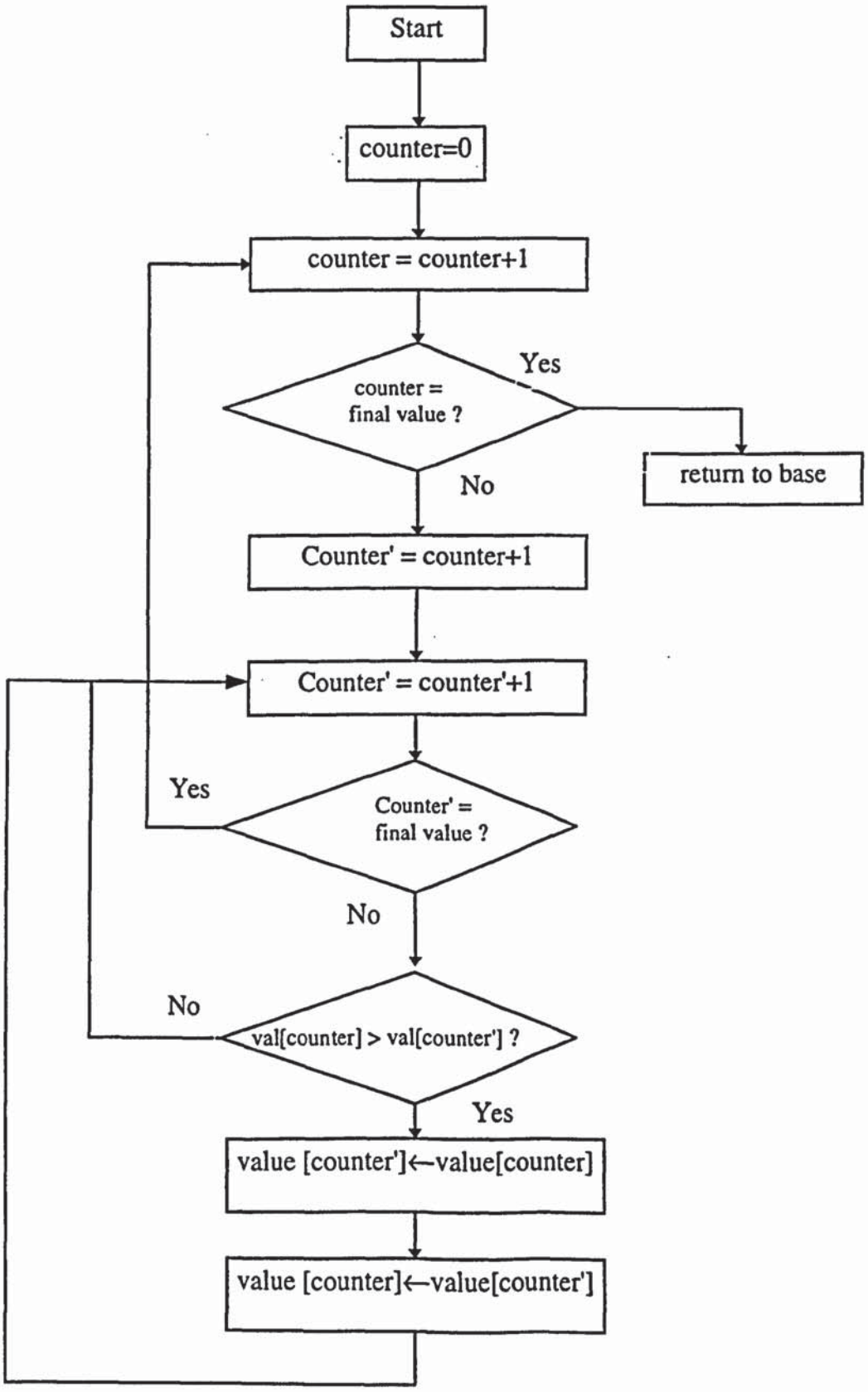

Arrangement of the grid points (function *arrange*)

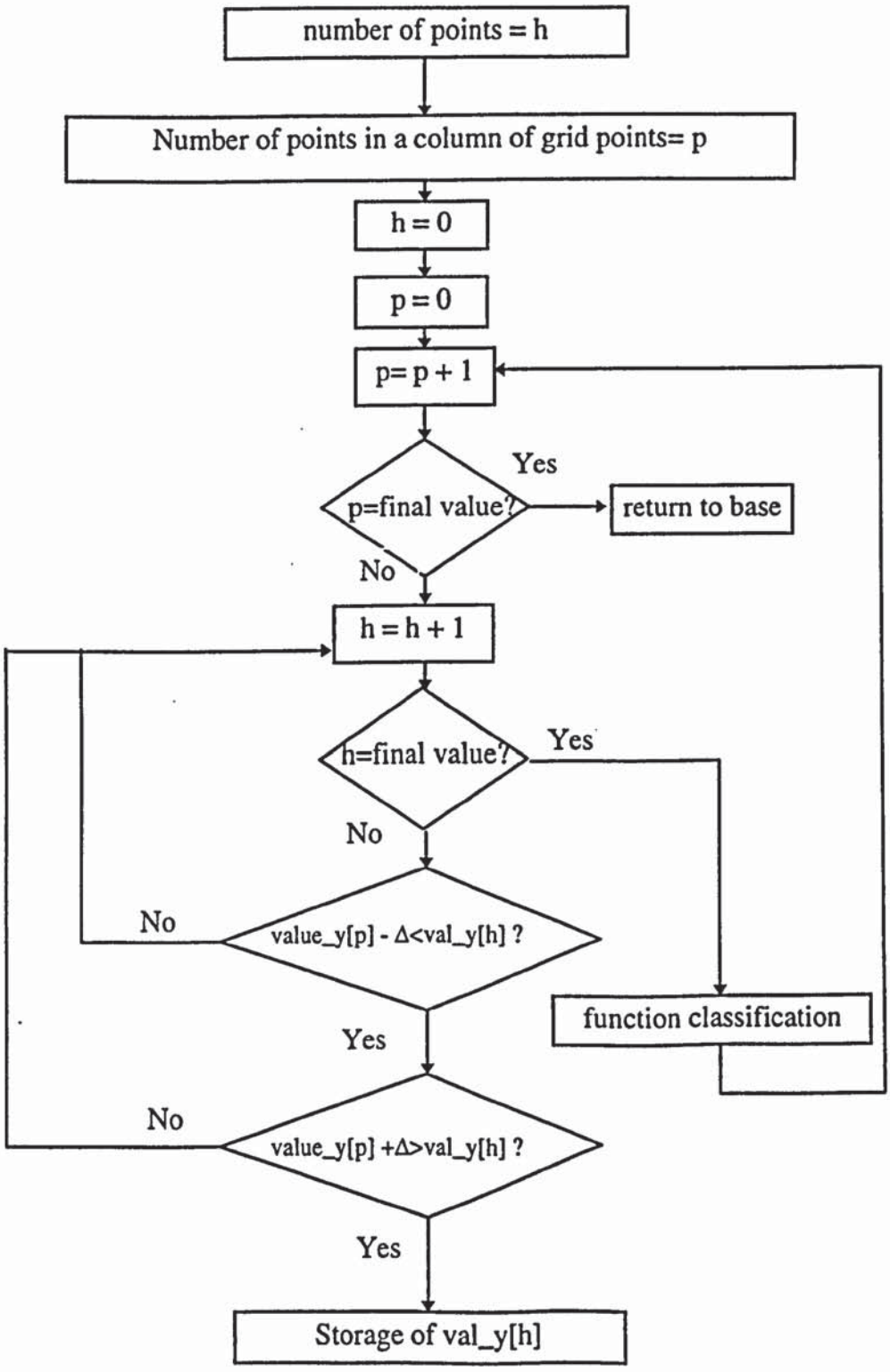

Calculations (function *calculus*)

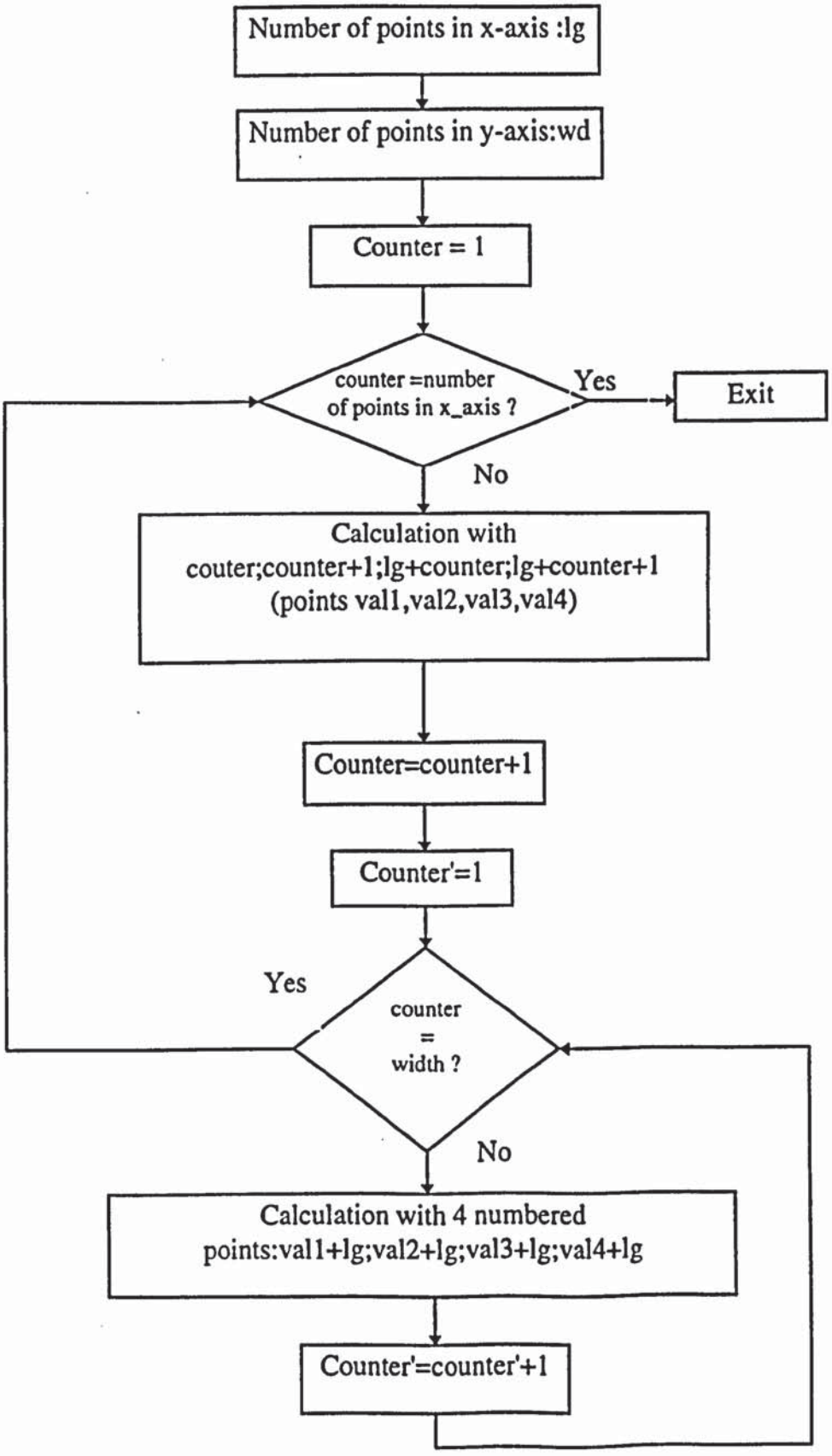

Flowchart of the program LINK.cl

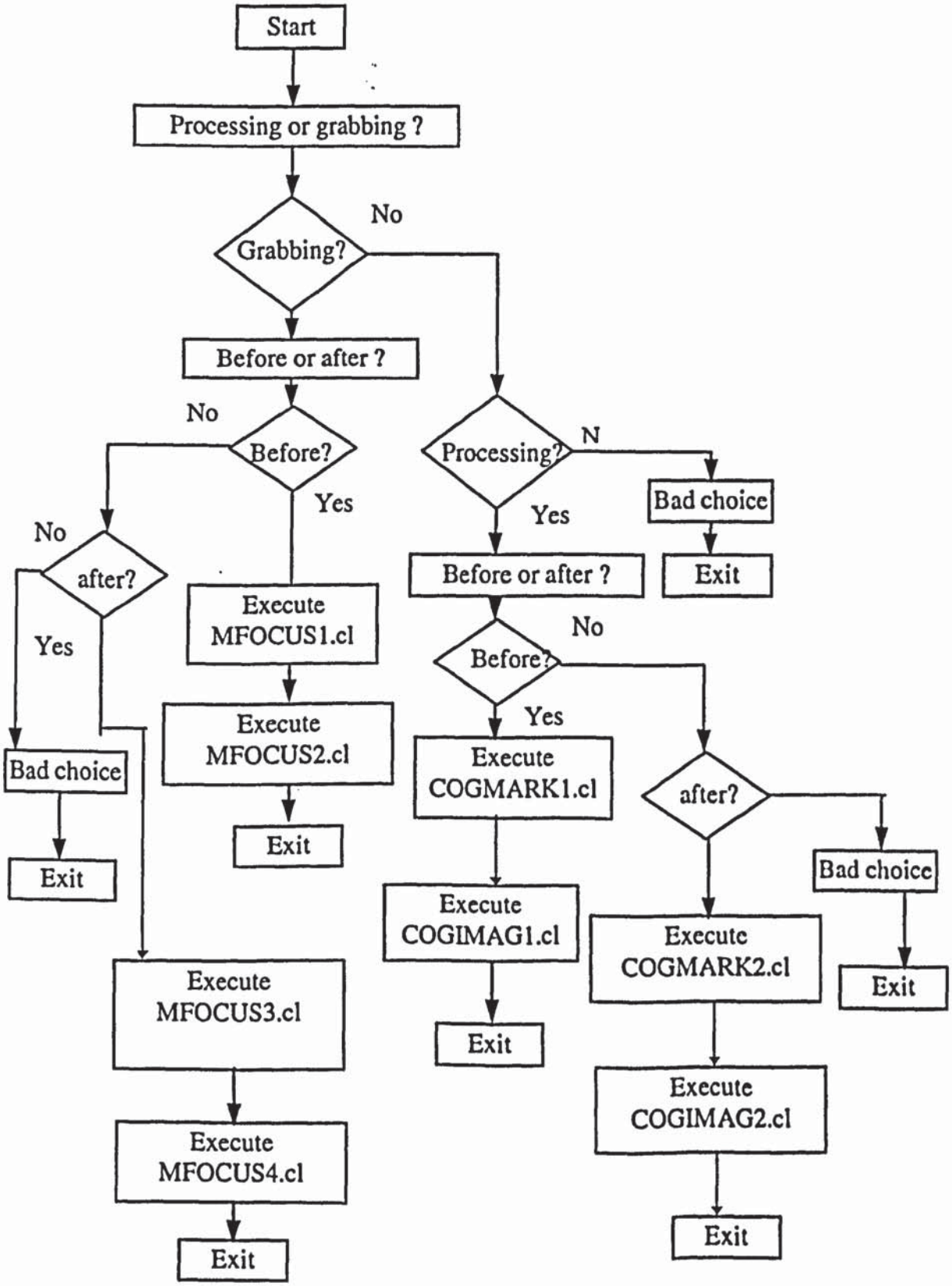

Flowchart for the programs MFOCUS1.cl, MFOCUS2.cl, MFOCUS3.cl and MFOCUS4.cl.

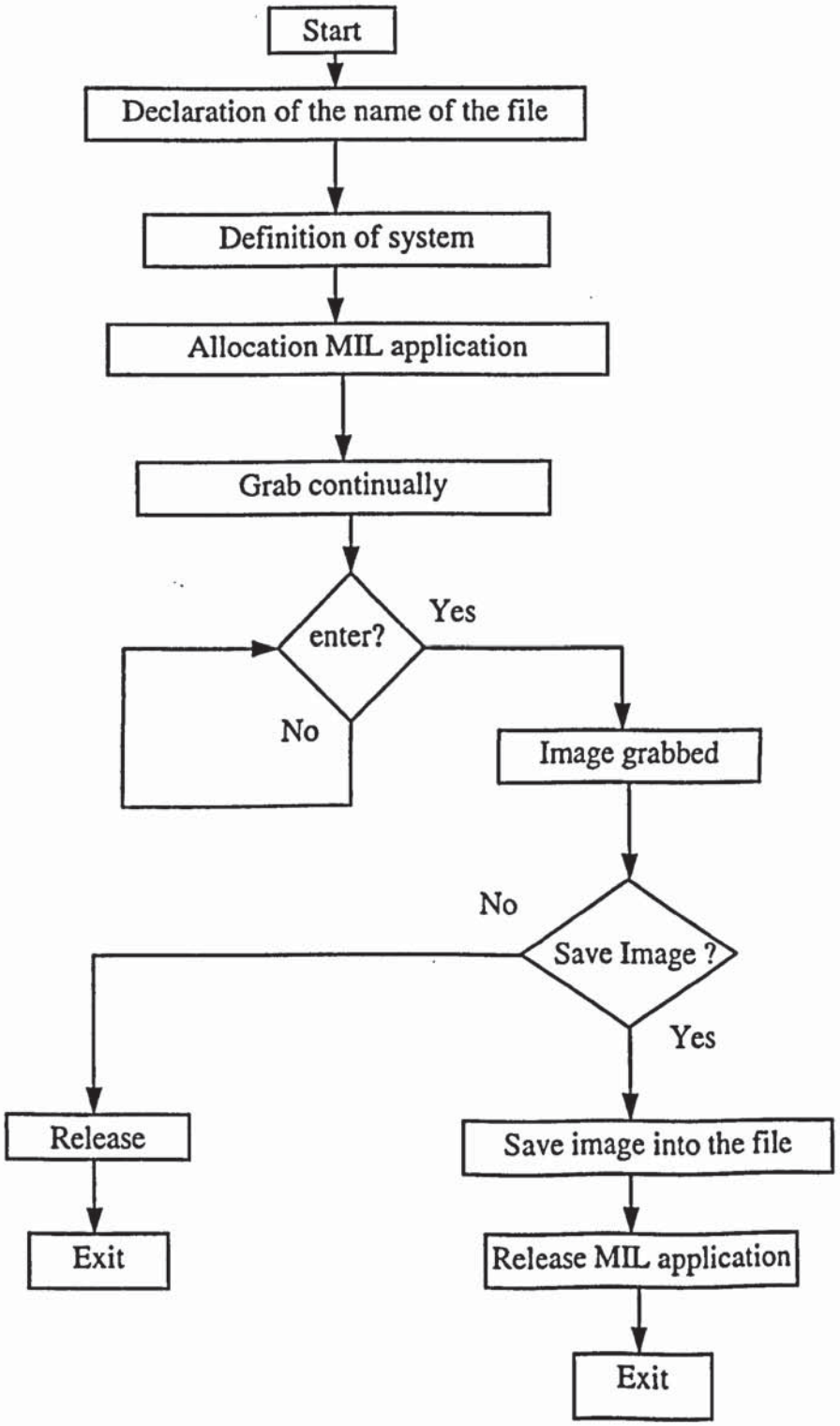

Appendix E

MIL Programs for image processing

```
;   PROGRAM  COGIMAG1.CL  WRITTEN IN MILINTER VERSION 2.0
;
;                                BY
;
;                            R.S.Senanayake
;
;                        Aston University, Birmingham, UK
;
;                   SUPERVISORS:Dr. I.M.Cole
;                                        A/Prof S.Thiruvarudchelvan
;


; File name: cogimag1.cl (Image 1:points before deformation)
; Synopsis:  This program counts the number of points in an image, marks the
;         centre of gravity of each and save the co-ordinates into files.

silence 1

; Target MIL image file specifications.

;File of the image to process.
macro IMAGE_FILE          "c:\image1.mim"
;Width of the image in pixels.
macro IMAGE_WIDTH         790
;Height of the image in pixels.
macro IMAGE_HEIGHT        590
;Threshold binarization default value.
macro IMAGE_THRESHOLD_VALUE 128

;results file
macro RESULTX_FILE        "c:\X1.c"
macro RESULTY_FILE        "c:\Y1.c"

;structuring element information
macro STRUCT_ELEM_WIDTH   50
macro STRUCT_ELEM_DEPTH   32

; Maximum number of blobs and maximum area of blobs in pixels.
macro MAX_BLOBS           50
macro MAX_BLOB_AREA       2000

; Radius of the smallest particles to keep in pixels.
macro SMALL_PARTICLE_RADIUS  1

; Size of the cross-hair used to mark centres of gravity in pixels.
macro CSIZE 10

MIL_ID MilApplication      ; Application identifier.
MIL_ID MilSystem           ; System identifier.
MIL_ID MilDisplay          ; Display identifier.
MIL_ID MilImage            ; Image buffer identifier.
MIL_ID MilSubImage         ; Sub-image buffer identifier.
MIL_ID BlobResult          ; Blob result buffer identifier.
MIL_ID FeatureList         ; Feature list identifier.
MIL_ID StructElemx         ; Result buffer identifier.
MIL_ID StructElemy         ; Result buffer identifier.
```

```
long  TotalBlobs          ; Total number of blobs.
allocarray CogX (4*MAX_BLOBS) ; X coordinate of center of gravity.
allocarray CogY (4*MAX_BLOBS) ; Y coordinate of center of gravity.

;Allocate defaults
MappAllocDefault M_SETUP &MilApplication &MilSystem &MilDisplay M_NULL &MilImage

;Restrict the region to be processed to the image size.
MbufChild2d MilImage 0 0 IMAGE_WIDTH IMAGE_HEIGHT &MilSubImage

;Load source image into image buffer.
MbufLoad IMAGE_FILE MilSubImage

;Pause to show the original image.
echo "This program determines the number of objects in the"
echo "displayed image and marks the center of gravity of each."
pause "Press <Enter> to continue."

;Binarize image.
;Grayscale variation
echo "Do you want to change the grayscale ? <y/n> (default=128)"
setnbr r [inkey]
if ([getnbr r]==110);no
{
echo "No"
;Binarization with the threshold default value.
MimBinarize MilSubImage MilSubImage M_GREATER_OR_EQUAL
IMAGE_THRESHOLD_VALUE M_NULL
}
while ([getnbr r]==121);yes
{
echo "Yes"
MbufLoad IMAGE_FILE MilSubImage
echo"Give me the new grayscale value (between 0 and 255)"
instr g

;Binarization with the new grayscale value.
MimBinarize MilSubImage MilSubImage M_GREATER_OR_EQUAL [strtonbr [getstr g]] M_NULL
echo "Do you want to change the grayscale one more time ? <y/n>)"
setnbr r [inkey]
}

;Remove small particles and then remove small holes.
MimOpen MilSubImage MilSubImage SMALL_PARTICLE_RADIUS M_BINARY
MimClose MilSubImage MilSubImage SMALL_PARTICLE_RADIUS M_BINARY

;Allocate a feature list.
MblobAllocFeatureList &FeatureList

;Enable feature to select blobs of interest.
MblobSelectFeature FeatureList M_AREA

;Allocate a blob result buffer.
MblobAllocResult &BlobResult

;change the foreground value
MblobControl BlobResult M_FOREGROUND_VALUE M_ZERO

;Calculate selected features for each blob.
```

```
MblobCalculate MilSubImage M_NULL FeatureList BlobResult

;Exclude blobs whose area is too small.
MblobSelect BlobResult M_EXCLUDE M_AREA M_GREATER_OR_EQUAL MAX_BLOB_AREA
M_NULL

;Get the total number of selected blobs.
MblobGetNumber BlobResult &TotalBlobs
echoln "There are "
echoln [nbrtostr TotalBlobs 10]
echo" objects in the image."
pause "Press <Enter> to continue."

;Select center of gravity feature.
MblobSelectFeature FeatureList M_CENTER_OF_GRAVITY_X
MblobSelectFeature FeatureList M_CENTER_OF_GRAVITY_Y

;Calculate selected features for each blob.
MblobCalculate MilSubImage M_NULL FeatureList BlobResult

;Check for array overflow.
if(TotalBlobs > MAX_BLOBS)
{
echo "Error: too many blobs."
}
else
{
;Get the results.
MblobGetResult BlobResult (M_CENTER_OF_GRAVITY_X+M_TYPE_LONG) [getarray CogX]
MblobGetResult BlobResult (M_CENTER_OF_GRAVITY_Y+M_TYPE_LONG) [getarray CogY]

echo "The coordinates of the different centers of gravity are:"
for n 0 TotalBlobs 1
{
echoln "X="
echo [nbrtostr [getnbrarray CogX _n] 10]
echoln "Y="
echo [nbrtostr [getnbrarray CogY _n] 10]
pause
if ([getnbr n]==(TotalBlobs-1))
{
echo "end of list"
}
else
echo "next point"
}

;Draw gray cross-hairs at the center of gravity of each blob.
MgraColor M_DEFAULT 128

for n 0 TotalBlobs 1
{
setnbr cog_x_ ([getnbrarray CogX _n]-CSIZE)
setnbr cog_y [getnbrarray CogY _n]
setnbr cog_x_cs ([getnbrarray CogX _n]+CSIZE)
setnbr cog_x [getnbrarray CogX _n]
setnbr cog_y_ ([getnbrarray CogY _n]-CSIZE)
setnbr cog_y_cs ([getnbrarray CogY _n]+CSIZE)
```

```
MgraLine M_DEFAULT MilSubImage [getnbr cog_x_] [getnbr cog_y] [getnbr cog_x_cs] [getnbr cog_y]
MgraLine M_DEFAULT MilSubImage [getnbr cog_x] [getnbr cog_y_] [getnbr cog_x] [getnbr cog_y_cs]
}
;results buffers allocation
MbufAlloc1d M_DEFAULT STRUCT_ELEM_WIDTH (STRUCT_ELEM_DEPTH+M_SIGNED)
M_STRUCT_ELEMENT &StructElemx
MbufAlloc1d M_DEFAULT STRUCT_ELEM_WIDTH (STRUCT_ELEM_DEPTH+M_SIGNED)
M_STRUCT_ELEMENT &StructElemy

;put data from the array into a buffer
MbufPut1d StructElemx 0 STRUCT_ELEM_WIDTH [getarray CogX]
MbufPut1d StructElemy 0 STRUCT_ELEM_WIDTH [getarray CogY]

;save buffers into files
Mbufsave RESULTX_FILE StructElemx
Mbufsave RESULTY_FILE StructElemy

echo "The coordinates of the centers of gravity have been saved"
echo "into the files :c:\X1.c  and  c:\Y1.c."
echo
echo "The calculated centers of gravity have been marked."
pause "Press <Enter> to end."
}

;Free all allocations.
MblobFree BlobResult
MblobFree FeatureList
MbufFree MilSubImage
MbufFree StructElemx
MbufFree StructElemy
MappFreeDefault MilApplication  MilSystem MilDisplay M_NULL MilImage

; Enable the automatic printing of the return values of commands
silence 0
```

```
;
;   PROGRAM  COGIMAG2.CL  WRITTEN IN MILINTER VERSION 2.0
;
;                                   BY
;
;                                R.S.Senanayake
;
;                          Aston University, Birmingham, UK
;
;                          SUPERVISORS: Dr. I.M.Cole
;                                       A/Prof S.Thiruvarudchelvan
;
;
; File name: cogimag2.cl (Image 2:points after deformation)
; Synopsis:  This program counts the number of points in an image, marks the
;         center of gravity of each and save the coordinates into files.

silence 1

; Target MIL image file specifications.

;File of the image to process.
macro IMAGE_FILE        "c:\image2.mim"
;Width of the image in pixels.
macro IMAGE_WIDTH       790
;Height of the image in pixels.
macro IMAGE_HEIGHT      590
;Threshold binarization default value.
macro IMAGE_THRESHOLD_VALUE 128

;results file
macro RESULTX_FILE      "c:\X2.c"
macro RESULTY_FILE      "c:\Y2.c"

;structuring element information
macro STRUCT_ELEM_WIDTH    50
macro STRUCT_ELEM_DEPTH    32

; Maximum number of blobs and maximum area of blobs in pixels.
macro MAX_BLOBS         50
macro MAX_BLOB_AREA     2000

; Radius of the smallest particles to keep in pixels.
macro SMALL_PARTICLE_RADIUS  1

; Size of the cross-hair used to mark centers of gravity in pixels.
macro CSIZE 10

MIL_ID MilApplication     ; Application identifier.
MIL_ID MilSystem          ; System identifier.
MIL_ID MilDisplay         ; Display identifier.
MIL_ID MilImage           ; Image buffer identifier.
MIL_ID MilSubImage        ; Sub-image buffer identifier.
MIL_ID BlobResult         ; Blob result buffer identifier.
MIL_ID FeatureList        ; Feature list identifier.
MIL_ID StructElemx        ; Result buffer identifier.
MIL_ID StructElemy        ; Result buffer identifier.
```

```
long  TotalBlobs          ; Total number of blobs.
allocarray CogX (4*MAX_BLOBS) ; X coordinate of center of gravity.
allocarray CogY (4*MAX_BLOBS) ; Y coordinate of center of gravity.

;Allocate defaults
MappAllocDefault M_SETUP &MilApplication &MilSystem &MilDisplay M_NULL &MilImage

;Restrict the region to be processed to the image size.
MbufChild2d MilImage 0 0 IMAGE_WIDTH IMAGE_HEIGHT &MilSubImage

;Load source image into image buffer.
MbufLoad IMAGE_FILE MilSubImage

;Pause to show the original image.
echo "This program determines the number of objects in the"
echo "displayed image and marks the center of gravity of each."
pause "Press <Enter> to continue."

;Binarize image.
;Grayscale variation
echo "Do you want to change the grayscale ? <y/n> (default=128)"
setnbr r [inkey]
if ([getnbr r]==110);no
{
echo "No"
;Binarization with the threshold default value.
MimBinarize MilSubImage MilSubImage M_GREATER_OR_EQUAL
IMAGE_THRESHOLD_VALUE M_NULL
}
while ([getnbr r]==121);yes
{
echo "Yes"
MbufLoad IMAGE_FILE MilSubImage
echo"Give me the new grayscale value (between 0 and 255)"
instr g

;Binarization with the new grayscale value.
MimBinarize MilSubImage MilSubImage M_GREATER_OR_EQUAL [strtonbr [getstr g]] M_NULL
echo "Do you want to change the grayscale one more time ? <y/n>)"
setnbr r [inkey]
}

;Remove small particles and then remove small holes.
MimOpen MilSubImage MilSubImage SMALL_PARTICLE_RADIUS M_BINARY
MimClose MilSubImage MilSubImage SMALL_PARTICLE_RADIUS M_BINARY

;Allocate a feature list.
MblobAllocFeatureList &FeatureList

;Enable feature to select blobs of interest.
MblobSelectFeature FeatureList M_AREA

;Allocate a blob result buffer.
MblobAllocResult &BlobResult

;change the foreground value
MblobControl BlobResult M_FOREGROUND_VALUE M_ZERO
```

```
;Calculate selected features for each blob.
MblobCalculate MilSubImage M_NULL FeatureList BlobResult

;Exclude blobs whose area is too small.
MblobSelect BlobResult M_EXCLUDE M_AREA M_GREATER_OR_EQUAL MAX_BLOB_AREA
M_NULL

;Get the total number of selected blobs.
MblobGetNumber BlobResult &TotalBlobs
echoln "There are "
echoln [nbrtostr TotalBlobs 10]
echo" objects in the image."
pause "Press <Enter> to continue."

;Select center of gravity feature.
MblobSelectFeature FeatureList M_CENTER_OF_GRAVITY_X
MblobSelectFeature FeatureList M_CENTER_OF_GRAVITY_Y

;Calculate selected features for each blob.
MblobCalculate MilSubImage M_NULL FeatureList BlobResult

;Check for array overflow.
if(TotalBlobs > MAX_BLOBS)
{
echo "Error: too many blobs."
}
else
{
;Get the results.
MblobGetResult BlobResult (M_CENTER_OF_GRAVITY_X+M_TYPE_LONG) [getarray CogX]
MblobGetResult BlobResult (M_CENTER_OF_GRAVITY_Y+M_TYPE_LONG) [getarray CogY]

echo "The coordinates of the different centers of gravity are:"
for n 0 TotalBlobs 1
{
echoln "X="
echo [nbrtostr [getnbrarray CogX _n] 10]
echoln "Y="
echo [nbrtostr [getnbrarray CogY _n] 10]
pause
if ([getnbr n]==(TotalBlobs-1))
{
echo "end of list"
}
else
echo "next point"
}

;Draw gray cross-hairs at the center of gravity of each blob.
MgraColor M_DEFAULT 128

for n 0 TotalBlobs 1
{
setnbr cog_x_ ([getnbrarray CogX _n]-CSIZE)
setnbr cog_y [getnbrarray CogY _n]
setnbr cog_x_cs ([getnbrarray CogX _n]+CSIZE)
setnbr cog_x [getnbrarray CogX _n]
setnbr cog_y_ ([getnbrarray CogY _n]-CSIZE)
setnbr cog_y_cs ([getnbrarray CogY _n]+CSIZE)
```

```
MgraLine M_DEFAULT MilSubImage [getnbr cog_x_] [getnbr cog_y] [getnbr cog_x_cs] [getnbr cog_y]
MgraLine M_DEFAULT MilSubImage [getnbr cog_x] [getnbr cog_y_] [getnbr cog_x] [getnbr cog_y_cs]
}
;results buffers allocation
MbufAlloc1d M_DEFAULT STRUCT_ELEM_WIDTH (STRUCT_ELEM_DEPTH+M_SIGNED)
M_STRUCT_ELEMENT &StructElemx
MbufAlloc1d M_DEFAULT STRUCT_ELEM_WIDTH (STRUCT_ELEM_DEPTH+M_SIGNED)
M_STRUCT_ELEMENT &StructElemy

;put data from the array into a buffer
MbufPut1d StructElemx 0 STRUCT_ELEM_WIDTH [getarray CogX]
MbufPut1d StructElemy 0 STRUCT_ELEM_WIDTH [getarray CogY]

;save buffers into files
Mbufsave RESULTX_FILE StructElemx
Mbufsave RESULTY_FILE StructElemy

echo "The coordinates of the centers of gravity have been saved"
echo "into the files :c:\X2.c  and  c:\Y2.c."
echo
echo "The calculated centers of gravity have been marked."
pause "Press <Enter> to end."
}

;Free all allocations.
MblobFree BlobResult
MblobFree FeatureList
MbufFree MilSubImage
MbufFree StructElemx
MbufFree StructElemy
MappFreeDefault MilApplication  MilSystem MilDisplay M_NULL MilImage

; Enable the automatic printing of the return values of commands
silence 0
```

```
;
;
;   PROGRAM  COGMARK1.CL  WRITTEN IN MILINTER VERSION 2.0
;                          BY
;
;                                  R.S.Senanayake
;
;                                  Aston University, Birmingham, UK
;
;                                  SUPERVISORS: Dr. I.M.Cole
;                                                A/Prof S.Thiruvarudchelvan
;
;
; File name: cogmark1.cl (Coordinates system 1)
; Synopsis:  This program counts the number of points in an image, marks the
;          center of gravity of each and save the coordinates into files.

silence 1

; Target MIL image file specifications.

;File of the image to process.
macro IMAGE_FILE          "c:\mark1.mim"
;Width of the image in pixels.
macro IMAGE_WIDTH         790
;Height of the image in pixels.
macro IMAGE_HEIGHT        590
;Threshold binarization default value.
macro IMAGE_THRESHOLD_VALUE 128

;results file
macro RESULTX_FILE        "c:\mark1x.c"
macro RESULTY_FILE        "c:\mark1y.c"

;structuring element information
macro STRUCT_ELEM_WIDTH    50
macro STRUCT_ELEM_DEPTH    32

; Maximum number of blobs and maximum area of blobs in pixels.
macro MAX_BLOBS           50
macro MAX_BLOB_AREA       2000

; Radius of the smallest particles to keep in pixels.
macro SMALL_PARTICLE_RADIUS  1

; Size of the cross-hair used to mark centers of gravity in pixels.
macro CSIZE 10

MIL_ID MilApplication      ; Application identifier.
MIL_ID MilSystem           ; System identifier.
MIL_ID MilDisplay          ; Display identifier.
MIL_ID MilImage            ; Image buffer identifier.
MIL_ID MilSubImage         ; Sub-image buffer identifier.
MIL_ID BlobResult          ; Blob result buffer identifier.
MIL_ID FeatureList         ; Feature list identifier.
MIL_ID StructElemx         ; Result buffer identifier.
MIL_ID StructElemy         ; Result buffer identifier.
```

```
long  TotalBlobs          ; Total number of blobs.
allocarray CogX (4*MAX_BLOBS) ; X coordinate of center of gravity.
allocarray CogY (4*MAX_BLOBS) ; Y coordinate of center of gravity.

;Allocate defaults
MappAllocDefault M_SETUP &MilApplication &MilSystem &MilDisplay M_NULL &MilImage

;Restrict the region to be processed to the image size.
MbufChild2d MilImage 0 0 IMAGE_WIDTH IMAGE_HEIGHT &MilSubImage

;Load source image into image buffer.
MbufLoad IMAGE_FILE MilSubImage

;Pause to show the original image.
echo "This program determines the number of objects in the"
echo "displayed image and marks the center of gravity of each."
pause "Press <Enter> to continue."

;Binarize image.
;Grayscale variation
echo "Do you want to change the grayscale ? <y/n> (default=128)"
setnbr r [inkey]
if ([getnbr r]==110);no
{
echo "No"
;Binarization with the threshold default value.
MimBinarize MilSubImage MilSubImage M_GREATER_OR_EQUAL
IMAGE_THRESHOLD_VALUE M_NULL
}
while ([getnbr r]==121);yes
{
echo "Yes"
MbufLoad IMAGE_FILE MilSubImage
echo"Give me the new grayscale value (between 0 and 255)"
instr g

;Binarization with the new grayscale value.
MimBinarize MilSubImage MilSubImage M_GREATER_OR_EQUAL [strtonbr [getstr g]] M_NULL
echo "Do you want to change the grayscale one more time ? <y/n>)"
setnbr r [inkey]
}

;Remove small particles and then remove small holes.
MimOpen MilSubImage MilSubImage SMALL_PARTICLE_RADIUS M_BINARY
MimClose MilSubImage MilSubImage SMALL_PARTICLE_RADIUS M_BINARY

;Allocate a feature list.
MblobAllocFeatureList &FeatureList

;Enable feature to select blobs of interest.
MblobSelectFeature FeatureList M_AREA

;Allocate a blob result buffer.
MblobAllocResult &BlobResult

;change the foreground value
MblobControl BlobResult M_FOREGROUND_VALUE M_ZERO
```

```
;Calculate selected features for each blob.
MblobCalculate MilSubImage M_NULL FeatureList BlobResult

;Exclude blobs whose area is too small.
MblobSelect BlobResult M_EXCLUDE M_AREA M_GREATER_OR_EQUAL MAX_BLOB_AREA
M_NULL

;Get the total number of selected blobs.
MblobGetNumber BlobResult &TotalBlobs
echoln "There are "
echoln [nbrtostr TotalBlobs 10]
echo" objects in the image."
pause "Press <Enter> to continue."

;Select center of gravity feature.
MblobSelectFeature FeatureList M_CENTER_OF_GRAVITY_X
MblobSelectFeature FeatureList M_CENTER_OF_GRAVITY_Y

;Calculate selected features for each blob.
MblobCalculate MilSubImage M_NULL FeatureList BlobResult

;Check for array overflow.
if(TotalBlobs > MAX_BLOBS)
{
echo "Error: too many blobs."
}
else
{
;Get the results.
MblobGetResult BlobResult (M_CENTER_OF_GRAVITY_X+M_TYPE_LONG) [getarray CogX]
MblobGetResult BlobResult (M_CENTER_OF_GRAVITY_Y+M_TYPE_LONG) [getarray CogY]

echo "The coordinates of the different centers of gravity are:"
for n 0 TotalBlobs 1
{
echoln "X="
echo [nbrtostr [getnbrarray CogX _n] 10]
echoln "Y="
echo [nbrtostr [getnbrarray CogY _n] 10]
pause
if ([getnbr n]==(TotalBlobs-1))
{
echo "end of list"
}
else
echo "next point"
}

;Draw gray cross-hairs at the center of gravity of each blob.
MgraColor M_DEFAULT 128

for n 0 TotalBlobs 1
{
setnbr cog_x_ ([getnbrarray CogX _n]-CSIZE)
setnbr cog_y [getnbrarray CogY _n]
setnbr cog_x_cs ([getnbrarray CogX _n]+CSIZE)
setnbr cog_x [getnbrarray CogX _n]
setnbr cog_y_ ([getnbrarray CogY _n]-CSIZE)
setnbr cog_y_cs ([getnbrarray CogY _n]+CSIZE)
```

```
MgraLine M_DEFAULT MilSubImage [getnbr cog_x_] [getnbr cog_y] [getnbr cog_x_cs] [getnbr cog_y]
MgraLine M_DEFAULT MilSubImage [getnbr cog_x] [getnbr cog_y_] [getnbr cog_x] [getnbr cog_y_cs]
}
;results buffers allocation
MbufAlloc1d M_DEFAULT STRUCT_ELEM_WIDTH (STRUCT_ELEM_DEPTH+M_SIGNED)
M_STRUCT_ELEMENT &StructElemx
MbufAlloc1d M_DEFAULT STRUCT_ELEM_WIDTH (STRUCT_ELEM_DEPTH+M_SIGNED)
M_STRUCT_ELEMENT &StructElemy

;put data from the array into a buffer
MbufPut1d StructElemx 0 STRUCT_ELEM_WIDTH [getarray CogX]
MbufPut1d StructElemy 0 STRUCT_ELEM_WIDTH [getarray CogY]

;save buffers into files
Mbufsave RESULTX_FILE StructElemx
Mbufsave RESULTY_FILE StructElemy

echo "The coordinates of the centers of gravity have been saved"
echo "into the files :c:\mark1x.c  and  c:\mark1y.c."
echo
echo "The calculated centers of gravity have been marked."
pause "Press <Enter> to end."
}

;Free all allocations.
MblobFree BlobResult
MblobFree FeatureList
MbufFree MilSubImage
MbufFree StructElemx
MbufFree StructElemy
MappFreeDefault MilApplication  MilSystem MilDisplay M_NULL MilImage

; Enable the automatic printing of the return values of commands
silence 0
```

```
;
;
;   PROGRAM  COGMARK2.CL  WRITTEN IN MILINTER VERSION 2.0
;
;                          BY
;
;                                R.S.Senanayake
;
;                           SUPERVISORS:      Dr. I.M.Cole
;                                             A/Prof S.Thiruvarudchelvan
;
;
;
; File name: cogmark2.cl (Coordinates system 2)
; Synopsis:  This program counts the number of points in an image, marks the
;          center of gravity of each and save the coordinates into files.

silence 1

; Target MIL image file specifications.

;File of the image to process.
macro IMAGE_FILE          "c:\mark2.mim"
;Width of the image in pixels.
macro IMAGE_WIDTH         790
;Height of the image in pixels.
macro IMAGE_HEIGHT        590
;Threshold binarization default value.
macro IMAGE_THRESHOLD_VALUE 128

;results file
macro RESULTX_FILE        "c:\mark2x.c"
macro RESULTY_FILE        "c:\mark2y.c"

;structuring element information
macro STRUCT_ELEM_WIDTH    50
macro STRUCT_ELEM_DEPTH    32

; Maximum number of blobs and maximum area of blobs in pixels.
macro MAX_BLOBS           50
macro MAX_BLOB_AREA       2000

; Radius of the smallest particles to keep in pixels.
macro SMALL_PARTICLE_RADIUS  1

; Size of the cross-hair used to mark centers of gravity in pixels.
macro CSIZE 10

MIL_ID MilApplication      ; Application identifier.
MIL_ID MilSystem           ; System identifier.
MIL_ID MilDisplay          ; Display identifier.
MIL_ID MilImage            ; Image buffer identifier.
MIL_ID MilSubImage         ; Sub-image buffer identifier.
MIL_ID BlobResult          ; Blob result buffer identifier.
MIL_ID FeatureList         ; Feature list identifier.
MIL_ID StructElemx         ; Result buffer identifier.
MIL_ID StructElemy         ; Result buffer identifier.
```

```
long  TotalBlobs          ; Total number of blobs.
allocarray CogX (4*MAX_BLOBS) ; X coordinate of center of gravity.
allocarray CogY (4*MAX_BLOBS) ; Y coordinate of center of gravity.

;Allocate defaults
MappAllocDefault M_SETUP &MilApplication &MilSystem &MilDisplay M_NULL &MilImage

;Restrict the region to be processed to the image size.
MbufChild2d MilImage 0 0 IMAGE_WIDTH IMAGE_HEIGHT &MilSubImage

;Load source image into image buffer.
MbufLoad IMAGE_FILE MilSubImage

;Pause to show the original image.
echo "This program determines the number of objects in the"
echo "displayed image and marks the center of gravity of each."
pause "Press <Enter> to continue."

;Binarize image.
;Grayscale variation
echo "Do you want to change the grayscale ? <y/n> (default=128)"
setnbr r [inkey]
if ([getnbr r]==110);no
{
echo "No"
;Binarization with the threshold default value.
MimBinarize MilSubImage MilSubImage M_GREATER_OR_EQUAL
IMAGE_THRESHOLD_VALUE M_NULL
}
while ([getnbr r]==121);yes
{
echo "Yes"
MbufLoad IMAGE_FILE MilSubImage
echo"Give me the new grayscale value (between 0 and 255)"
instr g

;Binarization with the new grayscale value.
MimBinarize MilSubImage MilSubImage M_GREATER_OR_EQUAL [strtonbr [getstr g]] M_NULL
echo "Do you want to change the grayscale one more time ? <y/n>)"
setnbr r [inkey]
}

;Remove small particles and then remove small holes.
MimOpen MilSubImage MilSubImage SMALL_PARTICLE_RADIUS M_BINARY
MimClose MilSubImage MilSubImage SMALL_PARTICLE_RADIUS M_BINARY

;Allocate a feature list.
MblobAllocFeatureList &FeatureList

;Enable feature to select blobs of interest.
MblobSelectFeature FeatureList M_AREA

;Allocate a blob result buffer.
MblobAllocResult &BlobResult

;change the foreground value
MblobControl BlobResult M_FOREGROUND_VALUE M_ZERO
```

```
;Calculate selected features for each blob.
MblobCalculate MilSubImage M_NULL FeatureList BlobResult

;Exclude blobs whose area is too small.
MblobSelect BlobResult M_EXCLUDE M_AREA M_GREATER_OR_EQUAL MAX_BLOB_AREA
M_NULL

;Get the total number of selected blobs.
MblobGetNumber BlobResult &TotalBlobs
echoln "There are "
echoln [nbrtostr TotalBlobs 10]
echo" objects in the image."
pause "Press <Enter> to continue."

;Select center of gravity feature.
MblobSelectFeature FeatureList M_CENTER_OF_GRAVITY_X
MblobSelectFeature FeatureList M_CENTER_OF_GRAVITY_Y

;Calculate selected features for each blob.
MblobCalculate MilSubImage M_NULL FeatureList BlobResult

;Check for array overflow.
if(TotalBlobs > MAX_BLOBS)
{
echo "Error: too many blobs."
}
else
{
;Get the results.
MblobGetResult BlobResult (M_CENTER_OF_GRAVITY_X+M_TYPE_LONG) [getarray CogX]
MblobGetResult BlobResult (M_CENTER_OF_GRAVITY_Y+M_TYPE_LONG) [getarray CogY]

echo "The coordinates of the different centers of gravity are:"
for n 0 TotalBlobs 1
{
echoln "X="
echo [nbrtostr [getnbrarray CogX _n] 10]
echoln "Y="
echo [nbrtostr [getnbrarray CogY _n] 10]
pause
if ([getnbr n]==(TotalBlobs-1))
{
echo "end of list"
}
else
echo "next point"
}

;Draw gray cross-hairs at the center of gravity of each blob.
MgraColor M_DEFAULT 128

for n 0 TotalBlobs 1
{
setnbr cog_x_ ([getnbrarray CogX _n]-CSIZE)
setnbr cog_y [getnbrarray CogY _n]
setnbr cog_x_cs ([getnbrarray CogX _n]+CSIZE)
setnbr cog_x [getnbrarray CogX _n]
setnbr cog_y_ ([getnbrarray CogY _n]-CSIZE)
setnbr cog_y_cs ([getnbrarray CogY _n]+CSIZE)
```

```
MgraLine M_DEFAULT MilSubImage [getnbr cog_x_] [getnbr cog_y] [getnbr cog_x_cs] [getnbr cog_y]
MgraLine M_DEFAULT MilSubImage [getnbr cog_x] [getnbr cog_y_] [getnbr cog_x] [getnbr cog_y_cs]
}
;results buffers allocation
MbufAlloc1d M_DEFAULT STRUCT_ELEM_WIDTH (STRUCT_ELEM_DEPTH+M_SIGNED)
M_STRUCT_ELEMENT &StructElemx
MbufAlloc1d M_DEFAULT STRUCT_ELEM_WIDTH (STRUCT_ELEM_DEPTH+M_SIGNED)
M_STRUCT_ELEMENT &StructElemy

;put data from the array into a buffer
MbufPut1d StructElemx 0 STRUCT_ELEM_WIDTH [getarray CogX]
MbufPut1d StructElemy 0 STRUCT_ELEM_WIDTH [getarray CogY]

;save buffers into files
Mbufsave RESULTX_FILE StructElemx
Mbufsave RESULTY_FILE StructElemy

echo "The coordinates of the centers of gravity have been saved"
echo "into the files :c:\mark2x.c  and  c:\mark2y.c."
echo
echo "The calculated centers of gravity have been marked."
pause "Press <Enter> to end."
}

;Free all allocations.
MblobFree BlobResult
MblobFree FeatureList
MbufFree MilSubImage
MbufFree StructElemx
MbufFree StructElemy
MappFreeDefault MilApplication  MilSystem MilDisplay M_NULL MilImage

; Enable the automatic printing of the return values of commands
silence 0


;
```

```
;      PROGRAM LINK.CL WRITTEN IN MILINTER VERSION 2.0
;
;                                BY
;
;                          R.S.Senanayake
;
;                     Aston University, Birmingham, UK
;
;                          SUPERVISORS:      Dr.I.M.Cole
;                                            A/Prof S.Thiruvarudchelvan
;
;
;

;file name:link.cl
;synopsis: This program presents the choice between images grabbing and images
;processing.


silence 1

;selection between images grabbing and images processing.

echo "1.Grab images"
echo "2.Image processing"
echo "Please select <1/2>."

setnbr n [inkey]
echo [nbrtostr ([getnbr n] - 48 ) 10]

;bad choice

if (([getnbr n] < 49) || ([getnbr n] >50) )
   {
    echo "Incorrect option"
    echo "Exiting"
   }

;choice:grab images.

else
   {
   if ([getnbr n]==49) ;1
      {
          echo "MFOCUS1.CL (Image 1)"
          execcl "c:\mfocus1.cl"
      pause
          echo "MFOCUS2.CL (Mark 1:Coordinates system 1)"
          execcl "c:\mfocus2.cl"
          pause
          echo "MFOCUS3.CL (Image 2)"
          execcl "c:\mfocus3.cl"
          pause
          echo "MFOCUS4.CL (Mark 2:Coordinates system 2)"
          execcl "c:\mfocus4.cl"
      }

;choice:process images.
```

```
  if ([getnbr n]==50) ;2
    {
        echo "COGMARK1.CL"
        execcl "c:\cogmark1.cl"
    pause
        echo "COGIMAG1.CL"
        execcl "c:\cogimag1.cl"
    pause
        echo "COGMARK2.CL"
        execcl "c:\cogmark2.cl"
        pause
        echo "COGIMAG2.CL"
        execcl "c:\cogimag2.cl"
        pause
        }
  }

silence 0

;
```

```
;     PROGRAM MFOCUS1.CL WRITTEN IN MILINTER VERSION 2.0
;
;                                   BY
;
;                                R.S.Senanayake
;
;                                Aston University, Birmingham, UK
;
;                                      SUPERVISORS:Dr. I.M.Cole
;                                                  A/Prof S.Thiruvarudchelvan
;
; File name: mfocus1.cl (image1)
; Synopsis: This program allows you to adjust your camera by
;         grabbing continuously from the default camera until
;         a key is pressed and save this image into a file.
;
silence 1
macro IMAGE_FILE "a:\image1.mim"

MIL_ID MilApplication : Application identifier.
MIL_ID MilSystem     ; System identifier.
MIL_ID MilDisplay    ; Display identifier.
MIL_ID MilCamera     ; Camera identifier.
MIL_ID MilImage      ; Image buffer identifier.

; Allocate defaults.
MappAllocDefault M_SETUP &MilApplication &MilSystem &MilDisplay &MilCamera &MilImage

; Grab continuously.
MdigGrabContinuous MilCamera MilImage

; When a key is pressed, halt.
echo "Continuous grab in progress. Adjust your camera and"
pause"press <Enter> to stop grabbing."

; Stop continuous grab.
MdigHalt MilCamera

echo "Displaying the last grabbed image."
pause
echo "Do you want to save this image? <y/n>"
setnbr r [inkey]
if ([getnbr r]==110);no
  {
  pause "Press <enter> to end"
  }
else
  {
  ;saved an image to IMAGE_FILE
  MbufSave IMAGE_FILE MilImage
  echo "This image has been saved into the file a:\image1.mim"
  pause "Press <enter> to end."
  }
; Release defaults.
MappFreeDefault MilApplication MilSystem MilDisplay MilCamera MilImage
; Enable the automatic printing of the return values of commands
silence 0
;
```

```
;     PROGRAM  MFOCUS2.CL WRITTEN IN MILINTER VERSION 2.0
;
;                                   BY
;
;                                R.S.Senanayake
;
;                           Aston University, Birmingham, UK
;
;;                          SUPERVISORS:        Dr. I.M.Cole
;                                               A/Prof S.Thiruvarudchelvan
;
;
; File name: mfocus2.cl (mark 1 :coordinates system 1)
; Synopsis:  This program allows you to adjust your camera by
;         grabbing continuously from the default camera until
;         a key is pressed and save this image into a file.
;
; Disable the automatic printing of the return values of commands
silence 1

 macro IMAGE_FILE "a:\mark1.mim"

MIL_ID MilApplication : Application identifier.
MIL_ID MilSystem     ; System identifier.
MIL_ID MilDisplay    ; Display identifier.
MIL_ID MilCamera     ; Camera identifier.
MIL_ID MilImage      ; Image buffer identifier.


; Allocate defaults.
MappAllocDefault M_SETUP &MilApplication &MilSystem &MilDisplay &MilCamera &MilImage

; Grab continuously.
MdigGrabContinuous MilCamera MilImage

; When a key is pressed, halt.
echo "Continuous grab in progress. Adjust your camera and"
pause"press <Enter> to stop grabbing."


; Stop continuous grab.
MdigHalt MilCamera

echo "Displaying the last grabbed image."

pause
echo "Do you want to save this image? <y/n>"
setnbr r [inkey]
if ([getnbr r]==110);no
  {
  pause "Press <enter> to end"
  }
else
  {
  ;saved an image to IMAGE_FILE
  MbufSave IMAGE_FILE MilImage
  echo "This image has been saved into the file a:\mil\mark1.mim"
  pause "Press <enter> to end."
  }
```

```
; Release defaults.
MappFreeDefault MilApplication MilSystem MilDisplay MilCamera MilImage


; Enable the automatic printing of the return values of commands
silence 0
```

```
;       PROGRAM MFOCUS3.CL WRITTEN IN MILINTER VERSION 2.0
;
;                                   BY
;
;                              R.S.Senanayake
;
;                           Aston University, Birmingham, UK
;
;                                   SUPERVISORS:        Dr. I.M.Cole
;                                                       A/Prof S.Thiruvarudchelvan
;
; File name: mfocus3.cl (Image 2:points after deformation)
; Synopsis:  This program allows you to adjust your camera by
;         grabbing continuously from the default camera until
;         a key is pressed and save this image into a file.
;
; Disable the automatic printing of the return values of commands
silence 1

 macro IMAGE_FILE "a:\image2.mim"

MIL_ID MilApplication : Application identifier.
MIL_ID MilSystem     ; System identifier.
MIL_ID MilDisplay    ; Display identifier.
MIL_ID MilCamera     ; Camera identifier.
MIL_ID MilImage      ; Image buffer identifier.


; Allocate defaults.
MappAllocDefault M_SETUP &MilApplication &MilSystem &MilDisplay &MilCamera &MilImage

; Grab continuously.
MdigGrabContinuous MilCamera MilImage

; When a key is pressed, halt.
echo "Continuous grab in progress. Adjust your camera and"
pause"press <Enter> to stop grabbing."


; Stop continuous grab.
MdigHalt MilCamera

echo "Displaying the last grabbed image."

pause
echo "Do you want to save this image? <y/n>"
setnbr r [inkey]
if ([getnbr r]==110);no
  {
  pause "Press <enter> to end"
  }
else
  {
  ;saved an image to IMAGE_FILE
  MbufSave IMAGE_FILE MilImage
  echo "This image has been saved into the file a:\mil\image2.mim"
  pause "Press <enter> to end."
  }
```

```
; Release defaults.
MappFreeDefault MilApplication MilSystem MilDisplay MilCamera MilImage


; Enable the automatic printing of the return values of commands
silence 0


;
```

```
;
;    PROGRAM MFOCUS4.CL WRITTEN IN MILINTER VERSION 2.0
;
;                                   BY
;
;                                R.S.Senanayake
;
;                          Aston University, Birmingham, UK
;
;                           SUPERVISORS:        Dr. I.M.Cole
;                                               A/Prof S.Thiruvarudchelvan
;
;
; File name: mfocus4.cl (mark2:coordinates system 2)
; Synopsis:  This program allows  adjustment of the camera by
;          grabbing continuously from the default camera until
;          a key is pressed and save this image into a file.
;
; Disable the automatic printing of the return values of commands
silence 1

macro IMAGE_FILE "a:\mark2.mim"

MIL_ID MilApplication : Application identifier.
MIL_ID MilSystem     ; System identifier.
MIL_ID MilDisplay    ; Display identifier.
MIL_ID MilCamera     ; Camera identifier.
MIL_ID MilImage      ; Image buffer identifier.


; Allocate defaults.
MappAllocDefault M_SETUP &MilApplication &MilSystem &MilDisplay &MilCamera &MilImage

; Grab continuously.
MdigGrabContinuous MilCamera MilImage

; When a key is pressed, halt.
echo "Continuous grab in progress. Adjust your camera and"
pause"press <Enter> to stop grabbing."


; Stop continuous grab.
MdigHalt MilCamera

echo "Displaying the last grabbed image."

pause
echo "Do you want to save this image? <y/n>"
setnbr r [inkey]
if ([getnbr r]==110);no
  {
  pause "Press <enter> to end"
  }
else
```

```
{
  ;saved an image to IMAGE_FILE
  MbufSave IMAGE_FILE MilImage
  echo "This image has been saved into the file a:\mil\mark2.mim"
  pause "Press <enter> to end."
  }
; Release defaults.
MappFreeDefault MilApplication MilSystem MilDisplay MilCamera MilImage


; Enable the automatic printing of the return values of commands
silence 0
```

Appendix F

C Programs for calculating plastic strains

```
/*****************************************************************************/
/*      PROGRAM  STRAINS.C  WRITTEN IN QUICK-C VERSION 2.5
                                        BY
                                    R.S.Senanayake
                                Aston University, Birmingham, UK
                                SUPERVISORS:  Dr I.M.Cole
                                A/Prof  S.Thiruvarudchelvan          */

/*****************************************************************************/
#include <stdio.h>
#include <math.h>
#include <stdlib.h>
#include <graph.h>
#define DIM 15

/*****************************************************************************/
/************************ MAIN PROGRAM ***************************************/
/*****************************************************************************

                        list of variables:

actualsize:number of points in the grid.
i:counter for loops.
ptx,pty:arrays including coordinates of grid points before deformation.
ptx2,pty2:arrays including coordinates of grid points after deformation.

                        list of constants:

DIM:dimension of the arrays.

*****************************************************************************/
main()

{
int actualsize,i;
float ptx[DIM],pty[DIM],ptx2[DIM],pty2[DIM];

printf("Enter the number of points of your grid.(Reference grid not included)\n");
scanf("%d",&actualsize);
getchar();

/*opening of x2.c file*/

printf("Opening of the file including grid points after deformation(x_axis).\n");
fileopen(&ptx2);
for (i=1;i<actualsize+1;i++)
printf("ptx2[%d]=%f\n",i,ptx2[i]);
getchar();

/*opening of y2.c file*/

printf("Opening of the file including grid points after deformation(y_axis).\n");
fileopen(&pty2);
for (i=1;i<actualsize+1;i++)
printf("pty2[%d]=%f\n",i,pty2[i]);
getchar();

changement(&ptx2,&pty2,actualsize);
getchar();
```

```
/*opening of x1.c file*/

printf("Opening of the file including grid points before deformation(x_axis).\n");
fileopen(&ptx);
for (i=1;i<actualsize+1;i++)
printf("ptx[%d]=%f\n",i,ptx[i]);
getchar();

/*opening of y1.c file*/

printf("Opening of the file including grid points before deformation(y_axis).\n");
fileopen(&pty);
for (i=1;i<actualsize+1;i++)
printf("pty[%d]=%f\n",i,pty[i]);
getchar();

base(&ptx,&pty,&ptx2,&pty2,actualsize);

}
```

```
/*************************************************************************/
/*****************Ordering and Numbering of Grid Points *****************/
/*************************************************************************
```

Description :

The biggest part of this program; this includes:
- -determination of the origin (point at the left top of the grid)
- -determination of the columns of grid points
- -ordering of these points (from the top to the bottom)
- -numbering of these grid points

These operations will be done for the grid points after and before deformation.

list of variables:

*valx1:pointer for the x_axis of grid points before deformation (array).
*valy1:pointer for the y_axis of grid points before deformation (array).
*valx2:pointer for the x_axis of grid points after deformation (array).
*valy2:pointer for the y_axis of grid points after deformation (array).
size:number of grid points of the grid (reference not included).

i,j,counter:counters for loops.
rank:variable including the rank of the base.
smallest:variable including the smallest sum of valx and valy.
colbasex1,_y1:arrays including coordinates (column of base before deformation).
colbasex2,_y2:arrays including coordinates (column of base after deformation).
casex1,_y1:arrays including values of valx1 and valy1.
casex2,_y2:arrays including values of valx2 and valy2.
mem1x,_1y:arrays including values ready for the calculation(classified).
mem2x,_2y:arrays including values ready for the calculation(classified).

list of constants:

DELTA_X:difference allowable in x_axis.
DIM:Dimension of the arrays.

```
*************************************************************************/


base(valx1,valy1,valx2,valy2,size)

#define DELTA_X 50
#define DIM 15
float *valx1,*valy1,*valx2,*valy2;
int size;
{
int i,rank,j,counter;
float smallest;
float colbasex1[DIM],colbasey1[DIM];
float colbasex2[DIM],colbasey2[DIM];
float casex1[DIM],casey1[DIM];
float casex2[DIM],casey2[DIM];
float mem1x[DIM],mem1y[DIM];
float mem2x[DIM],mem2y[DIM];
rank=1;

for (smallest=*(valx1+1)+*(valy1+1),i=1;i<size+1;i++)
```

```
        if(*(valx1+i)+*(valy1+i)<smallest)
                {
                smallest=*(valx1+i)+*(valy1+i);
                rank=i;
                }
printf("base:x_axis=%5f;y_axis=%5f\n",*(valx1+rank),*(valy1+rank));
j=1;
for (i=1;i<size+1;i++)
        if ( *(valx1+rank) - DELTA_X < *(valx1+i) )
                {
                if( *(valx1+i) < *(valx1+rank) + DELTA_X )
                        {
                        colbasex1[j]= *(valx1+i);
                        colbasey1[j]=*(valy1+i); ;
                        j=j+1;
                        }
                }
printf("column of base:\n");
printf("x_axis---------y_axis\n");
counter=0;
for (i=1;i<j;i++)
        {
        printf("%5f %15f\n",colbasex1[i],colbasey1[i]);
        counter=counter+1;
        }
while(!kbhit());
for (i=1;i<size+1;i++)
        {
         casex1[i]=*(valx1+i);
         casey1[i]=*(valy1+i);
        }

classification(&colbasex1,&colbasey1,counter);
getchar();
printf("\n");
arrange1(&colbasey1,&casex1,&casey1,size,counter,&mem1x,&mem1y);
getchar();
rank=1;

for (smallest=*(valx2+1)+*(valy2+1),i=1;i<size+1;i++)
        if(*(valx2+i)+*(valy2+i)<smallest)
                {
                smallest=*(valx2+i)+*(valy2+i);
                rank=i;
                }
printf("base:x_axis=%5f;y_axis=%5f\n",*(valx2+rank),*(valy2+rank));
j=1;
for (i=1;i<size+1;i++)
        if ( *(valx2+rank) - DELTA_X < *(valx2+i) )
                {
                if( *(valx2+i) < *(valx2+rank) + DELTA_X )
                        {
                        colbasex2[j]= *(valx2+i);
                        colbasey2[j]=*(valy2+i); ;
                        j=j+1;
                        }
                }
```

```
printf("column of base:\n");
printf("x_axis----------y_axis\n");
counter=0;
for (i=1;i<j;i++)
        {
        printf("%5f %15f\n",colbasex2[i],colbasey2[i]);
        counter=counter+1;
        }
getchar();
for (i=1;i<size+1;i++)
        {
         casex2[i]=*(valx2+i);
         casey2[i]=*(valy2+i);
        }

classification(&colbasex2,&colbasey2,counter);
getchar();
printf("\n");
arrange2(&colbasey2,&casex2,&casey2,size,counter,&mem2x,mem2y);
getchar();

calculus(&mem1x,&mem1y,&mem2x,&mem2y,size);

while(!kbhit());
}
```

```
/*****************************************************************************/
/*order values of column grid points and order them from the smallest to the biggest*/
/*****************************************************************************
```

Description:

Take from the base function values of column grid points and order them
from the smallest to the biggest.

list of variables:

val:number of points in the column of base.
*colbx and _y:pointers including coordinates of points in the column of base.

a,b,p:counters for loops.
var1,var2:intermediate variables.

```
*****************************************************************************/

classification(colbx,colby,val)

int val;
float *colbx,*colby;
{
int a,b,p;
float var1,var2;
 for(a=1;a<val;a++)
         for(b=a+1;b<val+1;b++)
         if(colby[a]>colby[b])
         {
         var2=colby[b];
         colby[b]=colby[a];
         colby[a]=var2;
         var1=colbx[b];
         colbx[b]=colbx[a];
         colbx[a]=var1;
         }
 printf("Column of base classified:\n");
 for (p=1;p<val+1;p++)
 printf("x=%f y=%f\n",colbx[p],colby[p]);
}
```

```
/*************************************************************************/
/* This function calculates the new  position of a grid points : one translation and one rotation
**************************************************************************/
/*************************************************************************
```

Description:

This function recognises a change in position of a grid point : one translation and one rotation

list of variables:

*x2,*y2:pointers including the coordinates of the points after deformation.
u:number of points in the grid.

i:counter for loops.
a,b,c,d:intermediate variables for the calculation of the rotation angle.
alpha1,alpha2:intermediate variables for the calculation of the rotation angle.
thetdg:value of the rotation angle in degrees.
theta:value of the rotation angle in radians.
vx:value of the translation vector in x_axis.
vy:value of the translation vector in y_axis.
sx2,sy2:arrays of intermediate results.
arX1,arY1:value in x_axis and in y_axis of points forming the coordinate
system before deformation.
arX2,arY2:value in x_axis and in y_axis of points forming the coordinate
system after deformation.

list of constants:

PTNBR:constant for the loops.
DIM:dimension of the arrays.
pi:value of the constant pi.

```
*************************************************************************/

changement (x2,y2,u)

#define PTNBR 4
#define DIM 15
float *x2,*y2;
int u;
{
int i;
float sx2[DIM],sy2[DIM],arX1[DIM],arY1[DIM],arX2[DIM],arY2[DIM];
double alpha1,alpha2,thetdg,theta,vx,vy,a,b,c,d;
float pi=3.1415926535;

/*opening of rep1x.c file*/

printf("Opening of file including points of mark before deformation(x_axis).\n");
fileopen(&arX1);
for (i=1;i<PTNBR;i++)
printf("mark1x[%d]=%f\n",i,arX1[i]);
getchar();

/*opening of rep1y.c file*/

printf("Opening of file including points of mark before deformation(y_axis).\n");
```

```
fileopen(&arY1);
for (i=1;i<PTNBR;i++)
printf("mark1y[%d]=%f\n",i,arY1[i]);
getchar();

/*opening of rep2x.c file*/

printf("Opening of file including points of mark after deformation(x_axis).\n");
fileopen(&arX2);
for (i=1;i<PTNBR;i++)
printf("mark2x[%d]=%f\n",i,arX2[i]);
getchar();

/*opening of rep2y.c file*/

printf("Opening of file including points of mark after deformation(y_axis).\n");
fileopen(&arY2);
for (i=1;i<PTNBR;i++)
printf("mark2y[%d]=%f\n",i,arY2[i]);
getchar();

vx=(arX2[2]-arX1[2]);
vy=(arY2[2]-arY1[2]);
printf ("The coordinates of the translation vector are:%f,%5f.\n",vx,vy);

d=(arY1[3]-arY1[2]);
c=(arX1[3]-arX1[2]);
alpha1=atan2(d,c);

b=(arY2[3]-arY2[2]);
a=(arX2[3]-arX2[2]);
alpha2=atan2(b,a);

theta=alpha2-alpha1;
printf ("Rotation angle:%frad.\n",theta);
thetdg=(theta*360)/(2*pi);
printf("Rotation angle:%fdegres.\n",thetdg);
while(!kbhit());

for (i=1;i<u+1;i++)
   {
   sx2[i]=arX2[2]+(*(x2+i)-arX2[2])*cos(theta)+(*(y2+i)-arY2[2])*sin(theta);
   sy2[i]=arY2[2]-(*(x2+i)-arX2[2])*sin(theta)+(*(y2+i)-arY2[2])*cos(theta);
   }
for (i=1;i<u+1;i++)
        {
        *(x2+i)=sx2[i]-vx;
        *(y2+i)=sy2[i]-vy;
        printf("Xfinal=%5f  Yfinal=%5f \n",*(x2+i),*(y2+i));
        }
}
```

```
/*****************************************************************************/
/******************** CALCULATION OF DEFORMATIONS ********************/
/*****************************************************************************
```

Description: Calculation of deformations

list of variables:

a1x,a1y:coordinates of classified points before deformation.
a2x,a2y:coordinates of classified points after deformation.
val:number of points in the grid.

length,width,i,j:variables for the loops.
val1,val2,val3,val4:intermediate variables.
eps1,eps2,eps12:values of the strains.
number:number of pixels for one millimeter.

list of constants:

DIM:dimension of the arrays.

```
*****************************************************************************/

calculus(a1x,a1y,a2x,a2y,val)

#define DIM 15
float *a1x,*a1y,*a2x,*a2y;
int val;
{
float eps1[DIM],eps2[DIM],eps12[DIM],number;
int length,width,i,j,val1,val2,val3,val4;

printf("Enter the number of points in length of the grid.\n");
scanf("%d",&length);

printf("Enter the number of points in width of the grid.\n");
scanf("%d",&width);

printf("Enter the number of pixels for one millimeter.\n");
scanf("%f",&number);

for(i=1;i<length;i++)
{
val1=i;
val2=1+i;
val3=length+i;
val4=length+1+i;
printf("val1=%d,val2=%d,val3=%d,val4=%d\n",val1,val2,val3,val4);

eps1[i]=((*(a2x+val2)-*(a2x+val1))-(*(a1x+val2)-*(a1x+val1)))/(*(a1x+val2)-*(a1x+val1));
eps1[i]=(eps1[i]/number);

printf("eps1=%f\n",eps1[i]);

eps2[i]=((*(a2y+val3)-*(a2y+val1))-(*(a1y+val3)-*(a1y+val1)))/(*(a1y+val3)-*(a1y+val1));
eps2[i]=(eps2[i]/number);
printf("eps2=%f\n",eps2[i]);
```

```
eps12[i]=(*(a2y+val2)-*(a2y+val1))/(*(a1x+val2)-*(a1x+val1))+(*(a2x+val3)-
*(a2x+val1))/(*(a1y+val3)-*(a1y+val1));
eps12[i]=(eps12[i]/(2*number)); /*for the good deformation */
printf("eps12=%f\n",eps12[i]);
printf("\n");
getchar();
        for (j=1;j<width-1;j++)
        {
        val1=val1+length;
        val2=val2+length;
        val3=val3+length;
        val4=val4+length;
        printf("val1=%d;val2=%d;val3=%d;val4=%d\n",val1,val2,val3,val4);

        eps1[i]=((*(a2x+val2)-*(a2x+val1))-(*(a1x+val2)-*(a1x+val1)))/(*(a1x+val2)-*(a1x+val1));
        eps1[i]=(eps1[i]/number);
        printf("eps1=%f\n",eps1[i]);

        eps2[i]=((*(a2y+val3)-*(a2y+val1))-(*(a1y+val3)-*(a1y+val1)))/(*(a1y+val3)-*(a1y+val1));
        eps2[i]=(eps2[i]/number);
        printf("eps2=%f\n",eps2[i]);

        eps12[i]=(*(a2y+val2)-*(a2y+val1))/(*(a1x+val2)-*(a1x+val1))+(*(a2x+val3)-
*(a2x+val1))/(*(a1y+val3)-*(a1y+val1));
        eps12[i]=(eps12[i]/(2*number));
        printf("eps12=%f\n",eps12[i]);
        getchar();
        }
}
}
```

```
/*****************************************************************************/
/************* Ordering of the grid points before deformation ***************/
/*****************************************************************************
```

Description:

Ordering of the grid points before deformation.

list of the variables:

*boly:see colbasey1 in the base function(pointer used like an array).
*chix:see casex1 in the base function(pointer used like an array).
*chiy:see casey1 in the base function(pointer used like an array).
*ligx:see mem1x in the base function(pointer used like an array).
*ligy:see mem1y in the base function(pointer used like an array).
heigth:number of points in the grid.
nbr:number of points in the base column.

a,b,k,i,j,p:variables for loops.
flo1,flo2:intermediate variables.

list of constants:

DELTA_Y:difference allowable in y_axis.

```
*****************************************************************************/

arrange1(boly,chix,chiy,heigth,nbr,ligx,ligy)

#define DELTA_Y 50
float *boly,*chix,*chiy,*ligx,*ligy;
int heigth,nbr;
{
int a,b,k,i,j,p;
float flo1,flo2;
j=1;
k=1;
for (p=1;p<nbr+1;p++)
  {
        for (i=1;i<heigth+1;i++)
        if ( *(boly+p) - DELTA_Y < *(chiy+i) )
                {
                if( *(chiy+i) < *(boly+p) + DELTA_Y )
                        {
                        *(ligx+j)=*(chix+i);
                        *(ligy+j)=*(chiy+i);
                        j=j+1;
                        }
                }
        for(a=k;a<j;a++)
                for(b=a+1;b<j;b++)
                if( *(ligx+a) > *(ligx+b) )
                {
                flo1=*(ligx+b);
                *(ligx+b)=*(ligx+a);
                *(ligx+a)=flo1;
                flo2=*(ligy+b);
```

```
                    *(ligy+b)=*(ligy+a);
                    *(ligy+a)=flo2;
                    }
            k=j;
           }
printf("values of points classified:\n");
printf("x_axis----------y_axis\n");
for (i=1;i<j;i++)
           printf("point n§%d:%5f %15f\n",i,*(ligx+i),*(ligy+i));

}
```

```
/*************************************************************************/
/************ Ordering of the grid points after deformation ***************/
/*************************************************************************
```

Description: Ordering of the grid points after deformation

list of the variables:

*ripy:see colbasey2 in the base function(pointer used like an array).
*fiox:see casex2 in the base function(pointer used like an array).
*fioy:see casey2 in the base function(pointer used like an array).
*pox2:see mem2x in the base function(pointer used like an array).
*poy2:see mem2y in the base function(pointer used like an array).
high:number of points in the grid.
lue:number of points in the base column.

a,b,k,i,j,p:variables for loops.
put1,put2,put3,put4:intermediate variables.

list of constants:

DELTA_Y:difference allowable in y_axis.

```
*************************************************************************/

arrange2(ripy,fiox,fioy,high,lue,pox2,poy2)

#define DELTA_Y 50
float *ripy,*fiox,*fioy,*pox2,*poy2;
int high,lue;
{
int a,b,i,j,k,p;
float put1,put2,put3,put4;
j=1;
k=1;
for (p=1;p<lue+1;p++)
    {
  for (i=1;i<high+1;i++)
        if ( *(ripy+p) -DELTA_Y < *(fioy+i) )
                if( *(fioy+i) < *(ripy+p) + DELTA_Y )
                        {
                        put1=*(fiox+i);
                    *(pox2+j)=put1;
                        put2=*(fioy+i);
                    *(poy2+j)=put2;
                        j=j+1;
                        }
        for(a=k;a<j;a++)
                for(b=a+1;b<j;b++)
                if( *(pox2+a) > *(pox2+b) )
                {
                put3=*(pox2+b);
                *(pox2+b)=*(pox2+a);
                *(pox2+a)=put3;
                put4=*(poy2+b);
                *(poy2+b)=*(poy2+a);
                *(poy2+a)=put4;
                }
```

```
            k=j;
            }
printf("value of points classified:\n");
printf("x_axis----------y_axis\n");
for (i=1;i<j;i++)
            printf("point n§%d:%5f %15f\n",i,*(pox2+i),*(poy2+i));
while(!kbhit());
}
```

```
/*****************************************************************************/
/****** This function writes  files of saved values into discs ******************/
/*****************************************************************************
```

Description:

This function opens files of saved values into discs. Special opening because files saved are buffers.

list of variables:
*value:pointer including saved values in the files (pointer used like array).

i:variable for loops.
j:counter.
nbr:number of mesure points.
num_read,tab:intermediate variables.
floval:variable including the saved values into the files.
*fpin:pointer of FILE type to open the files.

```
*****************************************************************************/

fileopen(value)

float *value;
{
char filename[50];
int i,j,num_read,nbr,tab;
float floval;
FILE *fpin;
printf("Enter the name of the file:");
gets(filename);
if((fpin=fopen(filename,"rb"))==NULL)
 {
 printf("cannot open input file :%s\n",filename);


 exit(EXIT_FAILURE);
 }
printf("Enter the number of grid points:");
scanf("%d",&nbr);
j=1;

for(i=1;i<194;i++)
num_read=fread(&tab,sizeof(int),1,fpin);

for(i=194;i<194+(nbr*2);i=i+1)
  {
  num_read=fread(&tab,sizeof(int),1,fpin);
  if(num_read)
    {
    if(tab!=0)
      {
      floval=tab;
      *(value+j)=floval;
      j=j+1;
      }
    }
  else
```

```
printf("read error.Last value of tab=%d",tab);
  }
fclose(fpin);
}

/*****************************END OF PROGRAM*********************************/
```

Related Publications